KOPRI ABSTRACTS

Volume 12 (2020)

KOPRI 극지연구소
Korea Polar Research Institute

KOPRI ABSTRACTS

Volume 12 (2020)

CONTENTS

KOPRI ABSTRACTS

Volume 12 (2020)

KOPRI ABSTRACTS contains journal articles written by KOPRI researchers and other researchers funded by KOPRI. It is published once a year and has distributed worldwide by KOPRI since launching in 2014. In 2004, KOPRI was established as an autonomous institute in KORDI (current, KIOST). Volume 1 (1984-2003) contains KORDI's research activities in the arctic and the antarctic.

Published on 13 August 2021
Published by Korea Polar Research Institute

Editorial office KOPRI Library
26 Songdomirae-ro, Yeonsu-gu, Incheon, 21990, Korea

Cover Photo Seo, Myeongho (KOPRI)
Design Designintro Co.

ISSN 2289-0734

Compiled by Library of Korea Polar Research Institute.

Summary of 2020 Research Paper Performance

We examined three years of research activities by the Korea Polar Research Institute (KOPRI), including research paper results, collaborative research results at home and abroad, and the outlook for its subject fields of research and major journals registered. KOPRI's SCI/SCI(E)-level papers are analyzed based on indicators and data in Web of Science, a database of Clarvate Analytics (former Thomson Reuters).

01. Research papers in recent 3 years

The total number of papers

2018	2019	2020
218	234	222

The number of papers with lead authors

2018	2019	2020
121	127	119

The number of papers by category

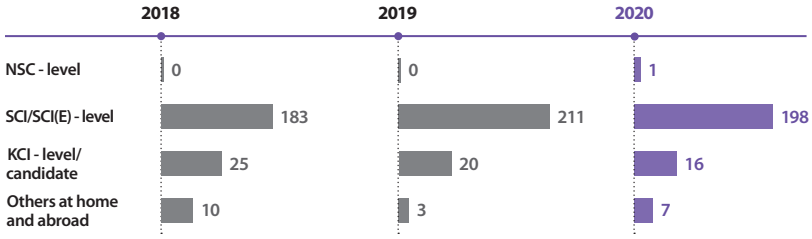

02. Collaborative research results at home and abroad

The analysis of papers published in 2020 found that KOPRI conducted collaborative research with individuals or institutions from a total number of **326** institutions and **37** countries.

Top 5 countries and number of research papers

Country	Number of records	% of 197
SOUTH KOREA	197	100%
USA	38	19.3%
CHINA	18	9.1%
JAPAN	14	7.1%
ENGLAND	13	6.6%
GERMANY	12	6.0%

Top 5 institutes and number of research papers

Institution	Number of records	% of 197
KOREA POLAR RESEARCH INSTITUTE (KOPRI)	195	99.0%
UNIVERSITY OF SCIENCE TECHNOLOGY (UST)	44	22.3%
SEOUL NATIONAL UNIVERSITY (SNU)	27	13.7%
KOREA UNIVERSITY	22	11.2%
PUKYONG NATIONAL UNIVERSITY	16	8.1%
KOREA INSTITUTE OF OCEAN SCIENCE TECHNOLOGY (KIOST)	16	8.1%

03. Subject fields of research

Research topics in 2020 KOPRI Abstracts are categorized into Climate Sciences, Life Sciences, Geosciences, Marine Sciences, and Polar Policy. ***Climate Sciences*** cover paleoclimate, atmosphere sciences, glaciology, remote sensing, and space sciences; ***Life Sciences*** include ecology and biodiversity, genomic & biotechnology; ***Geosciences*** include geology, geophysics, and underwater acoustics; and ***Marine Sciences*** cover oceanography(physical, chemical, biological and geological) as well as subjects in ecology and technological developments with marine environments.

Subject fields of research in 2020 KOPRI Abstracts

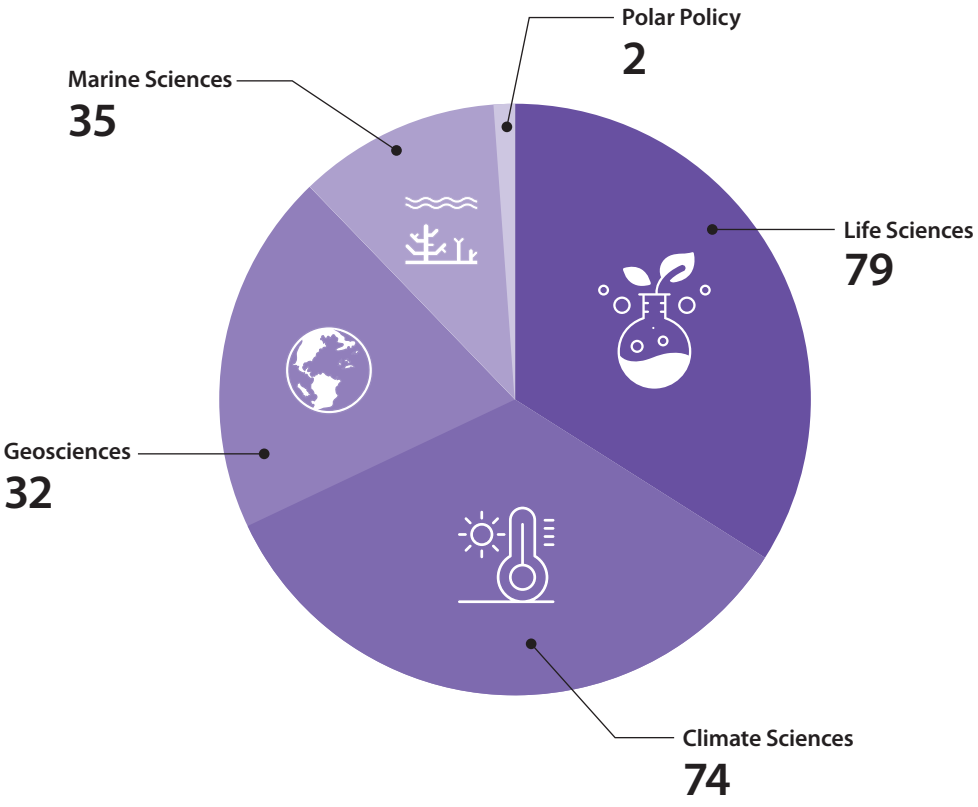

Top 25 Subject fields of research

· Source: Web of Science, Clarivate Analytics

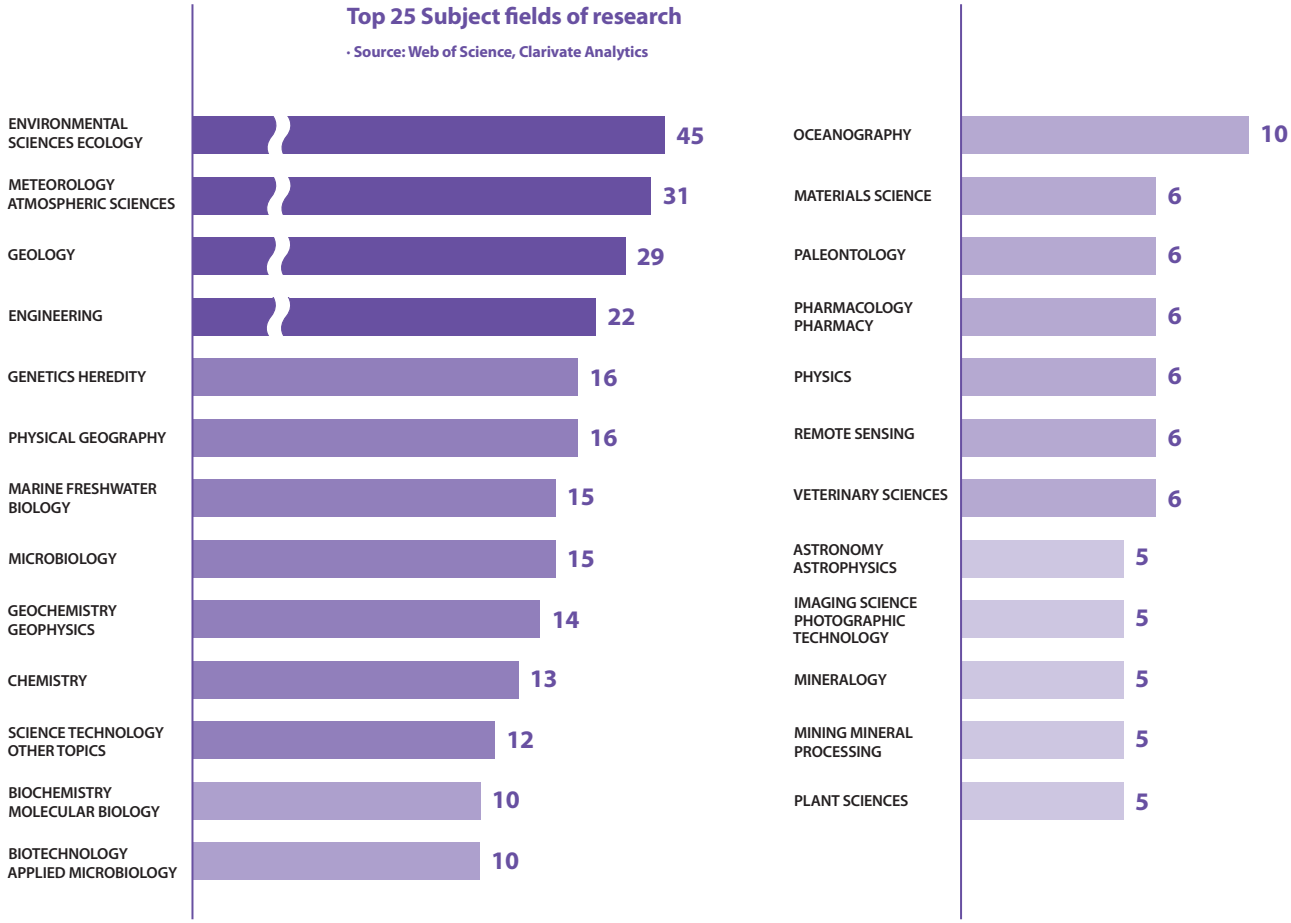

04. Major journals registered

Journals and the number of papers where more than 3 papers were registered

· Source: Web of Science, Clarivate Analytics

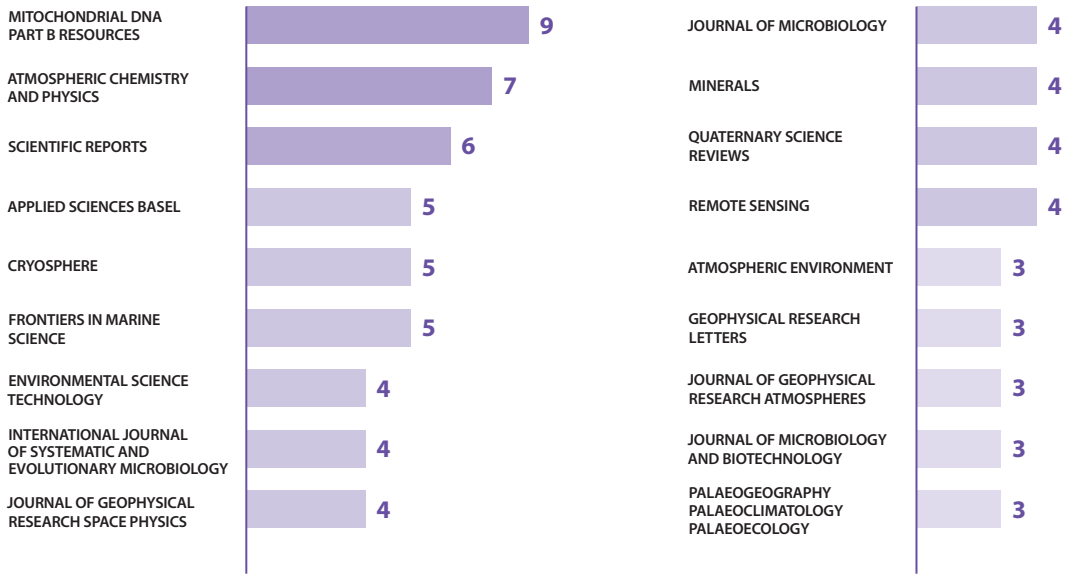

2020년 연구논문 성과 요약

최근 3년간 연구소의 연구논문 성과와 국내외 공동연구성과, 연구주제 분야 및 주요 등재 저널 동향을 살펴보았다. Clarivate Analytics(구 톰슨로이터)의 데이터베이스인 Web of Science 지표와 데이터를 기준으로, 본 연구소의 SCI/SCI(E)급 논문을 대상으로 분석하였다.

01. 최근 3년간 연구논문 성과

전체 논문 수

2018	2019	2020
218	234	222

주저자 논문 편수

2018	2019	2020
121	127	119

분류별 논문 수

	2018	2019	2020
NSC급	0	0	1
SCI/SCI(E)급	183	211	198
KCI등재/후보	25	20	16
국내외 기타	10	3	7

02. 국내외 공동 연구성과

2020년 WOS에 등재된 SCI/SCI(E)급 논문 197편의 논문 분석 결과, 극지연구소는 국내외 **326**개 기관, **37**개 국가와 공동연구를 수행하였다.

공동연구 수행 국가 TOP 5 및 논문 수

국가	논문 수	%(197 기준)
대한민국	197	100%
미국	38	19.3%
중국	18	9.1%
일본	14	7.1%
영국	13	6.6%
독일	12	6.0%

공동연구 수행 기관 TOP 5 및 논문 수

기관	논문 수	%(197 기준)
극지연구소(KOPRI)	195	99.0%
과학기술연합대학원대학교(UST)	44	22.3%
서울대학교	27	13.7%
고려대학교	22	11.2%
부경대학교	16	8.1%
한국해양과학기술원(KIOST)	16	8.1%

03.
연구 주제 분야

2020 KOPRI Abstracts에서 포함하고 있는 연구 주제는 기후과학, 생명과학, 지구시스템, 해양과학, 정책 분야로 분류하였다. **기후과학**은 대기, 고층대기, 빙하, 고기후, 고환경, 원격탐사 등을 포함하며, **생명과학**은 유전학·유전체학, 생리·생화학, 생물다양성·생태·진화, 생물공학을, **지구과학**은 지질, 지구물리, 수중음향을, **해양과학**은 해양학(물리, 화학, 생물학, 지질학)뿐만 아니라 해양환경에 따른 생태학 및 기술개발 등의 주제를 포함하였다.

2020 KOPRI Abstracts의 연구주제 분야

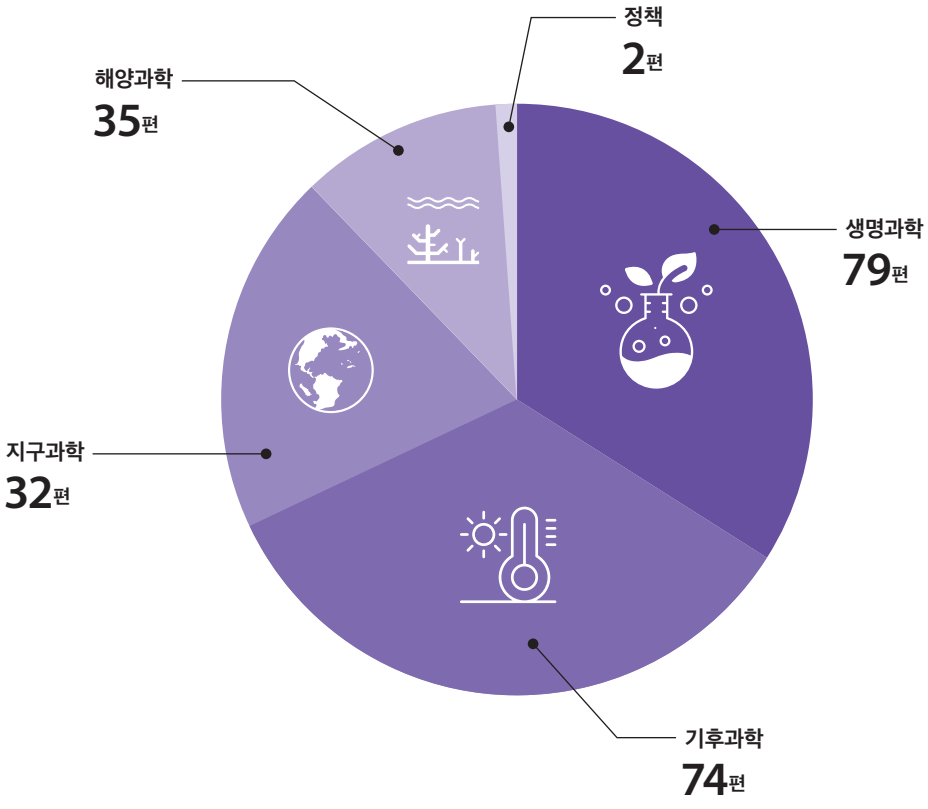

연구 분야 TOP 25

· Source: Web of Science, Clarivate Analytics

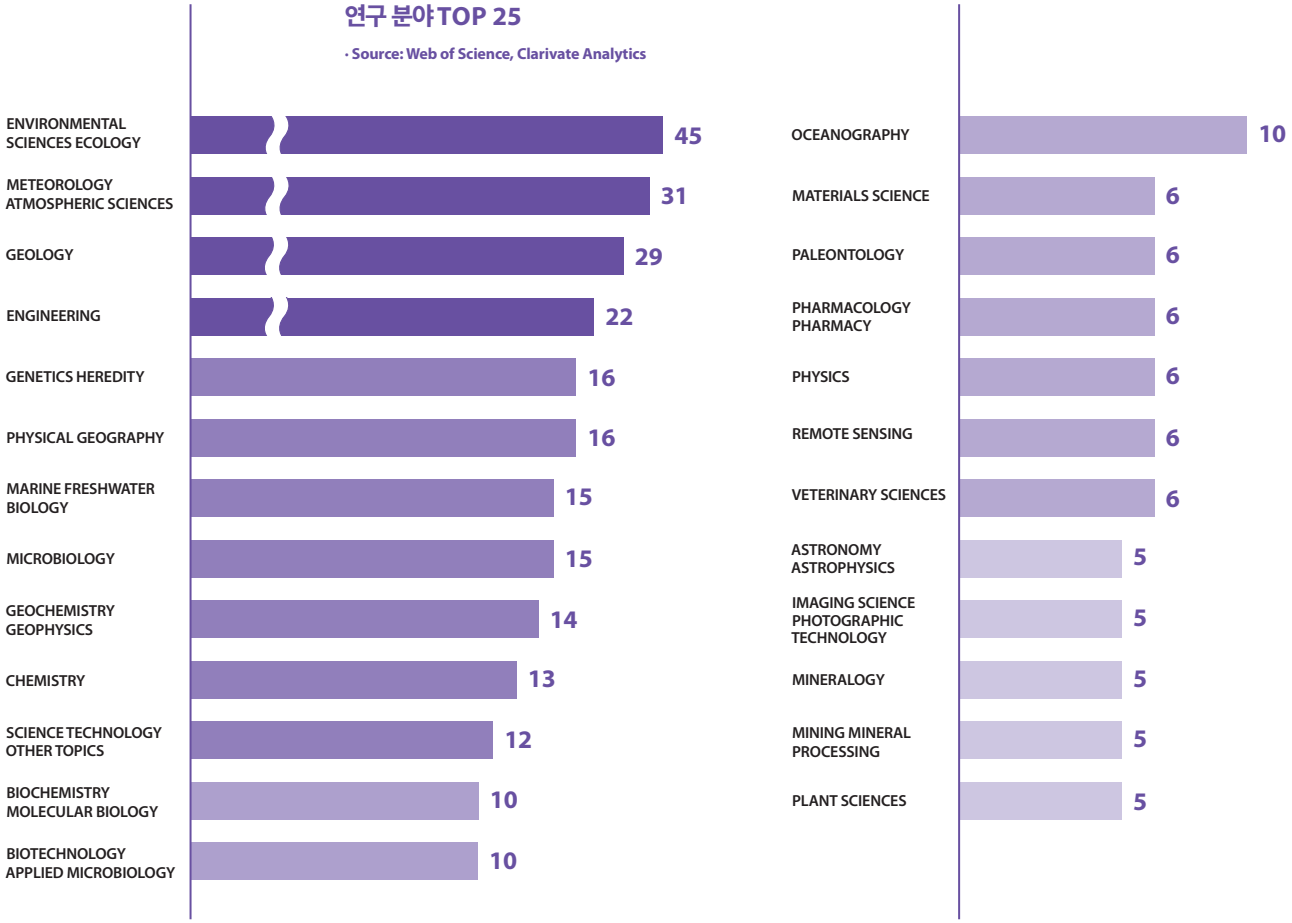

04. 주요 등재 저널

3편 이상 등재된 저널과 논문 수

· Source: Web of Science, Clarivate Analytics

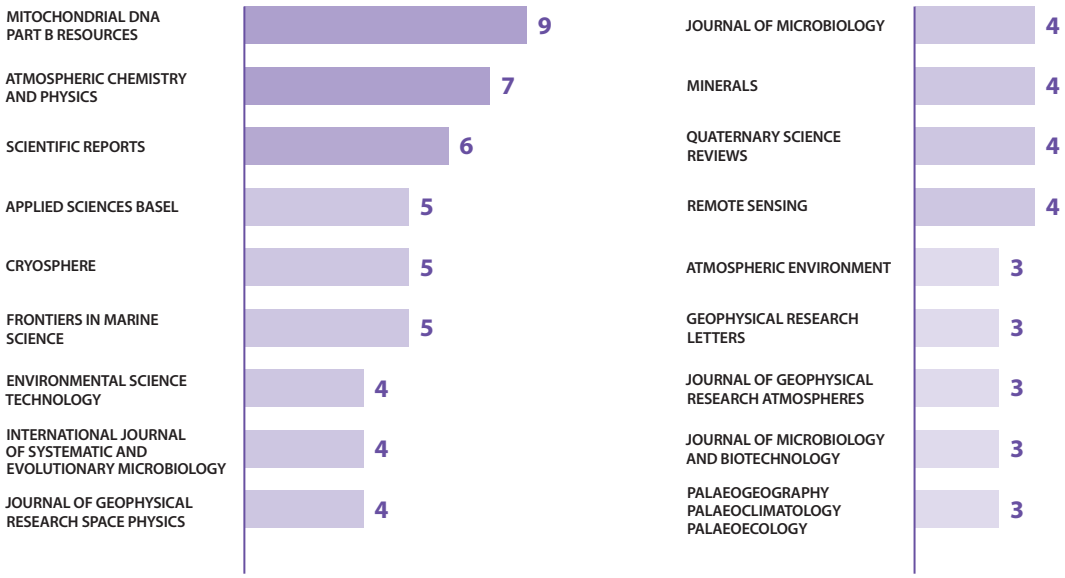

| NOTICE |

1-1 *Geography, Physical; Geosciences, Multidisciplinary*

Aerogeophysical characterization of an active subglacial lake system in the David Glacier catchment, Antarctica

Lindzey, Laura E., Beem, Lucas H., Young, Duncan A., Quartini, Enrica., Blankenship, Donald D., **Lee, Choon-Ki., Lee, Won Sang., Lee, Jong Ik.** and **Lee, Joohan.**

Cryosphere. 2020. 14(7): 2217-2233.

doi: 10.5194/tc-14-2217-2020.

In the 2016-2017 austral summer, the University of Texas Institute for Geophysics (UTIG) and the Korea Polar Research Institute (KOPRI) collaborated to perform a helicopter-based radar and laser altimeter survey of lower David Glacier with the goals of characterizing the subglacial water distribution that supports a system of active subglacial lakes and informing the site selection for a potential subglacial access drilling project. This survey overlaps with and expands upon an earlier survey of the Drygalski Ice Tongue and the David Glacier grounding zone from 2011 and 2012 to create a 5 km resolution survey extending 200 km upstream from the grounding zone.

Keywords: Active Subglacial Lakes; Aerogeophysics; David Glacier Catchment

• **Web of Science Subject**

*If there is no Web of Science Subject in this bibliography, this article is a journal not registered in Web of Science.

• **Reference**

*The following KOPRI authors can be seen as highlighted in bold text

• **Abstract**

• **Keywords**

PART 1

Climate Sciences

1-1 *Geography, Physical; Geosciences, Multidisciplinary*

Aerogeophysical characterization of an active subglacial lake system in the David Glacier catchment, Antarctica

Lindzey, Laura E., Beem, Lucas H., Young, Duncan A., Quartini, Enrica., Blankenship, Donald D., **Lee, Choon-Ki., Lee, Won Sang., Lee, Jong Ik.** and **Lee, Joohan.**

Cryosphere. 2020. 14(7): 2217-2233.

doi: 10.5194/tc-14-2217-2020.

In the 2016-2017 austral summer, the University of Texas Institute for Geophysics (UTIG) and the Korea Polar Research Institute (KOPRI) collaborated to perform a helicopter-based radar and laser altimeter survey of lower David Glacier with the goals of characterizing the subglacial water distribution that supports a system of active subglacial lakes and informing the site selection for a potential subglacial access drilling project. This survey overlaps with and expands upon an earlier survey of the Drygalski Ice Tongue and the David Glacier grounding zone from 2011 and 2012 to create a 5 km resolution survey extending 200 km upstream from the grounding zone. The surveyed region covers two active subglacial lakes and includes reflights of ICESat ground tracks that extend the surface elevation record in the region. This is one of the most extensive aerogeophysical surveys of an active lake system and provides higher-resolution boundary conditions and basal characterizations that will enable process studies of these features. This paper introduces a new helicopter-mounted ice-penetrating radar and laser altimetry system, notes a discrepancy between the original surface-elevation-derived lake outlines and locations of possible water collection based on basal geometry and hydraulic potential, and presents radar-based observations of basal conditions that are inconsistent with large collections of ponded water despite laser altimetry showing that the hypothesized active lakes are at a highstand.

Keywords: Active Subglacial Lakes; Aerogeophysics; David Glacier Catchment

1-2 *Green & Sustainable Science & Technology; Energy & Fuels; Engineering, Environmental; Engineering, Chemical*

Application of noble gas tracers to identify the retention mechanisms of CO_2 migrated from a deep reservoir into shallow groundwater

Ju, YeoJin., Gilfillan, Stuart M., V., Lee, Seong-Sun., Kaown, Dugin., Hahm, Doshik., Lee, Sanghoon., Park, In-Woo., Ha, Seung-Wook., **Park, Keyhong.** and 3 others.

International Journal of Greenhouse Gas Control. 2020. 97.

doi: 10.1016/j.ijggc.2020.103041.

Carbon Capture and Storage (CCS) is a valuable climate-mitigation technology, which offers the potential to cost-effectively reduce the emissions associated with the burning of fossil fuels. However, there is a potential risk of a small portion of the stored CO_2 unintentionally migrating from a storage site to a shallow groundwater aquifer which is the final retaining zone for any migrated CO_2 before it escapes to the atmosphere. Hence, it is imperative to identify the physical retention mechanisms of CO_2 within a shallow aquifer. In this study $1.70x10^2$ kg of CO_2 and noble gas tracers (He, Ar and Kr) were continuously injected into a groundwater aquifer over 28 days with the aim of identifying the mechanisms and amount of CO_2 retention. Among the tracers, Kr was found to be the earliest indicator of CO_2 migration. The other tracers - He and Ar - arrived later and exhibited diluted signals. The diluted signals were attributed to degassing of the plume mass (1.6 % of CO_2) during the early stages of CO_2 migration. Diffusion accelerated the dilution of the lighter elements at the plume boundaries. Consequently, the clear relation of the noble gases with the CO_2 proved that degassing and mixing primarily control the mass retention of CO_2 in shallow groundwater, and the relative importance of these processes varies along the evolving path of migrating CO_2.

Keywords: CCS; Monitoring; CO_2 leakage; Noble gas tracing; Artificial tracer; Geochemical Monitoring

1-3 *Engineering, Environmental; Environmental Sciences*

Approximation of most penetrating particle size for fibrous filters considering Cunningham slip correction factor

Jung, Chang Hoon., **Yoon, Young Jun.** and 5 others.

Environmental Engineering Research. 2020. 25(3): 439-445.

doi: 10.4491/eer.2019.058.

In the estimation of the aerosol single fiber efficiency using fibrous filters, there is a size range, where the particles penetrate most effectively through the fibrous collectors, and corresponding minimum single fiber efficiency. For small particles in which the diffusion mechanism is dominant, the Cunningham slip correction factor (C_C) affects the single fiber efficiency and the most penetrating particle size (MPPS). Therefore, for accurate estimation, C_C is essential to be considered. However, many previous studies have neglected this factor because of its complexity and the associated difficulty in deriving the appropriate parameterization particularly for the MPPS. In this study, the expression for the MPPS, and the corresponding expression for the minimum single fiber efficiency are analytically derived, and the effects of C_C are determined. In order to accommodate the slip factor for all particle-size ranges, C_C is simplified and modified. Overall, the obtained analytical expression for the MPPS is in a good agreement with the exact solution.

keywords: Aerosol single fiber efficiency; Cunningham slip correction factor; Fibrous collector; Minimum single fiber efficiency; Most penetrating particle size

---

1-4 *Environmental Sciences; Meteorology & Atmospheric Sciences*

Arctic ship-based evidence of new particle formation events in the Chukchi and East Siberian Seas

Dall'Osto, M., **Park**, **Jiyeon.**, **Kim**, **Joo-Hong.**, **Kang**, **Sung-Ho.**, Park, Kihong., Beddows, D. C. S., Harrison, Roy M. and **Yoon**, **Young Jun.**

Atmospheric Environment. 2020. 223.

doi: 10.1016/j.atmosenv.2019.117232.

Arctic aerosol-climate interactions are controlled by multiple factors including sources, processes and removal mechanisms of particles. The Arctic is mostly ocean, surrounded by mostly land, and our understanding of Arctic aerosol processes is incomplete due to scarce measurements carried out in sea ice regions. In particular, it is currently not known if these particular regions are sources of aerosols of primary or secondary origin. We present new results from ship-based measurements illustrating that marine new particle production and growth events occur in open ocean and melting sea ice regions in the Chukchi and East Siberian Seas. We report two new particle formation events during which a recently formed nucleation mode (<15 nm diameter) is detected and is observed to slowly grow into an Aitken mode (0.1-3.8 nm h^{-1}). Our results suggest that new particle formation occurs in the marine boundary layer contributing to the Arctic aerosol population in the study region for the first time studied and herein reported.

Keywords: Arctic; New particle formation; NPF; Sea ice; Open ocean; SMPS

1-5 *Environmental Sciences; Meteorology & Atmospheric Sciences*

Atmospheric new particle formation characteristics in the Arctic as measured at Mount Zeppelin, Svalbard, from 2016 to 2018

Lee, Haebum., Lee, Kwangyul., Lunder, Chris Rene., Krejci, Radovan., Aas, Wenche., **Park, Jiyeon., Park, Ki-Tae., Lee, Bang Yong., Yoon, Young Jun.** and Park, Kihong.

Atmospheric Chemistry and Physics. 2020. 20(21): 13425-13441.

doi: 10.5194/acp-20-13425-2020.

We conducted continuous measurements of nanoparticles down to 3 nm size in the Arctic at Mount Zeppelin, Ny Ålesund, Svalbard, from October 2016 to December 2018, providing a size distribution of nanoparticles (3-60 nm). A significant number of nanoparticles as small as 3 nm were often observed during new particle formation (NPF), particularly in summer, suggesting that these were likely produced near the site rather than being transported from other regions after growth. The average NPF frequency per year was 23 %, having the highest percentage in August (63 %). The average formation rate (*J*) and growth rate (GR) for 3-7 nm particles were 0.04 cm^{-3} s^{-1} and 2.07 nm h^{-1}, respectively. Although NPF frequency in the Arctic was comparable to that in continental

areas, the *J* and GR were much lower. The number of nanoparticles increased more frequently when air mass originated over the south and southwest ocean regions; this pattern overlapped with regions having strong chlorophyll *a* concentration and dimethyl sulfide (DMS) production capacity (southwest ocean) and was also associated with increased NH_3 and H_2SO_4 concentration, suggesting that marine biogenic sources were responsible for gaseous precursors to NPF. Our results show that previously developed NPF occurrence criteria (low loss rate and high cluster growth rate favor NPF) are also applicable to NPF in the Arctic.

keywords: Arctic atmospheric aerosol; New particle formation; climate

1-6 *Environmental Sciences; Geosciences, Multidisciplinary; Meteorology & Atmospheric Sciences*

Atmospheric Nitrous Oxide Variations on Centennial Time Scales During the Past Two Millennia

Ryu, Y., Ahn, J., Yang, J. -W., Brook, E. J., Timmermann, A., Blunier, T., **Hur, Soon Do.** and **Kim, Seong-Joong.**

Global Biogeochemical Cycles. 2020. 34(9).

doi: 10.1029/2020gb006568.

The continuous growth of atmospheric nitrous oxide (N_2O) is of concern for its potential role in global warming and future stratospheric ozone destruction. Climate feedbacks that enhance N_2O emissions in response to global warming are not well understood, and past records of N_2O from ice cores are not sufficiently well resolved to examine the underlying climate-N_2O feedbacks on societally relevant time scales. Here, we present a new high-resolution and high-precision N_2O reconstruction obtained from the Greenland NEEM (North Greenland Eemian Ice Drilling) and the Antarctic Styx Glacier ice cores. Covering the N_2O history of the past two millennia, our reconstruction shows a centennial-scale variability of ~10 ppb. A pronounced minimum at ~600 CE coincides with the reorganizations of tropical hydroclimate and ocean productivity changes. Comparisons with proxy records suggest association of centennial- to millennial-scale variations in N_2O with changes in tropical and subtropical land hydrology and marine productivity.

keywords: nitrous oxide; paleoclimate; ice core

1-7 *Environmental Sciences & Ecology*

Changes Detection of Ice Dimension in Cheonji, Baekdu Mountain Using Sentinel-1 Image Classification

Park, Sungjae., Eom, Jinah., Ko, Bokyun., **Park, Jeong-Won.** and Lee, Changwook.

The Journal of The Korean Earth Science Society. 2020. 41(1): 31-39.

doi: 10.5467/JKESS.2020.41.1.31.

Cheonji, the largest caldera lake in Asia, is located at the summit of Baekdu Mountain. Cheonji is covered with snow and ice for about six months of the year due to its high altitude and its surrounding environment. Since most of the sources of water are from groundwater, the water temperature is closely related to the volcanic activity. However, in the 2000s, many volcanic activities have been monitored on the mountain. In this study, we analyzed the dimension of ice produced during winter in Baekdu Mountain using Sentinel-1 satellite image data provided by the European Space Agency (ESA). In order to calculate the dimension of ice from the backscatter image of the Sentinel-1 satellite, 20 Gray Level Co-occurrence Matrix (GLCM) layers were generated from two polarization images using texture analysis. The method used in calculating the area was utilized with the Support Vector Machine (SVM) algorithm to classify the GLCM layer which is to calculate the dimension of ice in the image. Also, the calculated area was correlated with temperature data obtained from Samjiyeon weather station. This study could be used as a basis for suggesting an alternative to the new method of calculating the area of ice before using a long-term time series analysis on a full scale.

keywords: Cheonji; Sentinel-1; Texture analysis; Change detection

1-8 *Astronomy & Astrophysics; Geochemistry & Geophysics; Meteorology & Atmospheric Sciences*

Characteristics of Ionospheric Irregularities Using GNSS Scintillation Indices Measured at Jang Bogo Station, Antarctica (74.62°S, 164.22°E)

Hong, Junseok., Chung, Jong-Kyun., Kim, Yong Ha., Park, Jaeheung., **Kwon, Hyuck-Jin.**, **Kim, Jeong-Han.** and 2 others.

Space Weather-the International Journal of Research and Applications. 2020. 18(10).

doi: 10.1029/2020sw002536.

Global Navigation Satellite System (GNSS) signals strongly depend on the ionospheric conditions, which are composed of electrons and ions generated by solar radiation and particle precipitation. Ionospheric plasma irregularities may cause the scintillation of the GNSS signals or even the loss of signal lock, resulting in the reduction of positioning accuracy and timing precision. Phase scintillation phenomenon is known to occur frequently at high latitudes and primarily related to a significant plasma density gradient, which is due to fast plasma flows in the polar region, energetic particle precipitation in the auroral region, polar cap patches, or several instability mechanisms. Statistical studies are required to understand the characteristics of ionospheric (both phase and amplitude) scintillations at high latitudes. Here, we report the results of ionospheric scintillation measurements at Jang Bogo Station (JBS; 74.62°S, 164.22°E), located inside the polar cap region in Antarctica. The occurrence rates of ionospheric scintillations over the JBS are recorded for 2 years (2017-2018) during solar minimum conditions. The occurrence rates of amplitude scintillations increase only at lower elevation angles (below 30°), which are hard to determine whether the source is ionospheric irregularity or ambient noise such as multipath. In contrast, the occurrence rates of phase scintillations depend on the azimuth angle, season, magnetic activity, magnetic local time, and signal frequency. The results of our analysis suggest that users of the GNSS should consider these parameters to prepare for the degradation of the GNSS performance at high latitudes in the Southern Hemisphere.

keywords: ionosphere; Global Navigation Satellite System; scintillation; high latitudes

1-9 *Engineering*, *Electrical & Electronic; Instruments & Instrumentation*

Characteristics of the Reanalysis and Satellite-Based Surface Net Radiation Data in the Arctic

Seo, Minji., **Kim**, **Hyun-Cheol.** and 5 others.

Journal of Sensors. 2020. 2020.

doi: 10.1155/2020/8825870.

In this study, we compared four net radiation products: the fifth generation of European Centre for Medium-Range Weather Forecasts atmospheric reanalysis of the global climate (ERA5), National Centers for Environmental Prediction (NCEP), Clouds and the Earth's Radiant Energy System Energy Balanced and Filled (EBAF), and Global Energy and Water Exchanges (GEWEX), based on ground observation data and intercomparison data. ERA5 showed the highest accuracy, followed by EBAF, GEWEX, and NCEP. When analyzing the validation grid, ERA5 showed the most similar data distribution to ground observation data. Different characteristics were observed between the reanalysis data and satellite data. In the case of satellite-based data, the net radiation value tended to increase at high latitudes. Compared with the reanalysis data, Greenland and the central Arctic appeared to be overestimated. All data were highly correlated, with a difference of 6-21 W/m^2 among the products examined in this study. Error was attributed mainly to difficulties in predicting long-term climate change and having to combine net radiation data from several sources. This study highlights criteria that may be helpful in selecting data for future climate research models of this region.

keywords: Arctic; Net Radiation; Reanalysis; Satellite

1-10 *Geography*, *Physical; Geosciences*, *Multidisciplinary*

Chronological characteristics for snow accumulation on Styx Glacier in northern Victoria Land, Antarctica

Nyamgerel, **Yalalt.**, **Han**, **Yeongcheol.**, **Kim**, **Songyi.**, **Hong**, **Sang-Bum.**, Lee, Jeonghoon. and **Hur**, **Soon Do.**

Journal of Glaciology. 2020. 66(260): 916-926.

doi: 10.1017/jog.2020.53.

Under the potential to reconstruct the past climatic and atmospheric conditions from a deep ice core in the coastal Antarctic site (Styx Glacier), an 8.84 m long firn core (73°50.975′ S, 163°41.640′f E; 1623 m a.s.l.) was initially studied to propose a reliable age scale for

the local estimation of snow accumulation rate. The seasonal variations of $\delta^{18}O$, methanesulfonic acid (MSA) and non-sea-salt sulfate ($nssSO_4^{2-}$) were used for the firn core dating and revealed 25 annual peaks (from 1990 to 2014) with volcanic sulfate signal. The observed declining trend in annual accumulation rate with a mean value of 146 ± 60 kg m^{-2} a^{-1} is likely to be linked to the changes of sea-ice extent in the Ross Sea region. Moreover, the temporal variation of the annual mean $\delta^{18}O$, an annual flux of MSA and $nssSO_4^{2-}$ also likely to be under the influence of ice-covered and open water area. This study suggests a potential to recover past changes in an oceanic environment and will be useful for the interpretation of the long ice core drilled at the same site.

keywords: Annual layer counting; ionic species; snow accumulation; stable water isotopes; Styx Glacier

1-11 *Geography, Physical; Geosciences, Multidisciplinary*

Classification of sea ice types in Sentinel-1 synthetic aperture radar images

Park, Jeong-Won., Korosov, Anton Andreevich., Babiker, Mohamed., Won, Joong-Sun., Hansen, Morten Wergeland. and **Kim, Hyun-Cheol.**

Cryosphere. 2020. 14(8): 2629-2645.

doi: 10.5194/tc-14-2629-2020.

A new Sentinel-1 image-based sea ice classification algorithm using a machine-learning-based model trained in a semi-automated manner is proposed to support daily ice charting. Previous studies mostly rely on manual work in selecting training and validation data. We show that the readily available ice charts from the operational ice services can reduce the amount of manual work in preparation of large amounts of training/testing data. Furthermore, they can feed highly reliable data to the trainer by indirectly exploiting the best ability of the sea ice experts working at the operational ice services. The proposed scheme has two phases training and operational. Both phases start from the removal of thermal, scalloping, and textural noise from Sentinel-1 data and calculation of grey level co-occurrence matrix and Haralick texture features in a sliding window. In the training phase, the weekly ice charts are reprojected into the SAR image geometry. A random forest classifier is trained with the texture features on input and labels from the rasterized ice charts on output. Then, the trained classifier is directly applied to the texture features from Sentinel-1 images operationally. Test results from the two datasets spanning winter (January-March) and summer (June-August) seasons acquired over the Fram Strait and the Barents Sea showed that the classifier is capable of retrieving three generalized cover types (open water, mixed first-year ice, old ice) with overall accuracies of 87 % and 67 % in winter and summer seasons, respectively. For the summer season, the classifier failed in distinguishing mixed first-year ice from old ice with accuracy of only 12 %; however, it performed rather like an ice-water discriminator with high accuracy of 98 % as the misclassification between the mixed first-year ice and old ice was between them. The accuracy for five cover types (open water, new ice, young ice, first-year ice, old ice) in the winter season was 60 %. The errors are attributed both to incorrect manual classification on the ice charts and to the semi-automated algorithm. Finally, we demonstrate the potential for near-real-time service of the ice map using daily mosaicked Sentinel-1 images.

1-12 *Geochemistry & Geophysics; Meteorology & Atmospheric Sciences*

Climatology of polar ionospheric density profile in comparison with mid-latitude ionosphere from long-term observations of incoherent scatter radars: A review

Kim, Eunsol., **Jee, Geonhwa.**, Ji, Eun-Young., Kim, Yong Ha., **Lee, Changsup.** and 2 others.

Journal of Atmospheric and Solar-Terrestrial Physics. 2020. 211.

doi: 10.1016/j.jastp.2020.105449.

Although the horizontal density structures of the polar ionosphere have been extensively studied mostly using the F-region peak density or total electron content, there are relatively few studies on the vertical density structures. In this review, we present the climatology of the polar ionospheric density not only in the F-region but also in the E-region and topside ionosphere, in comparison with the mid-latitude ionosphere, using long-term incoherent scatter radar (ISR) observations at Millstone Hill, Tromsø, and Svalbard. The ISR data during the period of 1995-2015 are analyzed to study on the variations with local time,

season, and solar/geomagnetic activity. The diurnal variations of the F-region density are much smaller in the polar region than in the mid -latitude, particularly in summer. At Svalbard, there is a characteristic double-peak structure in the diurnal variation of the polar ionosphere in winter only for high solar activity. The diurnal variation of hmF2 decreases with increasing latitude and eventually disappears at Svalbard for low solar activity but the hmF2 and its diurnal variations in the polar ionosphere are remarkably enhanced for high solar activity. The distinctive irregularity in the mid-latitude F1-layer nearly disappears in the polar region, especially at Svalbard. The anomalous seasonal variations of the F-region density are less evident in the polar ionosphere especially for low solar activity and for high magnetic activity conditions. The polar E-region density shows characteristic nighttime peaks induced by auroral precipitation but it does not necessarily increase with solar activity. The topside ionospheric density variations are much stronger in the polar region for high solar activity. Finally, it is found that the polar ionospheric density profiles more strongly respond to increasing solar activity as well as the magnetic activity compared with the mid-latitude ionosphere.

keywords: Polar ionosphere; Climatology; Incoherent scatter radar; Review

1-13 *Engineering, Environmental; Environmental Sciences*

Cr(VI) Formation via Oxyhalide-Induced Oxidative Dissolution of Chromium Oxide/Hydroxide in Aqueous and Frozen Solution

Min, Dae Wi., **Kim**, **Kitae.**, **Kim**, **Bomi.** and 2 others.

Environmental Science & Technology. 2020. 54(22): 14413-14421.

doi: 10.1021/acs.est.0c04851.

The oxidative dissolution of Cr(III) species (Cr_2O_3 and $Cr(OH)_3$) by oxyhalide species, which produces hexavalent chromium (Cr(VI)), was studied in aqueous and frozen solution. The oxyhalide-induced oxidation of Cr(III) in frozen solution showed a different trend from that in aqueous solution. Cr(VI) production was higher in frozen than aqueous solution with hypochlorous acid (HOCl) and bromate (BrO_3^-) but suppressed in frozen solution with hypobromous acid (HOBr) and periodate (IO_4^-). In particular, bromate markedly enhanced Cr(VI) production in frozen solution, whereas it had a negligible activity in aqueous solution. On the contrary, periodate produced Cr(VI) significantly in aqueous solution but greatly suppressed it in frozen solution. Bromate was found to be much more concentrated in the ice grain boundary than periodate according to both chemical and Raman spectral analyses. The oxidative transformation of Cr(III) to Cr(VI) was accompanied by the concurrent and stoichiometric reduction of oxyhalide species. Dissolved O_2 had little effect on the oxidative dissolution, but dissolved organic matter retarded the oxidation of Cr_2O_3 in both aqueous and frozen conditions. This study proposes that the oxyhalide-induced oxidation of Cr(III) (particularly by bromate) in frozen conditions might have a significant effect on the generation of Cr(VI) in the frozen environment.

keywords: hexavalent chromium; ice chemistry; oxyhalides

1-14 *Meteorology & Atmospheric Sciences*

A Critical Role of Extreme Atlantic Windstorms in Arctic Warming

Hong, **Ja-Young.**, Kim, Baek-Min., Baek, Eun-Hyuk., **Kim**, **Joo-Hong.**, Zhang, Xiangdong. and **Kim**, **Seong-Joong.**

Asia-Pacific Journal of Atmospheric Sciences. 2020. 56(1): 17-28.

doi: 10.1007/s13143-019-00123-y.

Here we show that Atlantic windstorms of extreme category in northern winter tend to follow a well-defined route toward the Atlantic sector of Arctic, and that heat and moisture transported by these extreme storms significantly warm the Arctic. A positive North Atlantic Oscillation (NAO) condition and the associated intensified upper-level Atlantic jet provide favorable conditions for those extreme storm developments through enhanced vertical wind shear. These extreme windstorms lead to two discernible impacts on the Arctic: 1) enhanced poleward energy transport by moisture intrusion to the Arctic, which accompanies increased longwave downward radiation and 2) the occurrence of blocking-like patterns after the storm break-up. During these periods, significant Arctic warming was observed of a 10-fold increase versus normal and weak storms. The poleward deflections of

extreme storms, and the Arctic warming driven by such storms, are well simulated in numerical experiments with ocean-atmosphere coupled models.

keywords: Atlantic windstorm; Arctic warming; Extreme windstorm; Storm intensity

1-15 *Environmental Sciences; Geosciences, Multidisciplinary; Remote Sensing; Imaging Science & Photographic Technology*

Data Reconstruction for Remotely Sensed Chlorophyll-a Concentration in the Ross Sea Using Ensemble-Based Machine Learning

Park, Jinku., **Kim**, **Hyun-Cheol.** and 2 others.

Remote Sensing. 2020. 12(11).

doi: 10.3390/rs12111898.

Polar regions are too harsh to be continuously observed using ocean color (OC) sensors because of various limitations due to low solar elevations, ice effects, peculiar phytoplankton photosynthetic parameters, optical complexity of seawater and persistence of clouds and fog. Therefore, the OC data undergo a quality-control process, eventually accompanied by considerable data loss. We attempted to reconstruct these missing values for chlorophyll-a concentration (CHL) data using a machine-learning technique based on multiple datasets (satellite and reanalysis datasets) in the Ross Sea, Antarctica. This technique-based on an ensemble tree called random forest (RF)-was used for the reconstruction. The performance of the RF model was robust, and the reconstructed CHL data were consistent with satellite measurements. The reconstructed CHL data allowed a high intrinsic resolution of OC to be used without specific techniques (e.g., spatial average). Therefore, we believe that it is possible to study multiple characteristics of phytoplankton dynamics more quantitatively, such as bloom initiation/termination timings and peaks, as well as the variability in time scales of phytoplankton growth. In addition, because the reconstructed CHL showed relatively higher accuracy than satellite observations compared with the in situ data, our product may enable more accurate planktonic research.

keywords: data reconstruction; chlorophyll-a concentration (CHL); random forest (RF); Ross Sea; Antarctica

1-16

Deglacial to Holocene variability in surface water characteristics and major floods in the Beaufort Sea

Wu, Junjie., Stein, Ruediger., Fahl, Kirsten., Syring, Nicole., **Nam**, **Seung-Il.** and 3 others.

Communications Earth & Environment. 2020. 27.

doi: 10.1038/s43247-020-00028-z.

Surface water characteristics of the Beaufort Sea have global climate implications during the last deglaciation and the Holocene, as (1) sea ice is a critical component of the climate system and (2) Laurentide Ice Sheet meltwater discharges via the Mackenzie River to the Arctic Ocean and further, to its outflow near the deep-water source area of the Atlantic Meridional Overturning Circulation. Here we present high-resolution biomarker records from the southern Beaufort Sea. Multi-proxy biomarker reconstruction suggests that the southern Beaufort Sea was nearly ice-free during the deglacial to Holocene transition, and a seasonal sea-ice cover developed during the mid-late Holocene. Superimposed on the long-term change, two events of high sediment flux were documented at ca. 13 and 11 kyr BP, respectively. The first event can be attributed to the Younger Dryas flood and the second event is likely related to a second flood and/or coastal erosion.

keywords: Beaufort Sea; Biomarker; Flood events; Laurentide Ice Sheet; Sea ice

1-17 *Geochemistry & Geophysics; Meteorology & Atmospheric Sciences*

Dependence of sudden stratospheric warming type-transition on preceding North Atlantic Oscillation conditions

Choi, **Hyesun.**, Choi, Wookap., **Kim**, **Seong-Joong.** and Kim, Baek-Min.

Atmospheric Science Letters. 2020. 21(3).

doi: 10.1002/asl.953.

Most sudden stratospheric warming (SSW) events initiate with their centers being displaced from the pole. Some retain their displaced form until termination but some split into two vortices during their course.

Here, we show that existence of a transition during the course of the SSW life cycle can be attributable to the condition of North Atlantic Oscillation (NAO) preceding before onset: Positive NAO favors SSW of displacement type with no transition while negative NAO favors the displacement-split type. We show that, in positive NAO precondition, vertical flux of wave activity immediately before onset is mostly contributed only by wavenumber 1 component, which contrasts with the relatively stronger contribution of wavenumber 2 in negative NAO precondition. Whole Atmosphere Community Climate Model (WACCM) simulation results are also consistent with the observational findings. Therefore, NAO can be regarded as a useful precursor for determining the type of forthcoming SSW events.

keywords: North Atlantic oscillation; precursor; sudden stratospheric warming; tropospheric-stratospheric dynamical processes; type-transition

1-18

Development of a calibration system for stable water vapor isotope measurements using Cavity Ring-Down Spectroscope

Lee, Daeun., **Han, Yeongcheol.**, **Kim, Songyi.**, **Hur, Soon Do.** and Lee, Jeonghoon.

Journal of the Geological Society of Korea. 2020. 56(3): 395-403.

doi: 10.14770/jgsk.2020.56.3.395.

Recent development of laser-based spectroscopy introduces continuous measurement method for water vapor isotopic compositions. The measurement precision and accuracy should precede to obtain high temporal resolution data. Here, we developed a calibration system for water vapor isotopic measurement for applications to field studies. Each standard water vapor, evaporated from two isotopically distinct standard waters, was constantly introduced to the Cavity Ring-Down Spectroscope (CRDS). The theoretical isotopic compositions of standard water vapor, calculated using an equilibrium fractionation accompanied by constant temperature, were used as references to calculate a measurement error. This study was conducted in various environment, such as on-board measurements and in Antarctica, to validate the stability of the system when the humidity was lower than the analyzer recommendations. The cavity humidity was calibrated using local Automatic Weather Station (AWS), and then the calibration equation was determined in each different humidity level using enriched ($\delta^{18}O$: -7.98‰, δD: -56.1‰) and depleted ($\delta^{18}O$: -37.44‰, δD: -294.8‰) standards. The calibration system successfully reproduced normalized errors(Δ) within reported values, less than 0.1±0.21‰ (1±1.4‰) for $\delta^{18}O$ (δD), without humidity dependency. As a result, the method is widely applicable for long-term high resolution observations at extremely dry environment like polar regions and high altitude regions.

keywords: stable water vapor isotopes; Cavity Ring-Down Spectroscope; calibration

1-19 *Chemistry, Multidisciplinary; Engineering, Multidisciplinary; Materials Science, Multidisciplinary; Physics, Applied*

Development of a Shallow-Depth Soil Temperature Estimation Model Based on Air Temperatures and Soil Water Contents in a Permafrost Area

Park, Keunbo. and 3 others.

Applied Sciences-Basel. 2020. 10(3).

doi: 10.3390/app10031058.

A model for predicting shallow depth soil temperatures is important and effective to assess the changes in soil conditions related to global climate change and local disturbances. Shallow-depth soil temperature estimation model in cold region in Alaska is developed based on thermal response using air temperature and shallow-depth soil water content during active layer development period of 160 days from May to October. Among the seven soil temperature measurement sites, data from four sites were used for model development, and the remaining three sites were used for model validation. Near the middle of the seven measurement sites, air temperature is monitored at one location. The proposed model implemented concepts of thermal response and cumulative temperature. Temperatures and soil water contents were measured using automated remote sensing technology. Consequently, it was confirmed that the developed model enables fast and accurate assessment of shallow-depth soil temperature during active soil layer development period.

keywords: air temperature; soil temperature; soil temperature modelling; permafrost dynamics; soil water content

1-20 *Meteorology & Atmospheric Sciences*

Differences Between ICESat and CryoSat-2 Sea Ice Thicknesses Over the Arctic: Consequences for Analyzing the Ice Volume Trend

Kim, **Jong-Min.**, Sohn, Byung-Ju., Lee, Sang-Moo., Tonboe, Rasmus Tage., Kang, Eui-Jong. and **Kim**, **Hyun-Cheol.**

Journal of Geophysical Research-Atmospheres. 2020. 125(22).

doi: 10.1029/2020jd033103.

Two sources of readily available and non-overlapping space-borne data on sea ice thickness over the Arctic (i.e., Ice, Cloud, and land Elevation Satellite [ICESat] and CryoSat-2 [CS2]) were compared using overlapping thermal microwave radiometer data to examine their respective differences. As a bridge connecting these two data sets, data on the vertically polarized emissivity difference between 10.65 and 18.7 GHz derived from the Advanced Microwave Sounding Radiometer were related to ICESat and CS2 thickness values via regression. The results indicate that there are substantial and systematic differences in the ice thickness between these two data sets over the Arctic; ICESat ice thickness was systematically lower than that of CS2 by ~50 cm, compared to ice thickness from Operation IceBridge and upper looking sonar data. The CS2 thickness observed later than that of ICESat was found to be thicker, contradicting the thinning expected under global warming conditions. Correcting for the 50-cm difference between ICESat or CS2 data revealed trends in ice volume that are consistent with the expected and modeled declines in the Pan-Arctic Ice-Ocean Modeling and Assimilation System data, further corroborating the 50 cm of relative bias observed between the two data sets.

keywords: CryoSat-2; ICESat; Ice volume trend; sea ice thickness

1-21 *Oceanography*

Discussion on the Late Miocene Biogenic Opal Crash in the Andaman Sea

Lee, Jongmin., **Kim**, **Sunghan.** and Khim, Boo-Keun.

Journal of the Korean Society of Oceanography. 2020. 25(1): 1-8.

doi: 10.7850/jkso.2020.25.1.001.

Biogenic opal crash at about 6.7 Ma was identified at both IODP Site U1447 and NGHP Site 17 in the Andaman Sea. The different biogenic opal content and general variation pattern between two sites may be attributed to the different concentration of analytical reagent and sedimentation rate estimated by the different chronological approaches. Nevertheless, this study suggests that the biogenic opal crash in the Andaman Sea is closely related to the restriction of Indonesian Throughflow and to the decreasing strength of Indian summer monsoon during the late Miocene, both of which resulted in the reduction of nutrient supply.

keywords: Nutrient; Productivity; Indonesian Throughflow; IODP; Indian Ocean

1-22 *Meteorology & Atmospheric Sciences*

Dominance of large-scale atmospheric circulations in long-term variations of winter PM_{10} concentrations over East Asia

Lee, Greem., Ho, Chang-Hoi., Chang, Lim-Seok., Kim, Jinwon., Kim, Maeng-Ki. and **Kim**, **Seong-Joong.**

Atmospheric Research. 2020. 238.

doi: 10.1016/j.atmosres.2020.104871.

Concentrations of wintertime particulate matters of diameters below 10 μm (PM_{10}) in South Korea and China have decreased since the 2000s largely owing to the emissions reduction policies of the two countries; however, this decreasing tendency has been notably weakened, or even been reversed, in recent years. This study examines the influence of large-scale atmospheric circulations on this PM_{10}, change over East Asia for the winters (December-February) of the 2004/05-2015/16 period using an empirical orthogonal function (EOF) analysis. The first EOF mode, which accounts for 32.7% of the total variance, indicates decreases in PM_{10}, concentrations until 2012 and thereafter increases in them particularly at most stations in eastern and northeastern China. Regression patterns of meteorological variables with respect to the first EOF time series indicate that the wintertime

PM_{10}, variations over East Asia are greatly influenced by the Ural blocking; the weakening of the Ural blocking after 2014 led to the weakening of cold air flows from the north and provided atmospheric conditions favorable for bad air quality events over East Asia. The second EOF mode, which accounts for 20.1% of the total variance, shows a similar spatial distribution as the linear trend of PM_{10}, concentrations during the analysis period and would be related to the long-term changes in emissions. Our findings emphasize that the long-term variations in air quality over East Asia are affected primarily by the variations in large-scale atmospheric circulations with secondary contributions from the changes in emissions.

keywords: Particulate matter; PM_{10}; Atmospheric circulation; Ural blocking; East Asia

1-23 *Environmental Sciences; Marine & Freshwater Biology*

Dual carbon isotope ($\delta^{13}C$ and $\Delta^{14}C$) characterization of particulate organic carbon in the Geum and Seomjin estuaries, South Korea

Kang, Sujin., **Kim**, **Jung-Hyun.** and 2 others.

Marine Pollution Bulletin. 2020. 150.

doi: 10.1016/j.marpolbul.2019.110719.

We investigated the source, composition, and reactivity of particulate organic carbon (POC) in two contrasting Korean estuary systems, a closed estuary (Geum) (i.e., with an estuary dam at the river mouth) and an open (Seomjin) estuary. A dual isotope ($\delta^{13}C_{POC}$ and $\Delta^{14}C_{POC}$) approach was applied to surface water samples collected along a salinity gradient in August 2016. Our results indicate that phytoplankton-derived POC was the main contributor to the total POC pool in the reservoir of the Geum estuary, while terrestrial-derived POC predominated the upper Seomjin estuary. A simple binary mixing model using $\Delta^{14}C_{POC}$ revealed a higher modem POC contribution (87-90%) in the Geum estuary reservoir than that (77%) of the upper Seomjin estuary. Accordingly, it appears that an estuary dam can alter the source and reactivity of POC in a reservoir, which can be transferred to the adjacent coastal ecosystem.

keywords: Particulate organic carbon; Estuary dam; Carbon isotopes; Geum estuary; Seomjin estuary

1-24 *Chemistry, Analytical*

Dual isotope ratio normalization of nitrous oxide by bacterial denitrification of USGS reference materials

Kim, Taewan., Lee, Jeongsoon., **Hong**, **Sang-bum.**, **Park**, **Ha Ju.** and Lim, Jeong Sik.

Talanta. 2020. 219.

doi: 10.1016/j.talanta.2020.121268.

We measured the δ values of N_2O using gas chromatography isotope ratio mass spectrometry with a pre concentrator (precon-GC-IRMS). The instrumental precision of the mass spectrometer was restricted to below the shot noise limit, which agreed with the theoretical and experimental results of 0.02‰ ($\delta^{15}N$) and 0.04‰ ($\delta^{18}O$), respectively. The precision of the measured delta values was significantly improved by the temperature regulation protocol of the LN_2 preconcentrator, which was monitored by various temperature sensors placed along the U trap. The reproducibility of the He-diluted N_2O gas measurements resulted in 0.063‰ ($\delta^{15}N$) and 0.075‰ ($\delta^{18}O$) due to additional sources of uncertainty in the vials used for autosampling and in the general pre concentration process. Multipoint normalization of the dual δ values of the measured N_2O samples was conducted using United States Geological Survey reference materials denitrified by *Pseudomonas aureofaciens*. Kaiser's ion correction method, based on International Atomic Energy Agency parameters, exhibited low bias for the atomic isotope ratio reduction of the nitrate reference material, for which the oxygen anomaly was considerably high. Dedicated corrections for net isotope fractionation and water exchange were important in improving uncertainties in the procedure for normalizing the oxygen isotope ratio. Blank measurements for correcting biases in isotope ratios caused by pre-dissolved nitrate and nitrite ions in the water solvent led to further improvements, i.e. beyond unevenly controlled net isotope fractionation, throughout the bacterial denitrification process. The uncertainty evaluation revealed that three-point normalization can significantly improve the normalization accuracy compared with two-point normalization. In addition, an alternative strategy was suggested for assigning $\delta^{18}O$ using a CO_2 lab tank, allowing its use as a reference material for N_2O gas tanks.

keywords: Isotope ratio mass spectrometry; $\delta^{15}N$; $\delta^{18}O$; Bacterial denitrification; Multipoint normalization; Uncertainty assessment

1-25 *Environmental Sciences; Meteorology & Atmospheric Sciences*

Dynamical response of atmospheric circulation to below-normal East Sea sea surface temperatures associated with heavy snowfall in eastern Korea

Kim, **Taekyun.**, Kim, Yoonjae., Moon, Jae-Hong. and **Jin**, **Emilia Kyung.**

Environmental Research Letters. 2020. 15(7).

doi: 10.1088/1748-9326/ab8dd9.

Prior studies have shown that above-normal sea surface temperatures (SSTs) enhance snowfall over Korea. Here, we show that heavy snow is also associated with below-normal East Sea SSTs, and we investigate the dynamical response of the atmosphere to this surface condition using observations and numerical modeling. The results indicate that anomalous southeasterly/easterly winds are induced by heavy snowfall-related cold SST anomalies, and consequently, the moisture flux is converged. The existence of the southeasterly winds and the accompanied moisture flux convergence appear to be instrumental in producing the heavy snowfall events. The anomalous southeasterly/easterly winds associated with heavy snowfall-related cold SST anomalies reduce the climatological northwesterly/westerly winds, leading to relatively warm and wet conditions over the east coast of Korea that are favorable for forming and intensifying snowfall events in the region.

keywords: heavy snowfall; East Sea; heavy snowfall-related sea surface temperature; atmospheric circulation

1-26 *Chemistry, Analytical; Environmental Sciences*

Emerging investigator series: influence of marine emissions and atmospheric processing on individual particle composition of summertime Arctic aerosol over the Bering Strait and Chukchi Sea

Kirpes, Rachel M., Rodriguez, Blanca., Kim, Saewung., China, Swarup., Laskin, Alexander., **Park**, **Keyhong.**, **Jung**, **Jinyoung.** and 2 others.

Environmental Science-Processes & Impacts. 2020. 22(5): 1201-1213.

doi: 10.1039/c9em00495e.

The Arctic is rapidly transforming due to sea ice loss, increasing shipping activity, and oil and gas development. Associated marine and combustion emissions influence atmospheric aerosol composition, impacting complex aerosol-cloud-climate feedbacks. To improve understanding of the sources and processes determining Arctic aerosol composition, atmospheric particles were collected aboard the Korean icebreaker R/V *Araon* cruising within the Bering Strait and Chukchi Sea during August 2016. Offline analyses of individual particles by microspectroscopic techniques, including scanning electron microscopy with energy dispersive X-ray spectroscopy and atomic force microscopy with infrared spectroscopy, provided information on particle size, morphology, and chemical composition. The most commonly observed particle types were sea spray aerosol (SSA), comprising ~60–90%, by number, of supermicron particles, and organic aerosol (OA), comprising ~50-90%, by number, of submicron particles. Sulfate and nitrate were internally mixed within both SSA and OA particles, consistent with particle multiphase reactions during atmospheric transport. Within the Bering Strait, SSA and OA particles were more aged, with greater number fractions of particles containing sulfate and/or nitrate, compared to particles collected over the Chukchi Sea. This is indicative of greater pollution influence within the Bering Strait from coastal and inland sources, while the Chukchi Sea is primarily influenced by marine sources.

keywords: Arctic; Marine Aerosol; atmospheric chemistry; sulfate; summer

1-27 *Engineering, Chemical*

Enhanced reduction of hexavalent chromium by hydrogen sulfide in frozen solution

Nguyen, **Quoc Anh.**, **Kim**, **Bomi.**, **Chung**, **Hyun Young.**, Kim, Jungwon. and **Kim**, **Kitae.**

Separation and Purification Technology. 2020. 251.

doi: 10.1016/j.seppur.2020.117377.

Significant enrichment of hexavalent chromium [Cr (VI)] has been detrimentally influenced both environment and human's health in the polar regions. We found that reduction of Cr (VI) by hydrogen sulfide (H_2S) was significantly enhanced in ice (–20 °C) but relatively slow in water (25 °C) under the same experimental conditions. This enhancement is ascribed to the freeze concentrations of Cr (VI), H_2S, and proton (H^+) in ice grain boundaries during freezing. Sulfate (SO_4^{2-}) was produced more appreciably in ice than in water. Cr (VI) reduction in ice was enhanced effectively under various H_2S concentrations (5.0–100 μM), pH_i (2.0–7.7), and increasing the freezing temperature from –30 to –15 °C. Optical and chemical observations with a confocal Raman microscope under frozen state supported the freeze concentration of Cr (VI) in ice grain boundaries. The accumulation of H^+ (pH decrease) in ice grain boundaries was verified with the UV–visible absorption spectra of cresol red (CR) in ice. Removal of Cr (VI) in electroplating wastewater was significant and comparable to that in distilled water by freezing. Therefore, Cr (VI) reduction by H_2S in ice phase indicates the occurrence of Cr (VI) removal in cold regions.

keywords: Hexavalent chromium; Hydrogen sulfide; Freeze concentration effect; Electroplating wastewater; Ice chemistry

1-28 *Chemistry, Physical; Physics, Atomic, Molecular & Chemical*

Entangled iodine and hydrogen peroxide formation in ice

Baek, Yong Su., **Kim**, **Kitae.**, Saiz-Lopez, Alfonso., Min, Dae Wi., **Kim**, **Bomi.** and 2 others.

Physical Chemistry Chemical Physics. 2020. 22(29): 16532-16535.

doi: 10.1039/d0cp02966a.

Ice-core records show that anthropogenic pollution has increased the global atmospheric concentrations of hydrogen peroxide and iodine since the mid-20th century. Here, for the first time, we demonstrate a highly efficient mechanism that synergistically produces them in icy water conditions. This reaction is aided by a key intermediate IO_2H, formed by an I^- ion with a dissolved O_2 in acidic icy water, which produces both I as well as O_2H radicals. I recombines with I^- to produce I_2^- at a diffusion-limited rate, followed by formation of I_3^- through disproportionation, while O_2H yields H_2O_2 with I^- and a proton dissolved in icy water.

keywords: ice chemistry; iodine; ozone depletion; polar regions

1-29 *Meteorology & Atmospheric Sciences*

Evaluating the Impact of Assimilating Aerosol Optical Depth Observations on Dust Forecasts Over North Africa and the East Atlantic Using Different Data Assimilation Methods

Choi, **Yonghan.** and 6 others.

Journal of Advances in Modeling Earth Systems. 2020. 12(4).

doi: 10.1029/2019ms001890.

This study evaluates the impact of assimilating moderate resolution imaging spectroradiometer (MODIS) aerosol optical depth (AOD) data using different data assimilation (DA) methods on dust analyses and forecasts over North Africa and tropical North Atlantic. To do so, seven experiments are conducted using the Weather Research and Forecasting dust model and the Gridpoint Statistical Interpolation analysis system. Six of these experiments differ in whether or not AOD observations are assimilated and the DA method used, the latter of which includes the three-dimensional variational (3D-Var), ensemble square root filter (EnSRF), and hybrid methods. The seventh experiment, which allows us to assess the impact of assimilating deep blue AOD data, assimilates only dark target AOD data using the hybrid method. The assimilation of MODIS AOD data clearly improves AOD analyses and forecasts up to 48 hr in length. Results also show that assimilating deep blue data has a primarily positive effect on AOD analyses and forecasts over and downstream of the major North African source regions. Without assimilating deep blue data (assimilating dark target only), AOD assimilation only improves AOD forecasts for up to 30 hr. Of the three DA methods examined, the hybrid and EnSRF methods produce better AOD analyses and forecasts than the 3D-Var method does. Despite the clear benefit of AOD assimilation for AOD analyses and forecasts, the lack of information regarding the vertical distribution of aerosols in AOD data means that AOD assimilation has very little positive effect on analyzed or forecasted vertical profiles of backscatter.

1-30 *Meteorology & Atmospheric Sciences*

Evaluation of land-atmosphere processes of the Polar WRF in the summertime Arctic tundra

Kim, Jeongwon., Lee, Junhong., Hong, Je-Woo., Hong, Jinkyu., Koo, Ja-Ho., **Kim**, **Joo-Hong.**, **Yun**, **Juyeol.**, **Nam**, **Sungjin.**, **Jung**, **Ji Young.**, **Choi**, **Taejin.** and **Lee**, **Bang Yong.**

Atmospheric Research. 2020. 240.

doi: 10.1016/j.atmosres.2020.104946.

Arctic tundra is undergoing a rapid transition due to global warming and will be exposed to snow-free conditions for longer periods under projected climate scenarios. Regional climate modeling is useful for understanding and predicting climate change in the Arctic tundra, however, the lack of in-situ observations of surface energy fluxes and the planetary boundary layer (PBL) structure hinders accurate predictions of local and regional climate around the Arctic. In this study, we investigate the performance of the Polar-optimized version of the Weather Research and Forecasting model (PWRF) in the Arctic tundra on clear days in summer. Based on simultaneous observations of surface fluxes and the PBL structure in Cambridge Bay, Nunavut, Canada, our validation shows that the PWRF simulates a drier environment, leading to a larger Bowen ratio and a warmer atmosphere compared to observations. Further sensitivity analyses indicate that the model biases are mainly from the uncertainties in physical parameters such as surface albedo and emissivity, the solar constant, and the model top height, rather than structural flaws in the model physics. Importantly, the PWRF reproduces the observations more accurately when the observed soil moisture is fed into the simulation. This indicates that there must be improvements in simulations of the land-atmosphere interaction at the Arctic tundra, not only in the accuracy of the initial soil moisture conditions but also in soil hydraulic properties and drainage processes. The mixing diagram analysis also shows that the entrainment process between the PBL and the overlying atmosphere needs to be improved for better weather and climate simulation. Our findings shed light on modeling studies in the Arctic region by disentangling the model error sources from uncertainties by parameters and physics package options.

keywords: Polar WRF; Arctic tundra; Land-atmosphere interaction; Surface energy balance; Soil moisture; Planetary boundary layer

1-31 *Environmental Sciences; Geosciences, Multidisciplinary; Remote Sensing; Imaging Science & Photographic Technology*

Evolution of Backscattering Coefficients of Drifting Multi-Year Sea Ice during End of Melting and Onset of Freeze-up in the Western Beaufort Sea

Kim, **Seung Hee.**, **Kim**, **Hyun-Cheol.**, **Hyun**, **Chang-Uk.**, **Lee**, **Sungjae.**, Ha, Jung-Seok., **Kim**, **Joo-Hong.**, **Kwon**, **Young-Joo.**, **Park**, **Jeong-Won.** and 3 others.

Remote Sensing. 2020. 12(9).

doi: 10.3390/rs12091378.

Backscattering coefficients of Sentinel-1 synthetic aperture radar (SAR) data of drifting multi-year sea ice in the western Beaufort Sea during the transition period between the end of melting and onset of freeze-up are analyzed, in terms of the incidence angle dependence and temporal variation. The mobile sea ice surface is tracked down in a 1 km by 1 km region centered at a GPS tracker, which was installed during a field campaign in August 2019. A total of 24 Sentinel-1 images spanning 17 days are used and the incidence angle dependence in HH- and HV-polarization are -0.24 dB/deg and -0.10 dB/deg, respectively. Hummocks and recently frozen melt ponds seem to cause the mixture behavior of surface and volume scattering. The normalized backscattering coefficients in HH polarization gradually increased in time at a rate of 0.15 dB/day, whereas the HV-polarization was relatively flat. The air temperature from the ERA5 hourly reanalysis data has a strong negative relation with the increasing trend of the normalized backscattering coefficients in HH-polarization. The result of this study is expected to complement other previous studies which focused on winter or summer seasons in other regions of the Arctic Ocean.

keywords: sea ice; synthetic aperture radar; multi-year; arctic; Beaufort Sea; backscattering coefficient; incidence angle

1-32 *Geosciences, Multidisciplinary*

The Far Ultraviolet Signatures of Conjugate Photoelectrons Seen by the Special Sensor Ultraviolet Spectrographic Imager

Kil, Hyosub., Schaefer, Robert K., Paxton, Larry J. and **Jee**, **Geonhwa.**

Geophysical Research Letters. 2020. 47(1).

doi: 10.1029/2019gl086383.

This study investigates the origin of anomalous far ultraviolet emissions observed at night at the subauroral region by the Special Sensor Ultraviolet Spectrographic Imager on board the Defense Meteorological Satellite System-F16 satellite. The global distribution of the anomalous emission is derived using the measurements of the oxygen atom 130.4-nm emission in 2017. Our results show the extension of the anomalous emission from high latitudes to middle latitudes in the Northern American-Atlantic sector during the December solstice and in the Southern Australia-New Zealand sector during the June solstice. These observations indicate that the anomalous emission occurs in the winter hemisphere and is pronounced at locations close to the magnetic poles. The good agreement between the morphology of the anomalous emission and the predicted distribution of conjugate photoelectrons leads to the conclusion that the anomalous emissions are the signatures of conjugate photoelectrons.

keywords: Conjugate Space Environment; FUV

1-33 *Astronomy & Astrophysics*

First Global-Scale Synoptic Imaging of Solar Eclipse Effects in the Thermosphere

Aryal, Saurav., Evans, J. S., Correira, John., Burns, Alan G., Wang, Wenbin., Solomon, Stanley C., Laskar, Fazlul I., McClintock, William E., Eastes, Richard W., Dang, Tong., Lei, Jiuhou., Liu, Huixin. and **Jee**, **Geonhwa.**

Journal of Geophysical Research-Space Physics. 2020. 125(9).

doi: 10.1029/2020ja027789.

A total solar eclipse occurred in the Southern Hemisphere on 2 July 2019 from approximately 17 to 22 UT. Its effect in the thermosphere over South America was imaged from geostationary orbit by NASA's Global-scale Observation of Limb and Disk (GOLD) instrument. GOLD observed a large brightness reduction (>80% around totality) in OI 135.6 nm and N_2 LBH band emissions compared to baseline measurements made 2 days prior. In addition, a significant enhancement (with respect to the baseline) in the $\Sigma O/N_2$ column density ratio (~ 80%) was observed within the eclipse's totality. This enhancement suggests that the eclipse induced compositional changes in the thermosphere. After the eclipse passed, a slight enhancement in $\Sigma O/N_2$ column density ratio (~ 7%) was also seen around the totality path when compared to measurements before the eclipse. These observations are the first synoptic imaging measurements of an eclipse's thermospheric effects with the potential to drastically improve and test our understanding of how the thermosphere responds to rapid, localized changes in solar short wavelength radiation.

keywords: Solar Eclipse; Thermosphere

1-34 *Meteorology & Atmospheric Sciences*

First observations of the McMurdo-South Pole oblique ionospheric HF channel

Chartier, Alex T., Vierinen, Juha. and **Jee**, **Geonhwa.**

Atmospheric Measurement Techniques. 2020. 13(6): 3023-3031.

doi: 10.5194/amt-13-3023-2020.

We present the first observations from a new low-cost oblique ionosonde located in Antarctica. The transmitter is located at McMurdo Station, Ross Island, and the receiver at Amundsen-Scott Station, South Pole. The system was demonstrated successfully in March 2019, with the experiment yielding over 30 000 ionospheric echoes over a 2-week period. These data indicate the presence of a stable E layer and a sporadic and variable F layer with dramatic spread F of sometimes more than 500 km (in units of virtual height). The most important ionospheric parameter, NmF2, validates well against the Jang Bogo Vertical Incidence Pulsed Iono-spheric (VIPIR) ionosonde (observing more than 1000 km away). GPS-derived TEC data from the Multi-Instrument Data Analysis Software (MIDAS) algorithm can be considered necessary but insufficient to predict 7.2MHz propagation between

McMurdo and the South Pole, yielding a true positive in 40% of cases and a true negative in 73% of cases. The success of this pilot experiment at a total grant cost of USD 116 000 and an equipment cost of ~ USD 15 000 indicates that a large multi-static network could be built to provide unprecedented observational coverage of the Antarctic ionosphere.

keywords: Jang Bogo Station; Polar Ionosphere; VIPIR

1-35 *Computer Science, Information Systems; Engineering, Electrical & Electronic; Telecommunications*

Fractal Analysis and Texture Classification of High-Frequency Multiplicative Noise in SAR Sea-Ice Images Based on a Transform-Domain Image Decomposition Method

Shahrezaei, Iman Heidarpour. and **Kim, Hyun-Cheol.**

Ieee Access. 2020. 8: 40198-40223.

doi: 10.1109/access.2020.2976815.

Texture in synthetic aperture radar (SAR) images is a combination of the intrinsic texture of scene backscattering and the texture due to noncoherent high-frequency multiplicative noise (HMN) interactions that reflect erroneous information and lead to observation misinterpretation. The focus of this paper is the fractal analysis of KOMPSAT-5 SAR images of noncoherent sea-ice textures while being decomposed by discrete wavelet transform (DWT) processing. As a novel approach, fractal analysis relies on SAR sea-ice spatial backscattering data generation and time-frequency domain (TFD) formulations from the perspective of uncorrelated HMN. To the best of our knowledge, this is the first time that the extraction of the resolution profile and raw data for the reference KOMPSAT-5 SAR sea-ice image have been derived, evaluated and compared both qualitatively and quantitatively at each scale of DWT decomposition on the basis of the presence of HMN. This paper also presents a novel detailed modeling of the multiresolution probability distribution function of the HMN and its power spectral density function modeling at each scale of the decomposition. Other quality assessment techniques, such as two K-means clustering algorithms and several visualized verification methods, such as gradient vector field, advection mapping and tensor field mapping, have been implemented in this regard to investigate embedded HMN suppression and its adverse effects on the presence of pixel anomalies. As a result, as the decomposition continues, the HMN at each scale of decomposition is constantly altering from high-frequency uncorrelated anomalies to low-frequency joint spatial information within the observed 2-D data. In other words, excessive multiscale HMN suppression will result in spatial information loss that makes the DWT scale selection quite important for texture classification. The results also show that the importance of HMN suppression in SAR sea-ice images in the form of pixel anomaly decomposition for the purpose of further texture investigation should be in accordance with the spectral behavior of the HMN. The results are helpful for SAR remote sensing image restoration and data preservation when dealing with high-resolution SAR images, such as in time series analysis, sea-ice texture change detection, and polar structural mapping. The proposed approach is implemented on real KOMPSAT-5 SAR satellite sea-ice images, while fractal spatial resolution profile simulations are carried out based on the inversed equalized hybrid domain image formation algorithm.

keywords: Discrete wavelet transform; fractal analysis; high-frequency multiplicative noise; raw data generation; synthetic aperture radar

1-36 *Engineering, Chemical*

Freezing-accelerated removal of chromate by biochar synthesized from waste rice husk

Han, Tae Uk., Kim, Jungwon. and **Kim, Kitae.**

Separation and Purification Technology. 2020. 250.

doi: 10.1016/j.seppur.2020.117233.

The application of biochar has been considered a promising method for remediating contaminated water, as biochar exhibits a redox activity for environmentally relevant redox reactions. Although the mechanisms of various redox reactions by biochar in water have been widely investigated, investigations of reaction in ice have not been attempted. In this study, the freezing-accelerated removal of chromate (Cr(VI)) by biochar synthesized from waste rice husks (RH-BC) was investigated in water (25 °C) and ice (-20 °C). The reduction of Cr(VI) with RH-BC was insignificant in water, whereas an enhanced reduction efficiency of Cr(VI) was observed in ice due to the

freeze concentration phenomenon. The enhanced redox reaction between Cr(VI) and dissolved organic matter (DOM) is primarily responsible for the accelerated Cr(VI) reduction in ice, wherein DOM is a primary component of RH-BC. Experiments on various conditions of pH and RH-BC concentrations reveal that Cr(VI) is heavily reduced at low pH values and an aggregation of RH-BC in ice can inhibit the reduction efficiency of Cr (VI) due to a decrease in active sites. The removal of Cr(VI) by RH-BC was successfully achieved with real Cr(VI)contaminated wastewater in ice; this elucidated the environmental relevance of freezing-assisted Cr(VI) removal in cold regions.

keywords: Ice; Freeze concentration effect; Chromate; Biochar; Dissolved organic matter

1-37 *Engineering, Environmental; Engineering, Chemical*

Freezing-enhanced non -radical oxidation of organic pollutants by peroxymonosulfate

Nhat Thi Hong Le., **Ju, Jinjung.**, **Kim, Bomi.**, Kim, Min Sik., Lee, Changha., Kim, Saewung., Choi, Wonyong., **Kim**, **Kitae.** and Kim, Jungwon.

Chemical Engineering Journal. 2020. 388.

doi: 10.1016/j.cej.2020.124226.

This study presents a freezing method for accelerating the peroxymonosulfate (PMS)-mediated degradation process. The degradation of furfuryl alcohol (FFA) in the presence of PMS was markedly accelerated by freezing. The degradation efficiency of FFA was only 10.4% in aqueous solution at 25 °C, but 100% degradation was achieved in frozen solution at –20 °C after 3 h of reaction at [FFA] = 20 μM and [PMS] = 100 μM. This accelerated PMS-mediated degradation of FFA in the frozen solution is due to the concentration of both PMS and FFA in ice grain boundaries, which increases the collision frequency between PMS and FFA thereby facilitating redox transformation. The mapping images of PMS and FFA in the frozen sample obtained using confocal Raman microscopy provide clear evidence of the accumulation of PMS and FFA in the ice grain boundaries after freezing. The experimental results with sulfate radical ($SO_4^{\cdot-}$) scavengers, no production of hydroxyl radicals ($^{\cdot}OH$) and $SO_4^{\cdot-}$, and the highly pollutant-dependent degradation efficiency suggest that the PMS-mediated degradation in frozen solution primarily proceeds through the direct electron transfer from organic pollutants to PMS (non-radical mechanism) rather than the reaction of $SO_4^{\cdot-}$ or $^{\cdot}OH$ with organic pollutants (radical mechanism). The degradation efficiency of the PMS/freezing system was similar across the pH range of 3–10. In addition, the PMS/freezing system worked efficiently in the temperature range of –10 to –35 °C. This result implies that the PMS/freezing system can be operated without external energy in cold regions.

keywords: Peroxymonosulfate; Freeze-concentration effect; Redox chemical reaction; Non-radical mechanism; Pharmaceutical pollutant

1-38 *Engineering, Environmental; Environmental Sciences*

Freezing-Induced Simultaneous Reduction of Chromate and Production of Molecular Iodine: Mechanism, Kinetics, and Practical Implications

Kim, Kitae., **Chung**, **Hyun Young.**, **Kim**, **Bomi.** and 4 others.

Environmental Science & Technology. 2020. 54(24): 16204-16211.

doi: 10.1021/acs.est.0c05322.

A new method for the concurrent treatment of Cr(VI)-contaminated wastewater and production of the useful I_2 chemical was developed. The method is based on the redox reaction between Cr(VI) and I^- that occurs when an aqueous wastewater solution containing Cr(VI) and I^- is frozen, producing I_2 and allowing for the effective removal of Cr. The redox reaction occurs primarily because of the accumulation of Cr(VI), I^-, and protons in the ice grain boundaries formed during freezing (i.e., the freeze concentration effect). This effect was verified by confocal Raman spectroscopy and the experiments varying I^- concentration and pH. The reduction of Cr(VI) (20 μM) was near complete after freezing at I^- concentrations ≥ 100 μM, pH ≤ 3.0, and temperatures ≤ –10 °C. The freezing method (liquid cooling vs air cooling) had little effect on the final Cr(VI) reduction efficiency but had a significant effect on the Cr(VI) reduction rate. The freezing method was also tested with Cr(VI)-contaminated electroplating wastewater samples, and simultaneous Cr(VI) reduction and I_2 production proceeded rapidly in a frozen solution but was not observed in an aqueous solution. Additionally,

other substances in electroplating wastewater did not reduce the rate and final efficiency of Cr(VI) reduction and I_2 production. Therefore, the freezing/Cr(VI)/I^- system can be considered a feasible approach to water-energy nexus technology for simultaneous I_2 production and Cr(VI)-contaminated wastewater treatment.

keywords: Chromate removal; Electroplating wastewater; Freezing; dual-function system; iodine production

1-39 *Geography, Physical; Geosciences, Multidisciplinary*

Getz Ice Shelf melt enhanced by freshwater discharge from beneath the West Antarctic Ice Sheet

Wei, Wei., Blankenship, Donald D., Greenbaum, Jamin S., Gourmelen, Noel., Dow, Christine F., Richter, Thomas G., Greene, Chad A., Young, Duncan A., **Lee**, **SangHoon.**, **Kim**, **Tae-Wan.**, **Lee**, **Won Sang.** and Assmann, Karen M.

Cryosphere. 2020. 14(4): 1399-1408.

doi: 10.5194/tc-14-1399-2020.

Antarctica's Getz Ice Shelf has been rapidly thinning in recent years, producing more meltwater than any other ice shelf in the world. The influx of fresh water is known to substantially influence ocean circulation and biological productivity, but relatively little is known about the factors controlling basal melt rate or how basal melt is spatially distributed beneath the ice shelf. Also unknown is the relative importance of subglacial discharge from the grounded ice sheet in contributing to the export of fresh water from the ice shelf cavity. Here we compare the observed spatial distribution of basal melt rate to a new sub-ice-shelf bathymetry map inferred from airborne gravity surveys and to locations of subglacial discharge from the grounded ice sheet. We find that melt rates are high where bathymetric troughs provide a pathway for warm Circumpolar Deep Water to enter the ice shelf cavity and that melting is enhanced where subglacial discharge fresh water flows across the grounding line. This is the first study to address the relative importance of meltwater production of the Getz Ice Shelf from both ocean and subglacial sources.

keywords: Airborne Gravity Surveys; Getz Ice Shelf

1-40 *Geochemistry & Geophysics*

Global temperature calibration of the Long chain Diol Index in marine surface sediments

de Bar, Marijke W., Weiss, Gabriella., Yildiz, Caglar., Rampen, Sebastiaan W., Lattaud, Julie., Bale, Nicole J., Mienis, Furu., Brummer, Geert-Jan A., Schulz, Hartmut., Rush, Darci., **Kim**, **Jung-Hyun.** and 6 others.

Organic Geochemistry. 2020. 142.

doi: 10.1016/j.orggeochem.2020.103983.

The Long chain Diol Index (LDI) is a relatively new organic geochemical proxy for sea surface temperature (SST), based on the abundance of the C_{30} 1,15-diols relative to the summed abundance of the C_{28} 1,13-, C_{30} 1,13- and C_{30} 1,15-diols. Here we substantially extend and re-evaluate the initial core top calibration by combining the original dataset with 172 data points derived from previously published studies and 262 newly generated data points. In total, we considered 595 globally distributed surface sediments with an enhanced geographical coverage compared to the original calibration. The relationship with SST is similar to that of the original calibration but with considerably increased scatter. The effects of freshwater input (e.g., river runoff) and long-chain diol contribution from Proboscia diatoms on the LDI were evaluated. Exclusion of core-tops deposited at a salinity < 32 ppt, as well as core-tops with high *Proboscia*-derived C_{28} 1,12-diol abundance, resulted in a substantial improvement of the relationship between LDI and annual mean SST. This implies that the LDI cannot be directly applied in regions with a strong freshwater influence or high C_{28} 1,12-diol abundance, limiting the applicability of the LDI. The final LDI calibration (LDI = 0.0325 x SST + 0.1082; R^2 = 0.88; n = 514) is not statistically different from the original calibration of Rampen et al. (2012) (http://doi.org/10.1016/j.gca.2012.01.024), although with a larger calibration error of 3 °C. This larger calibration error results from several regions where the LDI does not seem to have a strong temperature dependence with annual mean SST, posing a limitation on the application of the LDI.

keywords: LDI core-top calibration; Long-chain diols; SST; Freshwater; *Proboscia* diatoms

1-41 *Geosciences, Multidisciplinary*

Impact of Antarctic Meltwater Forcing on East Asian Climate Under Greenhouse Warming

Oh, Ji-Hoon., Park, Wonsun., Lim, Hyung-Gyu., Noh, Kyung Min., **Jin**, **Emilia Kyung.** and Kug, Jong-Seong.

Geophysical Research Letters. 2020. 47(21).

doi: 10.1029/2020gl089951.

In recent decades, Antarctic ice sheet/shelf melting has been accelerated, releasing freshwater into the Southern Ocean. It has been suggested that the meltwater flux could lead to cooling in the Southern Hemisphere, which would retard global warming and further induce a northward shift of the Intertropical Convergence Zone (ITCZ). In this study, we use experimental ensemble climate simulations to show that Antarctic meltwater forcing has distinct regional climate impacts over the globe, leading in particular to regional warming in East Asia, which offsets the global cooling effect by the meltwater forcing. It is suggested that Antarctic meltwater forcing leads to a negative precipitation anomaly in the Western North Pacific (WNP) via cooling in the tropics and the northward shift of the ITCZ. This suppressed convection in WNP induces an anticyclonic flow over the North Pacific, which leads to regional warming in East Asia. This hypothesis is supported by analyses of interensemble spread and long-term control simulations.

keywords: Antarctic Meltwater; Southern Ocean; East Asia

1-42 *Environmental Sciences; Meteorology & Atmospheric Sciences*

Impact of poleward heat and moisture transports on Arctic clouds and climate simulation

Baek, Eun-Hyuk., **Kim**, **Joo-Hong.** and 3 others.

Atmospheric Chemistry and Physics. 2020. 20(5): 2953-2966.

doi: 10.5194/acp-20-2953-2020.

Many general circulation models (GCMs) have difficulty simulating Arctic clouds and climate, causing substantial inter-model spread. To address this issue, two Atmospheric Model Intercomparison Project (AMIP) simulations from the Community Atmosphere Model version 5 (CAM5) and Seoul National University (SNU) Atmosphere Model version 0 (SAM0) with a unified convection scheme (UNICON) are employed to identify an effective mechanism for improving Arctic cloud and climate simulations. Over the Arctic, SAM0 produced a larger cloud fraction and cloud liquid mass than CAM5, reducing the negative Arctic cloud biases in CAM5. The analysis of cloud water condensation rates indicates that this improvement is associated with an enhanced net condensation rate of water vapor into the liquid condensate of Arctic low-level clouds, which in turn is driven by enhanced poleward transports of heat and moisture by the mean meridional circulation and transient eddies. The reduced Arctic cloud biases lead to improved simulations of surface radiation fluxes and near-surface air temperature over the Arctic throughout the year. The association between the enhanced poleward transports of heat and moisture and increase in liquid clouds over the Arctic is also evident not only in both models, but also in the multi-model analysis. Our study demonstrates that enhanced poleward heat and moisture transport in a model can improve simulations of Arctic clouds and climate.

keywords: Arctic climate; Arctic clouds; general circulation model; poleward transport

1-43 *Chemistry, Analytical*

An improved ion chromatography system coupled with a melter for high-resolution ionic species reconstruction in Antarctic firn cores

Ro, Seokhyun., **Hur**, **Soon Do.**, Hong, Sungmin., **Chang**, **Chaewon.**, **Moon**, **Jangil.**, **Han**, **Yeongcheol.**, **Jun**, **Seong Joon.**, **Hwang**, **Heejin.** and **Hong**, **Sang-bum.**

Microchemical Journal. 2020. 159.

doi: 10.1016/j.microc.2020.105377.

We improved an on-line multi-ion chromatography (IC) system combined with a custom firn core melter (ICmelter). Five anions (F^-, $CH_3SO_3^-$, Cl^-, NO_3^-, SO_4^{2-}) and five cations (Na^+, NH_4^+, K^+, Mg^{2+}, Ca^{2+}) are simultaneously determined every 1.3 min; high-resolution ion data, with a depth interval of approximately 1.8 cm, can thus be obtained from Antarctic firn cores using the IC-melter. The IC-melter

provides a processing speed of 1.1-1.7 h per ~0.7-0.8 m firn core. The depth resolution was designed to capture seasonal variations of ions based on the accumulation rate of Styx Glacier (Northern Victoria Land, Antarctica), where a firn core used herein was obtained, and variations of the firn core density. The analytical conditions (eluent concentration and flow rate, run time, peak separation, and sensitivity) of the multi-IC system were optimized to achieve the research goals. Cations and anions were separated through 4-min isocratic elution (CH_3SO_3H eluent) and 5-min isocratic elution (KOH eluent), respectively. The isocratic elution method for anion analysis was selected, rather than the gradient elution method, due to the exceptionally low ionic strength of the meltwater and easy operation of the multi-IC system. All ionic species showed calibration curves with determinant coefficients >0.997, standard errors of estimated values <0.015, and relative standard deviation values <4.17% for anions and <2.42% for cations at levels of 5–25 μg L^{-1}. The method detection limits (MDLs) for assessed ions were comparable to detection limits (DLs) previously reported for on-line IC-melter systems, except the limit of SO_4^{2-} (~3.0 μg L^{-1}). In particular, the MDLs of fluoride ion (F^-) and methanesulfonate ion ($CH_3SO_3^-$) were 0.03 and 0.3 μg L^{-1}, respectively; these species were successfully measured in an Antarctic firn core for the first time, using the improved on-line IC-melter. The relative errors for ions other than Na^+ and Cl^- were generally < 13.3% at a level of approximately 50 μg L^{-1}. The expanded measurement uncertainties (k = 2 at the 95% confidence level) were ~0.13 μg L^{-1} and ~1.59 μg L^{-1} at levels of ~1.0 μg L^{-1} for F– and ~5.0 μg L^{-1} for $CH_3SO_3^-$, respectively. The measured ions from parallel two firn core stick samples showed reproducibility values <29.3%. Pearson's r values between ions obtained from the IC-melter and conventional method were > 0.67. In this study, as an application of the IC-melter, high-resolution ion species data from the firn core (depth interval: ~20.11–22.85 m) are shortly presented.

keywords: On-line multi-ion chromatography system; Firn core melter; Fluoride ion; Methanesulfonate ion; Styx Glacier; Antarctica

1-44 *Meteorology & Atmospheric Sciences*

Inertia-Gravity Waves Revealed in Radiosonde Data at Jang Bogo Station, Antarctica (74°37′S, 164°13′E): 2. Potential Sources and Their Relation to Inertia-Gravity Waves

Yoo, J-H., **Song**, **In-Sun.**, Chun, H-Y. and **Song**, **Byeong-Gwon.**

Journal of Geophysical Research-Atmospheres. 2020. 125(7).

doi: 10.1029/2019jd032260.

Potential sources of inertia-gravity waves (IGWs) in the lower stratosphere (z = 15-22 km) at Jang Bogo Station, Antarctica (74°37′S, 164°13′E) are investigated using 3-year (December 2014 to November 2017) radiosonde data, including the 25-month result (December 2014 to December 2016) analyzed in Yoo et al. (2018, https://doi.org/10.1029/2018JD029164, Part 1). For this investigation, three-dimensional backward ray tracing calculations are conducted using the Gravity wave Regional Or Global RAy Tracer. Among 248 IGWs, 112, 68, and 68 waves are generated in the troposphere (z < 8 km), tropopause (z = 8-15 km), and lower stratosphere (z = 15-18.5 km), respectively. These waves mainly propagate from the northwestern and southwestern regions of Jang Bogo Station dominated by the prevailing westerlies between the upper troposphere and lower stratosphere. Potential sources of IGWs are categorized into orography, fronts, convection, and the flow imbalance including the upper-tropospheric jet stream. In the troposphere, relatively large numbers of waves are associated with fronts (37) and orography (35) compared with convection (28). In the tropopause (stratosphere), 36 (42) waves, including 11 cases associated with the upper-tropospheric jet stream, are excited by the flow imbalance. Waves related to the flow imbalance are characterized by low intrinsic frequency (1-2f), short vertical wavelength (1-2 km), and longer horizontal wavelength (50-1000 km), whereas the waves induced by the tropospheric sources have wider ranges of intrinsic frequency (1-20f) and vertical wavelengths (1-15 km) with relatively shorter horizontal wavelengths (less than 500 km).

keywords: inertia-gravity waves; potential sources; ray tracing

1-45 *Multidisciplinary Sciences*

Input of terrestrial organic matter linked to deglaciation increased mercury transport to the Svalbard fjords

Kim, Haryun., Kwon, Sae Yun., Lee, Kitack., Lim, Dhongil., Han, Seunghee., Kim, Tae-Wook., **Joo**, **Young Ji.**, Lim, Jaesoo., Kang, Moo-Hee. and **Nam**, **Seung-Il.**

Scientific Reports. 2020. 10(1).

doi: 10.1038/s41598-020-60261-6.

Deglaciation has accelerated the transport of minerals as well as modern and ancient organic matter from land to fjord sediments in Spitsbergen, Svalbard, in the European Arctic Ocean. Consequently, such sediments may contain significant levels of total mercury (THg) bound to terrestrial organic matter. The present study compared THg contents in surface sediments from three fjord settings in Spitsbergen: Hornsund in the southern Spitsbergen, which has high annual volume of loss glacier and receives sediment from multiple tidewater glaciers, Dicksonfjorden in the central Spitsbergen, which receives sediment from glacifluvial rivers, and Wijdefjorden in the northern Spitsbergen, which receive sediments from a mixture of tidewater glaciers and glacifluvial rivers. Our results showed that the THg (52 ± 15 ng g^{-1}) bound to organic matter (OM) was the highest in the Hornsund surface sediments, where the glacier loss (0.44 km^3 yr^{-1}) and organic carbon accumulation rates (9.3 ~ 49.4 g m^{-2} yr^{-1}) were elevated compared to other fjords. Furthermore, the delta $\delta^{13}C$ (–27 ~ –24‰) and $\delta^{34}S$ values (–10 ~ 15‰) of OM indicated that most of OM were originated from terrestrial sources. Thus, the temperature-driven glacial melting could release more OM originating from the meltwater or terrestrial materials, which are available for THg binding in the European Arctic fjord ecosystems.

keywords: Glaciers; Marine sediments; Organic matter; Svalbard Fjords; Total mercury

1-46

In-situ measurement of the Arctic ocean for optical property analysis during 2019 cruise

Lee, **Sungjae.** and **Kim**, **Hyun-Cheol.**

Geo Data. 2020. 2(2): 63-70.

doi: 10.22761/DJ2020.2.2.009.

The Arctic issue has increased due to global warming. The Arctic is losing the role of cooling because reducing sea ice by warming on the Arctic, which is changing the energy balance on the Earth system. Change of Arctic ocean, atmosphere, and cryosphere influence on an ecosystem of Arctic as well. These changes are monitoring by remote sensing due to the Arctic is difficult for human access, and where is a wide area. However, a low solar altitude on the Arctic limits Ocean Color Algorithms applies to the Arctic because most ocean color algorithms are based on empirical data in the mid-latitude. Continuous data sampling on the Arctic ocean is the best way to improve and develop a suitable ocean color algorithm for the Arctic. This paper aims to report ocean observation data acquired by Ice-Breaker research vessel Araon during the summer Arctic expedition of 2019. Acquired samples are chlorophyll-a, suspended sediment concentration, in-situ measured ocean optical properties. Sampled data showed that there is a significant effect of dissolved organic matter in its inherent optical properties. We use these data for the aims of improving and develop ocean color algorithms in the Arctic.

keywords: Arctic sea; IBRV ARAON; Ocean Color Remote Sensing; Inherent optical property; Apparent optical property

1-47 *Multidisciplinary Sciences*

The internal origin of the west-east asymmetry of Antarctic climate change

Jun, **Sang-Yoon.**, **Kim**, **Joo-Hong.**, Choi, Jung., **Kim**, **Seong-Joong.** and 2 others.

Science Advances. 2020. 6(24).

doi: 10.1126/sciadv.aaz1490.

Recent Antarctic surface climate change has been characterized by greater warming trends in West Antarctica than in East Antarctica. Although this asymmetric feature is well recognized, its origin remains poorly understood. Here, by analyzing observation data and multimodel results, we show that a west-east asymmetric internal mode amplified in austral winter originates from the harmony of the atmosphere-ocean coupled feedback off West Antarctica and the Antarctic terrain. The warmer ocean temperature over the West Antarctic sector has positive feedback, with an anomalous upper-tropospheric anticyclonic circulation response centered over West Antarctica, in which the strength of the feedback is

controlled by the Antarctic topographic layout and the annual cycle. The current west-east asymmetry of Antarctic surface climate change is undoubtedly of natural origin because no external factors (e.g., orbital or anthropogenic factors) contribute to the asymmetric mode.

keywords: Antarctic climate change; west-east Antarctic asymmetry

1-48

Iron in the NEEM ice core relative to Asian loess records over the last glacial–interglacial cycle

Xiao, Cunde., Du, Zhiheng., Handley, Mike., Mayewski, Paul., Cao, Junji., Schupbach, Simon., Zhang, Tong., Petit, Jean-Robert., Li, Chuanjin., **Han**, **Yeongcheol.** and 2 others.

National Science Review. 2020. nwaa144.

doi: 10.1093/nsr/nwaa144.

Mineral dust can indirectly affect the climate by supplying bioavailable iron (Fe) to the ocean. Here, we present the records of dissolved Fe (DFe) and total Fe (TDFe) in North Greenland Eemian Ice Drilling (NEEM) ice core over the past 110 kyr BP. The Fe records are significantly negatively correlated with the carbon-dioxide (CO_2) concentrations during cold periods. The results suggest that the changes in Fe fluxes over the past 110 kyr BP in the NEEM ice core are consistent with those in Chinese loess records because the mineral-dust distribution is controlled by the East Asian deserts. Furthermore, the variations in the dust input on a global scale are most likely driven by changes in solar radiation during the last glacial–interglacial cycle in response to Earth's orbital cycles. In the last glacial–interglacial cycle, the DFe/TDFe ratios were higher during the warm periods (following the post-Industrial Revolution and during the Holocene and last interglacial period) than during the main cold period (i.e. the last glacial maximum (LGM)), indicating that the aeolian input of iron and the iron fertilization effect on the oceans have a non-linear relationship during different periods. Although the burning of biomass aerosols has released large amounts of DFe since the Industrial Revolution, no significant responses are observed in the DFe and TDFe variations during this period, indicating that severe anthropogenic contamination has no significant effect on the DFe (TDFe) release in the NEEM ice core.

keywords: Greenland NEEM ice core; iron fertilization; carbon dioxide; Chinese loess; glacial–interglacial cycle

1-49 *Engineering, Environmental; Engineering, Civil; Geosciences, Multidisciplinary*

Isotopic characteristics of snow and its meltwater over the Barton Peninsula, Antarctica

Lee, Jeonghoon., **Hur, Soon Do.** and 2 others.

Cold Regions Science and Technology. 2020. 173.

doi: 10.1016/j.coldregions.2020.102997.

The stable isotopic compositions of snow and meltwater are a very useful tool to investigate water provenances and to increase the accuracy of paleoclimate studies in glacial watershed systems. To better understand the factors that affect the isotopic compositions of snow and meltwater in the western Antarctic Peninsula, the isotopic compositions of snow/ice and meltwater from the Barton Peninsula in Antarctica were examined. The isotopic compositions of snow are more enriched than those of meltwater and the variability of the isotopic compositions decreases from snow to meltwater. The melting process changes the linear slope between two water isotopes, which is different from the meteoric water line. We observe that the isotopic compositions of snow are altered by tephra, which results in isotopically enriched snow that is covered by tephra. This tephra decreases the snow's albedo, and the increased energy that is absorbed by the snow surface increases the melting rate, which causes isotopic exchange between liquid water and ice. Hydrological processes, such as daily variations in the melting rate and contributions from groundwater/runoff to seawater, also affect the isotopic compositions of water over the Barton Peninsula. Our works imply that uncertainty caused by these variations should be considered when applying stable water isotopes in this area for water flowpath and paleoclimate study.

keywords: Barton Peninsula, Antarctica; snow; water isotopes; snow meltwater

1-50 *Geography, Physical; Geosciences, Multidisciplinary*

Late pleistocene paleoceanographic changes in the Ross Sea - Glacial-interglacial variations in paleoproductivity, nutrient utilization, and deep-water formation

Kim, Sunghan., **Lee, Jae Il.**, McKay, Robert M., **Yoo, Kyu-Cheul.**, Bak, Young-Suk., **Lee**, **Min Kyung.**, **Roh**, **Youn Ho.**, **Yoon**, **Ho Il.**, **Moon**, **Heung Soo.** and **Hyun**, **Chang-Uk.**

Quaternary Science Reviews. 2020. 239.

doi: 10.1016/j.quascirev.2020.106356.

The outer Ross Sea continental shelf has experienced large variations in ice sheet extent over the Pleistocene that are theorized to be largely driven by changes in the westward-flowing Antarctic Slope Current (ASC) at the continental shelf break. This current regulates southward incursions of warm modified Circumpolar Water, and it is thought to have triggered past marine ice sheet retreat. Additionally, expansions of grounded ice sheets on the continental shelf have fundamentally altered the Ross Sea water mass formation processes, influencing surface water salinity, sea ice cover, nutrient utilization, deep-water ventilation, and primary productivity. Here, we report the geochemical, physical properties, grain size, bulk $\delta^{15}N$, and diatom records during the late Pleistocene from two sediment cores from the Iselin Bank on the outermost continental shelf in the Ross Sea. These core sites were not overridden by grounded ice sheets during the late Pleistocene glacial-interglacial cycles, allowing for a continuous archive of glacimarine environments that were influenced by the ASC. Interglacial periods are typically characterized by high surface water productivity and nutrient utilization, with Chaetoceros resting spores indicating nutrient limitation under open ocean conditions, and glacial periods are typically characterized by low surface water productivity and nutrient utilization, with sea ice diatoms and planktonic foraminifers indicating light limitation under extensive sea ice/ice margin proximal conditions. A grain size analysis indicates coarse-skewed distributions and winnowing in the Iselin Bank region during cold periods. The winnowing may be related to enhanced ASC flow instead of density driven shelf water outflow.

keywords: Ross sea; Antarctic slope current; Pleistocene; Paleoproductivity; Nutrient utilization; Carbonate; Deep-water formation

1-51 *Geography, Physical; Geosciences, Multidisciplinary*

Late Quaternary depositional and glacial history of the Arliss Plateau off the East Siberian margin in the western Arctic Ocean

Joe, **Young Jin.**, Polyak, Leonid., Schreck, Michael., Niessen, Frank., Yoon, Seok Hoon., Kong, Gee Soo. and **Nam**, **Seung-Il.**

Quaternary Science Reviews. 2020. 228.

doi: 10.1016/j.quascirev.2019.106099.

Sedimentary stratigraphy and facies analysis along with seismostratigraphic and multibeam bathymetry data are used to reconstruct the last glacial impact on the Arliss Plateau (AP) and attendant sedimentation in the adjacent Chukchi Basin (CB) in the western Arctic Ocean off the East Siberian margin. Sediment core ARA02B/16B-GC from the AP lower slope captures glacier-related depositional history during the last estimated ca. 100 ka (Marine Isotope Stage, MIS 1 to 5c) based on regional lithostrati-graphic correlation. The sedimentary record shows distinguishable interglacial (interstadial) and glacial (stadial) patterns. The identified sedimentary fades reflect several modes of glaciogenic deposition by drifting icebergs, suspension settling from turbid meltwater plumes and/or detached underfiows, and turbidity currents. Based on strong seismic reflectors related to lithological boundaries, a downslope subbottom profile from AP to CB is divided into seismostratigraphic units (SSU) 1 and 2 corresponding in the core record to MIS 1-3 and MIS 3-5c, respectively. An acoustically transparent lens within SSU 2 correlates on the upper slope to debris lobes downslope from the AP top covered by megascale glacial lineations. This geomorphic/sedimentary pattern indicates a glacial erosional impact on the AP and proglacial deposition of eroded sediments on the slope and in the basin. Based on the developed sediment stratigraphy and facies analysis, the last debris lobe horizon was deposited in glacial/deglacial environments during late MIS 4 to early MIS 3. The absence of similar glaciogenic debris lobes within SSU 1 indicates no direct glacial impact on the AP during the Last Glacial Maximum (LGM). These results suggest that the last glacial erosion of the AP occurred during or immediately after MIS 4, possibly related to major glaciation in northern Siberia at ~50-70 ka.

keywords: Arctic Ocean sediments; Late Quaternary; Glacial history; Sediment facies; Seismostratigraphy

1-52 *Ecology; Geosciences, Multidisciplinary*

The linkages between Antarctic sea ice extent and Indian summer monsoon rainfall

Azhar, Siti Syairah Atiqah., Chenoli, Sheeba Nettukandy., Abu Samah, Azizan. and **Kim**, **Seong-Joong.**

Polar Science. 2020. 25.

doi: 10.1016/j.polar.2020.100537.

Teleconnection between the Antarctic sea ice and the tropical climate has been extensively investigated. This study examines the interannual relationship between the variability of sea ice extent in the Indian Ocean sector (20–90°E) and Indian summer monsoon rainfall under the influence of the Mascarene High. Sea ice extent during April-May-June (AMJ) appears to have a significant correlation with the summer monsoon rainfall over Peninsular India region during June-July-August-September from 1979 to 2013. Composites of mean sea level pressure (MSLP), 500 hPa geopotential height, and 850 hPa wind anomalies during high and low ice phases show a positive relation between the sea ice extent and the Mascarene High, revealing that high (low) ice phase corresponds respectively to the strengthening (weakening) of the Mascarene High as well as an increase (decrease) in Indian summer monsoon rainfall. During the respective high (low) ice phase years, positive (negative) MSLP anomalies were found, particularly over the Mascarene High region, associated with the eastwards (westwards) shifts of its climatology locations. Similar features were observed at 500 hPa geopotential height anomalies. In addition, strong anticyclonic (cyclonic) anomalies in the Mascarene High region were found in 850 hPa winds, which led to corresponding strong (weak) south westerlies and thus respective positive (negative) Indian summer monsoon rainfall anomalies.

keywords: Sea ice extent in the Indian ocean sector; Teleconnection; High and low ice phase; Mascarene high; Indian summer monsoon rainfall

1-53 *Astronomy & Astrophysics*

Long-Lasting Ground-Satellite High Coherence of Compressional Dayside Pc3-Pc4 Pulsations

Kim, Gi-Jeong., Kim, Khan-Hyuk., **Kwon**, **Hyuck-Jin.** and 3 others.

Journal of Geophysical Research-Space Physics. 2020. 125(8).

doi: 10.1029/2020ja028074.

We present observations of broadband (~ 10-50 mHz) Pc3-Pc4 waves on 4 January 2014. The waves were detected on the dayside simultaneously in a compressional component (δB_z) at the Radiation Belt Storm Probes A (RBSP-A) in the inner magnetosphere and in the north-south component (δH) on the ground at a low-latitude Bohyun (BOH) station (L = 1.3) during an interval of small interplanetary magnetic field cone angle, suggesting that upstream ultralow frequency (ULF) waves were the source of the magnetospheric Pc3-Pc4 waves. We observed the ground-satellite high coherence between RBSP-A δB_z and BOH δH for a prolonged time interval lasting 6.5hr, which has not been reported previously, during which RBSP-A was on the inbound and outbound legs moving from L = ~3.3 to ~6.3. In order to understand the spatial mode structure of the compressional waves, we examined the ground-satellite cross phase for the high-coherence interval and found that the waves observed in and out of the plasmasphere propagated earthward at the average fast-mode speed of ~700-1,000km/s. We also observed cross-phase values smoothly changing with the radial distance of the spacecraft across the plasmapause. This indicates that the presence of the plasmapause has little effect on our fast-mode waves propagating into the inner magnetosphere and to the ground low-latitude station.

keywords: Ground-satellite coherence; Long-lasting Pc3-Pc4 pulsations; Propagation of broadband waves

1-54 *Chemistry, Multidisciplinary; Engineering, Multidisciplinary; Materials Science, Multidisciplinary; Physics, Applied*

Mass Extinction Efficiency Approximation for Polydispersed Aerosol Using Harmonic Mean-Type Approximation

Um, Junshik., Jang, Seonghyeon., **Yoon**, **Young Jun.** and 7 others.

Applied Sciences-Basel. 2020. 10(23).

doi: 10.3390/app10238637.

Among many parameters characterizing atmospheric aerosols, aerosol mass extinction efficiency (MEE) is important for understanding the optical properties of aerosols. MEE is expressed as a function of the refractive indices (i.e., composition) and size distributions of aerosol particles. Aerosol MEE is often considered as a size-independent constant that depends only on the chemical composition of aerosol particles. The famous Malm's reconstruction equation and subsequent revised methods express the extinction coefficient as a function of aerosol mass concentration and MEE. However, the used constant MEE does not take into account the effect of the size distribution of polydispersed chemical composition. Thus, a simplified expression of size-dependent MEE is required for accurate and conventional calculations of the aerosol extinction coefficient and also other optical properties. In this study, a simple parameterization of MEE of polydispersed aerosol particles was developed. The geometric volume-mean diameters of up to 10 μm with lognormal size distributions and varying geometric standard deviations were used to represent the sizes of various aerosol particles (i.e., ammonium sulfate and nitrate, elemental carbon, and sea salt). Integrating representations of separate small mode and large mode particles using a harmonic mean-type approximation generated the flexible and convenient parameterizations of MEE that can be readily used to process in situ observations and adopted in large-scale numerical models. The calculated MEE and the simple forcing efficiency using the method developed in this study showed high correlations with those calculated using the Mie theory without losing accuracy.

keywords: mass extinction efficiency; extinction coefficient; polydispersed aerosol; reconstruction method; Mie scattering; harmonic mean type approximation

1-55 *Environmental Sciences; Meteorology & Atmospheric Sciences*

Molecular Distributions and Compound-Specific Stable Carbon Isotopic Compositions of Plant Wax *n*-Alkanes in Marine Aerosols along a North-South Transect in the Arctic-Northwest Pacific Region

Kim, Jung-Hyun., **Park**, **Jiyeon.**, Kim, Sol-Bin., Shin, Kyung-Hoon., **Kim**, **Sookwan.** and **Gim**, **Yeontae.**

Atmosphere. 2020. 11(5).

doi: 10.3390/atmos11050499.

A geographical source of *n*-alkanes in marine aerosols was assessed along a North-South transect in the Arctic-Northwest Pacific region. Marine aerosol samples were collected during the ARA08 cruise with the R/V Araon between 28 August and 28 September 2017. We investigated molecular distributions of *n*-alkanes (homologous series of C_{16} to C_{34}) and compound-specific stable carbon isotopes ($\delta^{13}C$) of *n*-C_{27}, *n*-C_{29}, and *n*-C_{31}. Unresolved complex mixtures (UCM) showed a latitudinal trend from the Arctic Ocean to the northwest Pacific Ocean, highlighting an increasing influence of the plume of polluted air exported from East Asian countries. The anthropogenic input was further evidenced by high U/R ratios (>5) and low CPI_{17-23}(0.6-1.4). The occurrence of high molecular weight (HMW) *n*-alkanes with high CPI_{27-31}(>3) indicated the biogenic input of terrestrial higher plant leaf waxes in all studied samples. The $\delta^{13}C$ of HMW *n*-alkanes was influenced by both the relative contributions from the C_3/C_4 plant sources and from fossil fuel combustions. The back-trajectory analyses provided evidence that changes in molecular distributions and $\delta^{13}C$ of *n*-alkanes were due to the long-range atmospheric transport of anthropogenic and biogenic organic materials from North American and East Asian countries to the Arctic Ocean and the remote northwest Pacific Ocean, respectively.

keywords: marine aerosol; *n*-alkanes; compound-specific carbon isotopes; Arctic Ocean; northwest Pacific Ocean

1-56 *Geography, Physical; Geosciences, Multidisciplinary; Paleontology*

Monsoon-influenced variation of clay mineral compositions and detrital Nd-Sr isotopes in the western Andaman Sea (IODP Site U1447) since the late Miocene

Lee, Jongmin., **Kim**, **Sunghan.**, **Lee**, **Jae Il.** and 3 others.

Palaeogeography Palaeoclimatology Palaeoecology. 2020. 538.

doi: 10.1016/j.palaeo.2019.109339.

Nd-Sr isotopes (ε_{Nd}, $^{87}Sr/^{86}Sr$) of detrital particles, clay mineral compositions, and $\delta^{13}C$ of sediment

organic matter ($\delta^{13}C_{SOM}$) at the International Ocean Discovery Program (IODP) Expedition 353 Site U1447 in the western Andaman Sea were measured to reveal the sediment provenance changes and/or weathering intensity variations in association with the Indian monsoon intensity change. The shipboard age model based on biostratigraphic data and paleomagnetic reversals shows that IODP Site U1447 preserves late Miocene (~10 Ma) sediments. Nd/Sr isotope systematics demonstrates that the sediments originated mainly from the Myanmar region, including the Irrawaddy River, Salween River, Sittang River and Indo-Burman-Arakan Ranges without a significant change of sediment provenance since the late Miocene. Thus, temporal variations of clay mineral compositions, represented as smectite/(illite + chlorite) [S/(I + C)], indicate the long-term variations of physical/chemical weathering intensity attributable to intensity changes of Indian winter/summer monsoon. A gradual decreasing trend of S/(I + C) ratios indicates stronger physical and/or weaker chemical weathering since the late Miocene, as a result of strengthening of Indian winter monsoon (and/or weakening of Indian summer monsoon), which seems be closely related to global cooling since the late Miocene. Distinct decrease of S/(I + C) ratios occurred at ~9.2-8.5 Ma, ~3.6 Ma, ~2.4 Ma, and ~1.2 Ma, which may be attributed to the combined effect of both global cooling and Tibetan Plateau Uplift as a local response. In addition, $\delta^{13}C_{SOM}$ values at IODP Site U1447 were higher at ~3.5 Ma and after 1.5 Ma when S/(I + C) ratio was minima, which may imply an increase of C_4 plant in Myanmar region as a result the strong Indian winter monsoon (or weak Indian summer monsoon).

keywords: Provenance; Weathering intensity; Indian monsoon; Paleodimate

1-57 *Geochemistry & Geophysics*

Neodymium isotope constraints on chemical weathering and past glacial activity in Svalbard

Jang, Kwangchul., Bayon, Germain., **Han**, **Yeong cheol.**, **Joo**, **Young Ji.**, Kim, Ji-Hoon., Ryu, Jong-Sik., Woo, Jusun., Forwick, Matthias., Szczucinski, Witold., **Kim**, **Jung-Hyun.** and **Nam**, **Seung-Il.**

Earth and Planetary Science Letters. 2020. 542.

doi: 10.1016/j.epsl.2020.116319.

Neodymium (Nd) isotopes in leached authigenic components of marine sediments have been increasingly used as a tracer of past ocean-water masses. Despite the general assumption that the Nd isotopic composition of solutes released during chemical weathering fingerprints the source rocks on continents, preferential dissolution of easily dissolvable phases may result in significant deviations in Nd isotopic composition between the solutes and the source rocks, with potential implications for the utility of Nd isotopes in paleoenvironmental studies. Here, we present the Nd isotopic compositions of leached and detrital fractions separated from bedrock and marine sediment samples from the Svalbard archipelago. Our goal is to further understand the behaviour of Nd isotopes during chemical weathering in glacial catchments and evaluate how glacier fluctuations and associated weathering congruency may have affected the export of dissolved Nd isotope signatures to seawater. Our results confirm that terrestrial weathering on Svalbard causes considerable Nd isotopic decoupling between the leached and detrital fractions of fjord sediments ($\Delta\varepsilon_{Nd}$), resulting from the preferential dissolution of marine precipitates in glaciated catchments dominated by sedimentary rocks. We also show that the degree of Nd isotopic decoupling has fluctuated in response to climate variability on Svalbard during the Holocene, which is also as suggested by the occurrence of generally higher $\Delta\varepsilon_{Nd}$ values during periods of glacier advances in sediment cores retrieved from two different fjords (Dicksonfjorden and Woodfjorden). We posit that the high $\Delta\varepsilon_{Nd}$ values can be ascribed to incongruent chemical weathering of fresh rock flour produced by glacial abrasion. This finding suggests that the degree of Nd isotopic decoupling could be used as a new proxy for tracing glacial fluctuations and associated glacier-derived nutrient inputs to the marine realm.

keywords: neodymium isotopes; isotopic decoupling; incongruent weathering; glacier fluctuation; Svalbard

1-58 *Environmental Sciences*

Ny-Ålesund-oriented organic pollutants in sewage effluent and receiving seawater in the Arctic region of Kongsfjorden

Choi, Younghun., **Kim**, **Kitae.** and 3 others.

Environmental Pollution. 2020. 258.

doi: 10.1016/j.envpol.2019.113792.

Ny-Ålesund, one of four permanent settlements on Spitsbergen in Svalbard, is a research town that includes scientific institutes from many countries. Because of daily-used chemicals (e.g., pharmaceutical and personal care products (PPCPs)) used by residents in the area, generated sewage is considered as a point source in the Kongsfjorden. The aim of the present study was to identify and quantify organic pollutants in the effluent and along the shoreline and offshore via target, suspect, and non-target screening using liquid chromatography high-resolution mass spectrometry. We tentatively identified 30 compounds using the suspect and non-target screening methods in effluent samples from our first visit to the settlement in 2016. Among these, 3 were false positive, 24 were confirmed, and the 3 remaining compounds were not confirmed because of a lack of reference standards. Of the confirmed, 21 were quantifiable and considered target compounds for the 2nd year study. The quantified compounds in the effluent samples in 2017 totaled 17, including PPCP5, pesticides, perfluorinated compounds, and their metabolites. Some of the compounds, such as caffeine, paraxanthine/theophylline, acetaminophen, cetirizine, diethyl toluamide (DEET), and icaridin, were also detected in the receiving seawater. The concentration range was from 4 to 280,000 ng/L in the effluent and 2-98 ng/L in the seawater. Other 24 compounds were tentatively identified in the second-year effluent samples. Five were further confirmed using reference standards. Prioritization was performed on the 47 substances screened in Ny-Ålesund using the exposure and toxicity index. As the result, the top seven substances of concern present were perfluorooctanesulfonic acid (PFOS), triphenyl phosphate (TPHP), irbesartan, DEET, acetaminophen, caffeine, and paraxanthine/theophylline. As the effluent was identified as a source of the concerned organic pollutants, an emission reduction strategy should take place for protection of Arctic Fjorden environment.

keywords: Arctic; Ny-Ålesund; LC-HRMS; Nontarget screening; Effluent

1-59 *Environmental Sciences; Remote Sensing; Imaging Science & Photographic Technology*

Object-based landfast sea ice detection over West Antarctica using time series ALOS PALSAR data

Kim, Miae., **Kim, Hyun-Cheol.** and 3 others.

Remote Sensing of Environment. 2020. 242.

doi: 10.1016/j.rse.2020.111782.

Landfast sea ice (fast ice) is an important feature prevalent around the Antarctic coast, which is affected by climate change and energy exchanges with the atmosphere and ocean. This study proposed a method for detection of the West Antarctic fast ice using the Advanced Land Observing Satellite Phased Array L-band SAR (ALOS PALSAR) images. The algorithm has combined image segmentation, image correlation analysis, and machine learning techniques (i.e., random forest (RF), extremely randomized trees (ERT), and logistic regression (LR)). We used SAR images with a baseline of 5 days that are not in the same orbit but overlap each other as overlaps between swaths in adjacent orbits are often available in the polar regions. The underlying assumption for the proposed fast ice detection algorithm is that fast ice regions in SAR images with a time interval of 5 days are highly correlated. The object-based approach proposed in this study was well suited to high-resolution SAR images in deriving spatially homogeneous fast ice regions. The image segmentation results using the optimized parameters showed a distinct difference in the backscatter temporal evolution between fast ice and pack ice regions. Correlation and STD of backscattering coefficients were found to be the most significant variables for the object-based fast ice detection from two temporally separated images. In overall, the quantitative and qualitative evaluation demonstrated that the algorithm was an effective approach to detect fast ice with high accuracies. The models well detected various fast ice regions in the West Antarctica but misclassified some objects. The misclassifications occurred toward the edge of fast ice regions with relatively rapid changes in backscattering between both data acquisitions. On the other hand, few fast ice objects were misclassified as uniform backscattering over time occurred by chance on very small objects far from the coast. Very old multi-year fast ice regions with high backscattered signals were also a source for some misclassifications. This may be due to the sensitivity of L-band to snow structure to some extent and a thinner ice over the region with either ice growth (no deformation) or closing (slight deformation) between both images. Heavy snow load on the ice could be another error source for some misclassification as well. The approach allowed for the reliable detection of fast ice regions by using L-band SAR images with a small

local incidence angle difference.

keywords: Landfast sea ice; L-band SAR; ALOS PALSAR; Object correlation analysis; Machine learning

1-60

Observations of the Polar Ionosphere by the Vertical Incidence Pulsed Ionospheric Radar at Jang Bogo Station, Antarctica

Ham, Young-Bae., **Jee, Geonhwa.**, **Lee, Changsup.**, **Kwon, Hyuck-Jin.**, **Kim, Jeong-Han.** and 2 others.

Journal of Astronomy and Space Sciences. 2020. 37(2): 143-156.

doi: 10.5140/JASS.2020.37.2.143.

Korea Polar Research Institute (KOPRI) installed an ionospheric sounding radar system called Vertical Incidence Pulsed Ionospheric Radar (VIPIR) at Jang Bogo Station (JBS) in 2015 in order to routinely monitor the state of the ionosphere in the auroral oval and polar cap regions. Since 2017, after two-year test operation, it has been continuously operated to produce various ionospheric parameters. In this article, we will introduce the characteristics of the JBS-VIPIR observations and possible applications of the data for the study on the polar ionosphere. The JBS-VIPIR utilizes a log periodic transmit antenna that transmits 0.5-25 MHz radio waves, and a receiving array of 8 dipole antennas. It is operated in the Dynasonde B-mode pulse scheme and utilizes the 3-D inversion program, called NeXtYZ, for the data acquisition and processing, instead of the conventional 1-D inversion procedure as used in the most of digisonde observations. The JBS-VIPIR outputs include the height profiles of the electron density, ionospheric tilts, and ion drifts with a 2-minute temporal resolution in the bottomside ionosphere. With these observations, possible research applications will be briefly described in combination with other observations for the aurora, the neutral atmosphere and the magnetosphere simultaneously conducted at JBS.

keywords: Vertical Incidence Pulsed Ionospheric Radar (VIPIR); polar ionosphere; Jang Bogo Station; Antarctica

1-61

Occurrence Characteristics of Sea Breeze in the Gangneung Region for 2009~2018

Hwang, Hyewon., Eun, Seung-Hee., Kim, Byung-Gon., **Park, Sang-Jong.** and Park, Gyun-Myeong.

Atmosphere. 2020. 30(3): 221-236.

doi: 10.14191/Atmos.2020.30.3.221.

The Gangneung region has the complicated geographical characteristics being adjacent to East Sea and Taeback mountains, and thus sea breeze could play an important role in local weather in various aspects. This study aims to understand overall characteristics of sea breeze largely based on long-term (2009~2018) ground-based observation data. We also propose a selection criteria of sea breeze occurrence day; 1) daily precipitation is less than 10 mm, 2) surface wind direction is 0~110° (northerly to easterly) for more than 3 hours during the daytime, 3) wind direction is 110~360° for more than 3 hours during the nighttime, and 4) land and sea temperature difference is positive during the daytime, 5) sea and land sea-level pressure difference is more than 0.5 hPa. As a result, a total of 595 days was selected for the past 10 years. The occurrence of sea breeze is the highest in late Spring to early Summer (May to June). The passage time of sea breeze at the inland station (1.6 km farther inland) is one hour later than the coastal station. On the typical sea breeze event of April 12, 2019, the passage speed and duration of sea breeze was 15 km hr^{-1} and about 9 hours, respectively, with its depth of about 500 m and its head swelling. The current results emphasize the critical role of sea breeze in forecasting surface temperature and wind, and contribute to relieve heat wave especially in summer in the Yeongdong region.

keywords: Sea breeze; East Sea; occurrence; Gangneung

1-62 *Environmental Sciences; Meteorology & Atmospheric Sciences*

On the annual variability of Antarctic aerosol size distributions at Halley Research Station

Lachlan-Cope, Thomas., Beddows, David C. S., Brough, Neil., Jones, Anna E., Harrison, Roy M., Lupi, Angelo., **Yoon, Young Jun.** and 2 others.

Atmospheric Chemistry and Physics. 2020. 20(7): 4461-4476.

doi: 10.5194/acp-20-4461-2020.

The Southern Ocean and Antarctic region currently best represent one of the few places left on our planet with conditions similar to the preindustrial age. Currently, climate models have a low ability to simulate conditions forming the aerosol baseline; a major uncertainty comes from the lack of understanding of aerosol size distributions and their dynamics. Contrasting studies stress that primary sea salt aerosol can contribute significantly to the aerosol population, challenging the concept of climate biogenic regulation by new particle formation (NPF) from dimethyl sulfide marine emissions. We present a statistical cluster analysis of the physical characteristics of particle size distributions (PSDs) collected at Halley (Antarctica) for the year 2015 (89 % data coverage; 6-209 nm size range; daily size resolution). By applying the Hartigan-Wong k-mean method we find eight clusters describing the entire aerosol population. Three clusters show pristine average low particle number concentrations (< 121-179 cm^{-3}) with three main modes (30, 75-95 and 135-160 nm) and represent 57 % of the annual PSD (up to 89 %-100 % during winter and 34 %-65 % during summer based on monthly averages). Nucleation and Aitken mode PSD clusters dominate summer months (September January, 59 %-90 %), whereas a clear bimodal distribution (43 and 134 nm, respectively; Hoppel minimum at mode 75 nm) is seen only during the December-April period (6%-21 %). Major findings of the current work include: (1) NPF and growth events originate from both the sea ice marginal zone and the Antarctic plateau, strongly suggesting multiple vertical origins, including the marine boundary layer and free troposphere; (2) very low particle number concentrations are detected for a substantial part of the year (57 %), including summer (34 %-65 %), suggesting that the strong annual aerosol concentration cycle is driven by a short temporal interval of strong NPF events; (3) a unique pristine aerosol cluster is seen with a bimodal size distribution (75 and 160 nm, respectively), strongly associated with high wind speed and possibly associated with blowing snow and sea spray sea salt, dominating the winter aerosol population (34 %-54 %). A brief comparison with two other stations (Dome C - Concordia- and King Sejong Station) during the year 2015 (240 d overlap) shows that the dynamics of aerosol number concentrations and distributions are more complex than the simple sulfate-sea-spray binary combination, and it is likely that an array of additional chemical components and processes drive the aerosol population. A conceptual illustration is proposed indicating the various atmospheric processes related to the Antarctic aerosols, with particular emphasis on the origin of new particle formation and growth.

keywords: Antarctic aerosol size distribution; Halley station; king Sejong station

---

1-63 *Geography, Physical; Geosciences, Multidisciplinary*

Paleoceanographic changes in the Southern Ocean off Elephant Island since the last glacial period: Links between surface water productivity, nutrient utilization, bottom water currents, and ice-rafted debris

Kim, Sunghan., **Yoo, Kyu-Cheul.**, **Lee, Jae Il.**, **Roh, Youn Ho.**, Bak, Young-Suk., Um, In-Kwon., **Lee, Min Kyung.** and **Yoon, Ho Il.**

Quaternary Science Reviews. 2020. 249.

doi: 10.1016/j.quascirev.2020.106563.

To understand past changes in ocean-cryosphere interactions in the Southern Ocean off the Antarctic Peninsula, multi-proxy analyses of three sediment cores located off Elephant Island were used to reconstruct changes in paleoproductivity, nutrient utilization, bottom current intensity, and iceberg calving since the last glacial period. The glacial period was characterized by low surface water productivity with high nutrient utilization, indicating surface water stratification. During the deglaciation, surface water productivity increased with decreasing nutrient utilization, implying that the increase is associated with increased nutrient supply from the subsurface water by enhancing Antarctic Circumpolar Current (ACC) influence as fronts migrate southward with warming. Abundant occurrence of grains >1 mm during the deglacial period indicates rapid ice sheet retreat with large-scale melting and calving. During the glacial period, however, coarse silt-fine sand-sized fraction represented ice-rafted debris (IRD). The different IRD grain size characteristics are thought to be related to the IRD source material characteristics. Regardless of IRD input, the running downcore correlation (5 to 9-point) between sortable silt mean grain size and percentage showed that sediments are well sorted

by bottom current. However, the cross plot of them showed different temporal relationships. Sediments were sorted by the ACC and southwestward flowing bottom current. Along with southward migration of fronts and the ACC, southwestward flowing bottom current influence diminished, whereas the ACC influence increased particularly from 7 ka. Our results indicate that the sedimentary processes in the Scotia Sea largely depend on the regional interactions between the ocean and the cryosphere.

keywords: Paleoceanography; Marine core; Geochemistry; Nutrient utilization; Ocean-cryosphere interaction; Ice-rafted debris

1-64 *Geography, Physical; Geosciences, Multidisciplinary; Paleontology*

A paleoproductivity shift in the northwestern Bay of Bengal (IODP Site U1445) across the Mid-Pleistocene transition in response to weakening of the Indian summer monsoon

Lee, Jongmin., **Kim**, **Sunghan.** and Khim, Boo-Keun.

Palaeogeography Palaeoclimatology Palaeoecology. 2020. 560.

doi: 10.1016/j.palaeo.2020.110018.

The long-term variability of the Indian monsoon in the Bay of Bengal remains inconclusive due to the lack of proximal sedimentary records. To further elucidate the long-term variability of the Indian monsoon, we analyzed the paleoproductivity regime over the last 2.3 Myr at the International Ocean Discovery Program (IODP) Expedition 353 Site U1445 located near the Mahanadi Basin in the northwestern Bay of Bengal. We measured the downcore concentrations and mass accumulation rates (MARs) of biogenic opal, $CaCO_3$, total organic carbon (TOC), and total nitrogen over the Mid-Pleistocene Transition (MPT) to identify the links between surface water marine biogenic production and the Indian summer monsoon. TOC MARs were found to reflect both surface water marine productivity and terrestrial organic matter through the measurements of sediment C/N ratios and $\delta^{13}C_{SOM}$ values. Nonetheless, we identified a shift in the paleoproductivity regime from a dominance of biogenic opal deposition prior to the MPT to the dominance of $CaCO_3$ deposition following the MPT. The shift in biogenic marine productivity across the MPT was closely related to riverine discharge, which was primarily controlled by the intensity of the Indian monsoon. Our results, therefore, infer a decrease in riverine discharge to the Bay of Bengal across the MPT in response to a weakened Indian summer monsoon (and/or strengthened Indian winter monsoon). In addition, changes in the intensity of the Indian monsoon across the MPT were more closely linked to the global climate cooling rather than the gradual uplift of the Himalaya and Tibetan Plateau.

keywords: Organic carbon; Biogenic opal; Calcium carbonate; Organic carbon isotopes; Surface water productivity; Riverine discharge

1-65 *Geography, Physical; Geosciences, Multidisciplinary; Paleontology*

Particle-size dependent magnetic properties of Scotia Sea sediments since the Last Glacial Maximum: Glacial ice-sheet discharge controlling magnetic proxies

Shin, Ji Young., **Kim, Sunghan.**, Zhao, Xiang., **Yoo, Kyu-Cheul.**, Yu, Yongjae., **Lee, Jae Il.**, **Lee, Min Kyung.** and **Yoon, Ho Il.**

Palaeogeography Palaeoclimatology Palaeoecology. 2020. 557.

doi: 10.1016/j.palaeo.2020.109906.

The strong glacial-interglacial similarity between the magnetic susceptibility (MS) of Southern Ocean sediments and Antarctic ice core dust records has often been used to reconstruct Southern Hemisphere atmospheric variability. Although evaluation of various magnetic properties is essential for identifying the magnetic carriers linked to sedimentological variation, detailed magnetic studies are not sufficient in the Scotia Sea. Here we investigate the bulk and particle-size dependent magnetic properties of Scotia Sea sediments over the past ~22 kyr, to determine the main sediment transport mechanism driving bulk magnetic proxies including MS. In bulk sediments, MS is highest during the last glacial period and is accompanied by an increase in the concentration and grain size of ferrimagnetic and antiferromagnetic minerals. For magnetic mineral assemblages, coarse detrital magnetite is dominant. Of three particle-size fractions (> 63, 16-63, and < 16 μm), the coarse silt

fraction (16-63 μm) is responsible for the magnetic properties of bulk glacial sediments. Such dominant contribution of coarse silts rules out a major input of dust, which is expected as finer silt and clay. The silt fraction exhibits a co-varying magnetic mineral concentration with that of the sand fraction (> 63 μm) throughout the last deglaciation, indicating a close linkage between their input mechanisms. Thus, the sediment particles ranging from sand to coarse silt, which control the bulk glacial magnetic proxies, are most plausibly transported by iceberg-rafted debris (IRD). As hematite is relatively concentrated in the sand fraction, the hematite contribution in the bulk sediment can highlight IRD-related magnetic signals rather than magnetite. The bulk hematite contribution simultaneously varies with the deglacial influx of coarse IRD particles (> 1 mm) in Scotia Sea sediments, although their glacial inconsistency possibly suggests a different IRD input mechanism during the advancement and retreat of the ice sheet. Consequently, the glacial increase in the bulk magnetic concentration indicates vigorous iceberg calving activity in the Scotia Sea and further suggests the coupled cryosphere-atmosphere system.

keywords: Magnetic property; Particle-size dependence; Southern Ocean; Glacial period; Iceberg-rafted debris

1-66 *Geography, Physical; Geosciences, Multidisciplinary*

Post-LGM dynamic deglaciation along the Victoria Land coast, Antarctica

Rhee, Hyun Hee., **Lee, Min Kyung.**, Seong, Yeong Bae., **Lee, Jae Il.**, **Yoo, Kyu-Cheul.** and Yu, Byung Yong.

Quaternary Science Reviews. 2020. 247.

doi: 10.1016/j.quascirev.2020.106595.

The post-Last Glacial Maximum (LGM) deglaciation of Antarctica holds important clues for understanding past environmental changes and predicting future changes in the Antarctic Ice Sheet. Cosmogenic nuclide exposure dating of glacial erratics documents the spatial and temporal glacier changes during the most recent deglaciation. We collected 55 erratic cobbles from the eight glaciated benches on Inexpressible Island, which is at the terminal area of Priestley Glacier, Terra Nova Bay, Victoria Land, to elucidate its post-LGM deglaciation pattern. Analyses of the ^{10}Be ages and ^{26}Al/^{10}Be ratios suggest that Priestley Glacier underwent ~254 m of lowering during the mid-Holocene, between 8.9 and 5.9 ka. This lowering rate (~0.09 m a^{-1}) is faster than those observed along other Victoria Land outlet glaciers to the north (Tucker and Aviator), but slower than the one to the south (Mackay). The post-LGM lowering of these outlet glaciers was triggered by marine ice sheet instability, with their asynchronous onsets of deglaciation derived from their diachronous response times to the southwestward migration of the grounding-line retreat until their synchronous termination of deglaciation at ~6 ka. A post-LGM deglaciation model with the southwestward migration of the western Ross Ice Shelf grounding line provides the best match to the terrestrial exposure dating results of the thinning patterns of the outlet glaciers along the Victoria Land coast.

keywords: Antarctica; Terra Nova bay; Inexpressible island; Deglaciation; Cosmogenic exposure dating; Ross ice shelf

1-67 *Geography, Physical; Geosciences, Multidisciplinary*

Prediction of monthly Arctic sea ice concentrations using satellite and reanalysis data based on convolutional neural networks

Kim, Young Jun., **Kim, Hyun-Cheol.** and 3 others.

Cryosphere. 2020. 14(3): 1083-1104.

doi: 10.5194/tc-14-1083-2020.

Changes in Arctic sea ice affect atmospheric circulation, ocean current, and polar ecosystems. There have been unprecedented decreases in the amount of Arctic sea ice due to global warming. In this study, a novel 1-month sea ice concentration (SIC) prediction model is proposed, with eight predictors using a deep-learning approach, convolutional neural networks (CNNs). This monthly SIC prediction model based on CNNs is shown to perform better predictions (mean absolute error - MAE - of 2.28 %, anomaly correlation coefficient - ACC - of 0.98, root-mean-square error - RMSE - of 5.76 %, normalized RMSE - nRMSE - of 16.15 %, and NSE - Nash-Sutcliffe efficiency - of 0.97) than a random-forest-based (RF-based) model (MAE of 2.45 %, ACC of 0.98, RMSE of 6.61 %, nRMSE of 18.64 %, and NSE of 0.96) and the persistence model based on the monthly trend (MAE of 4.31 %, ACC of 0.95, RMSE of 10.54 %, nRMSE of 29.17 %, and NSE of 0.89) through hindcast validations. The spatio-temporal analysis also confirmed the superiority of the CNN

model. The CNN model showed good SIC prediction results in extreme cases that recorded unforeseen sea ice plummets in 2007 and 2012 with RMSEs of less than 5.0 %. This study also examined the importance of the input variables through a sensitivity analysis. In both the CNN and RF models, the variables of past SICs were identified as the most sensitive factor in predicting SICs. For both models, the SIC-related variables generally contributed more to predict SICs over ice-covered areas, while other meteorological and oceanographic variables were more sensitive to the prediction of SICs in marginal ice zones. The proposed 1-month SIC prediction model provides valuable information which can be used in various applications, such as Arctic shipping-route planning, management of the fishing industry, and long-term sea ice forecasting and dynamics.

keywords: Arctic Sea Ice; Convolution Neural Network; Prediction; Reanalysis Data; Satellite Data

1-68 *Environmental Sciences; Meteorology & Atmospheric Sciences*

Propagation of gravity waves and its effects on pseudomomentum flux in a sudden stratospheric warming event

Song, In-Sun., **Lee, Changsup.**, Chun, Hye-Yeong., **Kim, Jeong-Han.**, **Jee, Geonhwa.**, **Song, Byeong-Gwon.** and Bacmeister, Julio T.

Atmospheric Chemistry and Physics. 2020. 20(12): 7617-7644.

doi: 10.5194/acp-20-7617-2020.

Effects of realistic propagation of gravity waves (GWs) on distribution of GW pseudomomentum fluxes are explored using a global ray-tracing model for the 2009 sudden stratospheric warming (SSW) event. Four-dimensional (4D; *x-z* and *t*) and two-dimensional (2D; *z* and *t*) results are compared for various parameterized pseudomomentum fluxes. In ray-tracing equations, refraction due to horizontal wind shear and curvature effects are found important and comparable to one another in magnitude. In the 4D, westward pseudomomentum fluxes are enhanced in the upper troposphere and northern stratosphere due to refraction and curvature effects around fluctuating jet flows. In the northern polar upper mesosphere and lower thermosphere, eastward pseudomomentum fluxes are increased in the 4D. GWs are found to propagate more to the upper atmosphere in the 4D, since horizontal propagation and change in wave numbers due to refraction and curvature effects can make it more possible that GWs elude critical level filtering and saturation in the lower atmosphere. GW focusing effects occur around jet cores, and ray-tube effects appear where the polar stratospheric jets vary substantially in space and time. Enhancement of the structure of zonal wave number 2 in pseudomomentum fluxes in the middle stratosphere begins from the early stage of the SSW evolution. An increase in pseudomomentum fluxes in the upper atmosphere is present even after the onset in the 4D. Significantly enhanced pseudomomentum fluxes, when the polar vortex is disturbed, are related to GWs with small intrinsic group velocity (wave capture), and they would change nonlocally nearby large-scale vortex structures without substantially changing local mean flows.

keywords: Gravity waves; Propagation; Pseudomomentum; Sudden stratospheric warming

1-69 *Geosciences, Multidisciplinary; Oceanography*

Quantitative reconstruction of Holocene sediment source variations in the Yellow and northern East China Seas and their forcings

Lim, Dhongil., Kim, Jihun., Xu, Zhaokai., Jung, Hoisoo., Yoo, Dong-Geun., Choi, Mansik. and **Kim, So-Young.**

Marine Geology. 2020. 430.

doi: 10.1016/j.margeo.2020.106345.

Sediment provenance in the Yellow Sea and northern East China Seas (YECSs) has long been a subject of interest, but its quantification is still inconclusive. Here, we present an improved Al-Mg regression analysis by refining its methodological approach to strengthen quantification of sediment source-to-sink transports in the YECSs, with focus on its forcing mechanisms during the Holocene. Our quantitative source estimates clearly depict a considerable supply of the Chinese river (CR) sediments (~50%) to the southwestern Korean coastal region, and the Korean river (KR) sediments (30-40%) to the Central Yellow Sea Mud deposit, which accounts for a good balance between the sediment supply and budget of the shelf deposit. Of particular note is an abrupt decline in the CR contributions around 124°E, which indicates

that the CR sediments do not directly reach the eastern part of the Yellow Sea blocked by a strong physical boundary. Further, the observed variations in proportions between Huanghe-, Changjiang- and Korean river-derived sediments over the last 15 kyr - notably an abrupt increase of CR contribution since ~7 ka, followed by a sudden drop at ~3-4 ka - exhibit a good correspondence with other mineralogical proxy records. These temporal provenance changes witnessed robust palaeoenvironmental signals which fit to major climatic and oceanographic events linked with sea-level, intensity of the Kuroshio Current inflow and the East Asian monsoon. This study improves understanding of what pathways and sinks exist within the YECS basin, and how rates of sediment supply from adjacent rivers have changed over time.

keywords: Sediment source; Al-Mg regression analysis; Quantitative apportionment; Yellow Sea

1-70 *Meteorology & Atmospheric Sciences*

Recent changes in heatwave characteristics over Korea

Yoon, Donghyuck., Cha, Dong-Hyun., Lee, Myong-In., Min, Ki-Hong., Kim, Joowan., **Jun, Sang-Yoon.** and **Choi, Yonghan.**

Climate Dynamics. 2020. 55(7-8): 1685-1696.

doi: 10.1007/s00382-020-05420-1.

Global warming and abnormal climate change have resulted in an increase in the frequency of severe heatwave events. Recently, a series of extreme heatwave events have occurred in South Korea, and the damage from these events has also been increasing. Thus, it is necessary to analyze the mechanisms for generating and developing heatwaves. In this study, the long-term trend for heatwave events in South Korea was investigated using cluster analysis. Heatwave events in a 38-year period in South Korea were defined, and their synoptic patterns were categorized into three clusters. The number of heatwave days of cluster 2, which is related to the anomalous positive geopotential height (GPH) over the Kamchatka Peninsula, was found to significantly increase in recent years (2000-2018) compared with the past (1981-1999). In contrast, the frequency of cluster 3 associated with a negative GPH anomaly over the Kamchatka Peninsula decreased in the same period. There were five regions, including northern China and the Kamchatka Peninsula, where the mid-level GPH significantly increased between 2000 and 2018. This change in GPH was positively (negatively) correlated with the patterns associated to long-term variability of heatwave days of cluster 2 (cluster 3). The long-term trends of the GPH anomalies over five regions showed a significant correlation with the North Atlantic Oscillation (NAO) index during midsummer. As a result, it is likely that the heatwave events related to cluster 2 (cluster 3) have increased (decreased) in South Korea because the long-term variability of the summer NAO has recently induced a favorable (unfavorable) atmospheric condition for cluster 2 (cluster 3).

keywords: Heat wave; Cluster analysis; Long-term variability; North Atlantic Oscillation; South Korea

1-71 *Environmental Sciences; Meteorology & Atmospheric Sciences*

Recent weakening of the southern stratospheric polar vortex and its impact on the surface climate over Antarctica

Kwon, Hataek., **Choi, Hyesun.**, Kim, Baek-Min., Kim, Sang-Woo. and **Kim, Seong-Joong.**

Environmental Research Letters. 2020. 15(9).

doi: 10.1088/1748-9326/ab9d3d.

The variability in the southern stratospheric polar vortex (SSPV) and its downward coupling with the troposphere are known to play a crucial role in driving climate variability over Antarctica. In this study, SSPV weakening events and their impacts on the surface climate of Antarctica are examined using *in-situ* observation and reanalysis data. Combining criteria from several previous studies, we introduce a new detection method for SSPV weakening events. Based on the new criteria, the occurrence frequency of SSPV weakening events has exhibited a systematic increasing trend since the 2000 s. However, the weakened anomalies of individual SSPV events are not statistically different (95% confidence level) between the earlier (1979-1999) and later (2000-2017) periods examined in this study. The recent increase in the occurrence of SSPV weakening events is largely controlled by tropospheric mechanisms, i.e. the poleward heat flux carried by southern hemispheric planetary waves and associated vertical wave propagation. Among the

various scales of planetary waves, the wavenumber 1 contributes most of the poleward eddy heat flux. We show that SSPV weakening events induce statistically significant cooling over the Antarctic Peninsula (AP) region and warming over the rest of Antarctica. Typically, surface air temperature anomalies with large negative values smaller than - 0.6 °C and positive values larger than + 0.8 °C are observed over the east coast of the tip of the AP and King Edward VII Land, respectively. The influence of an SSPV weakening event on the surface lasts for approximately three months with higher height anomalies off western Antarctica, providing favorable conditions for the atmosphere to transport cold air from the interior of Antarctica to the AP via the Weddell Sea. Distinct positive surface air temperature anomalies over the rest of Antarctica are associated with the northerly circulation anomaly from the eastern Weddell Sea to east Antarctica.

keywords: southern stratospheric polar vortex; polar cap height(PCH); Antarctic surface air temperature

1-72

Reconstruction of the relative sea-level (RSL) of the Gulf of Dvina (White Sea) based on the study of lake sediments on the Onega Peninsula

Kublitskiy, Y.A., Repkina, T.Y., Leontiev, P.A., Zaretskaya, N.E., Peretrukhina, A.O., Shilova, O.S., Subetto, D.A., **Nam, Seung-Il.** and **Kim, Jung-Hyun.**

Limnology and Freshwater Biology. (4): 451-452.

doi: 10.31951/2658-3518-2020-A-4-451.

We present the preliminary results of the granulometric and geochemical analyses of lake-bottom sediments obtained from the Murmanskoe and Maloe Murmanskoe lakes. Based on the collected data, we reconstructed changes of relative sea-level (RSL) in the Gulf of Dvina (White Sea) during the Holocene. The conditions and maximum levels of two transgressions (Late Glacial and Tapes) and one Early Holocene regression were identified.

keywords: lake sediments; Holocene; White Sea; sea-level change; grain-size; geochemistry

1-73 *Biochemistry & Molecular Biology; Chemistry, Multidisciplinary*

Reliable Ultra Trace Analysis of Cd, U and Zn Concentrations in Greenland Snow and Ice by Using Ultraclean Methods for Contamination Control

Han, Changhee., **Hwang, Heejin.**, **Kang, Jung-Ho.**, **Hong, Sang-Bum.**, **Han, Yeongcheol.**, **Lee, Khanghyun.**, **Hur, Soon Do.** and Hong, Sungmin.

Molecules. 2020. 25(11).

doi: 10.3390/molecules25112519.

This study presents ultraclean procedures used in the challenging task of determining trace elements at or below the pg/g concentration level encountered in Greenland snow and ice. In order to validate these ultraclean procedures, recent snowfall and Holocene ice from northwest Greenland were analyzed for Cd, U, and Zn concentrations. The total procedural blanks brought through the entire measurement procedure proved to be negligible, compared to trace element concentrations, measured in snow and ice samples. This validates the overall practicality of the proposed ultraclean procedures, thereby ensuring the reliable measurements of ultra-trace analysis. A comparison between our study and published data shows that improper procedures employed throughout all stages, from field sampling to analysis to elevate the concentrations by several orders of magnitude, relative to the reliable concentration ranges. The risk of contamination exposure for selected trace elements appears to increase in the order of U < As ≤ Pb < Cd < Zn. Reliable measurements of Cd, U, and Zn concentrations in snow and ice allowed us to interpret the data in terms of seasonal variations in the inputs of crustal and anthropogenic sources to Greenland ice sheet.

keywords: ultraclean procedure; ultralow trace elements; contamination; Greenland snow and ice; seasonal variations; anthropogenic inputs

1-74 *Environmental Sciences; Geosciences, Multidisciplinary; Remote Sensing; Imaging Science & Photographic Technology*

Robust Mosaicking of Lightweight UAV Images Using Hybrid Image Transformation Modeling

Kim, Jae-In., **Kim, Hyun-cheol.** and Kim, Taejung.

Remote Sensing. 2020. 12(6).

doi: 10.3390/rs12061002.

This paper proposes a robust feature-based mosaicking method that can handle images obtained by lightweight unmanned aerial vehicles (UAVs). The imaging geometry of small UAVs can be characterized by unstable flight attitudes and low flight altitudes. These can reduce mosaicking performance by causing insufficient overlaps, tilted images, and biased tiepoint distributions. To solve these problems in the mosaicking process, we introduce the tiepoint area ratio (TAR) as a geometric stability indicator and orthogonality as an image deformation indicator. The proposed method estimates pairwise transformations with optimal transformation models derived by geometric stability analysis between adjacent images. It then estimates global transformations from optimal pairwise transformations that maximize geometric stability between adjacent images and minimize mosaic deformation. The valid criterion for the TAR in selecting an optimal transformation model was found to be about 0.3 from experiments with two independent image datasets. The results of a performance evaluation showed that the problems caused by the imaging geometry characteristics of small UAVs could actually occur in image datasets and showed that the proposed method could reliably produce image mosaics for image datasets obtained in both general and extreme imaging environments.

keywords: lightweight UAV; image mosaic; imaging geometry; tiepoint area ratio

1-75 *Meteorology & Atmospheric Sciences*

Role of Gravity Waves in a Vortex-Split Sudden Stratospheric Warming in January 2009

Song, Byeong-Gwon., Chun, Hye-Yeong. and **Song, In-Sun.**

Journal of the Atmospheric Sciences. 2020. 77(10): 3321-3342.

doi: 10.1175/jas-d-20-0039.1.

The role of gravity waves (GWs) in a sudden stratospheric warming (SSW) event that occurred in January 2009 (SSW09) is investigated using the MERRA-2 dataset. Nearly 2 weeks prior to the central date (lag = 0), at which the zonal-mean zonal wind at 10 hPa and 60°N first becomes negative, westward GW drag (GWD) is significantly enhanced in the lower mesosphere and stratosphere. At 5 days before lag = 0, planetary waves (PWs) of zonal wavenumber 2 (ZWN-2) in the stratosphere are enhanced, while PWs of ZWN-1 are weakened, which are evident from the amplitudes of the PWs and their Eliassen-Palm flux divergence (EPD). To examine the relationship between PWs and GWs, a nonconservative GWD (NCGWD) source term of the linearized quasigeostrophic potential vorticity equation is considered. A ZWN-2 pattern of the NCGWD forcing is developed around z = 55-60 km with a secondary peak around z = 40 km just before the PWs of ZWN-2 in the stratosphere began to enhance. Asignificant positive correlation between the NCGWD forcing in the upper stratosphere and lower mesosphere (USLM; 0.3-0.1 hPa in the present data) and the PWs of ZWN-2 in the stratosphere (5-1 hPa) exists. This result demonstrates that the amplification of the PWs of ZWN-2 in the stratosphere before the onset of SSW09 is likely related to the generation of PWs by GWD in the USLM, which is revealed by the enhanced downward-propagating PWs of ZWN-2 into the stratosphere from above.

keywords: Gravity waves; Planetary waves; Potential vorticity; Stratospheric circulation; Waves; atmospheric; Middle atmosphere

1-76 *Engineering*, *Environmental; Environmental Sciences; Water Resources*

Seasonal contrast of particulate organic carbon (POC) characteristics in the Geum and Seomjin estuary systems (South Korea) revealed by carbon isotope ($\delta^{13}C$ and $\Delta^{14}C$) analyses

Kang, Sujin., **Kim, Jung-Hyun.** and 4 others.

Water Research. 2020. 187.

doi: 10.1016/j.watres.2020.116442.

In this study, we newly investigated surface water samples collected in two contrasting Korean estuary systems (i.e., closed Geum and open Seomjin estuaries) along a salinity gradient in winter (December) in 2016. The main objectives were to determine the source of particulate organic carbon (POC) in winter and to

assess the environmental factors inducing seasonal differences in POC characteristics. Concentrations and dual carbon isotopes ($\delta^{13}C$ and $\Delta^{14}C$) of POC were analyzed together with concentrations and stable carbon isotopes ($\delta^{13}C$) of dissolved inorganic carbon (DIC) and compared with those obtained in summer (August) in 2016. Our study provided a new insight that for both estuarine systems, the seasonal contrast in POC characteristics was associated with stronger wind-induced estuarine sediment resuspensions in winter than in summer providing a greater contribution of aged POC to the total POC pool in winter.

keywords: Particulate organic carbon; Dissolved inorganic carbon; Carbon isotopes; Sediment resuspension; Geum estuary; Seomjin estuary

1-77 *Environmental Sciences; Meteorology & Atmospheric Sciences*

Seasonality of aerosol chemical composition at King Sejong Station (Antarctic Peninsula) in 2013

Hong, Sang-bum., **Yoon, Young Jun.**, Becagli, Silvia., **Gim, Yeontae.**, Chambers, S. D., **Park, Ki-Tae.**, **Park, Sang-Jong.**, Traversi, Rita., Severi, Mirko., Vitale, V., **Kim, Joo-Hong.**, **Jang, Eunho.** and 2 others.

Atmospheric Environment. 2020. 223.

doi: 10.1016/j.atmosenv.2019.117185.

Seasonal variations of ionic species concentrations in PM_{10} and $PM_{2.5}$ aerosols were investigated at King Sejong Station (King George Island, Antarctic Peninsula) in 2013. Seasonal variations of $PM_{2.5}$ mass were also determined, and found to be in the range: 2482.2 ± 944.4 ng m^{-3} (austral winter) to 3493.3 ± 1223.8 ng m^{-3} (austral fall). On a weight basis, the $PM_{2.5}$ ionic species consisted mainly of primary ions from sea spray (~30% in summer, ~50% in winter) and partly from secondary ions (~20% in summer), with the ratios of sea spray and secondary ion components to $PM_{2.5}$ mass showing clear seasonal variation. The seasonal cycle of sea spray components was not well defined, but was weakly correlated with wind speed ($r^2 = 0.38$). This correlation was likely attributable to a combination of the seasonal properties of wind and the measurement site's location at the western tip of Barton Peninsula. The concentrations of sulphur species ($CH_3SO_3^-$ and non sea salt SO_4^{2-}) were clearly higher during austral summer. Notably, these concentrations were ~2-3 times higher during in January 2013 than in other summer months of the field observation period. This was attributed to an increased biomass of algae in the ocean area surrounding King George Island and more frequent air mass passage over ocean areas with algae blooms. The NH_4^+ concentration was also clearly higher in austral summer 2013, mainly due to secondary formation from the NH_3 released from local emission sources such as penguin colonies and ocean areas near the measurement site with acidic aerosol, but also affected by local meteorology specific to the summer of 2014.

keywords: PM_{10} and $PM_{2.5}$ aerosol; King sejong station; Seasonal variations of ionic components; Sea spray; Biogenic sulphur compounds; Ammonium

1-78 *Environmental Sciences; Meteorology & Atmospheric Sciences*

Shipborne observations reveal contrasting Arctic marine, Arctic terrestrial and Pacific marine aerosol properties

Park, Jiyeon., Dall'Osto, Manuel., Park, Kihong., **Gim, Yeontae.**, **Kang, Hyo Jin.**, **Jang, Eunho.**, **Park, Ki-Tae.**, Park, Minsu., Yum, Seong Soo., **Jung, Jinyoung.**, **Lee, Bang Yong.** and **Yoon, Young Jun.**

Atmospheric Chemistry and Physics. 2020. 20(9): 5573-5590.

doi: 10.5194/acp-20-5573-2020.

There are few shipborne observations addressing the factors influencing the relationships of the formation and growth of aerosol particles with cloud condensation nuclei (CCN) in remote marine environments. In this study, the physical properties of aerosol particles throughout the Arctic Ocean and Pacific Ocean were measured aboard the Korean icebreaker R/V *Araon* during the summer of 2017 for 25 d. A number of new particle formation (NPF) events and growth were frequently observed in both Arctic terrestrial and Arctic marine air masses. By striking contrast, NPF events were not detected in Pacific marine air masses. Three major aerosol categories are therefore discussed: (1) Arctic marine (aerosol number concentration $CN_{2.5}$: 413±442 cm^{-3}), (2) Arctic terrestrial ($CN_{2.5}$: 1622±1450 cm^{-3}) and (3) Pacific marine ($CN_{2.5}$: 397±185 cm^{-3}), following air mass back-trajectory analysis. A major conclusion of this study is not only

that the Arctic Ocean is a major source of secondary aerosol formation relative to the Pacific Ocean but also that open-ocean sympagic and terrestrially influenced coastal ecosystems both contribute to shaping aerosol size distributions. We suggest that terrestrial ecosystems - including river outflows and tundra - strongly affect aerosol emissions in the Arctic coastal areas, possibly more than anthropogenic Arctic emissions. The increased river discharge, tundra emissions and melting sea ice should be considered in future Arctic atmospheric composition and climate simulations. The average CCN concentrations at a supersaturation ratios of 0.4 % were 35±40 cm^{-3}, 71±47 cm^{-3} and 204±87 cm^{-3} for Arctic marine, Arctic terrestrial and Pacific marine aerosol categories, respectively. Our results aim to help evaluate how anthropogenic and natural atmospheric sources and processes affect the aerosol composition and cloud properties.

keywords: Nano particles; Arctic Ocean; Formation-growth-cloud formation

1-79 *Meteorology & Atmospheric Sciences*

Simulations of Winter Arctic Clouds and Associated Radiation Fluxes Using Different Cloud Microphysics Schemes in the Polar WRF: Comparisons With CloudSat, CALIPSO, and CERES

Cho, Heeje., **Jun, Sang-Yoon.** and 2 others.

Journal of Geophysical Research-Atmospheres. 2020. 125(2).

doi: 10.1029/2019jd031413.

Arctic cloud simulations of the polar-optimized version of the Weather Research and Forecasting model (Polar WRF) were compared with retrievals using the CloudSat and Cloud-Aerosol Lidar and Infrared Pathfinder Satellite Observation measurements. For the period from 1 December 2015 to 31 January 2016, a series of 24-to 48-hr simulations initialized daily at 00 UTC were examined. In particular, two cloud microphysics schemes, the Morrison double moment and the WRF single-moment 6-class (WSM6), were tested. The modeled cloud top heights had a correlation coefficient (*r*) of 0.69-0.72 with those from satellite retrievals, and a mean bias of less than 400 m. For the mean ice water content profile and mixed-phase cloud occurrence, the Morrison scheme's clouds were in better agreement with satellite retrievals than the WSM6. However, the use of the Morrison scheme resulted in underestimates of outgoing longwave radiation by -11.7 W m^{-2} compared to satellite observations. The bias was reduced to -0.4 W m^{-2} with the WSM6 which produced a stronger precipitation rate (by 10%) resulting in a drier and less-cloudy atmosphere. This also leads to the 7-W m^{-2} mean difference in the surface downward longwave radiation (DLR) between the schemes, which is large enough to explain the spread of the Arctic DLR in the current climate models. However, as the temporal variation in DLR showed good agreement with ground observations (*r*: 0.68-0.92), it is concluded that the Polar WRF can be useful for studying cloud effects on the winter Arctic surface climate.

keywords: Arctic cloud; Polar WRF

1-80 *Astronomy & Astrophysics*

Simultaneous Observations of SAR Arc and Its Ionospheric Response at Subauroral Conjugate Points (L≃2.5) During the St. Patrick's Day Storm in 2015

Hong, J., **Kim, Jeong-Han.**, Chung, J-K., Kim, Y. H., **Kam, Hosik.** and 2 others.

Journal of Geophysical Research-Space Physics. 2020. 125(4).

doi: 10.1029/2019ja027321.

During the St. Patrick's Day storm on 17 March 2015, an all-sky imager at King Sejong Station (KSS; geo: 62.2°S, 58.8°W; mag: 50.2°S) captured diffuse aurora and a stable auroral red (SAR) arc. Ground-based Global Positioning System observations were also simultaneously conducted at KSS, but there was no significant increase in the total electron content's rate-of-change index or the ionospheric scintillation indices around the SAR arc region. Auroral activities including a SAR arc were also detected by the all-sky imager at Millstone Hill Station (geo: 42.6°N, 71.4°W; mag: 52.5°N), which is magnetically conjugate to KSS. The total electron content's rate-of-change index map around Millstone Hill Station, too, indicates that the ionospheric irregularities occurred only near the diffuse aurora and not in the SAR arc. The northern SAR arc is broader than the southern one and also shows a multiplicity pattern, which may be due to latitude

structure within the seasonally dependent midlatitude ionospheric trough. These conjugate observations, despite their hemispheric differences, validate the classical SAR arc mechanism of emission driven by heat conduction from the inner magnetosphere that does not generate small-scale ionospheric irregularities that can affect Global Positioning System radio signals. Previous studies of SAR arcs and very high frequency radiowave scintillations did show a positive correlation.

keywords: GPS; Ionosphere; SAR arc; Scintillation; St. Patrick's day storm

1-81 *Geochemistry & Geophysics; Meteorology & Atmospheric Sciences*

Statistical study of EMIC Pc1-Pc2 waves observed at subauroral latitudes

Kwon, Jong-Woo., Kim, Khan-Hyuk., Jin, Ho., **Kwon, Hyuck-Jin.**, **Jee, Geonhwa.** and 2 others.

Journal of Atmospheric and Solar-Terrestrial Physics. 2020. 205.

doi: 10.1016/j.jastp.2020.105292.

Although the occurrence rate of electromagnetic ion cyclotron (EMIC) waves is high in the outer magnetosphere ($L > 7$), it has been suggested in the past that a steep plasma density gradient region of the plasmapause is a preferred location for the generation of EMIC waves. To examine spectral properties of the EMIC waves occurred near the nominal location of the plasmapause ($L = 4$-5), we focus on Pc1-Pc2 waves observed at subauroral latitude Athabasca station (magnetic latitude: ~62°, and $L \sim 4.6$). A statistical study of 10,494 wave samples identified from Athabasca data for 2007-2008 reveals the following wave characteristics. (1) Wave frequencies are higher in the postmidnight-to-dawn sector and lower in the late afternoon sector. (2) They mostly appear to be in frequency band between helium and oxygen gyrofrequencies (i.e., He-band) calculated from the dipole field model magnetic field intensity at $L = 4.6$. (3) The occurrence rate of Pc1-Pc2 waves has a peak in the prenoon sector at 0900-1100 LT under quiet geomagnetic conditions ($Kp \leq 1$), but is peaked in the afternoon sector under moderate and disturbed geomagnetic conditions ($Kp \geq 2$). (4) The Pc1-Pc2 waves observed at Athabasca were composed of a mixture of left-hand, right-hand, and linearly polarized waves. By comparing previous and recent studies with these observations, we suggest that the subauroral latitude Pc1-Pc2 waves are associated with EMIC waves generated near the plasmapause and discuss the EMIC wave properties in a region of cold and dense plasmas containing heavy ions in the inner magnetosphere.

keywords: Pc1-Pc2 waves; Subauroral latitude; He-band; Plasmapause

1-82 *Astronomy & Astrophysics*

A Statistical Study of Pi2 Pulsations Observed in the Upper Ionosphere Using Swarm Magnetic Field Data

Park, Jae-Hee., Kim, Khan-Hyuk., **Kwon, Hyuck-Jin.**, **Jee, Geonhwa.** and Hwang, Junga.

Journal of Geophysical Research-Space Physics. 2020. 125(1).

doi: 10.1029/2019ja027293.

The properties of Pi2 pulsations observed in the upper ionosphere are studied using magnetic field data acquired by the Swarm A spacecraft in low Earth orbit and at the low-latitude Bohyun ground station (BOH, $L = 1.3$) for January 2014 to June 2015. From time intervals when Swarm A was on the nightside (magnetic local time (MLT) = 1800-0600 hr) and the BOH station was near midnight (MLT = 2100-0300 hr), we identified 621 Pi2 events in the horizontal H component of the BOH data. For each event we examined the coherence between the horizontal H component on the ground and the B_x (radial), B_y (azimuthal), or B_z (compressional) components at Swarm A. Out of 621 events, the B_x - H high-coherence (> 0.7) events are ~6%, the B_y - H high-coherence events are ~2%, and the B_z - H high-coherence events are ~25%. The ground satellite high-coherence events occurred when the spacecraft was located at magnetic latitudes between −50° and 50°. Using the ground satellite high-coherence events, we statistically examined the latitudinal structure of the relative amplitude and phase of the ionospheric Pi2 pulsations and found that their latitudinal variations is consistent with the north-south mode structure expected from the plasmaspheric resonance model. Our statistical results indicate that the source of ionospheric Pi2 pulsations is the plasmaspheric resonance.

keywords: Magnetosphere; Magnetosphere-Ionosphere Coupling; Ionosphere

1-83 *Geography, Physical; Remote Sensing*

Surface roughness signatures of summer arctic snow-covered sea ice in X-band dual-polarimetric SAR

Han, Hyangsun., **Kim, Jae-In.**, **Hyun, Chang-Uk.**, **Kim, Seung Hee.**, **Park, Jeong-Won.**, **Kwon, Young-Joo.**, **Lee, Sungjae.**, Lee, Sanggyun. and **Kim, Hyun-Cheol.**

Giscience & Remote Sensing. 2020. 57(5): 650-669.

doi: 10.1080/15481603.2020.1767857.

Surface roughness of sea ice is primary information for understanding sea ice dynamics and air-ice-ocean interactions. Synthetic aperture radar (SAR) is a powerful tool for investigating sea ice surface roughness owing to the high sensitivity of its signal to surface structures. In this study, we explored the surface roughness signatures of the summer Arctic snow-covered first-year sea ice in X-band dual-polarimetric SAR in terms of the root mean square (RMS) height. Two ice campaigns were conducted for the first-year sea ice with dry snow cover in the marginal ice zone of the Chukchi Sea in August 2017 and August 2018, from which high-resolution (4 cm) digital surface models (DSMs) of the sea ice were derived with the help of a terrestrial laser scanner to obtain the in situ RMS height. X-band dual-polarimetric (HH and VV) SAR data (3 m spatial resolution) were obtained for the 2017 campaign, at a high incidence angle (49.5°) of TerraSAR-X, and for the 2018 campaign, at a mid-incidence angle (36.1°) of TanDEM-X 1-2 days after the acquisition of the DSMs. The sea ice drifted during the time between the SAR and DSM acquisitions. As it is difficult to directly co-register the DSM to SAR owing to the difference in spatial resolution, the two datasets were geometrically matched using unmanned aerial vehicle (4 cm resolution) and helicopter-borne (30 cm resolution) photographs acquired as part of the ice campaigns. A total of five dual-polarimetric SAR features—backscattering coefficients at HH and VV polarizations, co-polarization ratio, co-polarization phase difference, and co-polarization correlation coefficient—were computed from the dual-polarimetric SAR data and compared to the RMS height of the sea ice, which showed macroscale surface roughness. All the SAR features obtained at the high incidence angle were statistically weakly correlated with the RMS height of the sea ice, possibly influenced by the low backscattering close to the noise level that is attributed to the high incidence angle. The SAR features at the mid-incidence angle showed a statistically significant correlation with the RMS height of the sea ice, with Spearman's correlation coefficient being higher than 0.7, except for the co-polarization ratio. Among the intensity-based and polarimetry-based SAR features, HH-polarized backscattering and co-polarization phase difference were analyzed to be the most sensitive to the macroscale RMS height of the sea ice. Our results show that the X-band dual-polarimetric SAR at mid-incidence angle exhibits potential for estimation of the macroscale surface roughness of the first-year sea ice with dry snow cover in summer.

keywords: Sea ice surface roughness; root mean square (RMS) height; snow-covered first-year sea ice; synthetic aperture radar (SAR); x-band dual polarimetry

1-84 *Geosciences, Multidisciplinary*

Unusual Changes in the Antarctic Middle Atmosphere During the 2019 Warming in the Southern Hemisphere

Eswaraiah, S., **Kim, Jeong-Han.** and 4 others.

Geophysical Research Letters. 2020. 47(19).

doi: 10.1029/2020gl089199.

A rare sudden stratosphere warming (SSW) occurred in the Southern Hemisphere polar region in 2019. The polar stratosphere temperature and planetary wave (PW) enhancements are found to be unusual from the history for 40 years; hence, it is an "Extremely-Rare" SSW. The distinct features of the mesosphere winds were observed during the SSW, in association with the traveling PWs in the stratosphere. The mesosphere zonal winds reversed for about 20 days before the peak SSW. Meteor radar (MR) and Modern-Era Retrospective Analysis for Research and Applications (MERRA)-2 observations indicate that the zonal wind reversal was descended with time, and the reversal was larger over ~72°S than the MR site (62°S). The MR detected the PWs of 14-22 days before and 8-12 days following the SSW in the mesosphere. We further noticed the enhancement of wavenumber 1 signature in the mesosphere during the peak SSW over the polar region. Thus, the polar

middle-atmosphere is greatly affected by the SSW.

keywords: sudden stratospheric warming (SSW); Antarctic middle atmosphere; meteor radar; mesosphere wind reversal; planetary waves

1-85 *Astronomy & Astrophysics*

Vertical Structures of Temperature and Ozone Changes in the Stratosphere and Mesosphere during Stratospheric Sudden Warmings

Kim, Jeong-Han., **Jee, Geonhwa.**, **Choi, Hyesun.**, Kim, Baek-Min. and **Kim, Seong-Joong.**

Journal of Astronomy and Space Sciences. 2020. 37(1): 69-75.

doi: 10.5140/jass.2020.37.1.69.

We analyze the observations of temperature and ozone measured by the Microwave Limb Sounder (MLS) during the period of 2005–2016, to investigate the vertical structures of temperature and ozone in the stratosphere and mesosphere during stratospheric sudden warming (SSW). We compute the height profiles of the correlation coefficients between 55 height levels of MLS temperature anomalies and compare them with the results of Whole Atmosphere Community Climate Model simulations for three major SSWs. We also construct the temperature and ozone anomalies for the events to investigate the changes in the temperature and ozone distributions with height. There seems to always be a relatively weak but broad negative correlation between the temperature anomaly at 10 hPa and temperature anomalies over the entire mesosphere during the period before SSW events. However, this pattern gets stronger in the lower mesosphere but becomes a positive correlation in the upper mesosphere and lower thermosphere after the onset of SSW. We also found that the temperatures from the simulations show a similar trend to the observational results but with smaller variations and the transition height from negative to positive correlation in the mesosphere is much lower in the simulation than in the actual observations.

keywords: temperature and ozone changes; stratospheric sudden warming; middle atmosphere; northern polar region

1-86 *Meteorology & Atmospheric Sciences*

The Year of Polar Prediction in the Southern Hemisphere (YOPP-SH)

Bromwich, David H., Werner, Kirstin., Casati, Barbara., Powers, Jordan G., Gorodetskaya, Irina, V., Massonnet, Francois., Vitale, Vito., Heinrich, Victoria J., Liggett, Daniela., Arndt, Stefanie., Barja, Boris., Bazile, Eric., Carpentier, Scott., Carrasco, Jorge F., **Choi, Taejin.**, **Choi, Yonghan.**, Colwell, Steven R., Cordero, Raul R., Gervasi, Massimo., Haiden, Thomas., Hirasawa, Naohiko., Inoue, Jun., Jung, Thomas., Kalesse, Heike., **Kim, Seong-Joong.**, Lazzara, Matthew A., Manning, Kevin W., Norris, Kimberley., **Park, Sang-Jong.** and 9 others.

Bulletin of the American Meteorological Society. 2020. 101(10): E1653-E1676.

doi: 10.1175/bams-d-19-0255.1.

The Year of Polar Prediction in the Southern Hemisphere (YOPP-SH) had a special observing period (SOP) that ran from 16 November 2018 to 15 February 2019, a period chosen to span the austral warm season months of greatest operational activity in the Antarctic. Some 2,200 additional radiosondes were launched during the 3-month SOP, roughly doubling the routine program, and the network of drifting buoys in the Southern Ocean was enhanced. An evaluation of global model forecasts during the SOP and using its data has confirmed that extratropical Southern Hemisphere forecast skill lags behind that in the Northern Hemisphere with the contrast being greatest between the southern and northern polar regions. Reflecting the application of the SOP data, early results from observing system experiments show that the additional radiosondes yield the greatest forecast improvement for deep cyclones near the Antarctic coast. The SOP data have been applied to provide insights on an atmospheric river event during the YOPP-SH SOP that presented a challenging forecast and that impacted southern South America and the Antarctic Peninsula. YOPP-SH data have also been applied in determinations that seasonal predictions by coupled atmosphere-ocean-sea ice models struggle to capture the spatial and temporal characteristics of the Antarctic sea ice minimum. Education, outreach, and communication activities have supported the YOPP-SH SOP efforts. Based on the success of this Antarctic summer YOPP-SH SOP, a winter YOPP-SH SOP is being organized to support explorations of Antarctic

atmospheric predictability in the austral cold season when the southern sea ice cover is rapidly expanding.

PART 2

Geosciences

2-1 *Chemistry, Multidisciplinary; Engineering, Multidisciplinary; Materials Science, Multidisciplinary; Physics, Applied*

Analysis of Effects of Rock Physical Properties Changes from Freeze-Thaw Weathering in Ny-Ålesund Region: Part 1-Experimental Study

Park, Keunbo. and 3 others.

Applied Sciences-Basel. 2020. 10(5).

doi: 10.3390/app10051707.

In order to investigate the weathering characteristics of rocks in response to freeze-thaw conditions in northern latitudes, we analysed meteorological data from the Ny-Ålesund region in Norway, and observed changes in the physical and mechanical properties of rocks of dolomite and quartzite. To assess the effects of freeze-thaw weathering on these rock properties, 900 cycles of long-term freeze-thaw tests were conducted for the sampled rocks in two locations. P-wave velocity, absorption, shore hardness, and the uniaxial compressive strength of the sampled rocks were measured at every 150 cycles in order to analyse physical and mechanical mediator variables of freeze-thaw weathering. It was found that an increasing number of freeze-thaw cycle on the sampled rocks decreases uniaxial compressive strength, shore hardness, and P-wave velocity and increases absorption.

keywords: air temperature; freezing-thaw cycle; rock weathering; dolomite; quartzite; rock physical property

2-2 *Chemistry, Multidisciplinary; Engineering, Multidisciplinary; Materials Science, Multidisciplinary; Physics, Applied*

Analysis of Effects of Rock Physical Properties Changes from Freeze-Thaw Weathering in Ny- Ålesund Region: Part 2-Correlations and Prediction of Weathered Properties

Park, Keunbo., **Lee, Bang Yong.** and 2 others.

Applied Sciences-Basel. 2020. 10(10).

doi: 10.3390/app10103392.

From the examination of rock physical parameters' changes of compressive strength, shore hardness, water absorption, P-wave velocity with increasing freeze-thaw cycles, correlations of these parameters were investigated. Rock samples were collected from Ny- Ålesund region in Norway. As compressive strength and shore hardness inherently have high uncertainties due to inhomogeneous rock composition and internal fissures and cracks, only the relationship between water absorption and P-wave velocity revealed high correlations, providing meaningful linear fitting equations. From the correlation analysis results and clear trends of increasing water absorption and decreasing P-wave velocity with increasing freeze-thaw cycle found in part one of the companion study, prediction equations of future changes of rock physical parameters are proposed using P-wave velocity or water absorption. In addition, future rock weathering grade changes with time can be predicted from estimation of water absorption or P-wave velocity change due to freeze-thaw cycles.

keywords: rock weathering; rock weathering grade; freeze-thaw cycle; air temperature; P-wave velocity; water absorption; regression analysis

2-3 *Geochemistry & Geophysics; Mineralogy; Mining & Mineral Processing*

Chemical Weathering of Granite in Ice and Its Implication for Weathering in Polar Regions

Chung, Hyun Young., **Jung, Jaewoo.**, **Lee, Du Hyeong.**, **Kim, Sunghan.**, **Lee, Min Kyung.**, **Lee, Jae Il.**, **Yoo, Kyu-Cheul.**, Lee, Yong Il. and **Kim, Kitae.**

Minerals. 2020. 10(2).

doi: 10.3390/min10020185.

Recently, it has been reported that some chemical reactions are enhanced in below-freezing conditions. Despite the high denudation typical of polar regions, chemical weathering that occurs under ice has not been investigated. In this study, we investigated the dissolution of granite in ice. The mixture of granite and deionized water (DW) or solution adjusted to pH 2 or 3 was split into two groups: the test group was frozen at -20 °C, while the control was maintained at room temperature. After 29 days of batch experiments, the filtrate was analyzed to measure the concentrations of cations and silica. The filtered powder was analyzed to investigate the mineral compositions and crystallinities of the granite before and after the experiments. Despite the low temperature, a significant quantity of cations (Na^+, K^+, Mg^{2+}, Ca^{2+}) were dissolved out, even from the ice samples. During X-ray diffraction (XRD) analysis, the decreased crystallinities of granite in ice samples were identified regardless of the pH condition. To verify the observed freeze concentration effect, the concentration of granite in the ice grain boundaries was observed using optical microscopy with a cold chamber. The low concentration of silica in the ice samples could explain the silica anomaly in polar regions. This study also provides a new perspective for the dissolution mechanism in polar regions.

keywords: chemical weathering; dissolution; granite; ice chemistry; polar regions

2-4

Classification of Transport Vehicle Noise Events in Magnetotelluric Time Series Data in an Urban area Using Random Forest Techniques

Kwon, Hyoung-Seok., Ryu, Kyeongho., Sim, Ickhyeon., **Lee, Choon-Ki.** and Oh, Seokhoon.

Geophysics and Geophysical Exploration. 2020. 23(4): 230-242.

doi: 10.7582/GGE.2020.23.4.230.

We performed a magnetotelluric (MT) survey to delineate the geological structures below the depth of 20 km in the Gyeongju area where an earthquake with a magnitude of 5.8 occurred in September 2016. The measured MT data were severely distorted by electrical noise caused by subways, power lines, factories, houses, and farmlands, and by vehicle noise from passing trains and large trucks. Using machine-learning methods, we classified the MT time series data obtained near the railway and highway into two groups according to the inclusion of traffic noise. We applied three schemes, stochastic gradient descent, support vector machine, and random forest, to the

time series data for the highspeed train noise. We formulated three datasets, Hx, Hy, and Hx & Hy, for the time series data of the large truck noise and applied the random forest method to each dataset. To evaluate the effect of removing the traffic noise, we compared the time series data, amplitude spectra, and apparent resistivity curves before and after removing the traffic noise from the time series data. We also examined the frequency range affected by traffic noise and whether artifact noise occurred during the traffic noise removal process as a result of the residual difference.

keywords: MT time series; traffic noise; high-speed train (HST) noise; truck noise; random forest

2-5 *Geography, Physical; Geosciences, Multidisciplinary*

Cyclostratigraphic age constraining for Quaternary sediments in the Makarov Basin of the western Arctic Ocean using manganese variability

Park, Kwangkyu., **Kim, Jung-Hyun.**, **Asahi, Hirofumi.**, Polyak, Leonid., Khim, Boo-Keun., **Schreck, Michael.**, Niessen, Frank., Kong, Gee Soo. and **Nam, Seung-Il.**

Quaternary Geochronology. 2020. 55.

doi: 10.1016/j.quageo.2019.101021.

The Quaternary paleoenvironmental history of the Arctic Ocean remains uncertain, mainly due to the limited chronological constraints, especially beyond the ^{14}C dating limits of accelerator mass spectrometry (AMS). The difficulty in establishing reliable chronostratigraphies is mainly attributed to low sedimentation rates and diagenetic sediment changes, resulting in very poor preservation of microfossils and altered paleomagnetic records. In the absence of independent chronostratigraphic data, the age model of Pleistocene sediments from the Arctic Ocean is mainly based on cyclostratigraphy, which relates lithologic changes to climatic variability on orbital time scales. In this study, we used the Mn/Al record measured from the sediment core ARA03B-41GC retrieved from the Makarov Basin in the western Arctic Ocean. The Mn/Al variation was tuned to the global benthic oxygen isotope stack (LR04) curve under different assumptions for computational correlation. Regardless of assumptions, our computational approach led to similar ages of about 600-1,000 ka for the bottom part of the core. These age models were up to about 200 ka older than those derived from lithostratigraphic approaches. Interestingly, our new age models show that the Ca/Al peak, a proxy for a detrital input from the Laurentide Ice Sheet, first occurred about 150 ka earlier than those previously proposed. Therefore, our results suggest that the glaciers in northern North America developed more extensively at about 810 ka than in earlier glacial periods, and influenced the sedimentary and paleoceanographic environments of the Arctic Ocean much earlier than previously thought. In order to establish a more comprehensive age model, more work is needed to validate our findings with different sediment cores recovered from the western Arctic Ocean.

keywords: Cyclostratigraphy; Manganese; Western Arctic Ocean; Laurentide Ice Sheet; Glacial-interglacial cycles

2-6 *Paleontology*

Earliest known spatial competition between stromatoporoids: evidence from the Upper Ordovician Xiazhen Formation of South China

Jeon, Juwan., Liang, Kun., **Lee, Mirinae.** and Kershaw, Stephen.

Journal of Paleontology. 2020. 94(1): 1-10.

doi: 10.1017/jpa.2019.63.

The earliest known interpreted spatial competition between two species of stromatoporoids, *Clathrodictyon* cf. *C. mammillatum* (Schmidt, 1858) and *Labechia* sp. is found in the Upper Ordovician Xiazhen Formation at Zhuzhai, South China. The interaction between these taxa was initiated by settlement of *Labechia* sp. on the surface of *Clathrodictyon* cf. *C. mammillatum*. Distortions of the intraskeletal elements of stromatoporoids represented by abnormally large, wide cysts and thick cyst plates in *Labechia* sp. are observed, along with zigzag crumpled distorted laminae and antagonistic behavior of the skeleton in *Clathrodictyon* cf. *C. mammillatum*, indicating syn-vivo interactions. The growth of *Labechia* sp. was terminated by the overgrowth of *Clathrodictyon* cf. *C. mammillatum*, possibly reflecting the ecological superiority of *Clathrodictyon* cf. *C. mammillatum* over *Labechia* sp. The observations are interpreted as

competitive interaction between stromatoporoids that was most likely facultative, thus most likely occurring by chance, but the interaction allows assessment of different growth behaviors of the stromatoporoid species. Analysis of the interaction provides evidence to improve understanding of the paleoecology and growth behaviors of early stromatoporoids.

2-7

Evaluation of time series of soil moisture and soil temperature and computation of apparent thermal diffusivity of active layer in the Barton Peninsula, Antarctica

Kim, Chang-Seong., Lee, Jin-Yong., Kim, Heejung., Jeon, Woo-Hyun. and **Kim, Kitae.**

Journal of the Geological Society of Korea. 2020. 56(5): 571-585.

doi: 10.14770/jgsk.2020.56.5.571.

We have examined soil moisture and soil temperature of three sites in the Barton Peninsula, Antarctica. Auto-correlation, spectral analysis, and cross-correlation analysis were conducted using time series data. In addition, apparent thermal diffusivity was computed and active layer thickness was calculated. Soil moisture and soil temperature meters were installed at depths of 5, 10, 15, 20 cm, and measured every five minutes during summer 2019-2020. The soil moisture content was the largest at 20 cm depth at all sites. Rainfall below 0.5 mm/day could not affect the soil moisture content. The soil temperature in deeper depth was low. The soil temperature was above zero except for one day (December 20, 2019). The auto-correlation of soil moisture indicated shorter lag time at gradual slope and that of soil temperature indicated shorter lag time at shallower depth. The cycle of soil moisture was between 2.5 and 4.7 days, and the cycle of soil temperature was between 1.0 and 1.1 days. The cross-correlation of air temperature-soil temperature showed shorter lag time and larger correlation coefficient than that of solar radiation-soil temperature. The apparent thermal diffusivity (ATD) ranged from 0.01 to 121.94 mm^2/sec (median=0.34-0.59 mm^2/sec). The median values were close to that of minimum of previous study (0.4-3.3 mm^2/sec) using same methods. The active layer thickness ranged from 23.6 to 38.6 cm. The ATD is smaller and active layer thickness is thinner than that near the coast (within 0.2 km) because the study area is located 1.5 km from the sea.

keywords: soil moisture; soil temperature; time series analysis; apparent thermal diffusivity; active layer thickness

2-8 *Geology; Mineralogy; Mining & Mineral Processing*

Geology, mineralogy and stable isotope geochemistry of the Dzuunmod area in northern Mongolia: Constraints for gold ore genesis and sources

Kim, Yeongmin., Lee, Insung., Oyungerel, Sodnom., Altanzul, Chikalov., Jargal, Luvsanchultem. and **Kim, Nak Kyu.**

Ore Geology Reviews. 2020. 118.

doi: 10.1016/j.oregeorev.2019.103213.

The Dzuunmod area located in the North Khentii Gold belt (NKGB) of northern Mongolia includes lode gold deposits such as Gatsuurt, Sujigtei and Boroo with several minor gold deposits and occurrences. They show similar hydrothermal alteration assemblages (sericitic, siliceous and potassic) and ore mineral assemblages (pyrite and arsenopyrite with minor amount of galena, sphalerite and chalcopyrite). Gold occurs as native form and invisible gold in pyrite and arsenopyrite. The major sulfide minerals are separated into earlier non-auriferous stage and later auriferous grains containing invisible gold. Native gold postdates the major sulfide mineralization. Gold and arsenic content of pyrite grains indicates that gold exists mainly as solid solution form (Au^{+1}) in the Gatsuurt and Boroo deposit whereas gold nanoparticle (Au^0) is present in the Sujigtei deposit. High Co/Ni and Mo/Ni ratios of pyrite grain suggest a post-sedimentary or hydrothermal origin and the ore-forming fluid was significantly affected by fluid-host rock interactions during mineralization processes. Large variation of $\delta^{34}S$ values of pyrite and arsenopyrite from -2.6‰ to 17.2‰, indicates that sulfur seems to be mainly derived from a source with heterogeneous sulfur isotope composition, even though the role of magmatic sulfur as one of possible sulfur sources cannot be ruled out. Consistent with geological evidence, relatively positive $\delta^{34}S$ values suggest that sulfidation plays an important role for gold and sulfide precipitation. The calculated $\delta^{18}O$ values of hydrothermal fluid from the measured $\delta^{18}O$ values of quartz samples (from 14.7‰ to 17.7‰) indicate a metamorphic derivation of ore-forming fluid. Gold mineralization processes in the Dzuunmod area seem to

occur several times by multiple input of hydrothermal fluid and fluid-host rock interactions. The gold deposits in the Dzuunmod area are considered to be orogenic gold type influenced by fluid-host rock interactions in the deposit area.

keywords: Dzuunmod area; Orogenic gold; Stable isotope geochemistry; Ore genesis; Mongolia

2-9 *Multidisciplinary Sciences*

Groundwater oxygen anomaly related to the 2016 Kumamoto earthquake in Southwest Japan

Sano, Yuji., Onda, Satoki., Kagoshima, Takanori., Miyajima, Toshihiro., Takahata, Naoto., Shibata, Tomo., Nakagawa, Chika., Onoue, Tetsuji., **Kim**, **Nak Kyu.** and 3 others.

Proceedings of the Japan Academy Series B-Physical and Biological Sciences. 2020. 96(7): 322-334.

doi: 10.2183/pjab.96.024.

Here, we report the groundwater oxygen isotope anomalies caused by the 2016 Kumamoto earthquake (M_{JMA}7.3) that occurred in Southwest Japan on April 16, 2016. One hundred and seventeen groundwater samples were collected from a deep well located 3 km to the southeast of the epicenter in Mifune Town, Kumamoto Prefecture; they were drinking water packed in PET bottles and distributed in the area between April 2015 and March 2018. Further, the oxygen and hydrogen isotopes were evaluated via cavity ring-down spectroscopy without performing any pretreatment. An anomalous increase was observed with respect to the $\delta^{18}O$ value (up to 0.51 ‰) soon after the earthquake along with a precursory increase of 0.38‰ in January 2016 before the earthquake. During these periods, there was no noticeable change in the hydrogen isotopic ratios. Rapid crustal deformation related to the earthquake may have enhanced the microfracturing of the aquifer rocks and the production of new surfaces, inducing $\delta^{18}O$ enrichment via oxygen isotopic exchange between rock and porewater without changing $\delta^{2}H$.

keywords: groundwater; earthquake precursors; hydrogen isotopes; oxygen isotopes; 2016 Kumamoto earthquake

2-10 *Engineering, Civil; Geosciences, Multidisciplinary; Water Resources*

Hydrogeological characteristics of groundwater and surface water associated with two small lake systems on King George Island, Antarctica

Kim, Jisun., Jeen, Sung-Wook., Lim, Hyoun Soo., Lee, Jeonghoon., **Kim, Ok-Sun.**, **Lee, Hyoungseok.** and **Hong, Soon Gyu.**

Journal of Hydrology. 2020. 590.

doi: 10.1016/j.jhydrol.2020.125537.

Although groundwater is an important component of the water cycle in the polar regions, groundwater in Antarctica has rarely been studied. This study evaluated the physical and chemical characteristics of groundwater, surface water, and snow in two lakes on the Barton Peninsula, King George Island, Antarctica, with a particular focus on groundwater. Influxes/outfluxes of groundwater were measured using seepage meters, and hydraulic conductivities were calculated based on grain size analysis for the sediments. A total of 41 water samples were used to determine the chemical compositions and isotopic ratios of oxygen and hydrogen. The groundwater fluxes measured in one lake (referred to as "Lake A") were -9.9 x 10^{-10} ~2.7 x 10^{-9} m/s (average of -9.1 x 10^{-10} ± 3.6 x 10^{-9} m/s) and in a second lake (referred to as "Lake B") were 2.2 x 10^{-9} ~3.0 x 10^{-9} m/s (average of 2.6 x 10^{-9} ± 4.0 x 10^{-10} m/s). This indicates that groundwater flux is highly dynamic in Lake A, whereas groundwater influx in Lake B is relatively stable. Hydraulic conductivity for the lake sediments ranged between 1.7 x 10^{-6} m/s and 2.1 x 10^{-4} m/s. Oxygen and hydrogen isotopic compositions followed the global meteoric water line (GMWL) and local meteoric water line (LMWL), indicating that groundwater and surface water in the study area originate from the atmosphere. Evaporation may not be an influential factor probably due to the relatively humid climate during the summer season in the study area. Groundwater and surface water might partially experience isotopic exchange fractionation during and after the snow melting process. The chemical composition of groundwater was distinguished from that of surface water and snow by higher concentrations of major anions (Cl, SO_4, and alkalinity), major cations (Ca, Mg, K, and Na), and trace elements (Si, Li, Sr, Mn, Zn, and Cu), resulting from water-rock interactions. To the best of our knowledge, this is the first study to directly measure groundwater fluxes in lake systems in Antarctica, and to evaluate the characteristics of groundwater in the Barton Peninsula. It may therefore serve as a basis for studying

the role of groundwater in the water cycle of Antarctica.

keywords: Water cycle; Antarctica; Lake; Hydraulic conductivity; Groundwater flux; Isotope

2-11 *Environmental Sciences; Geosciences, Multidisciplinary; Remote Sensing; Imaging Science & Photographic Technology*

Identification of Phyllosilicates in the Antarctic Environment Using ASTER Satellite Data: Case Study from the Mesa Range, Campbell and Priestley Glaciers, Northern Victoria Land

Pour, Amin Beiranvand., Sekandari, Milad., Rahmani, Omeid., Crispini, Laura., Laeufer, Andreas., **Park, Yongcheol.**, **Hong, Jong Kuk.** and 5 others.

Remote Sensing. 2021. 13(1).

doi: 10.3390/rs13010038.

In Antarctica, spectral mapping of altered minerals is very challenging due to the remoteness and inaccessibility of poorly exposed outcrops. This investigation evaluates the capability of Advanced Spaceborne Thermal Emission and Reflection Radiometer (ASTER) satellite remote sensing imagery for mapping and discrimination of phyllosilicate mineral groups in the Antarctic environment of northern Victoria Land. The Mixture-Tuned Matched-Filtering (MTMF) and Constrained Energy Minimization (CEM) algorithms were used to detect the sub-pixel abundance of Al-rich, Fe^{3+}-rich, Fe^{2+}-rich and Mg-rich phyllosilicates using the visible and near-infrared (VNIR), short-wave infrared (SWIR) and thermal-infrared (TIR) bands of ASTER. Results indicate that Al-rich phyllosilicates are strongly detected in the exposed outcrops of the Granite Harbour granitoids, Wilson Metamorphic Complex and the Beacon Supergroup. The presence of the smectite mineral group derived from the Jurassic basaltic rocks (Ferrar Dolerite and Kirkpatrick Basalts) by weathering and decomposition processes implicates Fe^{3+}-rich and Fe^{2+}-rich phyllosilicates. Biotite (Fe^{2+}-rich phyllosilicate) is detected associated with the Granite Harbour granitoids, Wilson Metamorphic Complex and Melbourne Volcanics. Mg-rich phyllosilicates are mostly mapped in the scree, glacial drift, moraine and crevasse fields derived from weathering and decomposition of the Kirkpatrick Basalt and Ferrar Dolerite. Chlorite (Mg-rich phyllosilicate) was generally mapped in the exposures of Granite Harbour granodiorite and granite and partially identified in the Ferrar Dolerite, the Kirkpatrick Basalt, the Priestley Formation and Priestley Schist and the scree, glacial drift and moraine. Statistical results indicate that Al-rich phyllosilicates class pixels are strongly discriminated, while the pixels attributed to Fe^{3+}-rich class, Fe^{2+}-rich and Mg-rich phyllosilicates classes contain some spectral mixing due to their subtle spectral differences in the VNIR+SWIR bands of ASTER. Results derived from TIR bands of ASTER show that a high level of confusion is associated with mafic phyllosilicates pixels (Fe^{3+}-rich, Fe^{2+}-rich and Mg-rich classes), whereas felsic phyllosilicates (Al-rich class) pixels are well mapped. Ground truth with detailed geological data, petrographic study and X-ray diffraction (XRD) analysis verified the remote sensing results. Consequently, ASTER image-map of phyllosilicate minerals is generated for the Mesa Range, Campbell and Priestley Glaciers, northern Victoria Land of Antarctica.

keywords: phyllosilicates; alteration; ASTER; Antarctic environments; mesa range; Priestley Glacier; northern Victoria Land; Antarctica

2-12 *Multidisciplinary Sciences*

The International Bathymetric Chart of the Arctic Ocean Version 4.0

Jakobsson, Martin., Mayer, Larry A., Bringensparr, Caroline., Castro, Carlos F., Mohammad, Rezwan., Johnson, Paul., Ketter, Tomer., Accettella, Daniela., Amblas, David., An, Lu., Arndt, Jan Erik., Canals, Miquel., Casamor, Jose Luis., Chauche, Nolwenn., Coakley, Bernard., Danielson, Seth., Demarte, Maurizio., Dickson, Mary-Lynn., Dorschel, Boris., Dowdeswell, Julian A., Dreutter, Simon., Fremand, Alice C., Gallant, Dana., Hall, John K., Hehemann, Laura., Hodnesdal, Hanne., **Hong, Jong Kuk.** and 25 others.

Scientific Data. 2020. 7(1).

doi: 10.1038/s41597-020-0520-9.

Bathymetry (seafloor depth), is a critical parameter providing the geospatial context for a multitude of marine scientific studies. Since 1997, the International Bathymetric Chart of the Arctic Ocean (IBCAO) has been the authoritative source of bathymetry for the Arctic Ocean. IBCAO has merged its efforts with the

Nippon Foundation-GEBCO-Seabed 2030 Project, with the goal of mapping all of the oceans by 2030. Here we present the latest version (IBCAO Ver. 4.0), with more than twice the resolution (200 x 200m versus 500 x 500m) and with individual depth soundings constraining three times more area of the Arctic Ocean (~19.8% versus 6.7%), than the previous IBCAO Ver. 3.0 released in 2012. Modern multibeam bathymetry comprises ~14.3% in Ver. 4.0 compared to ~5.4% in Ver. 3.0. Thus, the new IBCAO Ver. 4.0 has substantially more seafloor morphological information that offers new insights into a range of submarine features and processes; for example, the improved portrayal of Greenland fjords better serves predictive modelling of the fate of the Greenland Ice Sheet.

keywords: Arctic Ocean; Bathymetric Chart; IBCAO

2-13 *Geochemistry & Geophysics*

Melilite condensed from an ^{16}O-poor gaseous reservoir: Evidence from a fine-grained Ca-Al-rich inclusion of Northwest Africa 8613

Wada, Sohei., Kawasaki, Noriyuki., **Park, Changkun.** and Yurimoto, Hisayoshi.

Geochimica Et Cosmochimica Acta. 2020. 288: 161-175.

doi: 10.1016/j.gca.2020.08.004.

Fine-grained Ca-Al-rich inclusions (FGIs) in CV chondrites are suggested to be condensates from the solar nebular gas and thus captured O-isotopes from the gas. We conducted a combined study of petrographic observations and *in situ* O-isotope analysis using secondary ion mass spectrometry for an FGI, named HKD01, from the reduced CV chondrite Northwest Africa 8613. HKD01 has an irregular shape and petrographically three-layered structures: a hibonite-rich core, a spinel-rich core, and a mantle. Each petrographic domain contains melilite, hibonite, and spinel with variable proportions of those minerals. The O-isotopic compositions of the constituent minerals plotted along the slope-1 line on an O three-isotope diagram ranged between Δ^{17}O ~ -23‰ and 1‰. Hibonite and spinel are uniformly ^{16}O-rich (Δ^{17}O=-23‰) irrespective of their occurrences, while melilite crystals exhibit wide O-isotope variations ranging between Δ^{17}O ~ -23‰ and 1‰. The O-isotopic composition in a melilite crystal changes abruptly within ~2 μm, indicating that disturbances of O-isotopes in melilite after condensation are less than ~2 μm. Because the melilite in the FGI typically has grain sizes of 5-10 μm, the abrupt change of O-isotopic composition demonstrates that melilite crystals in the FGI preserve the O-isotopic composition of the nebular gas from which they condensed. In the mantle, aggregates of melilite crystals, having relatively large grain sizes (10-25 μm) and oscillatory chemical zoning, exhibit ^{16}O-poor compositions with small variations ranging between Δ^{17}O ~ -4 and 1‰. Among them, a large melilite crystal (~20 μm) with homogeneously ^{16}O-poor composition (Δ^{17}O ~ 0‰) across the single crystal was found. The coexistence of ^{16}O-poor and ^{16}O-rich melilite crystals without O-isotope disturbances in the FGI reveals that ^{16}O-poor (Δ^{17}O ~ 0‰) nebular gas existed in the formation region of the FGI HKD01 in addition to ^{16}O-rich (Δ^{17}O ~ -23‰) nebular gas.

keywords: Ca-Al-rich inclusions; Oxygen isotope; Al-Mg systematics; Early solar system; Secondary ion mass spectrometry

2-14 *Geochemistry & Geophysics; Mineralogy; Mining & Mineral Processing*

Microstructures and Fabric Transitions of Natural Ice from the Styx Glacier, Northern Victoria Land, Antarctica

Kim, Daeyeong., Prior, David J., **Han, Yeongcheol.**, Qi, Chao., Han, Hyangsun. and **Ju, Hyeon Tae.**

Minerals. 2020. 10(10).

doi: 10.3390/min10100892.

We investigated the microstructures of five ice core samples from the Styx Glacier, northern Victoria Land, Antarctica. Evidence of dynamic recrystallization was found in all samples: those at 50 m mainly by polygonization, and those at 170 m, largely by grain boundary migration. Crystallographic preferred orientations of all analyzed samples (view from the surface) typically showed a single cluster of *c*-axes normal to the surface. A girdle intersecting the single cluster occurs at 140-170 m with a tight cluster of *a*-axes normal to the girdle. We interpret the change of crystallographic preferred orientations (CPOs) at <140 m as relating to a combination of vertical compression, and shear on a horizontal plane, and the girdle CPOs at depths >140 m, as the result of

horizontal extension. Based on the data obtained from the ground penetrating radar, the underlying bedrock topography of a nunatak could have generated the extensional stress regime in the study area. The results imply changeable stress regimes that may occur during burial as a result of external kinematic controls, such as an appearance of a small peak in the bedrock.

keywords: Ice; microstructure; crystallographic preferred orientation (CPO); Styx Glacier; electron backscatter diffraction (EBSD)

2-15 *Paleontology*

New fossil woods from lower Cenozoic volcano-sedimentary rocks of the Fildes Peninsula, King George Island, and the implications for the trans-Antarctic Peninsula Eocene climatic gradient

Oh, Changhwan., Philippe, Marc., Mcloughlin, Stephen., **Woo**, **Jusun.**, Leppe, Marcelo., Torres, Teresa., **Park**, **Tae-Yoon S.** and **Choi**, **Han-Gu.**

Papers in Palaeontology. 2020. 6(1): 1-29.

doi: 10.1002/spp2.1256.

Ten embedded fossil logs sampled *in situ* from the middle Eocene volcano-sedimentary rocks close to Suffield Point in the Fildes Peninsula, King George Island, Antarctica, are assigned to *Protopodocarpoxylon araucarioides* Schultze-Motel *ex* Vogellehner, *Phyllocladoxylon antarcticum* Gothan, *Agathoxylon antarcticum* (Poole & Cantrill) Pujana *et al.*, *A. pseudoparenchymatosum* (Gothan) Pujana *et al.* and an unidentified angiosperm wood. Differences in the taxonomic representation and growth-ring characters of the Eocene woods on King George Island and coeval assemblages from Seymour Island, on the western and eastern sides of the Antarctic Peninsula respectively, are interpreted to result from environmental and climatic gradients across the Peninsula Orogen during the early Palaeogene. In particular, a precipitation gradient inferred across the Peninsula at that time might have been induced by a rain-shadow effect.

keywords: fossil woods; Eocene; Antarctica; growth-ring analysis; rainfall gradient; palaeoclimate

2-16 *Geosciences, Multidisciplinary*

Occurrence of active gas hydrate mounds in the southwestern slope of the Chukchi Plateau, Arctic Ocean

Kim, Young-Gyun., **Kim, Sookwan.**, Lee, Dong-Hun., **Lee, Yung Mi.**, **Kim, Hyoung Jun.**, **Kang, Seung-Goo.** and **Jin, Young Keun.**

Episodes. 2020. 43(2): 811-823.

doi: 10.18814/epiiugs/2020/020053.

This study documents the discovery of mound morphologies containing gas hydrate and methane-derived authigenic carbonate (MDAC) in the southwestern slope of the Chukchi Plateau, during the IBRV Araon expeditions in 2016 and 2018. A multibeam bathymetric surveying was the basis for a new and detailed rendering around the mounds. Sub-bottom profiles and site-targeted gravity cores were also collected across these mounds which were located at water depths between 780 m and 580 m. Mounds are characterized by a circular plan shape of hundreds of meters in width and tens of meters in height. Below the mounds, gas accumulation in the sediment produces acoustic blanking in seismic data. MDACs are identified along the core collected from the top of a mound structure, indicating past methane oxidation processes. Gas hydrate has also been observed at the bottom of the core. Reverse geothermal gradients of the mound support the idea of active presentday seepage. We argue that the prolonged seepage activity of methane-rich fluid, possibly related to the formation of the rifted North Chukchi Basin, has led to the formation of the gas hydrate mounds, named hereafter the Araon Mounds, in the vicinity of the basin margin.

2-17 *Geochemistry & Geophysics; Mineralogy; Mining & Mineral Processing*

Quantitative Analysis of Asbestos-Containing Materials Using Various Test Methods

Yang, Kiho., **Yoo**, **Kyu-Cheul.** and **Jung**, **Jaewoo.**

Minerals. 2020. 10(6).

doi: 10.3390/min10060568.

The advantages of X-ray powder diffraction (XRPD) analysis are its non-destructive nature, reliability, fast and easy sample preparation, and low costs. XRPD analysis has been used for mineral identification and the

quantitative/qualitative determination of various types of fibrous minerals in asbestos-containing materials (ACMs). In order to test the detection limit of ACMs by XRPDD, standard samples with various concentrations of ACMs (0.1%, 1%, and 3%) were fabricated using three matrix materials (talc, vermiculite, and sepiolite). Asbestiform tremolite and chrysotile were identified in the XRPD profiles of the samples with 1% and 3% ACMs. Their integral intensities were positively correlated with the concentrations. However, the XRPD peak of asbestos was not found in the samples with 0.1% ACMs. Therefore, scanning and transmission electron microscopy were utilized to investigate the samples with a very low concentration of ACMs. Although the ACM concentration (0.1%) was negligible and its direct observation was time-consuming, electron microscopy allowed for the detection of asbestos in several matrix materials. Thus, a combination of XRPD and electron microscopy improve analytical performance and data reliability.

keywords: asbestos; elongate mineral particles; quantitative analysis; mineral identification; powder X-ray diffraction; scanning electron microscopy; transmission electron microscopy

2-18 *Geography, Physical; Geosciences, Multidisciplinary*

Revealing the former bed of Thwaites Glacier using sea-floor bathymetry: implications for warm-water routing and bed controls on ice flow and buttressing

Hogan, Kelly A., Larter, Robert D., Graham, Alastair G. C., Arthern, Robert., Kirkham, James D., Minzoni, Rebecca Totten., Jordan, Tom A., Clark, Rachel., Fitzgerald, Victoria., Wahlin, Anna K., Anderson, John B., Hillenbrand, Claus-Dieter., Nitsche, Frank O., Simkins, Lauren., Smith, James A., Gohl, Karsten., Arndt, Jan Erik., **Hong, Jong Kuk.** and Wellner, Julia.

Cryosphere. 2020. 14(9): 2883-2908.

doi: 10.5194/tc-14-2883-2020.

The geometry of the sea floor immediately beyond Antarctica's marine-terminating glaciers is a fundamental control on warm-water routing, but it also describes former topographic pinning points that have been important for ice-shelf buttressing. Unfortunately, this information is often lacking due to the inaccessibility of these areas for survey, leading to modelled or interpolated bathymetries being used as boundary conditions in numerical modelling simulations. At Thwaites Glacier (TG) this critical data gap was addressed in 2019 during the first cruise of the International Thwaites Glacier Collaboration (ITGC) project. We present more than 2000 km^2 of new multibeam echo-sounder (MBES) data acquired in exceptional sea-ice conditions immediately offshore TG, and we update existing bathymetric compilations. The cross-sectional areas of sea-floor troughs are under-predicted by up to 40% or are not resolved at all where MBES data are missing, suggesting that calculations of trough capacity, and thus oceanic heat flux, may be significantly underestimated. Spatial variations in the morphology of topographic highs, known to be former pinning points for the floating ice shelf of TG, indicate differences in bed composition that are supported by landform evidence. We discuss links to ice dynamics for an overriding ice mass including a potential positive feedback mechanism where erosion of soft erodible highs may lead to ice-shelf ungrounding even with little or no ice thinning. Analyses of bed roughnesses and basal drag contributions show that the sea-floor bathymetry in front of TG is an analogue for extant bed areas. Ice flow over the sea-floor troughs and ridges would have been affected by similarly high basal drag to that acting at the grounding zone today. We conclude that more can certainly be gleaned from these 3D bathymetric datasets regarding the likely spatial variability of bed roughness and bed composition types underneath TG. This work also addresses the requirements of recent numerical ice-sheet and ocean modelling studies that have recognised the need for accurate and high-resolution bathymetry to determine warm-water routing to the grounding zone and, ultimately, for predicting glacier retreat behaviour.

keywords: Thwaites Glacier; bathymetry; grounding zone; warm-water routing

2-19 *Geochemistry & Geophysics*

Structure of type A CAI-like melts: A view from multi-nuclear NMR study of melilite ($Ca_2Al_2SiO_7$-$Ca_2MgSi_2O_7$) glasses

Park, Sun Young., **Park, Changkun.** and 3 others.

Chemical Geology. 2020. 558.

doi: 10.1016/j.chemgeo.2020.119894.

Exploring the polymerization and structural disorder of Ca-Al-rich inclusion (CAI)-like melts is a key question in cosmochemistry due to strong implications for macroscopic properties of melts (i.e., viscosity and diffusivity). Here, we report experimental results showing the effect of composition on the structure of melilite glasses and melts [åkermanite (Åk, $Ca_2MgSi_2O_7$) - gehlenite (Gh, $Ca_2Al_2SiO_7$)] in type A CAIs with varying composition using high-resolution solid-state nuclear magnetic resonance (NMR). The ^{27}Al magic angle spinning (MAS) and 3Q (triple quantum) MAS NMR spectra of melilite glasses show predominant $^{[4]}Al$. A non-negligible fraction of $^{[5]}Al$ is observed in $Åk_{50}Gh_{50}$ and $Åk_{72}Gh_{28}$ glasses and it slightly increases with increasing åkermanite content. The ^{17}O 3QMAS NMR spectra of melilite glasses show that bridging oxygens (BOs, Si-O-Si, Al-O-Al, and Si-O-Al) and non-bridging oxygens (NBOs, Ca-O-Si, Ca-O-Al, and mixed {Ca, Mg}-NBO) are partially resolved. Despite the strong preference of Si over Al for NBOs, for the first time, Ca-O-Al is observed in natural melts (i.e., gehlenite and $Åk_{25}Gh_{75}$ glasses and melts). The results show that Al-NBO (~150 ppm in MAS dimension) can be distinguished from Si-NBO (~110 ppm) in melilite glasses and melts. The fraction of NBO increases with increasing åkermanite content. The experimental results suggest that composition-induced structural changes should be considered to interpret the melt viscosity, diffusivity, and oxygen isotopic composition of CAI-like melts in the early Solar System.

keywords: Melilite glasses and melts; Structure and disorder; High-resolution solid-state nuclear magnetic resonance; Viscosity and diffusivity

2-20 *Multidisciplinary Sciences*

Subnanosecond phase transition dynamics in laser-shocked iron

Hwang, H., Galtier, E., Cynn, H., Eom, I., Chun, S. H., Bang, Y., Hwang, G. C., Choi, J., Kim, T., Kong, M., Kwon, S., Kang, K., Lee, H. J., **Park, Changkun.**, **Lee, Jong Ik.** and 15 others.

Science Advances. 2020. 6(23).

doi: 10.1126/sciadv.aaz5132.

Iron is one of the most studied chemical elements due to its sociotechnological and planetary importance; hence, understanding its structural transition dynamics is of vital interest. By combining a short pulse optical laser and an ultrashort free electron laser pulse, we have observed the subnanosecond structural dynamics of iron from high-quality x-ray diffraction data measured at 50-ps intervals up to 2500 ps. We unequivocally identify a three-wave structure during the initial compression and a two-wave structure during the decaying shock, involving all of the known structural types of iron (α-, γ-, and ε-phase). In the final stage, negative lattice pressures are generated by the propagation of rarefaction waves, leading to the formation of expanded phases and the recovery of γ-phase. Our observations demonstrate the unique capability of measuring the atomistic evolution during the entire lattice compression and release processes at unprecedented time and strain rate.

keywords: iron; laser-shocked; phase transition; Subnanosecond

2-21

Time-Lapse Electrical Resistivity Structures for the Active Layer of Permafrost Terrain at the King Sejong Station: Correlation Interpretation with Vegetation and Meteorological Data

Kim, Kwansoo., **Lee, Joohan.**, Lee, Eungsang., **Ju, Hyeon Tae.**, **Hyun, Chang-Uk.**, **Park, Sang-Jong.**, **Kim, Ok-Sun.** and 2 others

Economic and Environmental Geology. 2020. 53(4): 413-423.

doi: 10.9719/EEG.2020.53.4.413.

Over the wide area, King Sejong Station and the nearby land are uncovered with snow and ice conditions. Therefore, the active layer on the permafrost has been formed to be much thicker than the other Antarctica region. Electrical resistivity survey of Wenner and dipole-dipole arrays was undertaken at a series of time in the freezing season at the King Sejong Station to delineate subsurface structure and to monitor active layer in permafrost terrain. Time-lapse resistivity structures are well in terms of the vegetation distribution, ground surface temperature, and snow depth. Horizontal high resistivity belt(>1826 Ωm) at very shallow depth is thickening with the lapse of time, probably caused by the freezing of the water in the pore spaces with decrease of ground

temperature. Subsurface structures for the area of low snow-cover and vegetated zone area are comprised of 0~0.5 m deep high-resistive gravel-rich soil, 0.5~3 m deep low-resistive active layer, and the underlying permafrost. In contrast, the unvegetated area and high snow-buildup is characterized with high resistivities larger than approximately 2000 Ωm due to freezing of the soil throughout the year. Data interpretation and correlation schemes explored in this paper can be applied to confirm the active layer, which is expected to get thinner in additional survey during the thawing season.

keywords: time-lapse electrical resistivity; active layer; permafrost; King Sejong Station; ground temperature

2-22 *Geochemistry & Geophysics; Mineralogy; Mining & Mineral Processing*

Timing and Metamorphic Evolution of the Ross Orogeny in and around the Mountaineer Range, Northern Victoria Land, Antarctica

Yi, Sang-Bong., **Lee, Mi Jung.**, **Lee, Jong Ik.** and **Kim, Hwayoung.**

Minerals. 2020. 10(10).

doi: 10.3390/min10100908.

The Ross(-Delamerian) Orogeny significantly impacted the formation of the tectonic structure of the Pacific Gondwana margin during the early Paleozoic era. Northern Victoria Land (NVL) in Antarctica preserves the aspect of the Ross Orogeny that led to the union of the Wilson (WT)-Bowers (BT)-Robertson Bay Terrane. The aspect of the Ross Orogeny in the NVL is characterized by subduction of oceanic domains toward the continental margin (continental arc) and the accretion of the associated marine-continental substances from 530-480 Ma. In the Mountaineer Range in NVL, the Ross Orogeny strain zone is identified at the WT/BT boundary regions. In these areas, fold and thrust shear zones are observed and aspects of them can be seen at Mt. Murchison, the Descent Unit and the Black Spider Greenschist zone. The Dessent Unit corresponds to a tectonic slice sheared between the WT and BT. The metamorphic evolution phase of the Dessent Unit is summarized in the peak pressure (M_1), peak temperature (M_2) and retrograde (M_3). The sensitive high-resolution ion microprobe (SHRIMP) zircon U-Pb ages of 514.6 ± 2.0 Ma and 499.2 ± 3.4 Ma obtained from the Dessent Unit amphibolite are comparable to the M_1 and M_2 stages, respectively. The Dessent Unit underwent intermediate pressure (P)/temperature (T)-type metamorphism characterized by 10.0-10.5 kbar/~600°C (M_1) and ~7 kbar/~700°C (M_2) followed by 4.0-4.5 kbar/~450°C (M_3). Mafic to intermediate magmatism (497-501 Ma) within the WT/BT boundary region may have given rise to the M_2 stage of the Dessent Unit, and this magmatism is synchronous with the migmatization period of Mt. Murchison (498.3 ± 3.4 Ma). This indicates that a continuous process of fold-shearing-magmatic intrusion-partial melting, which is typically associated with a continental arc orogeny, occurred before and after c. 500 Ma in the Mountaineer Range. During the Ross Orogeny, the Dessent unit was initially subducted underneath the WT at depth (10.0-10.5 kbar, ~35 km) and then thrust into the shallow (~7 kbar, ~23 km), hot (≥700°C) magmatic arc docking with the Mt. Murchison terrain, where migmatization prevailed.

keywords: Antarctica; Gondwana margin; Ross Orogeny; Northern Victoria Land; Dessent Unit; tectonic slice

2-23 *Chemistry, Analytical*

Two-point normalization for reducing inter-laboratory discrepancies in $\delta^{17}O$, $\delta^{18}O$, and $\Delta'^{17}O$ of reference silicates

Kim, Nak Kyu., **Park, Changkun.** and Kusakabe, Minoru.

Journal of Analytical Science and Technology. 2020. 11(1).

doi: 10.1186/s40543-020-00248-0.

The $\delta^{17}O$ and $\delta^{18}O$ values of a number of terrestrial minerals and rocks have been determined using laser fluorination method worldwide. For the comprehensive and congruous interpretation of oxygen isotope data, the δ-values should be normalized by the two-point method (i.e., the VSMOW-SLAP scale) to eliminate inter-laboratory bias. In this study, the $\delta^{17}O$ and $\delta^{18}O$ values of VSMOW and SLAP were measured to calibrate our laboratory working standard O_2 gas. The O_2 gas liberated from the water samples was purified using the preparation line normally employed for solid samples, and analyzed by the same mass spectrometer. From the analyses of VSMOW and SLAP, the oxygen isotope compositions of the international silicate

standards (UWG2 garnet, NBS28 quartz, and San Carlos olivine) were normalized to the VSMOW-SLAP scale (two-point calibration), and then the $\Delta'^{17}O$ values were determined. Using the δ-values obtained in this way, the inter-laboratory discrepancy of the $\delta^{17}O$ and $\delta^{18}O$ results of the silicate standards could be reduced. The VSMOW-SLAP scaling for $\delta^{17}O$ and $\delta^{18}O$ analysis of silicates provides the most effective way to obtain accurate and precise data. In reporting the $\Delta'^{17}O$ values, it is important to make the choice of the reference fractionation line into account because the $\Delta'^{17}O$ value is quite variable owing to the slope and y-intercept of the linear relation of the delta-values. The reference fractionation line obtained from the measurement of the low- and high- $\delta^{18}O$ reference silicates would help to compare $\Delta'^{17}O$ values. We confirmed that the $\Delta'^{17}O$ results of the international silicate standards based on the two-point silicate reference line were consistent with the results from other laboratories.

keywords: Oxygen three isotope; Silicates; VSMOW-SLAP scaling; Inter-laboratory comparison; $\Delta'^{17}O$

2-24 *Energy & Fuels; Engineering, Chemical*

Upwarding gas source and postgenetic processes in the shallow sediments from the ARAON Mounds, Chukchi Sea

Kim, Ji-Hoon., Hachikubo, Akihiro., Kida, Masato., Minami, Hirotsugu., Lee, Dong-Hun., **Jin, Young Keun.**, Ryu, Jong-Sik., **Lee, Yung Mi.**, Hur, Jin., Park, Myong-Ho., Kim, Young-Gyun., Kang, Moo-Hee., Park, Sanghee., Chen, Meilian., **Kang, Seung-Goo.** and **Kim, Sookwan.**

Journal of Natural Gas Science and Engineering. 2020. 76.
doi: 10.1016/j.jngse.2020.103223.

The methane (CH_4) emission from the Arctic Ocean is crucial to understand global carbon cycle. Here, we investigated sulfate (SO_4^{2-}) in pore water and compositional and isotopic gas signatures at ARAON Mounds (hydrate/nonhydrate-bearing sites) and background site in the Chukchi Sea. Sulfate-methane transition (SMT) did not reach at the background site but occurred at shallow depths (≤ 3.3 m below the seafloor) at all ARAON Mounds sites. The SO_4^{2-} profiles at ARAON Mounds also clearly indicate the unsteady state due to upward gas migration by high flux at the hydrate-bearing sites compared to the nonhydrate-bearing sites. The isotopic signatures of gas samples at the hydrate-bearing sites and below the SMT at the nonhydrate-bearing sites reflect thermogenic source transported across at least 1 km through faults/fractures in the Chukchi Sea. The headspace (HS) gas samples above/near the SMT at the nonhydrate-bearing sites are affected by the biogenic CH_4 with enriched ^{12}C; they indicate biogenic or thermogenic/biogenic mixed sources. The thermogenic gases below the SMT at ARAON Mounds have high C1/C2+ ratios (>300), much higher than those of normal thermogenic gases in offshore shallow sediments (<100), due to postgenetic processes during migration. The carbon isotopic fractionation ($\varepsilon_c = \delta^{13}C_{CO2} - \delta^{13}C_{CH4}$) in HS samples of the background site and ARAON Mounds above the SMT are consistent with the biogenic gas range generated via microbial CO_2 reduction. However, ε_c below the SMT is anomalously low (13-42‰) and is higher at the hydrate-bearing sites than at the nonhydrate-bearing sites. We postulate that this low ε_c is explained by the two-phase fluid transport model of Kim et al. (2012) and that gas hydrates highly influence this value. We suggest that ε_c can be used as a powerful geochemical proxy for the upward gas migration and gas hydrate occurrence in shallow marine sediment systems.

keywords: Arctic Ocean; ARAON Mounds; Thermogenic gas; Upward gas migration; Carbon isotopic fractionation

2-25 *Geochemistry & Geophysics*

Variations in initial Al-26/Al-27 ratios among fine-grained Ca-Al-rich inclusions from reduced CV chondrites

Kawasaki, Noriyuki., Wada, Sohei., **Park, Changkun.** and 2 others.

Geochimica Et Cosmochimica Acta. 2020. 279: 1-15.
doi: 10.1016/j.gca.2020.03.045.

Fine-grained Ca-Al-rich inclusions (FGIs) in CV chondrites are suggested to be condensates formed directly from the solar nebular gas. Al-Mg mineral isochrons of seven FGIs from reduced CV chondrites Efremovka, Vigarano, Thiel Mountains 07007, and Northwest Africa 8613 were obtained via *in situ* Al-Mg isotope measurements using secondary ion mass spectrometry. The slopes of the mineral isochrons for seven FGIs exhibit statistically significant variations in initial $^{26}Al/^{27}Al$ ratios, $(^{26}Al/^{27}Al)_0$, ranging from

(5.19 ± 0.17) to $(3.35 \pm 0.21) \times 10^{-5}$, which correspond to a relative age spread of 0.44 ± 0.07 Myr. Inferred upper limit of $(^{26}Al/^{27}Al)_0$ for the FGIs is identical to the Solar System $(^{26}Al/^{27}Al)_0$ of ~5.2×10^{-5} as determined by whole-rock Al-Mg isochron studies for CAIs in CV chondrites. The intercepts of the mineral isochrons, the initial $^{26}Mg/^{24}Mg$ ratios the FGIs formed with, are consistent with Mg-isotope evolution path of a solar-composition nebular gas. The observed variations in $(^{26}Al/^{27}Al)_0$ for FGIs are essentially similar to those (~5.2 to ~4.2×10^{-5}) for coarse-grained, igneous CAIs of CV chondrites that are formed by melting and solidification. If ^{26}Al was distributed homogeneously in the forming region, then our data indicate that thermal processes of condensation and melting for CAI formation occurred contemporaneously and continued for at least ~0.4 Myr at the very beginning of the Solar System. Alternatively, the observed variations in $(^{26}Al/^{27}Al)_0$ also indicate the possibility of heterogeneous distributions of ^{26}Al in the forming region, corresponding to a range of over at least $3.4 \times 10^{-5} < (^{26}Al/^{27}Al)_0 < 5.2 \times 10^{-5}$.

keywords: Ca-Al-rich inclusions; Al-Mg systematics; Secondary ion mass spectrometry; Early Solar System

PART 3

Marine Sciences

3-1 *Environmental Sciences; Marine & Freshwater Biology*

Acoustic Detection of Krill Scattering Layer in the Terra Nova Bay Polynya, Antarctica

Kang, Myounghee., Fajaryanti, Rina., **Son, Wuju.**, **Kim, Jeong-Hoon.** and **La, Hyoung Sul.**

Frontiers in Marine Science. 2020. 7.

doi: 10.3389/fmars.2020.584550.

Krill play a crucial role in the transfer of energy in the marine food web, connecting primary producers and the upper trophic levels in the Terra Nova Bay polynya (TNBP), which is part of the Ross Sea marine protected area. Despite the substantial ecological importance of krill, there are few studies on their distribution and abundance in the TNBP. An acoustic survey was conducted on 7-14 January 2019 in the TNBP, Ross Sea, using a Simrad EK60 echosounder (38 and 120 kHz) aboard the icebreaker RV Araon. The most commonly used range of the difference of the mean volume backscattering strength (MVBS) (2-16 dB) was applied to distinguish krill. The acoustic data (120 kHz) were extracted to examine the krill distribution characteristics. The study area was divided into low-value areas and high-value areas based on the third quartile of the nautical area scattering coefficient. The results showed that the krill aggregations were distributed in three layers at depths of 0-30 m, 70-110 m, and 270-300 m. The interpolated environmental parameters associated with the backscattering strength were compared. High-value areas of krill coincided with relatively low temperature, low salinity, and high chlorophyll, although very weak correlations were found. The primary goal of this study was to understand the vertical and horizontal distributions of krill acoustic biomass and to relate the observed patterns to the dominant environmental conditions.

keywords: krill; scattering layers; spatial distribution; Terra Nova Bay polynya; Antarctica; environmental attributes

3-2

Addressing Arctic Challenges Requires a Comprehensive Ocean Survey

Paasche, O., Olsen, A., Arthun, M., Anderson, L.G., Wangberg, S., Ashjian, C.J., Grebmeier, J.M., Kikuchi, T., Nishino, S., Yasunaka, S., **Kang, Sung-Ho.**, **Cho, Kyoung-Ho.** and 8 others.

Eos: Earth and Space Science News. 2020. 101(1):13-15

doi: 10.1029/2019EO136200.

A coordinated, multinational pan-Arctic Ocean research effort using icebreakers and research ships is scheduled to become a reality in 2020 and 2021. The effort to answer these and other scientific questions will benefit our understanding of how the Arctic Ocean operates and will also help foster the next generation of Arctic researchers. Ultimately, we must know how the Arctic system functions to assess risks and to develop policies that allow effective management.

keywords: International collaboration; Synoptic Arctic Survey; pan-Arctic Ocean Research

3-3

Assessment of Organic Matter Sources in the Singil Stream Flowing into Lake Shihwa, South Korea

Kim, Dahae., **Kim, Jung-Hyun.** and 3 others.

Korean Journal of Ecology and Environment. 2020. 53(2):138-147

doi: 10.11614/KSL.2020.53.2.138.

The Singil Stream, flowing into an artificial lake, Lake Shihwa (South Korea), experiences a strong anthropogenic pressure with continuous organic matter (OM) inputs from rural, urban, and industrial areas. In this study, we investigated suspended particulate matter (SPM) and streambed sediments collected along the Singil Stream in 2014 and 2016, by applying a dual element approach ($\delta^{13}C$ and $\delta^{15}N$) to identify OM sources. The SPM and streambed sediment samples from the indusrial area showed higher organic carbon and nitrogen concentrations (or contents) than those from the other areas, with distinctively lower $\delta^{15}N$ values. Accordingly, our dual element approach indicates that the industrial area was the predominant OM source influencing OM quality and thus water quality of the Singil Stream flowing into Lake Shihwa during the study periods. However, further studies are necessary to better constrain OM sources in the Singil Stream since OM sources from the industrial area appear to be complex.

keywords: Lake Shihwa; Singil Stream; Stable carbono isotope; Stable nitrogen isotope

3-4 *Oceanography*

Atmospheric dimethyl sulfide and its significant influence on the sea-to-air flux calculation over the Southern Ocean

Zhang, Miming., **Park, Ki-Tae.**, Yan, Jinpei., **Park, Keyhong.**, Wu, Yanfang., **Jang, Eunho.** and 4 others.

Progress in Oceanography. 2020. 186.

doi: 10.1016/j.pocean.2020.102392.

Our understanding about the atmospheric dimethyl sulfide (DMS) and its influence to sea-to-air flux calculation in the Southern Ocean is still limited due to insufficient investigations. Herein, high-resolution shipboard underway simultaneous surface seawater and atmospheric DMS measurements were conducted in the Southern Ocean from February 23 to March 31, 2018. A larger variation of DMS levels was found in atmosphere compared with that in seawater. Remarkably, a large-scale area with high seawater and atmospheric DMS concentrations up to 27.9 nM and 3.92 ppbv, respectively, was investigated outside of Ross Sea sector. Atmospheric DMS levels were strongly impacted by wind speed and air mass convection. The relationship between atmospheric DMS and air mass exposure to oceanic chlorophyll varied greatly depending on the area of investigation. Some other regions with high DMS production capacity were examined as well beside those along the cruise tracks based on the results of positive correlations with high slopes and back trajectories. Moreover, significant uncertainty of sea-to-air DMS flux over the Southern Ocean could be caused by follows: (1) the selecting of different gas transfer coefficients; (2) the negative flux values calculated under high atmospheric DMS levels together with low seawater DMS concentrations; and (3) the greatly overestimated flux, approximately 47.1-76.9%, without considering the atmospheric DMS. This study highlights the urgent demand of high-resolution

observations of atmospheric DMS over the Southern Ocean to estimate DMS emission with high accuracy.

keywords: Dimethyl sulfide; Southern Ocean; Atmospheric DMS; Seawater DMS; DMS sea-to-air flux

3-5 *Geography*, *Physical; Geosciences*, *Multidisciplinary*

Carbon and nitrogen uptake rates and macromolecular compositions of bottom-ice algae and phytoplankton at Cambridge Bay in Dease Strait, Canada

Kim, Kwanwoo., **Ha, Sun-Yong.**, **Kim, Bo Kyung.** and 4 others.

Annals of Glaciology. 2020. 61(82): 106-116.

doi: 10.1017/aog.2020.17.

Our understanding of ice algal responses to the recent changes in Arctic sea ice is impeded by limited field observations. In the present study, environmental characteristics of the landfast sea-ice zone as well as primary production and macromolecular composition of ice algae and phytoplankton were studied in the Kitikmeot Sea near Cambridge Bay in spring 2017. Averaged total chlorophyll-*a* (Chl- *a*) concentration was within the lower range reported previously for the same region, while daily carbon uptake rates of bottom-ice algae were significantly lower in this study than previously reported for the Arctic. Based on various indicators, the region's low nutrient concentrations appear to limit carbon uptake rates and associated accumulation of bottom-ice algal biomass. Furthermore, the lipids-dominant biochemical composition of bottom-ice algae suggests strong nutrient limitation relative to the distinctly different carbohydrates-dominant composition of phytoplankton. Together, the results confirm strong nitrate limitation of the local marine system.

keywords: Biochemical compositions; bottom-ice algae; Cambridge Bay; phytoplankton

3-6 *Environmental Sciences; Meteorology & Atmospheric Sciences*

Characteristics of methanesulfonic acid, non-sea-salt sulfate and organic carbon aerosols over the Amundsen Sea, Antarctica

Jung, Jinyoung., **Hong, Sang-Bum.**, Chen, Meilian., Hur, Jin., Jiao, Liping., **Lee, Youngju.**, **Park, Keyhong.**, Hahm, Doshik., **Choi, Jung-Ok.**, **Yang, Eun Jin.**, **Park, Jisoo.**, **Kim, Tae-Wan.** and **Lee, SangHoon.**

Atmospheric Chemistry and Physics. 2020. 20(9): 5405-5424.

doi: 10.5194/acp-20-5405-2020.

To investigate the characteristics of particulate methanesulfonic acid ($MSA_{(p)}$), non-sea-salt sulfate (nss SO_4^{2-}) and organic carbon (OC) aerosols, aerosol and seawater samples were collected over the Southern Ocean (43-70°S) and the Amundsen Sea (70-75°S) during the ANA06B cruise conducted in the austral summer of 2016 aboard the Korean icebreaker IBR/V *Araon*. Over the Southern Ocean, the atmospheric $MSA_{(p)}$ concentration was low (0.10±0.002 μg m^{-3}), whereas its concentration increased sharply up to 0.57 μg m^{-3} in the Amundsen Sea where *Phaeocystis antarctica* (*P. antarctica*), a producer of dimethylsulfide (DMS), was the dominant phytoplankton species. Unlike $MSA_{(p)}$, the mean nss SO_4^{2-} concentration in the Amundsen Sea was comparable to that in the Southern Ocean. Water-soluble organic carbon (WSOC) concentrations over the Southern Ocean and the Amundsen Sea varied from 0.048 to 0.16 and 0.070 to 0.18 μgCm^{-3}, with averages of 0.087±0.038 and 0.097±0.038 μgCm^{-3}, respectively. For water-insoluble organic carbon (WIOC), its mean concentrations over the Southern Ocean and the Amundsen Sea were 0.25±0.13 and 0.26±0.10 μgCm^{-3}, varying from 0.083 to 0.49 and 0.12 to 0.38 μgCm^{-3}, respectively. WIOC was the dominant organic carbon species in both the Southern Ocean and the Amundsen Sea, accounting for 73 %-75 % of the total aerosol organic carbon. WSOC/Na^+ and WIOC/Na^+ ratios in the fine-mode aerosol particles were higher, especially in the Amundsen Sea where biological productivity was much higher than the Southern Ocean. The fluorescence properties of water-soluble organic aerosols investigated using a fluorescence excitation-emission matrix coupled with parallel factor analysis (EEM-PARAFAC) revealed that protein-like components were dominant in our marine aerosol samples, representing 69 %-91 % of the total intensity. Protein-like components also showed a significant positive relationship with the relative biomass of diatoms; however, they were negatively correlated with the relative biomass of *P. antarctica*. These results suggest that the protein-like component is most likely produced as a result of biological processes of diatoms in the Amundsen Sea.

3-7 *Environmental Sciences; Water Resources*

Characteristics of the Biochemical Composition and Bioavailability of Phytoplankton-Derived Particulate Organic Matter in the Chukchi Sea, Arctic

Kim, Bo Kyung., **Jung, Jinyoung.**, **Lee, Youngju.**, **Cho, Kyoung-Ho.**, **Gal, Jong-Ku.**, **Kang, Sung-Ho.** and **Ha, Sun-Yong.**

Water. 2020. 12(9).

doi: 10.3390/w12092355.

Analysis of the biochemical composition (carbohydrates, CHO; proteins, PRT; lipids, LIP) of particulate organic matter (POM, mainly phytoplankton) is used to assess trophic states, and the quantity of food material is generally assessed to determine bioavailability; however, bioavailability is reduced or changed by enzymatic hydrolysis. Here, we investigated the current trophic state and bioavailability of phytoplankton in the Chukchi Sea (including the Chukchi Borderland) during the summer of 2017. Based on a cluster analysis, our 12 stations were divided into three groups: the southern, middle, and northern parts of the Chukchi Sea. A principal component analysis (PCA) revealed that relatively nutrient-rich and high-temperature waters in the southern part of the Chukchi Sea enhanced the microphytoplankton biomass, while picophytoplankton were linked to a high contribution of meltwater derived from sea ice melting in the northern part of the sea. The total PRT accounted for 41.8% (±7.5%) of the POM in the southern part of the sea, and this contribution was higher than those in the middle (26.5±7.5%) and northern (26.5±10.6%) parts, whereas the CHO accounted for more than half of the total POM in the northern parts. As determined by enzymatic hydrolysis, LIP were more rapidly mineralized in the southern part of the Chukchi Sea, whereas CHO were largely used as source of energy for higher trophic levels in the northern part of the Chukchi Sea. Specifically, the bioavailable fraction of POM in the northern part of the Chukchi Sea was higher than it was in the other parts. The findings indicate that increasing meltwater and a low nutrient supply lead to smaller cell sizes of phytoplankton and their taxa (flagellate and green algae) with more CHO and a negative effect on the total concentration of POM. However, in terms of bioavailability (food utilization), which determines the rate at which digested food is used by consumers, potentially available food could have positive effects on ecosystem functioning.

keywords: particulate organic matter; biochemical composition; phytoplankton; Chukchi Sea; Arctic Ocean

3-8 *Microbiology*

Contrasting Community Composition of Active Microbial Eukaryotes in Melt Ponds and Sea Water of the Arctic Ocean Revealed by High Throughput Sequencing

Xu, Dapeng., Kong, Hejun., **Yang, Eun Jin.**, Li, Xinran., Jiao, Nianzhi., Warren, Alan., Wang, Ying., **Lee, Youngju.**, **Jung, Jinyoung.** and **Kang, Sung-Ho.**

Frontiers in Microbiology. 2020. 11.

doi: 10.3389/fmicb.2020.01170.

Melt ponds (MPs), form as the result of thawing of snow and sea ice in the summer, have lower albedo than the sea ice and are thus partly responsible for the polar amplification of global warming. Knowing the community composition of MP organisms is key to understanding their roles in the biogeochemical cycles of nutrients and elements. However, the community composition of MP microbial eukaryotes has rarely been studied. In the present study, we assessed the microbial eukaryote biodiversity, community composition, and assembly processes in MPs and surface sea water (SW) using high throughput sequencing of 18S rRNA of size-fractionated samples. Alpha diversity estimates were lower in the MPs than SW across all size fractions. The community composition of MPs was significantly different from that of SW. The MP communities were dominated by members from Chrysophyceae, the ciliate classes Litostomatea and Spirotrichea, and the cercozoan groups Filosa-Thecofilosea. One open MP community was similar to SW communities, which was probably due to the advanced stage of development of the MP enabling the exchange of species between it and adjacent SW. High portions of shared species between MPs and SW may indicate the vigorous exchange of species between these two major types of environments in the Arctic Ocean. SW microbial eukaryote communities are mainly controlled by dispersal limitation whereas those of MP are mainly controlled by ecological drift.

keywords: assembly mechanism; community structure; diversity; high throughput cDNA sequencing; protist; 18S rRNA

3-9 *Environmental Sciences*

Effect of sea ice retreat on marine aerosol emissions in the Southern Ocean, Antarctica

Yan, Jinpei., **Jung, Jinyoung.** and 4 others.

Science of the Total Environment. 2020. 745.

doi: 10.1016/j.scitotenv.2020.140773.

Sea ice retreat in the polar region is expected to increase the emissions of sea salt aerosols and biogenic gases, which may significantly impact the climate by increasing cloud condensation nuclei (CCN) population and changing solar radiation. In this study, aerosol compositions were measured at high-time-resolution (1 h) with an in-situ gas and aerosol composition monitoring system in polynya regions of the Southern Ocean (SO) to access the effects of sea ice concentrations on the sea salt aerosol (SSA) and secondary biogenic aerosol (SBA) in the SO. SSA emissions increased by more than 30% as sea ice concentration decreased from 85% to 29%. However, SSA emissions did not increase monotonically as the sea ice concentration decreased. The highest SSA concentration occurred in drifting sea ice region. Sea ice melting increased SBA concentrations by enhancing the air-sea exchanges of SBA precursor gases and the release of algae from sea ice. Positive correlations between SSA and wind speed were present in different sea ice regions, while SBA didn't reveal an obvious correlation with wind speed in the SO. The impact of wind speed on the SSA emissions were very different, Higher slope value of 41.83 and 35.81 were present in the DSI and SIP region, while the value was only about 16.74 in the SIC region. The results extended the knowledge of the effect of future sea ice retreat on marine aerosol emissions and potential climate changes in the polar region.

keywords: Sea ice; Sea salt aerosols; Methane sulfonic acid (MSA); Nss-SO_{4}-; Climate

3-10 *Engineering, Marine; Engineering, Ocean; Oceanography*

Effects of Low pH and Low Salinity Induced by Meltwater Inflow on the Behavior and Physical Condition of the Antarctic Limpet, *Nacella concinna*

Sin, Eunchong., **Ahn, In-Young.** and 2 others.

Journal of Marine Science and Engineering. 2020. 8(10).

doi: 10.3390/jmse8100822.

Seawater acidification and freshening in the intertidal zone of Marian Cove, Antarctica, which occurs by the freshwater inflow from snow fields and glaciers, could affect the physiology and behavior of intertidal marine organisms. In this study, we exposed Antarctic limpets, *Nacella concinna*, to two different pH (8.00 and 7.55) and salinity (34.0 and 27.0 psu) levels and measured their righting ability after being flipped over, mortality, condition factor, and shell dissolution. During the 35-day exposure, there was no significant difference in behavior and mortality between different treatments. However, the condition factor was negatively affected by low salinity. Both low pH and low salinity negatively influenced shell formation by decreasing the aragonite saturation state (Ω_{arg}) and enhancing shell dissolution. Our results suggest that, though limpets can tolerate short-term low pH and salinity conditions, intrusions of meltwater accompanied by the glacial retreat may act as a serious threat to the population of *N. concinna*.

keywords: ocean acidification; glacial retreat; meltwater; *Nacella concinna*; Marian Cove; shell dissolution

3-11 *Oceanography*

Effects of Nitrogen Limitation on Phytoplankton Physiology in the Western Arctic Ocean in Summer

Ko, Eunho., Gorbunov, Maxim Y., **Jung, Jinyoung.**, **Joo, Hyoung Min.**, **Lee, Youngju**., **Cho, Kyoung-Ho.**, **Yang, Eun Jin.**, **Kang, Sung-Ho.** and **Park, Jisoo.**

Journal of Geophysical Research-Oceans. 2020. 125(11).

doi: 10.1029/2020jc016501.

Phytoplankton in the Arctic Ocean are subject to nitrogen limitation in the summer, however, how severely the nitrogen stress affects phytoplankton physiology remains largely unknown. In the summers of 2015-2018, we examined the distribution of phytoplankton photophysiological properties across two contrasting regions of the Arctic Ocean with

distinctly different levels of nitrogen availability in the upper water column. We quantified the extent of nitrogen stress using a highly sensitive fluorescence induction and relaxation system to obtain continuous underway measurements and via discrete sample analyses of phytoplankton physiology, as well as nutrient enrichment incubations. The results revealed vast regions in the Chukchi Sea where phytoplankton photosynthesis was severely nitrogen-stressed. Thereby, the maximum quantum yield of photochemistry in photosystem II showed only a small decrease (12 ± 9%) relative to its nutrient-replete values, while the maximum photosynthetic electron transport rates under saturating irradiance were impaired to a greater extent (40 ± 17%). This phytoplankton photosynthesis response is indicative of a severe nitrogen limitation, which results in dramatic reduction in growth and net primary production rates. Nutrient enrichment incubations also revealed a marked increase in large-size phytoplankton growth (>10 μm) after the nitrogen stress was alleviated, suggesting that the larger cells were more susceptible to nitrogen stress. These results are important for understanding how regional nitrogen fluxes control variability in the primary production and phytoplankton community structure and how these processes might change with rapid climate changes in the Arctic Ocean.

keywords: phytoplankton photophysiology; nitrogen limitation; variable fluorescence; maximum electron transfer rate; the western Arctic Ocean

3-12 *Engineering, Marine; Engineering, Ocean; Oceanography*

The Effects of Ocean Acidification and Warming on Growth of a Natural Community of Coastal Phytoplankton

Hyun, Bonggil., Kim, Ja-Myung., Jang, Pung-Guk., Jang, Min-Chul., Choi, Keun-Hyung., Lee, Kitack., **Yang, Eun Jin.** and 2 others.

Journal of Marine Science and Engineering. 2020. 8(10).

doi: 10.3390/jmse8100821.

An in situ mesocosm experiment was performed to investigate the combined effects of ocean acidification and warming on the coastal phytoplankton standing stock and species composition of a eutrophic coastal area in the temperate-subtropical region. Experimental treatments of natural seawater included three CO_2 and two temperature conditions (present control: ~400 μatm CO_2 and ambient temperature, acidification conditions: ~900 μatm CO_2 and ambient temperature, and greenhouse conditions: ~900 μatm CO_2 and ambient temperature +3 °C). We found that increased CO_2 concentration benefited the growth of small autotrophic phytoplankton groups: picophytoplankton (PP), autotrophic nanoflagellates (ANF), and small chain-forming diatoms (DT). However, in the greenhouse conditions, ANF and DT abundances were lower compared with those in the acidification conditions. The proliferation of small autotrophic phytoplankton in future oceanic conditions (acidification and greenhouse) also increased the abundance of heterotrophic dinoflagellates (HDF). These responses suggest that a combination of acidification and warming will not only increase the small autotrophic phytoplankton standing stock but, also, lead to a shift in the diatom and dinoflagellate species composition, with potential biogeochemical element cycling feedback and an increased frequency and intensity of harmful algal blooms.

keywords: mesocosm; acidification; warming; picophytoplankton; autotrophic nanoflagellates; diatoms; dinoflagellates

3-13 *Paleontology*

From bi-polar to regional distribution of modern dinoflagellate cysts, an overview of their biogeography

Marret, Fabienne., Bradley, Lee., de Vernal, Anne., Hardy, William., **Kim, So-Young.** and 6 others.

Marine Micropaleontology. 2020. 159.

doi: 10.1016/j.marmicro.2019.101753.

This paper examines the distribution of 91 modern dinoflagellate cyst taxa from 3636 locations across the world's oceans. Patterns of distributions among the taxa included bi-polarity, cosmopolitan, northern versus southern hemispheres, and geographically restricted. Of the 91 taxa, three dominate these 3636 assemblages at the global scale, *Brigantedinium* species, *Operculodinium centrocarpum* sensu Wall and Dale 1966 and some species of *Spiniferites*. Whereas *Brigantedinium* is a true cosmopolitan taxon, with high abundances in each ocean, *Operculodinium centrocarpum* sensu Wall and Dale 1966 shows high

abundances in polar to temperate regions in the Northern Hemisphere, and in tropical to sub-tropical waters in the Southern Hemisphere. *Spiniferites* species show highest occurrences in the Southern Hemisphere. This study also highlights three true bi-polar species, *Impagidinium pallidum*, *Islandinium minutum* and cyst of *Polarella glacialis*. Only a few taxa are strictly endemic, either being relics of ancient seas such as the Paratethys (*Spiniferites cruciformis*) or linked to specific environmental conditions. However, recent studies have shown recent worldwide dispersal of these endemic species possibly due to human activities. Overall, this compilation has highlighted the progress made since the early 1970s on our understanding of these important tracers of environmental conditions but also gaps in our knowledge of their distribution in pelagic regions of the Pacific and Indian Oceans as well as under Arctic sea ice.

keywords: Dinoflagellate cyst; Modern distribution; Global; Bi-polar; Endemism

3-14 *Multidisciplinary Sciences*

Ice front blocking of ocean heat transport to an Antarctic ice shelf

Wahlin, A. K., Steiger, N., Darelius, E., Assmann, K. M., Glessmer, M. S., Ha, H. K., Herraiz-Borreguero, L., Heuze, C., Jenkins, A., **Kim, Tae-Wan.** and 3 others.

Nature. 2020. 578(7796): 568-+.

doi: 10.1038/s41586-020-2014-5.

Mass loss from the Antarctic Ice Sheet to the ocean has increased in recent decades, largely because the thinning of its floating ice shelves has allowed the outflow of grounded ice to accelerate[1,2]. Enhanced basal melting of the ice shelves is thought to be the ultimate driver of change[2,3], motivating a recent focus on the processes that control ocean heat transport onto and across the seabed of the Antarctic continental shelf towards the ice[4-6]. However, the shoreward heat flux typically far exceeds that required to match observed melt rates[2,7,8], suggesting that other critical controls exist. Here we show that the depth-independent (barotropic) component of the heat flow towards an ice shelf is blocked by the marked step shape of the ice front, and that only the depth-varying (baroclinic) component, which is typically much smaller, can enter the sub-ice cavity. Our results arise from direct observations of the Getz Ice Shelf system and laboratory experiments on a rotating platform. A similar blocking of the barotropic component may occur in other areas with comparable ice-bathymetry configurations, which may explain why changes in the density structure of the water column have been found to be a better indicator of basal melt rate variability than the heat transported onto the continental shelf[9]. Representing the step topography of the ice front accurately in models is thus important for simulating ocean heat fluxes and induced melt rates.

keywords: Antarctic ice shelf; Getz Ice Shelf; heat transport

3-15 *Ecology; Marine & Freshwater Biology; Oceanography*

Impacts of meltwater discharge from marine-terminating glaciers on the protist community in Inglefield Bredning, northwestern Greenland

Matsuno, Kohei., Kanna, Naoya., Sugiyama, Shin., Yamaguchi, Atsushi. and **Yang, Eun Jin.**

Marine Ecology Progress Series. 2020. 642: 55-65.

doi: 10.3354/meps13324.

To evaluate the effects of meltwater discharge from marine-terminating glaciers on a fjord protist community in northwestern Greenland during summer, we investigated the distribution, abundance and biomass of the protist community and their relationships with hydrographic parameters. In the standing stock of protists, dinoflagellates (46.4%) and oligotrich ciliates (39.5 %) were dominant throughout the study region. With respect to vertical distribution, oligotrich ciliates were abundant in the surface layer, mainly due to suitable food conditions (abundance of diatom and nanoflagellates). Near glaciers, relatively high chlorophyll *a* (chl *a*) concentrations were found in the subsurface layers associated with the low-temperature, high-turbidity and slightly high nutrient levels, indicating that the nutrient inputs from the upwelling glacial melt-water plume increased primary production. Large-sized *Protoperidium* spp. were found only at stations near glaciers where nutrients were abundant, and heterotrophic dinoflagellates showed strong relationships with nanoflagellates. These findings suggest that the upwelling associated with subglacial meltwater discharge can stimulate nanoflagellate production, resulting in increases in

ciliate and heterotrophic dinoflagellate production.

keywords: Protist community; Meltwater discharge; Marine-terminating glacier; Ciliates; Dinoflagellates

3-16 *Environmental Sciences; Water Resources*

In Situ Rates of Carbon and Nitrogen Uptake by Phytoplankton and the Contribution of Picophytoplankton in Kongsfjorden, Svalbard

Kim, Bo Kyung., **Joo, Hyoung Min.**, **Jung, Jinyoung.**, **Lee, Boyeon.** and **Ha, Sun-Yong.**

Water. 2020. 12(10).

doi: 10.3390/w12102903.

Rapid climate warming and the associated melting of glaciers in high-latitude open fjord systems can have a significant impact on biogeochemical cycles. In this study, the uptake rates of carbon and nitrogen (nitrate and ammonium) of total phytoplankton and picophytoplankton (<2 μm) were measured in Kongsfjorden in early May 2017 using the dual stable isotope technique. The daily uptake rates of total carbon and nitrogen ranged from 0.3 to 1.1 g C m^{-2} day^{-1}, with a mean of 0.7 ± 0.3 g C m^{-2} day^{-1}, and 0.13 to 0.17 g N m^{-2} day^{-1}, with a mean of 0.16 ± 0.02 g N m^{-2} day^{-1}. Microphytoplankton (20-200 μm) accounted for 68.1% of the total chlorophyll a (chl-a) concentration, while picophytoplankton (<2 μm) accounted for 19.6% of the total chl-a, with a high contribution to the carbon uptake rate (42.9%) due to its higher particulate organic carbon-to-chl-a ratio. The contributions of picophytoplankton to the total nitrogen uptake rates were 47.1 ± 10.6% for nitrate and 74.0 ± 16.7% for ammonium. Our results indicated that picophytoplankton preferred regenerated nitrogen, such as ammonium, for growth and pointed to the importance of the role played by picophytoplankton in the local carbon uptake rate during the early springtime in 2017. Although the phytoplankton community, in terms of biovolume, in all samples was dominated by diatoms and *Phaeocystis* sp., a higher proportion of nano- and picophytoplankton chl-a (mean ± SD = 71.3 ± 16.4%) was observed in the relatively cold and turbid surface water in the inner fjord. Phytoplankton production (carbon uptake) decreased towards the inner fjord, while nitrogen uptake increased. The contrast in carbon and nitrogen uptake is likely caused by the gradient in glacial meltwater which affects both the light regime and nutrient availability. Therefore, global warming-enhanced glacier melting might support lower primary production (carbon fixation) with higher degrees of regeneration processes in fjord systems.

keywords: phytoplankton productivity; carbon and nitrogen; stable isotopes; Kongsfjorden; Svalbard

3-17 *Environmental Sciences; Meteorology & Atmospheric Sciences*

Influence on the conversion of DMS to MSA and SO_4^{2-} in the Southern Ocean, Antarctica

Yan, Jinpei., Zhang, Miming., **Jung, Jinyoung.** and 4 others.

Atmospheric Environment. 2020. 233.

doi: 10.1016/j.atmosenv.2020.117611.

Dimethyl sulfide (DMS), methanesulphonic acid (MSA) and sulfate (SO_4^{2-}) were measured simultaneously at high-time resolution in the Southern Ocean (SO) during February and March 2018, to characterize the conversion of DMS to MSA and SO_4^{2-} in the marine atmosphere. DMS concentrations ranged up to ~10890.5 ng m^{-3} (with an average of 899.8. ± 957.9 ng m^{-3}, representing the standard deviation), which were much higher than the MSA concentrations (with an average of 30.6. ± 16.8 ng m^{-3}) and SO_4^{2-} concentration (148.1. ± 32.5 ng m^{-3}) in the aerosol phase. The spatial distribution of MSA was different from the distribution of DMS. The ratio of MSA to DMS (R_M) ranged up to ~ 0.31, with an average of 0.044. ± 0.045. R_M value decreased dramatically as DMS concentration increased, when DMS concentration was below 1000 ng m^{-3}. The effects of temperature and relative humidity (RH) on R_M were mostly negligible, indicating that neither DMS concentration, nor RH and temperature was the key parameter for the conversion of DMS to MSA in the SO. Ratios of nss-SO_4^{2-} to DMS (R_S) were used to estimate the conversion of DMS to SO_4^{2-}. The calculated R_S with mean R_P (the ratio of MSA to nss-SO_4^{2-}) value correlated well with the observed R_S, which provided an useful method to estimate the biogenic SO_4^{2-} from the oxidation of DMS in the marine atmosphere, as biogenic SO_4^{2-} levels can be calculated with Rs and DMS concentrations. The

estimated biogenic SO_4^{2-} levels ranged up to 163.8 ng m^{-3}, with an average of 47.1 ± 30.2 ng m^{-3} in the SO during the cruise. The results extend the knowledge of the conversion of DMS to MSA and SO_4^{2-} in the marine atmosphere.

keywords: Dimethyl sulfide (DMS); Methanesulfonic acid (MSA); nss-SO_{4_2}.; Aerosol; Antarctica

3-18 *Ecology*

A marine carbon monoxide (CO) model with a new parameterization of microbial oxidation

Kwon, Young Shin., Kang, Hyoun-Woo., Polimene, Luca. and **Rhee, Tae Siek.**

Ecological Modelling. 2020. 432.

doi: 10.1016/j.ecolmodel.2020.109203.

Traditionally, marine carbon monoxide (CO) models assume that the microbial oxidation of CO is only dependent on the concentration of CO in the water column. However, CO oxidation rates in the ocean have been reported to vary up to two orders of magnitude both spatially and temporally. Here, we developed a new model assuming that CO microbial oxidation is dependent on bacterial carbon biomass other than CO concentration. In addition to microbial oxidation, the model also describes CO photochemical production, vertical mixing, and air-sea gas exchange. The new CO model has been embedded in the European Regional Seas Ecosystem Model (ERSEM) and coupled with the General Ocean Turbulence Model (GOTM). The CO-GOTM-ERSEM model was implemented at the Bermuda Atlantic Time Series (BATS) station to simulate CO concentrations observed in March 1993 by Kettle (1994). The proposed second-order function describing CO microbial oxidation introduces a new parameter, the bacteria biomass specific oxidation rate, which was estimated to be 5.7 ± 0.2 $(\mu g\ C\ m^{-3})^{-1}\ h^{-1}$. Statistical metrics indicates that the new CO model performs better than a previously published model with a first-order decay function to describe microbial oxidation, acknowledging the dependence of microbial oxidation on bacterial abundance is realistic. A long-term (1992-1994) simulation carried out with CO-GOTM-ERSEM reproduced the spatial and seasonal variability of CO reported in the literature. Our model provides a realistic description of the CO dynamics and is potentially usable in different environmental contexts worldwide.

keywords: Marine carbon monoxide; Microbial oxidation; Marine ecosystem; Modelling; Second-order kinetics

3-19 *Engineering, Environmental; Environmental Sciences*

Mass Budget of Methylmercury in the East Siberian Sea: The Importance of Sediment Sources

Kim, Jihee., Soerensen, Anne L., **Kim, Mi Seon.**, Eom, Sangwoo., **Rhee, Tae Siek.**, **Jin, Young Keun.** and Han, Seunghee.

Environmental Science & Technology. 2020. 54(16): 9949-9957.

doi: 10.1021/acs.est.0c00154.

Biological concentrations of methylmercury (MeHg) are elevated throughout the Arctic Ocean; however, to date, the major sources and the spatial variability of MeHg are not well quantified. To identify the major inputs and outputs of MeHg to the Arctic shelf water column, we measured MeHg concentrations in the seawater and sediment samples from the East Siberian Sea collected from August to September 2018. We found that the MeHg concentrations in seawater and pore water were higher on the slope than on the shelf, while the MeHg concentrations in the sediment were higher on the shelf than on the slope. We created a mass budget for MeHg and found that the benthic diffusion and resuspension largely exceed other sources, such as atmospheric deposition and river water input. The major sinks of MeHg in the water column were dark demethylation and evasion. When we extrapolated our findings on benthic diffusion to the entire Arctic shelf system, the annual MeHg diffusion from the shelf sediments was estimated to be 23,065 ± 939 mol $yr^{1})$, about 2 times higher than previously proposed river discharges. Our study suggests that the MeHg input from shelf sediments in the Arctic Ocean is significant and has been previously underestimated.

3-20 *Environmental Sciences; Marine & Freshwater Biology*

Mass Occurrence of Pacific Copepods in the Southern Chukchi Sea During Summer: Implications of the High-Temperature Bering Summer Water

Kim, Jee-Hoon., **Cho, Kyoung-Ho.**, **La, Hyoung Sul.**, **Choy, Eun Jung.**, Matsuno, Kohei., **Kang, Sung-Ho.**, Kim, Won. and **Yang, Eun Jin.**

Frontiers in Marine Science. 2020. 7.

doi: 10.3389/fmars.2020.00612.

The Bering Strait is the only gateway to the Chukchi Sea from the Pacific Ocean and is a major route of Pacific water inflow. We recently investigated the occurrence of Pacific copepod species along with the warming of the Chukchi Sea and sought to identify the cause of the mass occurrence these copepods through an analysis of the water masses flowing through the Bering Strait. Zooplankton and Conductivity-Temperature-Depth (CTD) data collection was conducted in the Chukchi Sea and Bering Strait from 2014 to 2016. In addition, mooring systems installed in the Bering Strait were analyzed to obtain water temperature and salinity data during summer to understand the properties of the water masses. In 2015, a high abundance of Pacific copepod species (*Eucalanus bungii*, *Metridia pacifica*, and *Neocalanus* spp.) was observed in Bering Summer Water (BSW), which was relatively warm compared to measurements obtained from 2014 to 2016. As further confirmation, our results were consistent with 2007, 2009, and 2012 data, which showed that the abundance of Pacific copepod species was proportional to the temperature of the BSW entering the Chukchi Sea. In conclusion, we reconfirmed that Pacific copepod species are entering the Chukchi Sea along with BSW, and we newly discovered that their high abundance coincided with the relatively warm BSW, instead of other water masses. These findings suggest that the inflow of the high-temperature BSW (>3°C) plays an important role in the mass occurrence of Pacific copepod species in the southern Chukchi Sea.

keywords: Pacific copepod; Arctic; Chukchi Sea; Bering Summer Water; mass occurrence

3-21 *Limnology; Oceanography*

Methane production in the oxygenated water column of a perennially ice-covered Antarctic lake

Li, Wei., Dore, John E., Steigmeyer, August J., Cho, Yong-Joon., **Kim, Ok-Sun.** and 4 others.

Limnology and Oceanography. 2020. 65(1): 143-156.

doi: 10.1002/lno.11257.

Aerobic methane production in aquatic ecosystems impacts the global atmospheric budget of methane, but the extent, mechanism, and taxa responsible for producing this greenhouse gas are not fully understood. Lake Bonney (LB), a perennially ice-covered Antarctic lake, has cold hypersaline waters underlying an oxygenated freshwater layer. We present temporal methane concentration profiles in LB indicating methane production in the oxygenated (> 200% air saturation) water. Experiments amended with methylphosphonate (MPn) yielded methane generation, suggesting in situ methanogenesis via the carbon-phosphorus (C-P) lyase pathway. Enrichment cultures from the lake were used to isolate five bacterial strains capable of generating methane when supplied with MPn as the sole P source. Based on 16S rRNA gene sequencing, the isolates belong to the Proteobacteria (closely related to *Marinomonas*, *Hoeflea*, and *Marinobacter* genera) and Bacteroidetes (*Algoriphagus* genus). 16S rRNA metagenomic sequencing confirms the presence of these taxa in LB. None of the isolated species were reported to be capable to produce methane. In addition, orthologs of the phosphoenolpyruvate mutase gene (*PepM*) and methylphosphonate synthase (*MPnS*), enzymes involved in phosphonate and MPn biosynthesis, were widely spread in the LB shotgun metagenomic libraries; genes related to C-P lyase pathways (*phn* gene clusters) were also abundant. 16S rRNA and *mcrA* genes of anaerobic methanogens were absent in both 16S rRNA and metagenomics libraries. These data reveal that in situ aerobic biological methane production is likely a significant source of methane in LB.

keywords: Antarctic lakes; aerobic methane production; methylphosphonate

3-22 *Environmental Sciences; Marine & Freshwater Biology*

Molecular-Level Chemical Characterization of Dissolved Organic Matter in the Ice Shelf Systems of King George Island, Antarctica

Jang, Jiyi., **Park, Jiyeon.**, **Ahn, Seohee.**, **Park, Ki-Tae.**, **Ha, Sun-Yong.** and 2 others.

Frontiers in Marine Science. 2020. 7.

doi: 10.3389/fmars.2020.00339.

Antarctic shelf systems play an important role in organic matter circulation on Earth; hence, identifying the characteristics of dissolved organic matter (DOM) can be a good indicator for understanding its origin, as well as climate change. In this study, to identify the characteristics of DOM in the ice shelf systems, surface water was collected from the open sea (OS) and Marian cove (fjord, FJ). Although there were no differences in DOM characteristics between sampling sites in the quantitative analyses, the DOM in the surface water of each region seemed to be more affected by terrestrial than marine biological sources in optical and molecular properties. This finding indicates that the terrestrial DOM related to mosses based on the results of molecular properties: high levels of lipid-like (35-39%) and unsaturated hydrocarbon-like (UH; 27-34%) in both the OS and the FJ regions and significantly higher tannin-like substance and condensed aromatic structures in the FJ than in the OS region. When comparing the FJ transect samples, those nearest to a glacier (FJ1; 0.93 km from the glacier) showed relatively low salinity, high dissolved organic carbon, and high chromophoric DOM, indicating that terrestrial DOM (possibly produced by moss) inflow occurred with the runoff from the freshly melting land ice and glacier. However, no significant differences in molecular composition were detected, suggesting that terrestrial DOM is introduced into the ice shelf systems by melting land ice, and glacier runoff could be a major source of DOM-rich seawater during austral fall when low marine biological activity occurs. This study has a great significance as background data for DOM characteristics in the ice shelf systems due to the enhanced biological activity during the austral summer.

keywords: dissolved organic matter; terrestrial DOM; glacier runoff; ice shelf systems; King George Island; Orbitrap

3-23 *Geochemistry & Geophysics*

Noble gas as a proxy to understand the evolutionary path of migrated CO_2 in a shallow aquifer system

Ju, YeoJin., Lee, Seong-Sun., Kaown, Dugin., Lee, Kang-Kun., Gilfillan, Stuart M., V., Hahm, Doshik. and **Park, Keyhong.**

Applied Geochemistry. 2020. 118.

doi: 10.1016/j.apgeochem.2020.104609.

To provide confidence in the safety of a carbon capture and storage (CCS) project, researchers have focused on developing monitoring techniques to trace the unlikely, but potentially possible, migration of CO_2 from a deep reservoir. Among the various techniques, noble gas tracing is a beneficial approach, owing to the unique noble gas fingerprints present in injection fluids, the deep reservoir, and the shallow aquifer above the storage area. However, the value of this approach has been limited to demonstrations in a natural analogue CO_2-rich reservoir and an artificial injection test site. Therefore, further efforts are required to link those valuable observations to an actual CCS site. In this study, we outline how to use these tracers for actual monitoring work in a shallow aquifer system. First, two artificial injection tests were performed using He, Ar, Kr, and SF_6 to understand the behavior of the leaked plume in the shallow aquifer system. In both tests, the noble gas ratio remarkably changed with the solubility -controlled process and the mixing process. To extend and link the valuable findings from the artificial injection tests to an actual CO_2 leakage event, we performed a leakage simulation using data from a real CO_2 injection site, i.e., the Weyburn -Midale site. This simulation suggested that combinations of ^4He with other heavier noble gases can be used to monitor CO_2 leakage, as they allow us to separate and explain the major interactions governing the migration of the leaked plume in the shallow aquifer system. Additionally, although the high CO_2 density of a dissolved plume is known to add uncertainty in quantitative approaches, the influence of those effects was negligible when compared to the errors arising from the wide variation in the noble gas fingerprints in the leaked CO_2. This study, therefore, provides insight into the evolutionary path of the migrated CO_2 plume in the shallow aquifer system and to the results can be used to inform the tracing of a leakage source within a shallow aquifer despite various mechanisms complicating the plume distribution.

keywords: Carbon capture and storage; CO2 leakage; Noble gas tracing; Degassing; Inherent tracer; Monitoring

3-24 *Oceanography*

Observation of Bottom-Trapped Topographic Rossby Waves on the Shelf Break of the Chukchi Sea

Ku, Ahyoung., Seung, Young Ho., Jeon, Chanhyung.,

Choi, Youngseok., **Yoshizawa, Eri.**, Shimada, Koji., **Cho, Kyoung-Ho.** and Park, Jae-Hun.

Journal of Geophysical Research-Oceans. 2020. 125(7).

doi: 10.1029/2019jc015436.

This study investigates topographic Rossby waves (TRWs) with a period of approximately 35 hr using a mooring observation at 194-m depth on the shelf break of the Chukchi Sea in the Arctic Ocean. We measured velocity, temperature, and salinity for about 1 year from August 2014 to August 2015. The observations reveal that the bottom-intensified upslope current fluctuations were significantly coherent with near-bottom temperature fluctuations, with a phase lag of approximately 90°. Near the seafloor, the temperature increased with depth. Therefore, the temperature increases (decreases) with the upslope (downslope) currents. Theoretical estimates of the wavelength, angle of wavenumber vector, and bottom-trapping depth confirmed that the observed near 35-hr TRWs are indeed plausible in the study area. Energetic TRWs were observed in September and October, during the sea ice free season, whereas weak TRWs were observed in months with sea ice cover. The TRW events coincided with local wind-stress events, suggesting that the TRWs were triggered by atmospheric forcing. These findings imply that a longer ice-free season may allow for a more frequent occurrence of energetic TRWs, which may enhance the water exchange between the shallow continental shelf and the deep ocean.

keywords: bottom-intensified fluctuations; topographic Rossby waves; wind forcing influence

3-25 *Environmental Sciences; Marine & Freshwater Biology; Toxicology*

Ocean freshening and acidification differentially influence mortality and behavior of the Antarctic amphipod *Gondogeneia antarctica*

Park, Seojeong., **Ahn, In-Young.** and 3 others.

Marine Environmental Research. 2020. 154.

doi: 10.1016/j.marenvres.2019.104847.

The Western Antarctic Peninsula (WAP) has experienced rapid atmospheric and ocean warming over the past few decades and many marine-terminating glaciers have considerably retreated. Glacial retreat is accompanied by fresh meltwater intrusion, which may result in the freshening and acidification of coastal waters. Marian Cove (MC), on King George Island in the WAP, undergoes one of the highest rates of glacial retreat. Intertidal and shallow subtidal waters are likely more susceptible to these processes, and sensitive biological responses are expected from the organisms inhabiting this area. The gammarid amphipod *Gondogeneia antarctica* is one of the most abundant species in the shallow, nearshore Antarctic waters, and it occupies an essential ecological niche in the coastal marine WAP ecosystem. In this study, we tested the sensitivity of *G. antarctica* to lowered salinity and pH by meltwater intrusion following glacial retreat. We exposed *G. antarctica* to four different treatments combining two salinities (34 and 27 psu) and pH (8.0 and 7.6) levels for 26 days. Mortality, excluding cannibalized individuals, increased under low pH but decreased under low salinity conditions. Meanwhile, low salinity increased cannibalism, whereas low pH reduced food detection. Shelter use during the daytime decreased under each low salinity and pH condition, indicating that the two stressors act as disruptors of amphipod behavior. Under low salinity conditions, swimming increased during the daytime but decreased at night. Although interactions between low salinity and low pH were not observed during the experiment, the results suggest that each stressor, likely induced by glacial melting, causes altered behaviors in amphipods. These environmental factors may threaten population persistence in Marian Cove and possibly other similar glacial embayments.

keywords: Amphipod; Cannibalism; Food detection; Glacial retreat; Marian Cove; Molting; Swimming

3-26 *Meteorology & Atmospheric Sciences*

On the Interpretation of the North Atlantic Averaged Sea Surface Temperature

Sun, Jing., Latif, Mojib., Park, Wonsun. and **Park, Taewook.**

Journal of Climate. 2020. 33(14): 6025-6045.

doi: 10.1175/jcli-d-19-0158.1.

The North Atlantic (NA) basin-averaged sea surface temperature (NASST) is often used as an index to study climate variability in the NA sector. However,

there is still some debate on what drives it. Based on observations and climate models, an analysis of the different influences on the NASST index and its low-pass filtered version, the Atlantic multidecadal oscillation (AMO) index, is provided. In particular, the relationships of the two indices with some of its mechanistic drivers including the Atlantic meridional overturning circulation (AMOC) are investigated. In observations, the NASST index accounts for significant SST variability over the tropical and subpolar NA. The NASST index is shown to lump together SST variability originating from different mechanisms operating on different time scales. The AMO index emphasizes the subpolar SST variability. In the climate models, the SST-anomaly pattern associated with the NASST index is similar. The AMO index, however, only represents pronounced SST variability over the extratropical NA, and this variability is significantly linked to the AMOC. There is a sensitivity of this linkage to the cold NA SST bias observed in many climate models. Models suffering from a large cold bias exhibit a relatively weak linkage between the AMOC and AMO and vice versa. Finally, the basin-averaged SST in its unfiltered form, which has been used to question a strong influence of ocean dynamics on NA SST variability, mixes together multiple types of variability occurring on different time scales and therefore underemphasizes the role of ocean dynamics in the multidecadal variability of NA SSTs.

keywords: Coupled models ; Atmosphere-ocean interaction; Ocean circulation; Ocean dynamics; Thermocline circulation

3-27 *Environmental Sciences; Marine & Freshwater Biology*

Trophic Dynamics of Zooplankton Before and After Polar Night in the Kongsfjorden (Svalbard): Evidence of Trophic Position Estimated by $\delta^{15}N$ Analysis of Amino Acids

Choi, Hyuntae., **Ha, Sun-Yong.**, Lee, Seunghan., **Kim, Jee-Hoon.** and Shin, Kyung-Hoon.

Frontiers in Marine Science. 2020. 7.

doi: 10.3389/fmars.2020.00489.

In polar ecology, zooplankton diets and survival rates vary according to the seasonality of solar radiation and oceanographic conditions. Each zooplankton species has evolved feeding strategies to survive in the diet-limited conditions of the "polar night." Many zooplankton studies have reported seasonal adaptations in feeding activity during polar night based on their trophic niches. Nitrogen isotope analysis of amino acids has provided improved accuracy in estimates of trophic position (TP) in various marine species. In this study, field work was conducted in Kongsfjorden before (October 2017) and after polar night (April 2018). As representative zooplankton, an amphipod (*Themisto abyssorum*), euphausids (*Meganycitiphanes norvegica* and *Thysanoessa* sp.), a chaetognath (*Parasagitta elegans*), and copepods (*Calanus* spp. and *Oithona similis*) were collected. trophic position values of each taxon were estimated using the nitrogen isotope ratio of glutamic acid ($\delta^{15}N_{Glu}$) and phenylalanine ($\delta^{15}N_{Phe}$). Results showed that TP values of *P. elegans* were relatively constant, averaging 3.2 in both seasons, likely due to continuous feeding activity during polar night. Trophic position values were also constant for *Calanus* spp., ranging 2.5-3.0 in both seasons, due to their ability to utilize stored high-energy wax. In contrast, average TP values for *O. similis*, an omnivorous zooplankton, were 2.9 in October and 2.3 the following April. Trophic position values for *O. similis* before polar night can be attributed to the relatively high availability of algae during longer periods of daylight. We found that TP variation in zooplankton before and after polar night differed according to feeding activities in diet-restricted circumstances.

keywords: trophic position; nitrogen isotope; amino acid; zooplankton; Kongsfjorden; Svalbard

3-28 *Environmental Sciences; Marine & Freshwater Biology*

A Unique Benthic Microbial Community Underlying the *Phaeocystis antarctica*-Dominated Amundsen Sea Polynya, Antarctica: A Proxy for Assessing the Impact of Global Changes

Cho, Hyeyoun., Hwang, Chung Yeon., Kim, Jong-Geol., Kang, Sanghoon., Knittel, Katrin., Choi, Ayeon., Kim, Sung-Han., Rhee, Sung-Keun., **Yang, Eun Jin.**, **Lee, SangHoon.** and Hyun, Jung-Ho.

Frontiers in Marine Science. 2020. 6.

doi: 10.3389/fmars.2019.00797.

Polynyas in the polar seas are regarded as windows through which ecosystem responses associated

with global climate changes are to be noticed. However, little information is available on benthic microbial communities in the Amundsen Sea polynya (ASP), where environmental changes due to global warming are occurring rapidly, from which future climate change-induced ecosystem responses could be assessed. We performed high-throughput sequencing of 16S rRNA genes and quantitative PCR in combination with biogeochemical analyses and metabolic rate measurements to determine the composition, diversity and controls of major microbial communities in sediments of the ASP. A large fraction of the sequenced benthic microbial community (40% on average) in the polynya was uniquely affiliated with the phylum *Planctomycetes*, whereas *Thaumarchaeota* (51% on average) predominated in non-polynya areas. The relative abundance of *Planctomycetes* correlated significantly with organic carbon (C_{org}) content in the polynya sediment underlying the *Phaeocystis*-dominated water column. These results suggest that *Planctomycetes* comprise a major bacterial group utilizing relatively recalcitrant C_{org} produced primarily by *Phaeocystis* blooms. In contrast, the predominance of chemolithoautotrohic *Thaumarchaeota* in the sea-ice zone was attributed to low C_{org} supply due to low primary productivity in the ice-covered water column. The *Planctomycetes*-dominated microbial communities in the ASP is in stark contrast to that *Proteobacteria* (*Delta-* and *Gamma-proteobacteria*) occupy ecological niches as primary mineralizers of organic materials in most benthic systems in the Southern Ocean, where organic materials in the sediments mostly originate from diatom blooms. Given that microbial communities respond quickly to environmental changes, and that global climate change is proceeding rapidly in the ASP, our results suggest that any modifications in the *Planctomycetes*-dominated microbial communities will provide valuable insight into changes in organic matter transport to the seafloor that may result from shifts in planktonic communities from *Phaeocystis* to diatoms associated with climate change.

keywords: Amundsen Sea polynya; Antarctica; benthic microbial community; global climate change; organic carbon mineralization; *Phaesocystis antarctica; Planctomycetes; Thaumarchaeota*

3-29 *Environmental Sciences; Meteorology & Atmospheric Sciences*

Uptake selectivity of methanesulfonic acid (MSA) on fine particles over polynya regions of the Ross Sea, Antarctica

Yan, Jinpei., **Jung, Jinyoung.** and 8 others.

Atmospheric Chemistry and Physics. 2020. 20(5): 3259-3271.

doi: 10.5194/acp-20-3259-2020.

The uptake of methanesulfonic acid (MSA) on existing particles is a major route of the particulate MSA formation, however, MSA uptake on different particles is still lacking in knowledge. Characteristics of MSA uptake on different aerosol particles were investigated in polynya (an area of open sea water surrounded by ice) regions of the Ross Sea, Antarctica. Particulate MSA mass concentrations, as well as aerosol population and size distribution, were observed simultaneously for the first time to access the uptake of MSA on different particles. The results show that MSA mass concentration does not always reflect MSA particle population in the marine atmosphere. MSA uptake on aerosol particle increases the particle size and changes aerosol chemical composition, but it does not increase the particle population. The uptake rate of MSA on particles is significantly influenced by aerosol chemical properties. Sea salt particles are beneficial for MSA uptake, as MSA-Na and MSA-Mg particles are abundant in the Na and Mg particles, accounting for 0.43 ± 0.21 and 0.41 ± 0.20 of the total Na and Mg particles, respectively. However, acidic and hydrophobic particles suppress the uptake of MSA, as MSA-EC (elemental carbon) and MSA-SO_4^{2-} particles account for only 0.24 ± 0.68 and 0.26 ± 0.47 of the total EC and SO_4^{2-} particles, respectively. The results extend the knowledge of the formation and environmental behavior of MSA in the marine atmosphere.

3-30 *Environmental Sciences*

Use of a broad β-diversity measure of pelagic ciliate communities for assessing vertical heterogeneity of water columns in the Pacific Arctic Ocean

Xu, Guangjian., **Yang, Eun Jin.**, **Lee, Youngju.** and **Kang, Sung-Ho.**

Environmental Science and Pollution Research. 2020. 27(31): 38769-38775.

doi: 10.1007/s11356-020-09753-6.

Multivariate dispersion has proven to be a broad β-diversity measure that shows the heterogeneity of environmental conditions. The dispersion patterns of pelagic ciliate communities were investigated at eight water depths in the northern Bering Sea of the western Arctic Ocean and Chukchi Sea. Multivariate analysis indicated that (1) pelagic ciliates showed significant variability in multivariate dispersion on a vertical scale, (2) dispersion patterns were shaped by both the species composition and individual abundance, (3) vertical variation in species occurrence was significantly related to nutrients and chlorophyll *a*, and (4) the dispersion measures at both species occurrence and species abundance resolutions were significantly negatively related to salinity and dissolved oxygen. This suggests that multivariate dispersion measures driven by both species composition and the individual abundance of pelagic ciliates may be a useful indicator of environmental heterogeneity in marine ecosystems.

keywords: Multivariate dispersion; β-diversity; Bioassessment; Vertical heterogeneity; Pelagic ciliate; Arctic Ocean

3-31 *Meteorology & Atmospheric Sciences; Oceanography*

Variability in high-salinity shelf water production in the Terra Nova Bay polynya, Antarctica

Yoon, Seung-Tae., **Lee, Won Sang.**, Stevens, Craig., Jendersie, Stefan., Nam, SungHyun., **Yun, Sukyoung.**, Hwang, Chung Yeon., Jang, Gwang Il. and **Lee, Jiyeon.**

Ocean Science. 2020. 16(2): 373-388.

doi: 10.5194/os-16-373-2020.

Terra Nova Bay in Antarctica is a formation region for high-salinity shelf water (HSSW), which is a major source of Antarctic Bottom Water. Here, we analyze spatiotemporal salinity variability in Terra Nova Bay with implications for the local HSSW production. The salinity variations in the Drygalski Basin and eastern Terra Nova Bay near Crary Bank in the Ross Sea were investigated by analyzing hydrographic data from instrumented moorings, vessel-based profiles, and available wind and sea-ice products. Near-bed salinity in the eastern Terra Nova Bay (~ 660 m) and Drygalski Basin (~ 1200 m) increases each year beginning in September. Significant salinity increases (> 0.04) were observed in 2016 and 2017, which is likely related to active HSSW formation. According to velocity data at identical depths, the salinity increase from September was primarily due to advection of the HSSW originating from the coastal region of the Nansen Ice Shelf. In addition, we show that HSSW can also be formed locally in the upper water column (< 300 m) of the eastern Terra Nova Bay through convection supplied by brine from the surface, which is related to polynya development via winds and ice freezing. While the general consensus is that the salinity of the HSSW was decreasing from 1995 to the late 2000s in the region, the salinity has been increasing since 2016. In 2018, it returned to values comparable to those in the early 2000s.

keywords: Hydrographic mooring; Terra Nova Bay polynya; high-salinity shelf water

3-32 *Marine & Freshwater Biology; Oceanography*

Verification of the Backscattering Strength Based on the Swimming Behavior of Antarctic Krill

Han, Inwoo., Oh, Wooseok., **La, Hyoung Sul.** and 4 others.

Ocean Science Journal. 2020. 55(3): 391-403.

doi: 10.1007/s12601-020-0031-9.

This study provides an estimate of the SDWBA-modelled mean target strength for given sets of krill length and swimming orientation. The range of the dB identification window for krill length was between 28 mm and 67 mm and the distribution of swimming orientation N[11.0°, 4.0°] was estimated to be between 0.06-10.97 dB, while the range estimated using N[53.1°, 21.4°], i.e., the distribution of orientation obtained under the brightest illuminance level, was 5.21-9.82 dB. The range of the dB window calculated using N[45.2°, 23.0°], obtained under the second brightest illuminance level, was 3.83-11.76 dB, and the range calculated with N[48.1°, 23.0°], obtained under the third illuminance level, was 3.83-11.76 dB. The range of the dB window calculated by N[45.9°, 23.0°] was 3.41-11.75 dB, and the range of the dB window for krill length ranging from 28 mm to 67 mm was 4.05-11.34 dB. In all the swimming orientations, the smaller the krill size was the lower the averaged target strength value was; likewise, the larger the krill size was the higher the averaged target strength value was. The result

indicated that swimming orientation impacted greatly on the range of frequency differences of Antarctic krill.

keywords: Antarctic krill; SDWBA model; swimming orientation; target strength

PART 4

Life Sciences

4-1 *Multidisciplinary Sciences*

30 years revisit survey for long-term changes in the Antarctic subtidal algal assemblage

Ko, Young Wook., **Choi, Han-Gu.** and 2 others.

Scientific Reports. 2020. 10(1).

doi: 10.1038/s41598-020-65039-4.

A long-term change of a subtidal macroalgal assemblage has been investigated in Maxwell Bay, King George Island (KGI) of the Antarctic coast by a revisit survey after 30 years. Field surveys were done by SCUBA diving at six sites in 2016-2018 to directly compare with the previous survey conducted in 1988-1993 at the same sites. The total number of macroalgal species was similar between the previous and the present survey, 25 and 27 species respectively. However, the macroalgal assemblage changed substantially with the average similarity of 48.2% between the two surveys. Also, the species-level abundance showed a high variability between surveys. On the other hand, over the 30 years interval there was little overall change at the between-site level hierarchical structure in the subtidal communities of Maxwell Bay. The sites near the penguin rookery consistently showed the highest biodiversity, indicating the importance of land-based nutrients input in Antarctic coastal habitats. A noticeable pattern change over 30 years was the increase of *Desmarestia* complex and *Plocamium cartilagineum* and the decrease of *Himantothallus grandifolius*. Both groups are still dominant, but the shift from *Himantothallus* to *Desmarestia-Plocamium* may reflects temperature rise on the Maxwell Bay coast compared to the past.

keywords: Antarctic; Long-term change; Macroalgae; Monitoring

4-2 *Multidisciplinary Sciences*

Antarcticibacterium arcticum sp. nov., a bacterium isolated from marine sediment

of the Canadian Beaufort Sea

Lee, **Yung Mi.**, **Baek**, **Kiwoon.**, Lee, Dong-Hun., **Park**, **Yerin.**, **Shin**, **Seung Chul.** and **Jin**, **Young Keun.**

International Journal of Systematic and Evolutionary Microbiology. 2020. 70(4): 2912-2917.

doi: 10.1099/ijsem.0.004122.

A Gram-stain-negative, aerobic, yellow-pigmented, flexirubin-negative, rod-shaped and non-motile bacterial strain, PAMC 28998^T, was isolated from a surface sediment sample collected from the Canadian Beaufort Sea. Strain PAMC 28998^T grew at 4-37 °C (optimum, 25 °C), at pH 7.0-9.0 (optimum, pH 7.5) and in the presence of 1.0-10.0% (w/v) NaCl. Phylogenetic analysis based on the 16S rRNA gene sequence revealed that strain PAMC 28998^T belongs to the genus *Antarcticibacterium* showing the highest sequence similarity (96.8%) with *Antarcticibacterium flavum* JB01H24^T. The average nucleotide identity and genome-to-genome distance values between PAMC 28998^T and the most closely related species (*A. flavum* JB01H24^T) were 74.1 and 18.5%. respectively, indicating that strain PAMC 28998^T is clearly distinguished from *A. flavum*. The genomic DNA G+C content calculated from genome sequences was 39.8%. The major fatty acids (>10%) were iso-$C_{15:0}$ (19.5%), anteiso-$C_{15:0}$ (18.0%), iso-$C_{16:0}$ (11.6%) and summed feature 3 ($C_{16:1}$ *ω6c* and/or $C_{16:1}$ *ω7c;* 11.4%). The major polar lipids were phosphatidylethanolamine. aminoglycolipid, two unidentified aminolipids, three unidentified phospholipids and four unidentified lipids. The major respiratory quinone was MK-6. Based on the phylogenetic, genomic and phenotypic data presented here, strain PAMC 28998^T is considered to represent a novel species of the genus *Antarcticibacterium*, for which the name *Antarcticibacterium arcticum* sp. nov. is proposed with the strain PAMC 28998^T (=KCCM 43316^T=JCM 33514^T).

keywords: *Antarcticibacterium arcticum* sp. nov.; polyphasic taxonomy; Arctic; Beaufort Sea

4-3 *Chemistry, Medicinal; Pharmacology & Pharmacy*

Anti-Inflammatory and Protein Tyrosine Phosphatase 1B Inhibitory Metabolites from the Antarctic Marine-Derived Fungal Strain *Penicillium glabrum* SF-7123

Ha, Tran Minh., Kim, Dong-Cheol., Sohn, Jae Hak., **Yim**, **Joung Han.** and Oh, Hyuncheol.

Marine Drugs. 2020. 18(5).

doi: 10.3390/md18050247.

A chemical investigation of the marine-derived fungal strain *Penicillium glabrum* (SF-7123) revealed a new citromycetin (polyketide) derivative (1) and four known secondary fungal metabolites, i.e, neuchromenin (2), asterric acid (3), myxotrichin C (4), and deoxyfunicone (5). The structures of these metabolites were identified primarily by extensive analysis of their spectroscopic data, including NMR and MS data. Results from the initial screening of anti-inflammatory effects showed that 2, 4, and 5 possessed inhibitory activity against the excessive production of nitric oxide (NO) in lipopolysaccharide (LPS)-stimulated BV2 microglial cells, with IC_{50} values of 2.7 μM, 28.1 μM, and 10.6 μM, respectively. Compounds 2, 4, and 5 also inhibited the excessive production of NO, with IC_{50} values of 4.7 μM, 41.5 μM, and 40.1 μM, respectively, in LPS-stimulated RAW264.7 macrophage cells. In addition, these compounds inhibited LPS-induced overproduction of prostaglandin E_2 in both cellular models. Further investigation of the most active compound (2) revealed that these anti-inflammatory effects were associated with a suppressive effect on the over-expression of inducible nitric oxide synthase and cyclooxygenase-2. Finally, we showed that the anti-inflammatory effects of compound 2 were mediated via the downregulation of inflammation-related pathways such as those dependent on nuclear factor kappa B and p38 mitogen-activated protein kinase in LPS-stimulated BV2 and RAW264.7 cells. In the evaluation of the inhibitory effects of the isolated compounds on protein tyrosine phosphate 1B (PTP1B) activity, compound 4 was identified as a noncompetitive inhibitor of PTP1B, with an IC_{50} value of 19.2 μM, and compound 5 was shown to inhibit the activity of PTP1B, with an IC_{50} value of 24.3 μM, by binding to the active site of the enzyme. Taken together, this study demonstrates the potential value of marine-derived fungal isolates as a bioresource for bioactive compounds.

keywords: marine-derived fungi; anti-inflammation; anti-neuroinflammation; PTP1B

4-4 *Biotechnology & Applied Microbiology*

Anti-inflammatory Effects of *Lecania*

gerlachei Extract Collected from the Antarctic King Sejong Island

Min, Seul Ki., **Kim, Jung Eun.**, **Hong, Ju-Mi.**, **Yim, Joung Han.**, Park, Hyun., **Youn, Ui Joung.**, **Han, Se Jong.** and **Kim, Il-Chan.**

Biotechnology and Bioprocess Engineering. 2020. 25(4): 543-550.

doi: 10.1007/s12257-019-0371-4.

Chronic inflammation is the cause of various diseases such as rheumatoid arthritis and asthma, with a large number of people suffering from them. There have been many reports that even link cancer to inflammation, so the development of sophisticated and powerful drugs continues to be in demand. Here we demonstrate that the methanol extract of *Lecania gerlachei*(LGME), a lichen member found in the extreme Antarctic environment, exhibits anti-inflammatory activities. Treatment of lipopoly-saccharide (LPS) stimulated Raw 264.7 murine macrophage cells with LGME reduced nitric oxide (NO) immune modulator production, and also down-regulated inducible nitric oxide synthase (iNOS), pro-inflammatory interleukin 6, 1β and 1α (IL-6, IL-1β and IL-1α), and tumor necrosis factor α (TNF-α) at both transcript and protein levels, in a concentration dependent manner. Furthermore, it was found that these effects were mediated by nuclear factor kappa B (NF-κB) signaling inhibition. Thus, our findings may contribute towards the development of novel inflammatory drugs.

keywords: *Lecania gerlachei*; lichens; Antarctica; antiinflammatory properties; nuclear factor kappa B (NF-κB) pathway

4-5 *Fisheries; Immunology; Marine & Freshwater Biology; Veterinary Sciences*

Anti-inflammatory effects of methanol extracts from the Antarctic lichen, *Amandinea* sp. in LPS-stimulated raw 264.7 macrophages and zebrafish

Kim, **Jung Eun.**, **Min**, **Seul Ki.**, **Hong**, **Ju-Mi.**, **Kim**, **Kyung Hee.**, **Han**, **Se Jong.**, **Yim**, **Joung Han.**, Park, Hyun. and **Kim**, **Il-Chan.**

Fish & Shellfish Immunology. 2020. 107: 301-308.

doi: 10.1016/j.fsi.2020.10.017.

The aim of the present study was to determine the anti-inflammatory effect of an extracts isolated from the lichen. *Amandinea* sp. was collected from the Antarctic and extracted with methanol. The basic screening of the anti-inflammatory property of the extracts was done using the NO assay. The extracts showed very little cytotoxicity, and reduced NO production in LPS-stimulated RAW 264.7 cells in a dose-dependent manner. Furthermore, the extracts inhibited LPS-induced release of pro-inflammatory cytokines such as interleukin-6 (IL-6), and tumor necrosis factor-α(TNF-α), and inflammatory mediators inducible nitric oxide synthase (iNOS), and cyclooxygenase-2 (COX-2). The extracts also reduced the cytosolic *p*-IκB-α level and the level of the nuclear factor p65. We examined the anti-inflammatory effects of the extracts using zebrafish *in vivo*. The extracts reduced the amount of reactive oxygen species (ROS) in LPS-induced zebrafish larvae and inhibited the mRNA expression of inflammatory cytokines and mediators in a tail-cutting induced model. These results are similar to those obtained in vitro with RAW 264.7 cells. Collectively, the data suggest that the extracts may contain one of more compounds with anti-inflammatory effects. Further studies are required to identify the candidate compound/s and to understand the mechanism of action of the extract.

keywords: Antarctic; *Amandinea* sp.; Anti-Inflammation; Pro-inflammatory cytokines; NF-κB pathway; Zebrafish

4-6 *Evolutionary Biology; Genetics & Heredity*

Bacterial Origin and Reductive Evolution of the CPR Group

Bokhari, Rijja Hussain., Amirjan, Nooreen., Jeong, Hyeonsoo., **Kim, Kyung Mo.** and 2 others.

Genome Biology and Evolution. 2020. 12(3): 103-121.

doi: 10.1093/gbe/evaa024.

The candidate phyla radiation (CPR) is a proposed subdivision within the bacterial domain comprising several candidate phyla. CPR organisms are united by small genome and physical sizes, lack several metabolic enzymes, and populate deep branches within the bacterial subtree of life. These features raise intriguing questions regarding their origin and mode of evolution. In this study, we performed a comparative and phylogenomic analysis to investigate CPR origin

and evolution. Unlike previous gene/protein sequence-based reports of CPR evolution, we used protein domain superfamilies classified by protein structure databases to resolve the evolutionary relationships of CPR with non-CPR bacteria, Archaea, Eukarya, and viruses. Across all supergroups, CPR shared maximum superfamilies with non-CPR bacteria and were placed as deep branching bacteria in most phylogenomic trees. CPR contributed 1.22% of new superfamilies to bacteria including the ribosomal protein L19e and encoded four core superfamilies that are likely involved in cell-to-cell interaction and establishing episymbiotic lifestyles. Although CPR and non-CPR bacterial proteomes gained common superfamilies over the course of evolution, CPR and Archaea had more common losses. These losses mostly involved metabolic superfamilies. In fact, phylogenies built from only metabolic protein superfamilies separated CPR and non-CPR bacteria. These findings indicate that CPR are bacterial organisms that have probably evolved in an Archaea-like manner via the early loss of metabolic functions. We also discovered that phylogenies built from metabolic and informational superfamilies gave contrasting views of the groupings among Archaea, Bacteria, and Eukarya, which add to the current debate on the evolutionary relationships among superkingdoms.

keywords: candidate phyla radiation; tree of life; phylogenetics; reductive evolution; protein structure

4-7 *Biotechnology & Applied Microbiology; Energy & Fuels*

Biodiesel and flavor compound production using a novel promiscuous cold-adapted SGNH-type lipase (*Ha*SGNH1) from the psychrophilic bacterium *Halocynthiibacter arcticus*

Le, Ly Thi Huong Luu., Yoo, Wanki., Jeon, Sangeun., **Lee, Chang Woo.**, Kim, Kyeong Kyu., **Lee, Jun Hyuck.** and Kim, T. Doohun.

Biotechnology for Biofuels. 2020. 13(1).

doi: 10.1186/s13068-020-01696-x.

Background: Biodiesel and flavor compound production using enzymatic transesterification by microbial lipases provides mild reaction conditions and low energy cost compared to the chemical process. SGNH-type lipases are very effective catalysts for enzymatic transesterification due to their high reaction rate, great stability, relatively small size for convenient genetic manipulations, and ease of immobilization. Hence, it is highly important to identify novel SGNH-type lipases with high catalytic efficiencies and good stabilities. Results: A promiscuous cold-adapted SGNH-type lipase (*Ha*SGNH1) from *Halocynthiibacter arcticus* was catalytically characterized and functionally explored. *Ha*SGNH1 displayed broad substrate specificity that included *tert*-butyl acetate, glucose pentaacetate, and *p*-nitrophenyl esters with excellent stability and high efficiency. Important amino acids (N83, M86, R87, F131, and I173F) around the substrate-binding pocket were shown to be responsible for catalytic activity, substrate specificity, and reaction kinetics. Moreover, immobilized *Ha*SGNH1 was used to produce high yields of butyl and oleic esters. Conclusions: This work provides a molecular understanding of substrate specificities, catalytic regulation, immobilization, and industrial applications of a promiscuous cold-adapted SGNH-type lipase (*Ha*SGNH1) from *H. arcticus*. This is the first analysis on biodiesel and flavor synthesis using a cold-adapted halophilic SGNH-type lipase from a *Halocynthiibacter* species.

keywords: *Ha*SGNH1; *Halocynthiibacter arcticus*; Immobilization; SGNH-type lipase; Substrate specificity; Biodiesel

4-8 *Pharmacology & Pharmacy*

Biological Activity of Chemical Constituents Isolated from Strain *Chlamydomonas* sp. KSF108 (Chlamydomonadaceae)

Tran, Huynh Nguyen Khanh., **Youn, Ui Joung.**, Kim, Minji., Cao, Thao Quyen., Kim, Jeong Ah., Woo, Mi Hee., **Kim, Sanghee.** and Min, Byung Sun.

Natural Product Sciences. 2020. 26(1): 59-63.

doi: 10.20307/nps.2020.26.1.59.

This study focused on investigation of the immunosuppressive inhibitory effect through determination of IL-2 production of nine compounds (1 - 9) isolated from *Chlamydomonas* sp. KSF108. Among them, compounds 1, 5, and 6 displayed moderately inhibitory effects on IL-2 production at a concentration of 100 μM. In addition, the related ones including

cytotoxic, anti-inflammatory, and anti-oxidant activities were also elucidated. 6 further displayed cytotoxic activity against the MCF-7 cell line, with an IC_{50} value of 17.2 μM and 4, 6 7, and 9 possessed significant DPPH radical scavenging activity, with IC_{50} values ranging from 3.1 to 4.4 μM. To the best of our knowledge, this is the first report on the bioactivity of isolated chemical constituents from the genus *Chlamydomonas*. Compounds 1 and 5 investigated for the first time in the activity of immunosuppressivity and 6 may come to serve as the most important marker in broad-spectrum activities of the secondary metabolites identified from *C.* sp. KSF108.

keywords: Chlamydomonadaceae; *Chlamydomonas* sp. KSF108; Immunosuppressive; Anti-inflammatory; Cytotoxic, Anti-oxidant

4-9 *Plant Sciences; Chemistry, Medicinal; Pharmacology & Pharmacy*

Calvatianone, a Sterol Possessing a 6/5/6/5-Fused Ring System with a Contracted Tetrahydrofuran B-Ring, from the Fruiting Bodies of *Calvatia nipponica*

Lee, **Seulah.** and 6 others.

Journal of Natural Products. 2020. 83(9): 2737-2742.

doi: 10.1021/acs.jnatprod.0c00673.

Calvatia nipponica is an extremely rare mushroom with a limited number of studies on its chemical components and biological activities published. Here we report the isolation of a novel sterol, calvatianone (1), possessing a 6/5/6/5-fused ring system with a contracted tetrahydrofuran B-ring, and four known steroids (2-5) from the fruiting bodies of *C. nipponica*. The structure of calvatianone including its absolute configuration was determined by NMR spectroscopic analyses, HR-ESIMS, gauge-including atomic orbital NMR chemical shift calculations, and ECD calculations. Ergosterol peroxide (3) and cyathisterol (4) suppressed the cell viability increase induced by 17*β*-estradiol in MCF-7 breast cancer cell lines, suggesting a possible approach for these compounds to serve as ER*α* antagonists.

4-10 *Genetics & Heredity*

Characterization of complete mitochondrial genome of *Pogonophryne albipinna* (Perciformes: Artedidraconidae)

Tabassum, Nazia., Alam, Md. Jobaidul., **Kim, Jeong-Hoon.** and 4 others.

Mitochondrial DNA Part B-Resources. 2020. 5(1): 156-157.

doi: 10.1080/23802359.2019.1698361.

The complete mitochondrial genome of *Pogonophryne albipinna* was determined by the MiSeq platform, which was the first report in the family Artedidraconidae. The circular form of its mitochondrial genome was 17,086bp, which contained the canonical eukaryotic 37 genes. The gene orders of *P. albipinna* was identical to the other icefish species, in which there was additional non-coding region and translocation of ND6 gene. Except for ATP6 gene and COI (GTG), 11 genes begin with the typical start codon, while incomplete stop codons (T--) were identified in COII, ND4, and CytB. Phylogenetic tree with the currently known mitogenomes in suborder Notothenioidei showed that *P. albipinna* was located distinctly from those in Bathydraconidae and Nototheniidae forming a unique cluster as Artedidraconidae. The first complete mitochondrial genome of *P. albipinna* would be the fundamental data to understand the evolutional relationship of icefish species in the Antarctic Oceans.

keywords: Artedidraconidae; mitogenome; MiSeq; *Pogonophryne albipinna*

4-11 *Biotechnology & Applied Microbiology; Microbiology*

Characterization of CYP125A13, the First Steroid C-27 Monooxygenase from *Streptomyces peucetius* ATCC27952

Rimal, Hemraj., Subedi, Pradeep., Kim, Ki-Hwa., Park, Hyun., **Lee, Jun Hyuck.** and Oh, Tae-Jin.

Journal of Microbiology and Biotechnology. 2020. 30(11): 1750-1759.

doi: 10.4014/jmb.2007.07004.

The characterization of cytochrome P450 CYP125A13 from *Streptomyces peucetius* was conducted using cholesterol as the sole substrate. The in vitro enzymatic assay utilizing putidaredoxin and putidaredoxin reductase from *Pseudomonas putida* revealed that CYP125A13 bound cholesterol and hydroxylated it. The

calculated K_D value, catalytic conversion rates, and Km value were 56.92 ± 11.28 μM, 1.95 nmol min^{-1} $nmol^{-1}$, and 11.3 ± 2.8 μM, respectively. Gas chromatography-mass spectrometry (GC-MS) analysis showed that carbon 27 of the cholesterol side-chain was hydroxylated, characterizing CYP125A13 as steroid C27-hydroxylase. The homology modeling and docking results also revealed the binding of cholesterol to the active site, facilitated by the hydrophobic amino acids and position of the C27-methyl group near heme. This orientation was favorable for the hydroxylation of the C27-methyl group, supporting the in vitro analysis. This was the first reported case of the hydroxylation of cholesterol at the C-27 position by *Streptomyces* P450. This study also established the catalytic function of CYP125A13 and provides a solid basis for further studies related to the catabolic potential of *Streptomyces* species.

keywords: *Streptomyces peucetius*; cytochrome P450; CYP125A13; 27-hydroxycholesterol; regio-selective hydroxylation

4-12 *Genetics & Heredity*

Characterization of the complete mitochondrial genome of the false trevally, *Lactarius lactarius* (Perciformes: Lactariidae)

Tabassum, Nazia., Lee, Ji-Hyun., Lee, Soo Rin., **Kim, Jeong-Hoon.** and Kim, Hyun-Woo.

Mitochondrial DNA Part B-Resources. 2020. 5(2): 1806-1807.

doi: 10.1080/23802359.2020.1750988.

The complete mitochondrion DNA sequence of *Lactarius lactarius* was determined by next generation sequencing (NGS) platform as the first mitogenome report in the family. The mitogenome of *L. lactarius* wa 16,642 bp in length that contains 13 gene-encoded proteins, 2 ribosomal RNA gene (12S and 16S), 22 tRNA gene, and a control region (D-loop). Besides COX1 gene (GTG), all the other protein-coding genes showed typical (ATG) start codon. Incomplete stop condons (TA-/T-) were identified in COX2, COX3, ND2, ND3, ND4 and Cyt B. A phylogenetic analysis with currently reported mitogenomes of its relative species, *L. lactarius* formed a Lactariidae clade distinct from other families. Two species, Pentaceros japonicus (AB739063) and Banjos banjos (KT345965) were among the most closely related species with 86.61% and 86.33% sequence identity, respectively.

keywords: MitochondrionMiseq; *Lactarius lactarius*; Lactariidae

4-13 *Biochemistry & Molecular Biology; Ecology; Evolutionary Biology*

Chromosomal-level assembly of *Takifugu obscurus* (Abe, 1949) genome using third-generation DNA sequencing and Hi-C analysis

Kang, Seunghyun., **Kim, Jin-Hyoung.**, **Jo, Euna.**, Lee, Seung Jae., **Jeong, Jihye.**, **Kim, Bo-Mi.**, **Lee, Jun Hyuck.** and 4 others.

Molecular Ecology Resources. 2020. 20(2): 520-530.

doi: 10.1111/1755-0998.13132.

The Tetraodontidae family are known to have relatively small and compact genomes compared to other vertebrates. The obscure puffer fish *Takifugu obscurus* is an anadromous species that migrates to freshwater from the sea for spawning. Thus the euryhaline characteristics of *T. obscurus* have been investigated to gain understanding of their survival ability, osmoregulation, and other homeostatic mechanisms in both freshwater and seawater. In this study, a high quality chromosome-level reference genome for *T. obscurus* was constructed using long-read Pacific Biosciences (PacBio) Sequel sequencing and a Hi-C-based chromatin contact map platform. The final genome assembly of *T. obscurus* is 381 Mb, with a contig N50 length of 3,296 kb and longest length of 10.7 Mb, from a total of 62 Gb of raw reads generated using single-molecule real-time sequencing technology from a PacBio Sequel platform. The PacBio data were further clustered into chromosome-scale scaffolds using a Hi-C approach, resulting in a 373 Mb genome assembly with a contig N50 length of 15.2 Mb and and longest length of 28 Mb. When we directly compared the 22 longest scaffolds of *T. obscurus* to the 22 chromosomes of the tiger puffer *Takifugu rubripes*, a clear one-to-one orthologous relationship was observed between the two species, supporting the chromosome-level assembly of *T. obscurus*. This genome assembly can serve as a valuable genetic resource for exploring fugu-specific compact

genome characteristics, and will provide essential genomic information for understanding molecular adaptations to salinity fluctuations and the evolution of osmoregulatory mechanisms.

keywords: chromosome-level assembly; fugu genome; Hi-C assembly; long-read sequencing; *Takifugu obscurus*

4-14 *Microbiology*

Comparative Genomic Study of Polar Lichen-Associated *Hymenobacter* sp. PAMC 26554 and *Hymenobacter* sp. PAMC 26628 Reveals the Presence of Polysaccharide-Degrading Ability Based on Habitat

Ghimire, Nisha., Han, So-Ra., Kim, Byeollee., Park, Hyun., **Lee, Jun Hyuck.** and Oh, Tae-Jin.

Current Microbiology. 2020. 77(10): 2940-2952.

doi: 10.1007/s00284-020-02120-1.

The genus *Hymenobacter* is classified in the family Hymenobacteraceae under the phylum Bacteroidetes. They have been isolated from diverse environments, such as air, soil, and lichen, along with extreme polar environments, including the Arctic and Antarctic regions. The polar regions have attracted intense research interest for the discovery of novel microorganisms and their functions. Analysis of the polysaccharide utilization-related carbohydrate-active enzyme among the two lichen-associated polar organisms *Hymenobacter* sp. PAMC 26554 and *Hymenobacter* sp. PAMC 26628 was performed, along with its comparison with the complete genome of the same genus available in the NCBI database. The study was conducted relying on the AZCL screening data for the two polar lichen-associated species. While comparing with eight other complete genomes, differences in polysaccharide preferences based on the isolation environment and biosample source were discovered. All the species showed almost similar percentage of cellulose synthesis and degradation genes. However, the polar lichen-associated microorganism was found to have a high percentage of hemicellulose degradation genes, and less starch and laminarin degradation. The *Hymenobacter* species with higher number of hemicellulose degradation genes was found to have a lower number of starch and laminarin degradation genes and vice versa, highlighting the differences in polysaccharide utilization among the species.

keywords: Biosample; Habitat; *Hymenobacter*; lichen; polar region; polysaccharide utilization

4-15 *Genetics & Heredity*

Complete chloroplast genome sequence of a medicinal landrace citrus Jinkyool (*Citrus sunki* Hort. ex Tanaka) in Jeju Island, Korea

Yoo, Yo-Han., Oh, Chang Jae., **Shin, Seung Chul.**, **Seo, Suyeon.**, Kim, Minju., Yun, Su-Hyun., Song, Kwan Jeong., **Lee, Hyoungseok.** and Kim, Ho Bang.

Mitochondrial DNA Part B-Resources. 2020. 5(3): 3719-3720.

doi: 10.1080/23802359.2020.1833771.

Citrus sunki (Jinkyool) is a medicinal landrace citrus belonging to the Rutaceae family. We determined the complete chloroplast genome (160,699 bp) of *C. sunki* CRS0085 in Jeju Island, Korea. The genome is composed of four distinct parts; a large single copy of 87,918 bp, a small single copy of 21,355 bp, and a pair of inverted repeat regions of 25,713 bp. A total of 134 genes including 89 protein-coding genes, 37 tRNA genes, and eight rRNA genes were identified. The phylogenetic tree showed that *C. sunki* CRS0085 has the closest relationship with *C. reticulata* within genus *Citrus*.

keywords: *Citrus sunki*; Jinkyool; Landrace; medicinal fruit; chloroplast genome; phylogenetic analysis

4-16 *Genetics & Heredity; Marine & Freshwater Biology*

Complete genome sequence of *Antarcticibacterium flavum* JBO1H24^T from an Antarctic marine sediment

Lee, Yung Mi., **Jin, Young Keun.** and **Shin, Seung Chul.**

Marine Genomics. 2020. 50.

doi: 10.1016/j.margen.2019.100695.

Antarcticibacterium flavum JB01H24^T was isolated from a marine sediment of the Ross Sea, Antarctica. Whole-

genome sequencing of the strain *Antarcticibacterium flavum* JB01H24^T was achieved using PacBio RS II platform. The resulting complete genome comprised of one closed, complete chromosome of 4,319,074 base pairs with a 40.87% G + C content, where genomic analyses demonstrated that it is constituted mostly by putative ORFs with unknown functions, representing a novel genetic feature. It is the first complete genome sequence of the *Antarcticibacterium* strain.

keywords: *Antarcticibacterium flavum*; Genome sequence; Marine sediment; Ross Sea; Antarctica

4-17 *Biochemistry & Molecular Biology; Biotechnology & Applied Microbiology; Genetics & Heredity*

Complete genome sequence of *Sphingobium* sp. strain PAMC 28499 reveals a potential for degrading pectin with comparative genomics approach

Han, So-Ra., Jang, Sung-Min., Chi, Young Min., Kim, Byeollee., Jung, Sang-Hee., **Lee, Yung Mi.**, Uetake, Jun., **Lee, Jun Hyuck.** and 2 others.

Genes & Genomics. 2020. 42(9): 1087-1096.

doi: 10.1007/s13258-020-00976-y.

Background *Spingobium sp.*PAMC 28499 is isolated from the glaciers of Uganda. Uganda is a unique region where hot areas and glaciers coexist, with a variety of living creatures surviving, but the survey on them is very poor. The genetic character and complete genome information of *Sphingobium* strains help with environmental studies and the development of better to enzyme industry. Objective In this study, complete genome sequence of *Spingobium* sp. PAMC 28499 and comparative analysis of *Spingobium* species strains isolated from variety of the region. Methods Genome sequencing was performed using PacBio sequel single-molecule real-time (SMRT) sequencing technology. The predicted gene sequences were functionally annotated and gene prediction was carried out using the program NCBI non-redundant database. And using dbCAN2 and KEGG data base were degradation pathway predicted and protein prediction about carbohydrate active enzymes (CAZymes). Results The genome sequence has 64.5% GC content, 4432 coding protein coding genes, 61 tRNAs, and 12 rRNA operons. Its genome encodes a simple set of metabolic pathways relevant to pectin and its predicted degradation protein an unusual distribution of CAZymes with extracellular esterases and pectate lyases. CAZyme annotation analyses revealed 165 genes related to carbohydrate active, and especially we have found GH1, GH2, GH3, GH38, GH35, GH51, GH51, GH53, GH106, GH146, CE12, PL1 and PL11 such as known pectin degradation genes from *Sphingobium yanoikuiae*. These results confirmed that this *Sphingobium* sp. strain PAMC 28499 have similar patterns to RG I pectin-degrading pathway. Conclusion In this study, isolated and sequenced the complete genome of *Spingobium* sp. PAMC 28499. Also, this strain has comparative genome analysis. Through the complete genome we can predict how this strain can store and produce energy in extreme environment. It can also provide bioengineered data by finding new genes that degradation the pectin.

keywords: Carbohydrate active enzyme; Comparative genomics; Genome sequencing; Pectin degradation; *Sphingobium* sp.

4-18 *Genetics & Heredity*

Complete mitochondrial genome and phylogenetic analysis of the Weddell seal, *Leptonychotes weddellii*

Kim, Jong-U. and **Kim, Jeong-Hoon.**

Mitochondrial DNA Part B-Resources. 2020. 5(3): 3357-3358.

doi: 10.1080/23802359.2020.1820390.

The Weddell seal, *Leptonychotes weddellii*, which belongs to the family Phocidae, is an abundant pinniped that inhabits the Antarctica. Here, we present the complete mitochondrial genome and phylogeny of *L. weddellii*. The total length of the mitogenome is 16,762 bp, consisting of 13 protein-coding genes (PCGs), 22 tRNA genes, and 2 rRNA genes. The base composition of the mitogenome is 34.26% (A), 25.51% (T), 27.09% (C), and 13.11% (G), and 40.22% for overall GC contents. The description of this mitogenome can provide information about variations at the intra-species level and aid phylogenetic studies in family Phocidae.

keywords: *Leptonychotes weddellii*; mitogenome; pinniped; Weddell seal

4-19 *Genetics & Heredity*

The complete mitochondrial genome of Eaton's skate, *Bathyraja eatonii* (Rajiformes, Arhynchobatidae)

Kim, Jinmu., Jang, Sung-Min., Choi, Eunkyung., **Jo, Euna.**, Lee, Seung Jae., Kim, Sun Hee., Chi, Young Min., **Kim, Jin-Hyoung.** and Park, Hyun.

Mitochondrial DNA Part B-Resources. 2021. 6(1): 91-92.

doi: 10.1080/23802359.2020.1847608.

The complete mitochondrial genome of Eaton's skate Bathyraja eatonii was studied using the long-read technology, PacBio Sequel System. The complete mitochondrial genome form of *B. eatonii* was 16,698 bp and it's comprised of 13 protein-coding genes, 22 tRNA and 2 rRNA. The base composition of *B. eatonii* is analyzed 31.94% for A, 33.94% for T, 13.49% for G, 20.64% for C, the result of GC content was 33.94%. Phylogenetic analysis showed that *B. eatonii* was closely related to *Bathyraja meridionalis* in Arhynchobatidae family, and this first mitochondrial genome of Antarctic skate would provide fundamental information to the evolutional relationship of Antarctic fishes

keywords: PacBio; mitochondria genome; *Bathyraja eatonii*; long-read technology; Arhynchobatidae

4-20 *Genetics & Heredity*

The complete mitochondrial genome of *Macrourus whitsoni* (Gadiformes, Macrouridae)

Lee, Seung Jae., Im, Tae-Eul., **Jo, Euna.**, Choi, Eunkyung., Chi, Young Min., **Kim, Jin-Hyoung.**, **Kim, Jeong-Hoon.** and Park, Hyun.

Mitochondrial DNA Part B-Resources. 2020. 5(3): 2326-2327.

doi: 10.1080/23802359.2020.1773339.

The complete mitochondrial genome of *Macrourus witsoni* was determined in this study by the Long-read Technology, such as PacBio Sequel System. The Long-read Technology, which can sequence continuously the whole vertebrate mitochondrial genome, allows more accurate genomes to be completed. The circular form of its mitochondrial genome was 16,714bp, which contained 13 protein-coding genes, 22 tRNA, and 2 rRNA. The gene orders of *M.witsoni* was identical to that of the other species of Macrouridae family. Phylogenetic analysis indicated *M. witsoni* was mostly close to *C.kishinouyei* in the Macrouridae family.

keywords: Mitochondria genome; PacBio; Macrouridae; *Macrourus witsoni*

4-21 *Genetics & Heredity*

The complete mitochondrial genome of Patagonian moray cod, *Muraenolepis orangiensis* Vaillant, 1888 (Gadiformes, Muraenolepididae)

Choi, Eunkyung., Park, Seong Hee., Lee, Seung Jae., **Jo, Euna.**, Kim, Jinmu., **Kim, Jeong-Hoon.**, **Kim, Jin-Hyoung.** and 2 others.

Mitochondrial DNA Part B-Resources. 2020. 5(3): 2707-2708.

doi: 10.1080/23802359.2020.1787275.

The full-length mitochondrial genome of *Muraenolepis orangiensis* (Vaillant, 1888) was studied using PacBio platform and it is first report in a Muraenolepididae family. The circular form of mitochondria genome is 16,833 bp including 13 protein-coding genes, two rRNA, and 22 tRNA. Start codon of 13 protein-coding genes was only ATG but three types of stop codons (TAA, T(AA), and TAG) were detected. To evaluate evolutionary position of *M. orangiensis*, the phylogenetic tree with other 13 Antarctic fishes belonged to five families were showed that *M. orangiensisis* unique cluster as a Muraenolepididae family and this study would provide fundamental data to understand the evolutionary relationship of fishes founded in Antarctic area.

keywords: Mitochondria genome; *Muraenolepis orangiensis*; Patagonian moray cod; PacBio

4-22 *Genetics & Heredity*

The complete mitochondrial genome of the Antarctic marbled rockcod, *Notothenia rossii* (Perciformes, Nototheniidae)

Jo, Euna., Cho, Yll Hwan., Lee, Seung Jae., Choi, Eunkyung., **Kim, Jeong-Hoon.**, Chi, Young Min., **Kim, Jin-Hyoung.** and Park, Hyun.

Mitochondrial DNA Part B-Resources. 2020. 5(3): 2421-2422.

doi: 10.1080/23802359.2020.1775507.

The complete mitochondrial genome of *Notothenia rossii* was obtained using PacBio Sequel long-read sequencing platform. The mitogenome of *N. rossii* was circular form and 18,274 bp long, which consists of 13 protein-coding genes, 24 tRNAs, 2 rRNAs, and non-coding control region. Particularly, we found duplicated $tRNA^{Thr}$ and $tRNA^{Pro}$ in addition to the typical 22 tRNAs. The phylogenetic tree revealed that *N. rossii* was most closely related to *N. coriiceps* among species in the Nototheniidae clade within the suborder Notothenioidei.

keywords: *Notothenia rossii*; mitochondrial genome; Antarctica; Notothenioidei; PacBio

4-23 *Genetics & Heredity*

Complete mitochondrial genome of the snow petrel, *Pagodroma nivea*

Kim, Jong-U. and **Kim, Jeong-Hoon.**

Mitochondrial DNA Part B-Resources. 2020. 5(3): 3355-3356.

doi: 10.1080/23802359.2020.1820389.

The snow petrel, *Pagodroma nivea* is a small sea bird endemic to Antarctica and the Southern Ocean. Herein, we assembled a complete mitochondrial genome of the snow petrel as a first revealed genetic resource in Pagodroma family. The mitogenome is 17,279 bp in length and consists of 13 protein-coding genes (PCGs), 22 *tRNA* genes, and two *rRNA* genes. Base composition is 31.3% A, 25.3% T, 30.1% C, and 13.2% G with CG content of 43.4%. These results will provide a useful basis for further genetic and phylogenetic studies of this species.

keywords: Mitogenome; *Pagodroma nivea*; sea bird; snow petrel

4-24 *Biotechnology & Applied Microbiology; Energy & Fuels*

Co-production of biodiesel and bioethanol using psychrophilic microalga *hlamydomonas* sp. KNM0029C isolated from Arctic sea ice

Kim, Eun Jae., **Kim, Sanghee.**, **Choi, Han-Gu.** and **Han, Se Jong.**

Biotechnology for Biofuels. 2020. 13(1).

doi: 10.1186/s13068-020-1660-z.

Background: Biofuels, generated using microalgae as sustainable energy, have received a lot of attention. Microalgae can be cultivated at low cost with CO_2 and solar energy without competition from edible crops. Psychrophilic microalgae can be a suitable feedstock to produce biofuels without the environmental constraints of low temperatures, because they can grow below 10 °C. However, there is a lack of efficient strategies using psychrophilic microalgae to produce biodiesel and bioethanol. Therefore, the current study aimed to optimize the production of biodiesel and bioethanol from Arctic *Chlamydomonas* sp. KNM0029C at low temperatures. Results: After incubation in a 20-L photobioreactor, fatty acid methyl ester (FAME) was extracted using modified FAME extraction methods, producing a maximum yield of 0.16-g FAME/g KNM0029C. Residual biomass was pretreated for bioethanol production, and the yields from different methods were compared. The highest bioethanol yield (0.22-g/g residual biomass) was obtained by pretreatment with enzyme (amyloglucosidase) after sonication. Approximately 300-mg biofuel was obtained, including 156-mg FAME biodiesel and 144-mg bioethanol per g dried cells, representing the highest recorded yield from psychrophilic microalgae. Conclusions: This is the first to attempt at utilizing biomass from psychrophilic Arctic microalga *Chlamydomonas* sp. KNM0029C for the co-production of bioethanol and biodiesel, and it yielded the highest values among reported studies using psychrophilic organisms. These results can be used as a source for the efficient biofuel production using polar microalgae.

keywords: Arctic; Biodiesel; Bioethanol; *Chlamydomonas*; Psychrophilic microalgae

4-25 *Biochemistry & Molecular Biology; Biophysics*

Crystal structure of the reactive intermediate/imine deaminase A homolog from the Antarctic bacterium *Psychrobacter* sp. PAMC 21119

Kwon, Sunghark., **Lee, Chang Woo.**, **Koh, Hye Yeon.**, Park, Hyun., **Lee, Jun Hyuck.** and Park, Hyun Ho.

Biochemical and Biophysical Research Communications. 2020. 522(3): 585-591.

doi: 10.1016/j.bbrc.2019.11.139.

The RidA subfamily proteins catalyze the deamination reaction of enamine/imine intermediates, which are metabolites of amino acids such as threonine and serine. Numerous structural and functional studies have been conducted on RidA isolated from mesophiles and thermophiles. However, little is known about the structure of the RidA proteins isolated from psychrophiles. In the present study, we elucidated the crystal structure of RidA from the Antarctic bacterium *Psychrobacter* sp. PAMC 21119 (Pp-RidA) at 1.6 Å resolution to identify the structural properties contributing to cold-adaptability. Although the overall structure of Pp-RidA is similar to those of its homologues, it exhibits specific structural arrangements of a loop positioned near the active site, which is assumed to play a role in covering the active site of catalysis. In addition, the surface electrostatic potential of Pp-RidA suggested that it exhibits stronger electrostatic distribution relative to its homologues. Our results provide novel insights into the key determinants of cold-adaptability.

keywords: RidA; Deamination; Psychrophile; Antarctic bacterium; Cold-adaptability

---

4-26 *Crystallography; Materials Science, Multidisciplinary*

Crystallization and Preliminary X-ray Diffraction Study of a Novel Bacterial Homologue of Mammalian Hormone-Sensitive Lipase (halip1) from *Halocynthiibacter arcticus*

Jeon, Sangeun., **Hwang, Jisub.**, Yoo, Wanki., **Do, Hackwon.**, **Kim, Han-Woo.**, Kim, Kyeong Kyu., **Lee, Jun Hyuck.** and Kim, T. Doohun.

Crystals. 2020. 10(11).

doi: 10.3390/cryst10110963.

Hormone sensitive lipase is a central enzyme in triacylglycerol hydrolysis, lipid modification, and transformation of various lipids. Microbial hormone-sensitive lipases, which are highly similar to a catalytic domain of mammalian equivalents, have attracted strong attention due to their application potentials. Here, characterization and a preliminary X-ray crystallographic analysis of a novel bacterial homologue of hormone-sensitive lipase (*Ha*Lip1) from Halocynthiibacter arcticus is reported. Sequence analysis shows that *Ha*Lip1 has a conserved serine residue within the GDSAG motif. In addition, a characteristic HGGG motif for oxyanion formation was identified. The *Ha*Lip1 protein was overexpressed in *E. coli*. SDS-PAGE, overlay assay, and mass analysis were performed to confirm purity and activity of *Ha*Lip1 protein. Furthermore, *Ha*Lip1 was crystallized in a condtion consisting of 25% (*w/v*) PEG 3350, 0.1 M Hepes-KOH, pH 7.5, 0.2 M sodium chloride. Diffraction data were processed to 1.30 Å with an R_{merge} of 7.3%. The crystals of *Ha*Lip1 belong to the $P2_12_12_1$, with unit cell parameters of a = 54.6 Å, b = 59.5 Å, and c = 82.9 Å.

keywords: hormone sensitive lipase; psychrophilic bacterium; crystallization

---

4-27 *Engineering, Environmental; Environmental Sciences*

Development and Evaluation of Olive Flounder *cyp1a1*-Luciferase Assay for Effective Detection of CYP1A-Inducing Contaminants in Coastal Sediments

Jung, Jee-Hyun., Yim, Bora., Jeong, Sol., Yoon, Mee-Sup., **Kim, Bo-Mi.** and 4 others.

Environmental Science & Technology. 2020. 54(23): 15170-15179.

doi: 10.1021/acs.est.0c06921.

Flounders have been widely used as indicator species for monitoring the benthic environment of marine coastal regions owing to their habitat and feeding preferences in or on sandy sediments. Here, a single-step, sensitive, specific, and simple luciferase assay was developed, using the olive flounder *cyp1a1* gene, for effective detection of CYP1A-inducing contaminants in coastal sediments. The developed *cyp1a1*-luciferase assay was highly sensitive to the widely used CYP1A inducers 2,3,7,8-tetrachlorodibenzo-*p*-dioxin (TCDD), benzo[*a*]pyrene (B[*a*]P), and 3,3',4,4',5-pentachlorobiphenyl (PCB 126). In the case of TCDD, significant dose-dependent increases in luciferase activity (0.3-300 ng/L) were detected. The assay was more sensitive to PCB 126 than to B[*a*]P. The assay also involved the highly sensitive expression of luciferase to extracted mixtures of PCBs and polycyclic

aromatic hydrocarbons (PAHs) collected from coastal sediments. PCBs were more capable of *cyp1a1* induction in the assay system at small doses than PAHs in environmental samples. Using the *cyp1a1*-luciferase assay along with water or sediment chemistry will certainly aid in diagnosing CYP1A-inducing contaminants in coastal environments.

keywords: *cyp1a1*; PAHs; *cyp1a1* luciferase assay

4-28 *Multidisciplinary Sciences*

Different types of agricultural land use drive distinct soil bacterial communities

Lee, Shin Ae., Kim, Jeong Myeong., Kim, Yiseul., Joa, Jae-Ho., Kang, Seong-Soo., Ahn, Jae-Hyung., **Kim, Mincheol.** and 2 others.

Scientific Reports. 2020. 10(1).

doi: 10.1038/s41598-020-74193-8.

Biogeographic patterns in soil bacterial communities and their responses to environmental variables are well established, yet little is known about how different types of agricultural land use affect bacterial communities at large spatial scales. We report the variation in bacterial community structures in greenhouse, orchard, paddy, and upland soils collected from 853 sites across the Republic of Korea using 16S rRNA gene pyrosequencing analysis. Bacterial diversities and community structures were significantly differentiated by agricultural land-use types. Paddy soils, which are intentionally flooded for several months during rice cultivation, had the highest bacterial richness and diversity, with low community variation. Soil chemical properties were dependent on agricultural management practices and correlated with variation in bacterial communities in different types of agricultural land use, while the effects of spatial components were little. *Firmicutes*, *Chloroflexi*, and *Acidobacteria* were enriched in greenhouse, paddy, and orchard soils, respectively. Members of these bacterial phyla are indicator taxa that are relatively abundant in specific agricultural land-use types. A relatively large number of taxa were associated with the microbial network of paddy soils with multiple modules, while the microbial network of orchard and upland soils had fewer taxa with close mutual interactions. These results suggest that anthropogenic agricultural management can create soil disturbances that determine bacterial community structures, specific bacterial taxa, and their relationships with soil chemical parameters. These quantitative changes can be used as potential biological indicators for monitoring the impact of agricultural management on the soil environment.

keywords: agricultural land; land use; soil bacterial community

4-29

Discrepancies between Mitochondrial DNA and AFLP Genetic Variation among Lineages of Sea Slaters *Ligia* in the East Asian Region

Kang, Seunghyun. and Jung, Jongwoo.

Animal Systematics, Evolution and Diversity. 2020. 36(4): 347-353.

doi: 10.5635/ASED.2020.36.4.061.

Although sea slaters *Ligia* have a significant role in rocky shore habitats, their taxonomic entities have not been clearly understood. In this study, we investigated whether genetic variation inferred from a nuclear genetic marker, namely amplified fragment length polymorphism (AFLP), would conform to that of a mitochondrial DNA marker. Using both the mitochondrial DNA marker and the AFLP marker amplified by the six selective primer sets, we analyzed 95 *Ligia* individuals from eight locations from East Asia. The direct sequencing of mitochondrial 16S rRNA gene revealed three distinct genetic lineages, with 9.8-11.7 Kimura 2-parameter genetic distance. However, the results of AFLP genotyping analysis with 691 loci did not support those of mitochondrial DNA, and revealed an unexpectedly high proportion of shared polymorphisms among lineages. The inconsistency between the two different genetic markers may be explained by difference in DNA evolutionary history, for example inheritance patterns, effective population size, and mutation rate. The other factor is a possible genomic island of speciation, in that most of the genomic parts are shared among lineages, and only a few genomic regions have diverged.

keywords: *Ligia*; AFLP; 16S rRNA gene; genetic variation; East Asia

Distinct gut microbiotas between southern elephant seals and Weddell seals of Antarctica

Kim, Mincheol., **Cho, Hyunjun.** and **Lee, Won Young.**

Journal of Microbiology. 2020. 58(12): 1018-1026.

doi: 10.1007/s12275-020-0524-3.

The gut microbiome provides ecological information about host animals, but we still have limited knowledge of the gut microbiome, particularly for animals inhabiting remote locations, such as Antarctica. Here, we compared fecal microbiota between southern elephant seals (*Mirounga leonina*) and Weddell seals (*Leptonychotes weddelli*), that are top predatory marine mammals in the Antarctic ecosystem, using 16S rRNA amplicon sequencing and assessed the relationships of the gut microbial communities to functional profiles using gut metabolite analysis. The bacterial community did not differ significantly by host species or sex at the phylum level, but the distinction at the family level was obvious. The family Ruminococcaceae (Firmicutes) was more abundant in southern elephant seals than in Weddell seals, and the families Acidaminococcaceae (Firmicutes) and Pasteurellaceae (Gammaproteobacteria) were uniquely present in Weddell seals. The fecal bacterial community structure was distinctively clustered by host species, with only 6.7% of amplicon sequence variants (ASVs) shared between host species. This result implies that host phylogeny rather than other factors, such as diet or age, could be the major driver of fecal microbiotic diversification. Interestingly, there was no apparent sex effect on bacterial community structure in Weddell seals, but the effect of sex was pronounced in adult southern elephant seals mainly due to the prevalence of *Edwardsiella* sp., suggesting that extreme sexual dimorphism may modulate the gut microbiota of southern elephant seals. Unlike the clear distinction in the taxonomic composition of fecal bacterial communities, there were no discernible differences in the profiles of potential microbial functions and gut metabolites between host species or sexes, indicating that functional redundancy dominates the gut microbiota of seals surveyed in this study.

keywords: gut microbiome; marine mammal; Phocidae; Antarctic seal; NMR

DNA Barcoding of Antarctic Freshwater Copepod *Boeckella poppei* (Crustacea: Copepoda: Calanoida: Centropagidae) Inhabiting King George Island, South Shetland Islands, Antarctica

Kang, Seunghyun. and **Jo, Euna.**

Animal Systematics, Evolution and Diversity. 2020. 36(4): 396-399.

doi: 10.5635/ASED.2020.36.4.044.

The Antarctic freshwater copepod, *Boeckella poppei* (Mrazek, 1901), has the widest range of distribution extending from southern South America to Antarctic continent, among all *Boeckella* species. *Boeckella poppei* is the only freshwater copepod known to be inhabiting the Antarctic continent. In present study, we analyzed the DNA barcodes of the mitochondrial cytochrome *c* oxidase subunit I (*COI*) gene of *B. poppei* from King George Island, Antarctica. The intraspecific genetic distances varied from 0% to 13% and interspecific genetic distances ranged from 11% to 14%. The overlap of DNA barcode gap suggests careful threshold-based delimitation of species boundaries.

keywords: *Boeckella poppei*; Antarctica; DNA barcode; *COI*; copepod

Draft Genome Sequence of the Psychrotolerant Bacterium *Methylobacterium* sp. Strain BTF04, Isolated from Freshwater in Antarctica

Cho, Ahnna., **Cho, Yong-Joon.**, **Kim, Soyeon.** and **Kim, Ok-Sun.**

Microbiology Resource Announcement. 2020. 9(21): e00171-20.

doi: 10.1128/MRA.00171-20.

Methylobacterium sp. strain BTF04, a pink-pigmented psychrotolerant bacterium, was isolated from freshwater on Barton Peninsula, King George Island, Antarctica. Here, we report the assembled draft genome sequence of *Methylobacterium* sp. strain BTF04.

keywords: Cold shock protein; Genome sequence; Heavy metal resistance genes; King George Island; *Methylobacterium* sp. BTF04

4-33

The Effect of Translationally Controlled Tumor Protein (TCTP) of the Arctic Copepod *Calanus glacialis* on Protecting *Escherichia coli* Cells against Oxidative Stress

Park, Yu Kyung., **Lee, Chang-Eun.**, **Lee, Hyoungseok.**, **Koh, Hye Yeon.**, Kim, Sojin., **Lee, Sung Gu.**, **Kim, Jung Eun.**, **Yim, Joung Han.**, **Hong, Ju-Mi.**, Kim, Ryeo-Ok., **Han, Se Jong.** and **Kim, Il-Chan.**

Journal of Life Science. 2020. 30(11): 931-938.

doi: 10.5352/JLS.2020.30.11.931.

Translationally controlled tumor protein (TCTP) is one of the most abundant proteins in various eukaryotic organisms. TCTPs play important roles in cell physiological processes in cancer, cell proliferation, gene regulation, and heat shock response. TCTP is also considered an important factor in the resistance to oxidative stress induced by dithiothreitol or hydrogen peroxide (H_2O_2). Arctic calanoid copepods have a variety of antioxidant defense systems to regulate the levels of potentially harmful reactive oxygen species generated by ultraviolet radiation in the Arctic marine ecosystem. However, information on the antioxidant activity of TCTP in the Arctic *Calanus glacialis* is still scarce. To understand the putative antioxidant function of the Arctic copepod *C. glacialis* TCTP (Cg-TCTP), its gene was cloned and sequenced. The Cg-*TCTP* comprised 522 bp and encoded a 174-amino acid putative protein with a calculated molecular weight of ~23 kDa. The recombinant Cg-TCTP (Cg-r TCTP) gene was overexpressed in *Escherichia coli* (BL21), and Cg-rTCTP-transformed cells were grown in the presence or absence of H_2O_2. Cg-rTCTP-transformed *E. coli* showed increased tolerance to high H_2O_2 concentrations. Therefore, TCTP may be an important antioxidant protein related to tolerance of the Arctic copepod *C. glacialis* to oxidative stress in the harsh environment of the Arctic Ocean.

keywords: Antioxidant; Arctic copepod; TCTP; *Calanus glacialis*; Recombinant TCTP; TCTP

4-34 *Biotechnology & Applied Microbiology*

Effects of a Δ-9-fatty acid desaturase and a cyclopropane-fatty acid synthase from the novel psychrophile *Pseudomonas* sp. B14-6 on bacterial membrane properties

Choi, Tae-Rim., Park, Ye-Lim., Song, Hun-Suk., Lee, Sun Mi., Park, Sol Lee., Lee, Hye Soo., Kim, Hyun-Joong., Bhatia, Shashi Kant., Gurav, Ranjit., **Lee, Yoo Kyung.** and 2 others.

Journal of Industrial Microbiology & Biotechnology. 2020. 47(12): 1045-1057.

doi: 10.1007/s10295-020-02333-0.

Psychrophilic bacteria, living at low and mild temperatures, can contribute significantly to our understanding of microbial responses to temperature, markedly occurring in the bacterial membrane. Here, a newly isolated strain, *Pseudomonas* sp. B14-6, was found to dynamically change its unsaturated fatty acid and cyclic fatty acid content depending on temperature which was revealed by phospholipid fatty acid (PLFA) analysis. Genome sequencing yielded the sequences of the genes Δ-9-fatty acid desaturase (*desA*) and cyclopropane-fatty acid-acyl-phospholipid synthase (*cfa*). Overexpression of *desA* in *Escherichia coli* led to an increase in the levels of unsaturated fatty acids, resulting in decreased membrane hydrophobicity and increased fluidity. Cfa proteins from different species were all found to promote bacterial growth, despite their sequence diversity. In conclusion, PLFA analysis and genome sequencing unraveled the temperature-related behavior of *Pseudomonas* sp. B14-6 and the functions of two membrane-related enzymes. Our results shed new light on temperature-dependent microbial behaviors and might allow to predict the consequences of global warming on microbial communities.

keywords: *Pseudomonas* strain; Phospholipid fatty acid; Genome sequencing; Hydrophobicity; Membrane fluidity

4-35 *Veterinary Sciences*

Effects of Leucosporidium-derived ice-binding protein (LeIBP) on bull semen cryopreservation

Jang, Hoon., Kwon, Hyo J., Sun, Wu S., Hwang, Seongsoo., Hwang, In S., Kim, Sungwoo., **Lee, Jun**

Hyuck., **Lee, Sung Gu.** and Lee, Jeong W.

Veterinary Medicine and Science. 2020. 6(3): 447-453.

doi: 10.1002/vms3.269.

We examined the effect of ice-binding protein derived from *Leucosporidium* (LeIBP) on the cryopreservation of bull semen and compared it with that derived from previously reported Antifreeze Protein III (AFPIII). Six concentrations of LeIBP ($10^{-1} \sim 10^{4}$ μg/ml) and AFPIII ($10^{-1} \sim 10^{4}$ μg/ml) were added to the bull semen extender, respectively. Sperm kinematic parameters were measured to examine sperm toxicity and cryopreserved sperm quality. Measures of antioxidant activity such as superoxide dismutase (SOD), reduced glutathione/oxidative glutathione (GSH/GSSG), and total antioxidant capacity (TAC) were analysed to identify the effect of LeIBP on sperm quality. In addition, sperm viability was analysed using a flow cytometer and fluorescence microscope by SYBR14/PI staining. The results showed that the LeIBP groups (0.1, 1 and 10 μg/ml) were less toxic, and the quality of the sperm were dramatically improved in the extenders containing 0.1 μg /ml LeIBP among concentrations of LeIBP and AFPIII. The SOD activity of LeIBP was greater than that of AFPIII and control. In addition, sperm viability was enhanced in the LeIBP-treated group. In summary, LeIBP is a useful cryoprotective adjuvant for bull sperm cryopreservation, and the most efficient concentration of LeIBP is 0.1 μg /ml.

keywords: Antioxidant activity; Bull sperm; Cryopreservation; LeIBP

4-36 *Biotechnology & Applied Microbiology; Microbiology*

Enzymatic Synthesis of Anabolic Steroid Glycosides by Glucosyltransferase from *Terribacillus* sp. PAMC 23288

Yu, Eun-Ji., Yamaguchi, Tokutaro., Lee, Joo-Ho., Lim, A-Rang., **Lee, Jun Hyuck.** and 2 others.

Journal of Microbiology and Biotechnology. 2020. 30(4): 604-614.

doi: 10.4014/jmb.1911.11057.

The application of steroids has steadily increased thanks to their therapeutic effects. However, alternatives are required due their severe side effects; thus, studies on the activities of steroid derivatives are underway. Sugar derivatives of nandrolone, which is used to treat breast cancer, as well as cortisone and prednisone, which reduce inflammation, pain, and edema, are unknown. We linked *O*-glucose to nandrolone and testosterone using UDP-glucosyltransferase (UGT-1) and, then, tested their bioactivities in vitro. Analysis by NMR showed that the derivatives were 17β-nandrolone β-D-glucose and 17β-testosterone β-D-glucose, respectively. The viability was higher and cytotoxicity was evident in PC12 cells incubated with rotenone and, testosterone derivatives, compared to the controls. SH-SY5Y cells incubated with H_2O_2 and nandrolone derivatives remained viable and cytotoxicity was attenuated. Both derivatives enhanced neuronal protective effects and increased the amounts of cellular ATP.

keywords: Testosterone; nandrolone; glucosylation; neuroprotective activity; rotenone-induced apoptosis; steroid

4-37 *Biotechnology & Applied Microbiology*

Evaluation of assembly methods combining long-reads and short-reads to obtain *Paenibacillus* sp. R4 high-quality complete genome

Shin, Seung Chul., **Choi, Woong.**, **Lee, Jun Hyuck.**, Kim, Hyo Jin. and **Kim, Han-Woo.**

3 Biotech. 2020. 10(11).

doi: 10.1007/s13205-020-02474-0.

We sequenced the *Paenibacillus* sp. R4 using Oxford Nanopore Technology (ONT), single molecule real-time (SMRT) technology from Pacific Biosciences (PacBio), and Illumina technologies to investigate the application of nanopore reads in de novo sequencing of bacterial genomes. We compared the differences in both genome sequences between genome assemblies using nanopore and PacBio reads and focused on the difference in the prediction of coding sequences. The results indicated that for more accurate predictions of open reading frames, contigs in the assemblies using only PacBio reads also needed to be corrected using short reads with high-quality bases, and repeat regions in genomes did not affect the increase of mispredicted coding sequences via genome polishing significantly. In assemblies using only nanopore reads, genome polishing was essential, but many repeat regions in

genomes might increase the number of mispredicted coding sequences via genome polishing. The hybrid assembly combining the long reads and short reads represents the best result for coding sequence predictions in genome assemblies using nanopore reads.

keywords: Hybrid assembly; Long-read sequencing; Oxford Nanopore technology; *Paenibacillus* sp.

4-38 *Genetics & Heredity*

The Genome Assembly and Annotation of the Southern Elephant Seal *Mirounga leonina*

Kim, Bo-Mi., Lee, Yoon Jin., **Kim, Jeong-Hoon.**, **Kim, Jin-Hyoung.**, **Kang, Seunghyun.**, **Jo, Euna.**, Lee, Seung Jae., **Lee, Jun Hyuck.** and 2 others.

Genes. 2020. 11(2).

doi: 10.3390/genes11020160.

The southern elephant seal *Mirounga leonina* is the largest phocid seal and one of the two species of elephant seals. They are listed as 'least concern' by the International Union for Conservation of Nature (IUCN) Red List of Threatened Species 2015. Here, we have assembled the reference genome for *M. leonina* using the 10x chromium sequencing platform. The final genome assembly of *M. leonina* was 2.42 Gb long, with a contig N50 length of 54 Mb and a maximum length of 111.6 Mb. The *M. leonina* genome contained 20,457 predicted protein-coding genes and possessed 41.51% repeated sequences. The completeness of the *M. leonina* genome was evaluated using benchmarking universal single-copy orthologous genes (BUSCOs): the assembly was highly complete, containing 95.6% of the core set of mammalian genes. The high-quality genomic information on *M. leonina* will be essential for further understanding of adaptive metabolism upon repeated breath-hold dives and the exploration of molecular mechanisms contributing to its unique biochemical and physiological characteristics. The southern elephant seal genome project was deposited at NCBI (National Center for Biotechnology Information) under BioProject number PRJNA587380.

keywords: southern elephant seal; *Mirounga leonina*; genome assembly; annotation; 10x genomics chromium technology

4-39 *Biochemistry & Molecular Biology; Genetics & Heredity*

Genome-wide identification and structural analysis of heat shock protein gene families in the marine rotifer *Brachionus* spp.: Potential application in molecular ecotoxicology

Park, Jun Chul., Kim, Duck-Hyun., Lee, Yoseop., Lee, Min-Chul., **Kim, Tai Kyoung.**, **Yim, Joung Han.** and Lee, Jae-Seong.

Comparative Biochemistry and Physiology D-Genomics & Proteomics. 2020. 36.

doi: 10.1016/j.cbd.2020.100749.

Heat shock proteins (Hsp) are class of conserved and ubiquitous stress proteins present in all living organisms from primitive to higher level. Various studies have demonstrated multiple cellular functions of Hsp in living organisms as an important biomarker in response to abiotic and biotic stressors including temperature, salinity, pH, hypoxia, environmental pollutants, and pathogens. However, full understanding on the mechanism and pathway involved in the induction of Hsp still remains challenging, especially in aquatic invertebrates. In this study, the entire Hsp family and subfamily members in the marine rotifers *Brachionus* spp., one of the cosmopolitan ecotoxicological model organisms, have been genome-widely identified. In *Brachionus* spp. Hsp family was comprised of Hsp10, small hsp (sHsp), Hsp40, Hsp60, Hsp70/105, and Hsp90, with highest number of genes found within Hsp40 DnaJ homolog subfamily C members. Also, the differences in the orientation of the conserved motifs within Hsp family may have induced differences in transcriptional gene modulation in response to thermal stress in *Brachionus koreanus*. Overall, Hsp family-specific domains were highly conserved in all three *Brachionus* spp., relative to *Homo sapiens* and across other animal taxa and these findings will be helpful for future ecotoxicological studies focusing on Hsps.

keywords: Stress proteins; Molecular chaperones; Invertebrates; Rotifer

4-40 *Marine & Freshwater Biology; Toxicology*

Genome-wide identification of DNA double-strand break repair genes and

transcriptional modulation in response to benzo[α]pyrene in the monogonont rotifer *Brachionus* spp.

Lee, Young Hwan., Kim, Min-Sub., Kim, Duck-Hyun., **Kim, Il-Chan.** and 2 others.

Aquatic Toxicology. 2020. 227.

doi: 10.1016/j.aquatox.2020.105614.

The DNA repair system has evolved from the common ancestor of all life forms and its function is highly conserved within eukaryotes. In this study, to reveal the role of DNA double-strand break repair (DSB) genes in response to benzo [α] pyrene (B[α]P), we first identified DSB genes in relation to homologous recombination and non-homologous end joining events in four *Brachionus* rotifer spp.: *B. calyciflorus*, *B. koreanus*, *B. plicatilis*, and *B. rotundiformis*. In all the *Brachionus* spp., 39 orthologous genes to human DSB repair genes were identified. Furthermore, three genes in *B. koreanus*, two genes in *B. plicatilis*, and one gene in *B. calyciflorus* and *B. rotundiformis* were present as duplicated genes, indicating that these genes were diversified over speciation in the genus *Brachionus*. Moreover, we compared DSB repair genes on the gene structures in four monogonont *Brachionus* rotifers and the bdelloid rotifer *Adineta vaga*, which possesses highly efficient DNA repair ability. The transcriptional responses of four monogonont *Brachionus* rotifers in response to B[α] P exposure showed how B[α]P exposure led to DSBs and subsequently recruited DNA DSB repair pathways in the rotifer *B. koreanus*. Taken together, this study provides a better understanding of the potential role of DSB repair genes in the monogonont rotifer *Brachionus* spp. in response to B[α]P.

keywords: DNA damage; DNA double-strand break repair genes; Rotifer; *Brachionus* spp.

4-41 *Biochemistry & Molecular Biology; Ecology; Evolutionary Biology*

Glycerols and fatty acids isolated from *Micractinium* sp. KSF0031

Huynh Nguyen Khanh Tran., **Youn, Ui Joung.**, Kim, Jeong Ah., **Chae, Hyunsik.**, **Kim, Sanghee.** and Min, Byung Sun.

Biochemical Systematics and Ecology. 2020. 89.

doi: 10.1016/j.bse.2019.104000.

From the collected extract from King Sejong Antarctic Station, strain *Micractinium* sp. KSF0031, led to the isolation of one new monoacyldigalactosyl glycerol (1) and seven known compounds (2-8). Their chemical structures were established using extensive spectroscopic techniques, including 1D, 2D-NMR, and MS, and compared with the published data. To the best of our knowledge, this is the first report to investigate the secondary metabolites from genus *Micractinium*. The monoacyldigalactosyl glycerol in *Micractinium* could serve as its chemotaxonomic markers.

keywords: Chlorellaceae; *Micractinium* sp. KSF0031; Glycerol

---

4-42 *Biotechnology & Applied Microbiology; Microbiology*

Heterologous Gene Expression System Using the Cold-Inducible *CnAFP* Promoter in *Chlamydomonas reinhardtii*

Kim, Minjae., Kim, Jongrae., **Kim, Sanghee.** and Jin, EonSeon.

Journal of Microbiology and Biotechnology. 2020. 30(11): 1777-1784.

doi: 10.4014/jmb.2007.07024.

To increase the availability of microalgae as producers of valuable compounds, it is necessary to develop novel systems for gene expression regulation. Among the diverse expression systems available in microalgae, none are designed to induce expression by low temperature. In this study, we explored a cold-inducible system using the antifreeze protein (AFP) promoter from a polar diatom, *Chaetoceros neogracile*. A vector containing the *CnAFP* promoter (*pCnAFP*) was generated to regulate nuclear gene expression, and reporter genes (*Gaussia* luciferase (*GLuc*) and mVenus fluorescent protein (*mVenus*)) were successfully expressed in the model microalga, *Chlamydomonas reinhardtii*. In particular, under the control of *pCnAFP*, the expression of these genes was increased at low temperature, unlike *pAR1*, a promoter that is widely used for gene expression in *C. reinhardtii*. Promoter truncation assays showed that cold inducibility was still present even when *pCnAFP* was shortened to 600 bp, indicating the presence of a low-temperature response element between -600 and -477 bp. Our results show the availability of new heterologous gene expression systems with cold-inducible promoters and the possibility to find novel low-temperature response

factors in microalgae. Through further improvement, this cold-inducible promoter could be used to develop more efficient expression tools.

keywords: Cold-inducible expression system; antifreeze protein; truncated promoter; *Chlamydomonas reinhardtii*; Gaussia luciferase; fluorescent protein

4-43 *Mycology*

Hispidopannaria and *Phormopsora*, two new and small, but evolutionary old Pannariaceae lichen genera from southern South America

Elvebakk, Arve., **Hong, Soon Gyu.** and **Park, Chae Haeng.**

Mycological Progress. 2020. 19(11): 1353-1364.

doi: 10.1007/s11557-020-01632-1.

Based on phylogenetic analyses of the ITS, nuclear large subunit rRNA, mitochondrial small subunit rRNA, and MCM7 genes, species previously treated as *Pannaria hispidula* and *P. isabellina* are shown to represent two new Pannariaceae genera, *Hispidopannaria* and *Phormospsora*. Each genus forms monophyletic clades, both in multilocus phylogeny and in single gene phylogenies. In the multilocus phylogeny, both genera together formed a monophyletic clade as a sister group to the genus *Pannaria*, whereas this monophyly was not maintained in single gene phylogenies. *Hispidopannaria* differs from *Pannaria* in having large, geotropically arranged, hispid squamules, IKI+ internal ascus structures, and perispores with irregular pulvinate verrucae and apical extensions. The southern South American, TLC-negative species *H. hispidula* is generitype and is concentrated to trunks in the evergreen *Nothofagus* forests of south-central Chile. *Psoroma dasycladum*, a similar endemic species from the Juan Fernández Archipelago, is also transferred to *Hispidopannaria*. *Phormopsora* is monospecific and is the only member of Pannariaceae which contains norstictic and connorstictic acids. Its thallus of large, branched squamules with large, foliose cephalodia and its bullate perispores with long-apiculate apical extensions also separate it from *Pannaria*. Its species, *Phormopsora isabellina*, has a similar distribution as *H. hispidula* on the South American mainland, but is more widespread. The position of these two small genera as a sister group to the large and diverse genus *Pannaria*, indicates a long period of slow evolutionary rate, with the island endemic *Hispidopannaria dasyclada* as an exception. Reproductive isolation and photobiont specialization are partly suggested to explain their slow evolution and lack of surviving speciation.

keywords: Endemism; Evolution; *Pannaria*; Photobionts; Phylogeny; Taxonomy

4-44 *Agriculture, Dairy & Animal Science; Veterinary Sciences*

Home Range Estimates and Habitat Use of Siberian Flying Squirrels in South Korea

Kim, Jong-U. and 3 others.

Animals. 2020. 10(8).

doi: 10.3390/ani10081378.

Conservation measures or management guidelines must be based on species' ecological data. The home range of the target species was studied to understand its spatial ecology, in order to protect it. The Siberian flying squirrel is the only flying squirrel species present and is considered as a protected species in South Korea. In this study, we investigated the home range, habitat use, and daily movement of Siberian flying squirrels from February 2015 to June 2016 at Mt. Baekwoon, Gangwon Province, South Korea. We tracked 21 flying squirrels using radio transmitters and analyzed the home range of 12 individuals. Flying squirrels appeared to have an overall mean home range of 18.92 ± 14.80 ha with a core area of 3.54 ha ± 3.88 ha. Movement activity peaked between 18:00-19:00 with the longest distance traveled, coinciding with sunset. In addition, we observed the preference of Siberian flying squirrels to the old deciduous forest with dense crowns. The results of the present study indicate that it is important to manage their habitat; for instance, preserving an appropriate size of mature deciduous forest is essential for Siberian flying squirrels. While our study provides needed baseline information on the spatial activity of the species, further research on topics such as the national distribution, behavior, and population dynamics of Siberian flying squirrels is needed in South Korea.

keywords: habitat use; home range; radio telemetry; Siberian flying squirrel

4-45 *Biochemistry & Molecular Biology; Genetics & Heredity*

An improved genome assembly and annotation of the Antarctic copepod *Tigriopus kingsejongensis* and comparison of fatty acid metabolism between *T. kingsejongensis* and the temperate copepod *T. japonicus*

Lee, Min-Chul., Choi, Beom-Soon., Kim, Min-Sub., Yoon, Deok-Seo., Park, Jun Chul., **Kim, Sanghee.** and Lee, Jae-Seong.

Comparative Biochemistry and Physiology D-Genomics & Proteomics. 2020. 35.

doi: 10.1016/j.cbd.2020.100703.

Copepods in the genus *Tigriopus* are widely distributed in the intertidal zone worldwide. To assess differences in fatty acid (FA) metabolism among congeneric species in this genus inhabiting polar and temperate environments, we analyzed and compared FA profiles of the Antarctic copepod *Tigriopus kingsejongensis* and the temperate copepod *T. japonicus*. Higher amounts of total FAs were found in the Antarctic copepod *T. kingsejongensis* than the temperate copepod *T. japonicus* under administration of the identical amount of *Tetraselmis suecica*. To determine the genomic basis for this, we identified fatty acid metabolism-related genes in an improved genome of *T. kingsejongensis*. The total length of the assembled genome was approximately 338 Mb with N50 = 1.473 Mb, 938 scaffolds, and a complete Benchmarking Universal Single-Copy Orthologs value of 95.8%. A total of 25,470 genes were annotated using newly established pipeline. We identified eight elongation of very long-chain fatty acid protein (*Elovl*) genes and nine fatty acid desaturase (*Fad*) genes in the genome of *T. kingsejongensis*. In addition, fatty acid profiling suggested that the duplicated Δ5/6 desaturase gene in *T. kingsejongensis* is likely to play an essential role in synthesis of different FAs in *T. kingsejongensis* to those in *T. japonicus*. However, further experimental research is required to validate our *in silico* findings. This study provides a better understanding of fatty acid metabolism in the Antarctic copepod *T. kingsejongensis*.

keywords: Copepod; Fatty acid; *Elovl*; *Fad*; *Tigriopus kingsejongensis*

4-46

Individual Human Recognition of Wild Animals: A Review and a Case Study in the Arctic Environment

Lee, Won Young. and Choe, Jae Chun.

Proceeding of National Institute of Ecology. 2020. 1(1): 1-8.

doi: 10.22920/PNIE.2020.1.1.1

Recent studies revealed that many animals identify individual humans. In this account, we review previous literatures on individual human recognition by wild or domestic animals and discuss the three hypotheses: "high cognitive abilities" hypothesis, "close human contact" and "pre-exposure to stimuli" hypothesis. The three hypotheses are not mutually exclusive. Close human contact hypothesis is an ultimate explanation for adaptive benefits whereas high cognitive abilities and pre-exposure to stimuli hypothesis are proximate explanations for mechanisms to perform such discriminatory behaviour. We report a case study of two bird species in a human-free habitat. Long-tailed skuas, which are known for having high cognitive abilities, exhibited the human discriminatory abilities whereas ruddy turnstones did not display such abilities toward approaching humans. This suggests that highly intelligent species may have this type of discriminatory ability so that they could learn to identify individual humans quickly by pre-exposure to stimuli, even in a human-free habitat. Here, we discuss that human recognition is more common in species with rapid learning ability and it could develop for a short period of time between an intelligent species and human.

keywords: Close human contact hypothesis; High cognitive abilities hypothesis; Individual human recognition; Longtailed skua; Pre-exposure to stimuli hypothesis; Ruddy turnstone

4-47 *Fisheries; Immunology; Marine & Freshwater Biology; Veterinary Sciences*

Inorganic nitrogen compounds reduce immunity and induce oxidative stress in red seabream

Seo, Jung Soo., Haque, Md Niamul., Nam, Sang-Eun., **Kim, Bo-Mi.** and Rhee, Jae-Sung.

Fish & Shellfish Immunology. 2020. 104: 237-244.

doi: 10.1016/j.fsi.2020.05.072.

In this study, the effect of ammonia derived from different stocking densities on immunological, hematological, and oxidative stress parameters was analyzed in the blood or liver of red seabream. Density- and time-dependent increases in inorganic nitrogen compounds were measured for 20 days by analyzing the three major inorganic nitrogen compounds, total ammonia nitrogen, nitrite nitrogen, and nitrate nitrogen. Three immunity parameters, alternative complement activity, lysozyme activity, and total immunoglobulin content were significantly decreased in the blood at the highest stocking density (10 kg m^{-3}). The concentrations of hemoglobin and white blood cells were significantly decreased at 10 kg m^{-3}, while there was no significant change in red blood cells. The significant increases in cortisol level and the enzymatic activities of alanine aminotransferase, aspartate aminotransferase, and alkaline phosphatase at 10 kg m^{-3} clearly supported inorganic nitrogen compounds-triggered stress. A significant elevation of lipid peroxidation value and depletion of intracellular glutathione were observed at 5 and/or 10 kg m^{-3} in the liver tissue. The hepatic enzymatic activities of antioxidant defense enzymes, catalase and superoxide dismutase were also significantly increased. When a protein skimmer removes the inorganic nitrogen compounds at the highest density, most parameters showed no significant change. Taken together, these results suggest that accumulated inorganic nitrogen compounds at the highest stocking density inhibit innate immunity and induce oxidative stress in red seabream. This information will be helpful to maintain homeostasis of red seabream by controlling immunity and oxidative status through inorganic nitrogen compounds removal in intensive culture condition.

keywords: Red seabream; Immunity; Stocking density; Inorganic nitrogen compound; Oxidative stress

4-48 *Multidisciplinary Sciences*

Integrative description of a new *Dactylobiotus* (Eutardigrada: Parachela) from Antarctica that reveals an intraspecific variation in tardigrade egg morphology

Kihm, Ji-Hoon., **Kim, Sanghee.**, McInnes, Sandra J., Zawierucha, Krzysztof., Rho, Hyun Soo., **Kang, Pilmo.** and **Park, Tae-Yoon S.**

Scientific Reports. 2020. 10(1).
doi: 10.1038/s41598-020-65573-1.

Tardigrades constitute one of the most important group in the challenging Antarctic terrestrial ecosystem. Living in various habitats, tardigrades play major roles as consumers and decomposers in the trophic networks of Antarctic terrestrial and freshwater environments; yet we still know little about their biodiversity. The Eutardigrada is a species rich class, for which the eggshell morphology is one of the key morphological characters. Tardigrade egg morphology shows a diverse appearance, and it is known that, despite rare, intraspecific variation is caused by seasonality, epigenetics, and external environmental conditions. Here we report *Dactylobiotus ovimutans* sp. nov. from King George Island, Antarctica. Interestingly, we observed a range of eggshell morphologies from the new species, although the population was cultured under controlled laboratory condition. Thus, seasonality, environmental conditions, and food source are eliminated, leaving an epigenetic factor as a main cause for variability in this case.

keywords: Antarctica; Biodiversity; King George Island; Laboratory culture; Morphological variation; Tardigrade

4-49 *Ecology; Evolutionary Biology*

Interspecific comparison of the fecal microbiota structure in three Arctic migratory bird species

Cho, Hyunjun. and **Lee, Won Young.**

Ecology and Evolution. 2020. 10(12): 5582-5594.
doi: 10.1002/ece3.6299.

The gut microbiota of birds is known to be characterized for different species, although it may change with feeding items. In this study, we compared the gut microbiota of birds with different feeding behaviors in the same habitat. We collected fecal samples from three Arctic species, snow buntings *Plectrophenax nivalis*, sanderlings *Calidris alba*, and pink-footed geese *Anser brachyrhynchus* that are phylogenetically quite distant in different families to evaluate effects of diet on gut microbiota. Also, we characterized the prevalence of fecal bacteria using the Illumina MiSeq platform to sequence bacterial 16S rRNA genes. Our NMDS results showed that

fecal bacteria of snow buntings and sanderlings were significantly distant from those of pink-footed geese. Although all three birds were occupied by three bacterial phyla, Proteobacteria, Firmicutes, and Bacteroidetes, dominant taxa still varied among the species. Our bacterial sequences showed that snow buntings and sanderlings were dominated by Firmicutes and Bacteroidetes, while pink-footed geese were dominated by Proteobacteria. In addition, the bacterial diversity in snow buntings and sanderlings was significantly higher than that in pink-footed geese. Our results suggest that insectivorous feeding diet of snow buntings and sanderlings could be responsible for the similar bacterial communities between the two species despite the distant phylogenetic relationship. The distinctive bacterial community in pink-footed geese was discussed to be related with their herbivorous diet.

keywords: Arctic birds; diet; fecal bacteria; feeding behavior; gut microbiota

4-50 *Green & Sustainable Science & Technology; Environmental Sciences; Environmental Studies*

Key Factors Controlling Primary Production and Cyanobacterial Harmful Algal Blooms (cHABs) in a Continuous Weir System in the Nakdong River, Korea

Choi, Jisoo., **Min, Jun Oh.**, Choi, Bohyung., Kim, Dokyun., Kang, Jae Joong., Lee, Sang Heon., Choi, Kwangsoon., Lee, Heesuk., **Jung, Jinyoung.** and Shin, Kyung-Hoon.

Sustainability. 2020. 12(15).

doi: 10.3390/su12156224.

To identify key factors that control primary production (P.P.) and trigger cyanobacterial harmful algal blooms (cHABs), we investigated spatio-temporal variations in P.P. in a continuous weir system in the Nakdong River once or twice a month from April to October 2018. P.P. was measured through an in-situ incubation experiment using a ^{13}C tracer. Relative proportion of pigment-based phytoplankton composition was calculated by the CHEMTAX program based on pigment analysis using a high-performance liquid chromatography (HPLC). P.P. was higher in spring (1130 ± 1140 mg C m^{-2} d^{-1}) and summer (1060 ± 814 mg C m^{-2} d^{-1}) than autumn (180 ± 220 mg C m^{-2} d^{-1}), and tended to increase downstream. P.P. was negatively related to PO_4^{3-} (r = -0.41, p< 0.01) due to utilization by phytoplankton during the spring and summer when it was high. The relative proportion of pigment-based cyanobacteria (mainly *Microcystis* sp.) was positively correlated with water temperature (r = 0.79, p< 0.01) and hydraulic retention time (HRT, r = 0.67, p< 0.01), suggesting that these two factors should affect cHABs in summer. Therefore, to control HRT could be one of the solutions for reducing cHABs in a continuous weir system.

keywords: continuous weir; cHABs; primary productivity; environmental factors; pigment; CHEMTAX

4-51 *Microbiology*

Lichenicola cladoniae gen. nov., sp. nov., a member of the family *Acetobacteraceae* isolated from an Antarctic lichen

Noh, Hyun-Ju., **Shin, Seung Chul.**, **Park, Yerin.**, Choi, Ahyoung., Baek, Kiwoon., **Hong, Soon Gyu.**, Cho, Yong-Joon., **Lee, Hyoungseok.** and **Lee, Yung Mi.**

International Journal of Systematic and Evolutionary Microbiology. 2020. 70(11): 5918-5925.

doi: 10.1099/ijsem.0.004495.

Two Gram-stain-negative, facultative anaerobic, chemoheterotrophic, pink-coloured, rod-shaped and non-motile bacterial strains, PAMC 26568 and PAMC 26569^T, were isolated from an Antarctic lichen. Phylogenetic analysis based on 16S rRNA gene sequences revealed that strains PAMC 26568 and PAMC 26569^T belong to the family *Acetobacteraceae* and the most closely related species are *Gluconacetobacter takamatsuzukensis* (96.1 %), *Gluconacetobacter tumulisoli* (95.9%) and *Gluconacetobacter sacchari* (95.7%). Phylogenomic and genomic relatedness analyses showed that strains PAMC 26568 and PAMC 26569^T are clearly distinguished from other genera in the family *Acetobacteraceae* by average nucleotide identity values (<72.8 %) and the genome-to-genome distance values (<22.5%). Genomic analysis revealed that strains PAMC 26568 and PAMC 26569^T do not contain genes involved in atmospheric nitrogen fixation and utilization of sole carbon compounds such as methane and methanol. Instead, strains PAMC 26568 and PAMC 26569^T possess genes to utilize nitrate and nitrite and certain monosaccharides and disaccharides.

The major fatty acids (>10%) are summed feature 8 ($C_{18:1}$ *ω7c* and/or $C_{18:1}$ *ω6c*; 40.3–40.4 %), $C_{18:1}$ 20H (22.7-23.7%) and summed feature 2 ($C_{14:0}$ 30H and/or $C_{16:1}$ iso I; 12.0 % in PAMC 26568). The major respiratory quinone is Q-10. The genomic DNA G+C content of PAMC 26568 and PAMC 26569^T is 64.6 %. Their distinct phylogenetic position and some physiological characteristics distinguish strains PAMC 26568 and PAMC 26569^T from other genera in the family *Acetobacteraceae* supporting the proposal of *Lichenicola* gen. nov., with the type species *Lichenicola cladoniae* sp. nov. (type strain, PAMC 26569^T = KCCM 43315^T = JCM 33604^T).

keywords: Antarctica; *Lichenicola cladoniae*; new genus; polyphasic taxonomy; lichen

4-52 *Biotechnology & Applied Microbiology; Genetics & Heredity*

Loci associated with variation in gene expression and growth in juvenile salmon are influenced by the presence of a growth hormone transgene

McClelland, Erin Kathleen., Chan, Michelle T. T., Lin, Xiang., Sakhrani, Dionne., Vincelli, Felicia., **Kim, Jin-Hyoung.** and 2 others.

Bmc Genomics. 2020. 21(1).

doi: 10.1186/s12864-020-6586-0.

Background: Growth regulation is a complex process influenced by genetic and environmental factors. We examined differences between growth hormone (GH) transgenic (T) and non-transgenic (NT) coho salmon to elucidate whether the same loci were involved in controlling body size and gene expression phenotypes, and to assess whether physiological transformations occurring from GH transgenesis were under the influence of alternative pathways. The following genomic techniques were used to explore differences between size classes within and between transgenotypes (T vs. NT): RNA-Seq/Differentially Expressed Gene (DEG) analysis, quantitative PCR (qPCR) and OpenArray analysis, Genotyping-by-Sequencing, and Genome-Wide Association Study (GWAS). Results: DEGs identified in comparisons between the large and small tails of the size distributions of T and NT salmon (NT_{Large}, NT_{Small}, T_{Large} and T_{Small}) spanned a broad range of biological processes, indicating widespread influence of the transgene on gene expression. Overexpression of growth hormone led to differences in regulatory loci between transgenotypes and size classes. Expression levels were significantly greater in T fish at 16 of 31 loci and in NT fish for 10 loci. Eleven genes exhibited different mRNA levels when the interaction of size and transgenotype was considered (IGF1, IGFBP1, GH, C3-4, FAS, FAD6, GLUT1, G6PASE1, GOGAT, MID1IP1). In the GWAS, 649 unique SNPs were significantly associated with at least one study trait, with most SNPs associated with one of the following traits: C3_4, ELA1, GLK, IGF1, IGFBP1, IGFII, or LEPTIN. Only 1 phenotype-associated SNP was found in common between T and NT fish, and there were no SNPs in common between transgenotypes when size was considered. Conclusions: Multiple regulatory loci affecting gene expression were shared between fast-growing and slow-growing fish within T or NT groups, but no such regulatory loci were found to be shared between NT and T groups. These data reveal how GH overexpression affects the regulatory responses of the genome resulting in differences in growth, physiological pathways, and gene expression in T fish compared with the wild type. Understanding the complexity of regulatory gene interactions to generate phenotypes has importance in multiple fields ranging from applications in selective breeding to quantifying influences on evolutionary processes.

keywords: Transgenic fish; Coho salmon; Growth hormone; Body size; Genome-wide association study; Genotyping-by-sequencing; SNPs

4-53 *Microbiology*

Microbiome in *Cladonia squamosa* Is Vertically Stratified According to Microclimatic Conditions

Noh, Hyun-Ju., **Lee, Yung Mi.**, **Park, Chae Haeng.**, **Lee, Hong Kum.**, Cho, Jang-Cheon. and **Hong, Soon Gyu.**

Frontiers in Microbiology. 2020. 11.

doi: 10.3389/fmicb.2020.00268.

Lichens are miniature ecosystems that contain fungi, microalgae, and bacteria. It is generally accepted that symbiosis between mycobiont and photobiont and microbial contribution to the ecosystem support the wide distribution of lichens in terrestrial ecosystems, including polar areas. The composition of symbiotic components can be affected by subtle

microenvironmental differences within a thallus, as well as large-scale climate differences. In this study, we investigated fine-scale profiles of algal, fungal, and bacterial compositions through horizontal and vertical positions of the Antarctic lichen *Cladonia squamosa* colonies by next-generation sequencing of the nuclear large subunit rRNA gene (nucLSU) of eukaryotes and the 16S rRNA gene of bacteria. Apical parts of thalli were exposed to strong light, low moisture, and high variability of temperature compared with basal parts. Microbial diversity increased from apical parts to basal parts of thalli. *Asterochloris erici* was the major photobiont in apical positions of thalli, but other microalgal operational taxonomic units (OTUs) of Trebouxiophyceae and Ulvophyceae were major microalgal components in basal positions. Photochemical responses of algal components from apical and basal parts of thalli were quite different under variable temperature and humidity conditions. Several fungal OTUs that belonged to Arthoniomycetes and Lecanoromycetes, and diverse bacterial OTUs that belonged to *Alphaproteobacteria*, *Acidobacteria_* Gp1, and candidate division WPS-2 showed a clear distribution pattern according to their vertical positions within thalli. The overall lichen microbiome was significantly differentiated by the vertical position within a thallus. These results imply that different microclimate are formed at different lichen thallus parts, which can affect microbial compositions and physiological responses according to positions within the thalli.

keywords: Antarctica; lichen; bacteria; fungi; microalgae; microbiome

4-54 *Microbiology*

Morphology, morphogenesis, and molecular phylogeny of a new freshwater ciliate, *Gonostomum jangbogoensis* n. sp. (Ciliophora, Hypotricha), from Victoria Land, Antarctica

Park, Kyung-Min., Jung, Jae-Ho., **Kim, Jeong-Hoon.**, Min, Gi-Sik. and **Kim, Sanghee.**

European Journal of Protistology. 2020. 73.

doi: 10.1016/j.ejop.2019.125669.

In a study on ciliate diversity, we discovered the new hypotrich species, *Gonostomum jangbogoensis* n. sp., in freshwater from Terra Nova Bay, Victoria Land, southeast Antarctica. We describe its morphology and morphogenesis using standard methods, and the SSU rRNA gene phylogeny is provided as well. Morphology of *Gonostomum jangbogoensis* n. sp. is characterized as follows: slender to elongated body shape; grayish under low magnification; cortical granules present; 32 - 1 adoral membranelles; 3 enlarged frontal cirri; 1 buccal cirrus; 2 frontoterminal cirri; 3 or 4 frontovemral cirral pairs, 2 pretransverse cirri, 6-7 transverse cirri; 13-19 left and 18-26 right marginal cirri; 17-23 paroral kinetids; 3 dorsal kinetics; 3 caudal cirri; 2 macronuclear nodules with 1-3 micronuclei. The morphogenesis of the new species confirms that it has at least seven frontal-ventral-transverse cirral anlagen, which is also reported in *Gonostomum* sp. 1 sensu Shin from Korea. Even though these two populations occur very far from each other, the morphometric data prove that this character state, the seven cirral anlagen, is a stable feature across these populations and might be an apomorphy. The phylogenetic analyses show that the genus *Gonostomum* is non-monophyletic and that the new species is a sister to *G. bromelicola*.

keywords: Ciliophora; Gonostomatidae; Ontogenesis; SSU rRNA gene; Taxonomy

4-55 *Chemistry, Medicinal; Food Science & Technology*

A New Chlorinated Phenolic Compound From the Antarctic Lichen, *Pertusaria dactylina*

Koo, Man Hyung., **Kim, Min Ju.**, **So, Jae Eun.**, **Kim, Ji Hee.**, **Han, Se Jong.**, **Kim, Il-Chan.**, **Lee, Jun Hyuck.** and **Youn, Ui Joung.**

Natural Product Communications. 2020. 15(3): 1-4.

doi: 10.1177/1934578x20902886.

A new chlorinated phenolic compound, methyl-3-chloro-2-hydroxy-4-methoxy-6-pentylbenzoate (1) and 4 known compounds (2-5) were isolated from the Antarctic lichen, *Pertusaria dactylina* (*Pertusariaceae*). The structure of the new compound was determined by means of One-dimensional and two dimensional nuclear magnetic resonance (1D and 2D NMR) and high-resolution fast atom bombardment mass spectrometry (HRFABMS) experiments. The antimicrobial activities of compounds 1 to 5 against *Staphylococcus aureus* and *Candida albicans* were

evaluated. The results showed that compound 1 exhibited a weak inhibitory effect against *C. albicans* with an IC_{50} value of 67 ± 7 μg/mL.

keywords: *Pertusaria dactylina*; Antarctic lichen; *Pertusariaceae*; antimicrobial activity; phenolic compound

4-56 *Biochemistry & Molecular Biology; Chemistry, Multidisciplinary*

Phytochemicals as Anti-Inflammatory Agents in Animal Models of Prevalent Inflammatory Diseases

Shin, Seong Ah, Joo, Byeong Jun, Lee, Jun Seob, Ryu, Gyoungah, Han, Minjoo, Kim, Woe Yeon, Park, Hyun Ho, **Lee, Jun Hyuck** and Lee, Chang Sup.

Molecules. 2020. 25(24).

doi: 10.3390/molecules25245932.

Phytochemicals are known to have anti-inflammatory effects in vitro and in vivo, such as in inflammatory disease model systems. Inflammation is an essential immune response to exogenous stimuli such as infection and injury. Although inflammation is a necessary host-defense mechanism, chronic inflammation is associated with the continuous local or systemic release of inflammatory mediators, non-cytokine mediators, such as ROS and NO, and inflammatory cytokines are strongly implicated in the pathogenesis of various inflammatory disorders. Phytochemicals that exhibit anti-inflammatory mechanisms that reduce sustained inflammation could be therapeutic candidates for various inflammatory diseases. These phytochemicals act by modulating several main inflammatory signaling pathways, including NF-κB, MAPKs, STAT, and Nrf-2 signaling. Here, we discuss the characteristics of phytochemicals that possess anti-inflammatory activities in various chronic inflammatory diseases and review the molecular signaling pathways altered by these anti-inflammatory phytochemicals, with a focus on transcription factor pathways. Furthermore, to evaluate the phytochemicals as drug candidates, we translate the effective doses of phytochemicals in mice or rat disease models into the human-relevant equivalent and compare the human-relevant equivalent doses of several phytochemicals with current anti-inflammatory drugs doses used in different types of chronic inflammatory diseases.

keywords: plant; phytochemical; anti-inflammation; inflammatory disease

4-57 *Plant Sciences; Cell Biology*

Poaceae Type II Galactinol Synthase 2 from Antarctic Flowering Plant *Deschampsia antarctica* and rice Improves Cold and Drought Tolerance by Accumulation of Raffinose Family Oligosaccharides in Transgenic Rice Plants

Cui, Li Hua., **Byun, Mi Young.**, Oh, Hyeong Geun., **Kim, Sung Jin.**, **Lee, Jungeun.**, **Park, Hyun.**, **Lee, Hyoungseok.** and Kim, Woo Taek.

Plant and Cell Physiology. 2020. 61(1): 88-104.

doi: 10.1093/pcp/pcz180.

Deschampsia antarctica is a Poaceae grass that has adapted to and colonized Antarctica. When *D. antarctica* plants were subjected to cold and dehydration stress both in the Antarctic field and in laboratory experiments, galactinol, a precursor of raffinose family oligosaccharides (RFOs) and raffinose were highly accumulated, which was accompanied by upregulation of galactinol synthase (GolS). The Poaceae monocots have a small family of *GolS* genes, which are divided into two distinct groups called types I and II. Type II GolSs are highly expanded in cold-adapted monocot plants. Transgenic rice plants, in which type II *D. antarctica GolS*2 (*DaGolS*2) and rice *GolS*2 (*OsGolS*2) were constitutively expressed, were markedly tolerant to cold and drought stress as compared to the wild-type rice plants. The RFO contents and GolS enzyme activities were higher in the *DaGolS*2 and *OsGolS*2-overexpressing progeny than in the wild-type plants under both normal and stress conditions. *DaGolS*2 and *OsGolS*2 overexpressors contained reduced levels of reactive oxygen species (ROS) relative to the wild-type plants after cold and drought treatments. Overall, these results suggest that Poaceae type II GolS2s play a conserved role in *D. antarctica* and rice in response to drought and cold stress by inducing the accumulation of RFO and decreasing ROS levels.

keywords: Antarctic flowering plant; *Deschampsia antarctica*; Cold and drought tolerance; Poaceae type II galactinol synthase; Raffinose family oligosaccharides; Transgenic rice plants

4-58 *Chemistry, Medicinal; Pharmacology & Pharmacy*

Protection of Alcohol Dehydrogenase against Freeze-Thaw Stress by Ice-Binding Proteins Is Proportional to Their Ice Recrystallization Inhibition Property

Lee, Young Hoon., **Kim, Kitae.**, **Lee, Jun Hyuck.** and Kim, Hak Jun.

Marine Drugs. 2020. 18(12).

doi: 10.3390/md18120638.

Ice-binding proteins (IBPs) have ice recrystallization inhibition (IRI) activity. IRI property has been extensively utilized for the cryopreservation of different types of cells and tissues. Recent reports demonstrated that IRI can also play a significant role in protecting proteins from freezing damage during freeze-thaw cycles. In this study, we hypothesized that the protective capability of IBPs on proteins against freeze-thaw damage is proportional to their IRI activity. Hence we used two IBPs: one with higher IRI activity (LeIBP) and the other with lower activity (FfIBP). Yeast alcohol dehydrogenase (ADH) was used as a freeze-labile model protein. IBPs and ADH were mixed, frozen at -20 °C, and thawed repeatedly. The structure of ADH was assessed using fluorescence emission spectra probed by 1-anilinonaphthalene-8-sulfonate over the repeated freeze-thaw cycles. The activity was monitored at 340 nm spectrophotometrically. Fluorescence data and activity clearly indicated that ADH without IBP was freeze-labile. However, ADH maintained about 70% residual activity after five repeated cycles at a minimal concentration of 0.1 mg mL^{-1} of high IRI-active LeIBP, but only 50% activity at 4 mg mL^{-1} of low active FfIBP. These results showed that the protection of proteins from freeze-thaw stress by IBPs is proportional to their IRI activity.

keywords: ice-binding protein; ice recrystallization inhibition; alcohol dehydrogenase; antifreeze protein; freezing damage

4-59 *Reproductive Biology; Veterinary Sciences*

The protective effect of *Leucosporidium*-derived ice-binding protein (LeIBP) on bovine oocytes and embryos during vitrification

Sun, Wu-Sheng., Jang, Hoon., Kwon, Hyo Jin., Kim, Ki Young., Bin Ahn, Soo., Hwang, Seongsoo., **Lee, Sung Gu.**, **Lee, Jun Hyuck.** and 2 others.

Theriogenology. 2020. 151: 137-143.

doi: 10.1016/j.theriogenology.2020.04.016.

Ice-binding proteins (IBPs) facilitate organism survival under extreme conditions by inhibiting thermal hysteresis and ice recrystallization. IBPs have been widely used as cryoprotectants to cryopreserve mammalian gametes and embryos. In the present study, we evaluated the protective effects of an Arctic yeast, *Leucosporidium* sp. AY30 derived ice-binding protein (LeIBP), on the vitrification of bovine metaphase II (MII) oocytes and embryos. When oocytes and embryos were frozen using the two-step vitrification method, the survival rate was significantly increased in the presence of LeIBP. The LeIBP supplementation decreased the levels of intracellular reactive oxygen species (ROS) and enhanced mitochondrial functions in the vitrifiedewarmed oocytes. Furthermore, LeIBP improved the developmental potential and suppressed apoptosis of the embryos derived from vitrifiedewarmed oocytes. Collectively, these data indicate that LeIBP can be used as a promising cryoprotectant to prevent cryoinjury during vitrification in bovine oocytes. (C) 2020 The Authors. Published by Elsevier Inc.

keywords: Bovine oocyte; Vitrification; Embryo development; LeIBP

4-60 *Microbiology*

Pseudomonas neustonica sp. nov., isolated from the sea surface microlayer of the Ross Sea (Antarctica)

Jang, Gwang Il., **Lee, Inae.**, Ha, Tran Thu., Yoon, Soo Jung., **Hwang, Yeon Ju.**, Yi, Hana., **Yun, Sukyoung.**, **Lee, Won Sang.** and Hwang, Chung Yeon.

International Journal of Systematic and Evolutionary Microbiology. 2020. 70(6): 3832-3838.

doi: 10.1099/ijsem.0.004240.

Gram- stain-negative, aerobic and rod-shaped bacterial strains, designated $SSM26^T$ and SSM44, were isolated from a sea surface microlayer sample from the Ross Sea, Antarctica. Analysis of the 16S rRNA gene sequences of strains $SSM26^T$ and SSM44 revealed a

clear affiliation with the genus *Pseudomonas*. Based on the results of phylogenetic analysis, strains SSM26^T and SSM44 showed the closest phylogenetic relationship with the species *Pseudomonas sabulinigri* KCTC 22137^T with the 16S rRNA gene sequence similarity level of 98.5 %. Strains SSM26^T and SSM44 grew optimally at 30 °C, pH 7.0-7.5 and 0.5- 10.0 % NaCl (w/v). The major cellular fatty acids were $C_{18:1}$ *ω7c* (31.3–34.9 %), $C_{16:0}$ (15.5–20.2 %), summed feature 3 ($C_{16:1}$ *ω7c* / $C_{16:1}$ *ω6c*; 19.5–25.4 %) and $C_{12:0}$ (6.0–9.3 %). The genomic DNA G+C content of each strain was 56.2 mol%. Genomic related-ness analyses based on the average nucleotide identity and the genome- to-genome distance showed that strains SSM26^T and SSM44 constituted a single species that was clearly distinguishable from its phylogenetically close relatives. The combined phenotypic, chemotaxonomic, genomic and phylogenetic data also showed that strains SSM26^T and SSM44 could be distin-guished from validly published members of the genus *Pseudomonas*. Thus, these strains should be classified as representing a novel species in the genus *Pseudomonas*, for which the name *Pseudomonas neustonica* sp. nov. is proposed with the type strain SSM26^T (=KCCM 43193^T=JCM 31284^T=PAMC 28426^T) and a sister strain SSM44 (=KCCM 43194=JCM 31285=PAMC 28427).

keywords: Antarctica; sea surface microlayer; marine bacteria; *Pseudomonas*

4-61 *Plant Sciences; Mycology*

Psoroma capense and *P. esterhuyseniae* (*Pannariaceae*), two new alpine species from South Africa

Elvebakk, Arve., **Hong, Soon Gyu.**, **Park, Chae Haeng.** and Rama, Teppo.

Lichenologist. 2020. 52(5): 345-352.

doi: 10.1017/s0024282920000377.

The new species *Psoroma capense* and *P. esterhuyseniae* are described from four alpine localities in the Western Cape Province of South Africa and are the only known *Psoroma* species from Africa. The specimens were all collected from moist sites near watercourses, on cool and mostly south-facing cliffs. *Psoroma capense* resembles *P. tenue* in gross morphology but differs in the ascending thallus squamules, lack of secondary compounds and short-ellipsoid to ovoid ascospores. However, a phylogenetic analysis involving the markers ITS, nucLSU, mtSSU and *Mcm7*, comparing the only recent collection of *P. capense* with previously published sequences, shows that it belongs to the *P. hypnorum* lineage, with no known, closely related species. *Psoroma esterhuyseniae* resembles *P. hypnorum* but has subglobose to short-ellipsoid ascospores without apical perispore extensions. The two species are thought to have evolved from one or two long-distance dispersal events during the Pleistocene.

keywords: biodiversity; evolution; lichens; phylogeny; taxonomy

4-62 *Agriculture, Dairy & Animal Science; Veterinary Sciences*

Remotely Piloted Aircraft System (RPAS)-Based Wildlife Detection: A Review and Case Studies in Maritime Antarctica

Hyun, Chang-Uk., **Park, Mijin.** and **Lee, Won Young.**

Animals. 2020. 10(12).

doi: 10.3390/ani10122387.

In wildlife biology, it is important to conduct efficient observations and quantitative monitoring of wild animals. Conventional wildlife monitoring mainly relies on direct field observations by the naked eyes or through binoculars, on-site image acquisition at fixed spots, and sampling or capturing under severe areal constraints. Recently, remotely piloted aircraft systems (RPAS), also called drones or unmanned aerial vehicles (UAV), were successfully applied to detect wildlife with imaging sensors, such as RGB and thermal-imaging sensors, with superior detection capabilities to those of human observation. Here, we review studies with RPAS which has been increasingly used in wildlife detection and explain how an RPAS-based high-resolution RGB image can be applied to wild animal studies from the perspective of individual detection and population surveys as well as behavioral studies. The applicability of thermal-imaging sensors was also assessed with further information extractable from image analyses. In addition, RPAS-based case studies of acquisition of high-resolution RGB images for the purpose of detecting southern elephant seals (*Mirounga leonina*) and shape property extraction using thermal-imaging sensor in King George Island, maritime Antarctica is presented as applications in an extreme environment. The case studies suggest that currently available cost-

effective small-sized RPAS, which are capable of flexible operation and mounting miniaturized imaging sensors, and are easily maneuverable even from an inflatable boat, can be an effective and supportive technique for both the visual interpretation and quantitative analysis of wild animals in low-accessible extreme or maritime environments.

keywords: wildlife biology; remotely piloted aircraft system; UAV; drone; quantitative monitoring; polar region; thermal-imaging sensor

4-63 *Soil Science*

Responses of surface SOC to long-term experimental warming vary between different heath types in the high Arctic tundra

Jung, Ji Young., Michelsen, Anders., **Kim, Mincheol.**, **Nam, Sungjin.**, Schmidt, Niels M., **Jeong, Sujeong.**, **Choe, Yong-Hoe.**, **Lee, Bang Yong.**, **Yoon, Ho Il.** and **Lee, Yoo Kyung.**

European Journal of Soil Science. 2020. 71(4): 752-767.

doi: 10.1111/ejss.12896.

Over the past few decades the Arctic has warmed up more than the lower latitudes. Soil organic carbon (SOC) in the Arctic is vulnerable to climate change, and carbon dioxide (CO_2) produced via SOC decomposition can amplify atmospheric temperature increase. Although SOC composition is relevant to decomposability, studies on its compositional changes with warming are scarce, particularly in the Arctic. Therefore, we investigated the responses of SOC and the bacterial community to climate manipulation under *Cassiope* and *Salix* heath vegetation communities in permafrost-affected soil in Zackenberg, Greenland. After 8-9 years of experimental warming, we evaluated changes in SOC quantity and quality of three density fractions of soil: free light fraction (FLF), occluded light fraction (OLF) and heavy fraction (HF). The SOC content at 0-5-cm depth was significantly reduced with warming under *Cassiope*, and it was accompanied by decreased FLF content, attributed to accelerated decomposition of the FLF by warming. However, SOC molecular composition and bacterial community composition were not affected by warming. By contrast, there was no warming effect on SOC under *Salix*, which could be partially due to smaller temperature increases caused by higher moisture levels associated with larger silt and clay contents, or to different responses of the dominant plant species to temperature. In both soils, more than 55% of SOC was associated with minerals, and its molecular composition indicated microbial decomposition. Our results suggested that long-term warming in the high Arctic could induce the loss of SOC, particularly in the FLF; however, the response could vary with vegetation type and/or soil properties, that is, soil texture.

keywords: $_{13}$C-NMR; bacterial community; climate change; SOC fractionation; soil organic carbon (SOC) and total nitrogen (TN) stocks

4-64 *Microbiology*

Sandaracinobacter neustonicus sp. nov., isolated from the sea surface microlayer in the Southwestern Pacific Ocean, and emended description of the genus *Sandaracinobacter*

Lee, Inae., Jang, Gwang Il., Cho, Yirang., Yoon, Soo Jung., Ha My Pham., Anh Vu Nguyen., **Lee, Yung Mi.**, Park, Hyun., **Rhee, Tae Siek.** and 2 others.

International Journal of Systematic and Evolutionary Microbiology. 2020. 70(8): 4698-4703.

doi: 10.1099/ijsem.0.004333.

A Gram stain negative, non-motile, facultatively anaerobic and rod-shaped bacterial strain, designated PAMC 28131^T, was isolated from a sea surface microlayer sample in the open water of the Pacific Ocean. Phylogenetic analysis of the 16S rRNA gene sequence of strain PAMC 28131^T revealed an affiliation to the genus *Sandaracinobacter* with the closest species *Sandaracinobacter sibiricus* RB16-17^T (sequence similarity of 98.2%). Strain PAMC 28131^T was able to grow optimally with 0.5-1.0% NaCl and at pH 6.5-7.0 and 30 °C The polar lipids were phosphatidylglycerol, phosphatidylethanolamine, two unidentified phospholipids, an unidentified aminolipid, an unidentified glycolipid and an unidentified lipid. The major cellular fatty acids (>10%) were $C_{18:1}$ *ω6c* and/or $C_{18:1}$ *ω7c*, (42.6 %), $C_{17:1}$ *ω6c* (19.3 %) and $C_{16:1}$ *ω6c* and/or $C_{16:1}$ *ω7c* (15.8 %), and the respiratory quinone was Q-10. The genomic DNA G+C content was 65.3mol%. The phylogenetic, phenotypic and chemotaxonomic data showed that strain PAMC 28131^T could be clearly

distinguished from *S. sibiricus* RB16-17^T. Thus, strain PAMC 28131^T should be classified as representing a novel species in the genus *Sandaracinobacter*, for which the name *Sandaracinobacter neustonicus* sp. nov. is proposed. The type strain is PAMC 28131^T (=KCCM 43127^T =JCM 30734^T).

keywords: new species; *Sandaracinobacter neustonicus*; sea surface microlayer; Pacific Ocean

4-65 *Microbiology*

Soil water content as a critical factor for stable bacterial community structure and degradative activity in maritime Antarctic soil

Kim, Dockyu., Chae, Namyi., **Kim, Mincheol.**, **Nam, Sungjin.**, Kim, Eungbin. and **Lee, Hyoungseok.**

Journal of Microbiology. 2020. 58(12): 1010-1017.

doi: 10.1007/s12275-020-0490-9.

Recent increases in air temperature across the Antarctic Peninsula may prolong the thawing period and directly affect the soil temperature (T_s) and volumetric soil water content (SWC) in maritime tundra. Under an 8°C soil warming scenario, two customized microcosm systems with maritime Antarctic soils were incubated to investigate the differential influence of SWC on the bacterial community and degradation activity of humic substances (HS), the largest constituent of soil organic carbon and a key component of the terrestrial ecosystem. When the microcosm soil (KS1-4Feb) was incubated for 90 days (T = 90) at a constant SWC of ~32%, the initial HS content (167.0 mg/g of dried soil) decreased to 156.0 mg (approximately 6.6% loss, $p < 0.05$). However, when another microcosm soil (KS1-4Apr) was incubated with SWCs that gradually decreased from 37% to 9% for T = 90, HS degradation was undetected. The low HS degradative activity persisted, even after the SWC was restored to 30% with water supply for an additional T = 30. Overall bacterial community structure remained relatively stable at a constant SWC setting (KS1-4Feb). In contrast, we saw marked shifts in the bacterial community structure with the changing SWC regimen (KS1-4Apr), suggesting that the soil bacterial communities are vulnerable to drying and re-wetting conditions. These microcosm experiments provide new information regarding the effects of constant SWC and higher T_s on bacterial communities for HS degradation in maritime Antarctic tundra soil.

keywords: Antarctic tundra soil; bacterial composition; degradative activity; humic substances; microcosm

4-66 *Biochemical Research Methods; Biochemistry & Molecular Biology; Biophysics; Crystallography*

Structural analysis of a novel substrate-free form of the aminoglycoside 6 ’-*N*-acetyltransferase from *Enterococcus faecium*

Jang, Hyunseok., Kwon, Sunghark., **Jeong, Chang-Sook.**, **Lee, Chang Woo.**, **Hwang, Jisub.**, Jung, Kyoung Ho., **Lee, Jun Hyuck.** and Park, Hyun Ho.

Acta Crystallographica Section F-Structural Biology Communications. 2020. 76: 364-371.

doi: 10.1107/s2053230x20009735.

Aminoglycoside acetyltransferases (AACs) catalyze the transfer of an acetyl group between acetyl-CoA and an aminoglycoside, producing CoA and an acetylated aminoglycoside. AAC(6’)-Ii enzymes target the amino group linked to the 6’ C atom in an aminoglycoside. Several structures of the AAC(6’)-Ii from *Enterococcus faecium* [Ef-AAC(6’)-Ii] have been reported to date. However, the detailed mechanism of its enzymatic function remains elusive. In this study, the crystal structure of Ef-AAC(6’)-Ii was determined in a novel substrate-free form. Based on structural analysis, it is proposed that Ef-AAC(6’)-Ii sequentially undergoes conformational selection and induced fit for substrate binding. These results therefore provide a novel viewpoint on the mechanism of action of Ef-AAC(6’)-Ii.

keywords: aminoglycoside acetyltransferases; *Enterococcus faecium*; acetyl-CoA; conformational selection; induced fit

4-67 *Multidisciplinary Sciences*

Structural and biochemical analyses of an aminoglycoside 2 ’-*N*-acetyltransferase from *Mycolicibacterium smegmatis*

Jeong, Chang-Sook., **Hwang, Jisub.**, **Do, Hackwon.**, Cha, Sun-Shin., Oh, Tae-Jin., Kim, Hak Jun., Park, Hyun Ho. and **Lee, Jun Hyuck.**

Scientific Reports. 2020. 10(1).

doi: 10.1038/s41598-020-78699-z.

The expression of aminoglycoside-modifying enzymes represents a survival strategy of antibiotic-resistant bacteria. Aminoglycoside 2'-*N*-acetyltransferase [AAC(2')] neutralizes aminoglycoside drugs by acetylation of their 2' amino groups in an acetyl coenzyme A (CoA)-dependent manner. To understand the structural features and molecular mechanism underlying AAC(2') activity, we overexpressed, purified, and crystallized AAC(2') from *Mycolicibacterium smegmatis* [AAC(2')-Id] and determined the crystal structures of its apo-form and ternary complexes with CoA and four different aminoglycosides (gentamicin, sisomicin, neomycin, and paromomycin). These AAC(2')-Id structures unraveled the binding modes of different aminoglycosides, explaining the broad substrate specificity of the enzyme. Comparative structural analysis showed that the α4-helix and β8–β9 loop region undergo major conformational changes upon CoA and substrate binding. Additionally, structural comparison between the present paromomycin-bound AAC(2')-Id structure and the previously reported paromomycin-bound AAC(6')-Ib and 30S ribosome structures revealed the structural features of paromomycin that are responsible for its antibiotic activity and AAC binding. Taken together, these results provide useful information for designing AAC(2') inhibitors and for the chemical modification of aminoglycosides.

keywords: crystal structure; antibiotics; aminoglycoside acetyltransferase; X-ray crystallography

4-68 *Microbiology*

Structural and sequence comparisons of bacterial enoyl-CoA isomerase and enoyl-CoA hydratase

Hwang, Jisub., **Jeong, Chang-Sook.**, **Lee, Chang Woo.**, **Shin, Seung Chul.**, **Kim, Han-Woo.**, **Lee, Sung Gu.**, **Youn, Ui Joung.**, Lee, Chang Sup., Oh, Tae-Jin., Kim, Hak Jun., Park, Hyun., Park, Hyun Ho. and **Lee, Jun Hyuck.**

Journal of Microbiology. 2020. 58(7): 606-613.

doi: 10.1007/s12275-020-0089-1.

Crystal structures of enoyl-coenzyme A (CoA) isomerase from *Bosea* sp. PAMC 26642 (*Bo*ECI) and enoyl-CoA hydratase from *Hymenobacter* sp. PAMC 26628 (*Hy*ECH) were determined at 2.35 and 2.70 Å resolution, respectively. *Bo*ECI and *Hy*ECH are members of the crotonase superfamily and are enzymes known to be involved in fatty acid degradation. Structurally, these enzymes are highly similar except for the orientation of their C-terminal helix domain. Analytical ultracentrifugation was performed to determine the oligomerization states of *Bo*ECI and *Hy*ECH revealing they exist as trimers in solution. However, their putative ligand-binding sites and active site residue compositions are dissimilar. Comparative sequence and structural analysis revealed that the active site of *Bo*ECI had one glutamate residue (Glu135), this site is occupied by an aspartate in some ECIs, and the active sites of *Hy*ECH had two highly conserved glutamate residues (Glu118 and Glu138). Moreover, *Hy*ECH possesses a salt bridge interaction between Glu98 and Arg152 near the active site. This interaction may allow the catalytic Glu118 residue to have a specific conformation for the ECH enzyme reaction. This salt bridge interaction is highly conserved in known bacterial ECH structures and ECI enzymes do not have this type of interaction. Collectively, our comparative sequential and structural studies have provided useful information to distinguish and classify two similar bacterial crotonase superfamily enzymes.

keywords: crystal structure; enoyl-CoA isomerase; enoyl-CoA hydratase; X-ray crystallography

4-69 *Microbiology*

Structural insights into the psychrophilic germinal protease *Pa*GPR and its autoinhibitory loop

Lee, Chang Woo., Lee, Saeyoung., **Jeong, Chang-Sook.**, **Hwang, Jisub.**, Chang, Jeong Ho., Choi, In-Geol., Kim, T. Doohun., Park, HaJeung., Kim, Hye-Yeon. and **Lee, Jun Hyuck.**

Journal of Microbiology. 2020. 58(9): 772-779.

doi: 10.1007/s12275-020-0292-0.

In spore forming microbes, germination protease (GPR) plays a key role in the initiation of the germination process. A critical step during germination is the degradation of small acid-soluble proteins (SASPs), which protect spore DNA from external stresses (UV, heat, low temperature, etc.). Inactive zymogen GPR can be activated by autoprocessing of the N-terminal pro-sequence domain. Activated GPR

initiates the degradation of SASPs; however, the detailed mechanisms underlying the activation, catalysis, regulation, and substrate recognition of GPR remain elusive. In this study, we determined the crystal structure of GPR from *Paenisporosarcina* sp. TG-20 (*Pa*GPR) in its inactive form at a resolution of 2.5 Å. Structural analysis showed that the active site of *Pa*GPR is sterically occluded by an inhibitory loop region (residues 202-216). The N-terminal region interacts directly with the self-inhibitory loop region, suggesting that the removal of the N-terminal pro-sequence induces conformational changes, which lead to the release of the self-inhibitory loop region from the active site. In addition, comparative sequence and structural analyses revealed that *Pa*GPR contains two highly conserved Asp residues (D123 and D182) in the active site, similar to the putative aspartic acid protease GPR from *Bacillus megaterium*. The catalytic domain structure of *Pa*GPR also shares similarities with the sequentially non-homologous proteins HycI and HybD. HycI and HybD are metal-loproteases that also contain two Asp (or Glu) residues in their active site, playing a role in metal binding. In summary, our results provide useful insights into the activation process of *Pa*GPR and its active conformation.

keywords: crystal structure; germination protease; X-ray crystallography; zymogen

4-70 *Plant Sciences*

Study of Ecophysiological Responses of the Antarctic Fruticose Lichen *Cladonia borealis* Using the PAM Fluorescence System under Natural and Laboratory Conditions

Cho, Sung Mi., **Lee, Hyoungseok.**, **Hong, Soon Gyu.** and **Lee, Jungeun.**

Plants-Basel. 2020. 9(1).

doi: 10.3390/plants9010085.

Antarctic lichens have been used as indicators of climate change for decades, but only a few species have been studied. We assessed the photosynthetic performance of the fruticose lichen *Cladonia borealis* under natural and laboratory conditions using the PAM fluorescence system. Compared to that of sun-adapted *Usnea* sp., the photosynthetic performance of *C. borealis* exhibits shade-adapted lichen features, and its chlorophyll fluorescence does not occur during dry days without rain. To understand its desiccation-rehydration responses, we measured changes in the PSII photochemistry in *C. borealis* under the average light intensity of dawn light and daylight and the desiccating conditions of its natural microclimate. Interestingly, samples under daylight and rapid-desiccation conditions showed a delayed reduction in *Fv'/Fm'* and rETRmax, and an increase in Y(II) and Y(NPQ) levels. These results suggest that the photoprotective mechanism of *C. borealis* depends on sunlight and becomes more efficient with improved desiccation tolerance. Amplicon sequencing revealed that the major photobiont of *C. borealis* was *Asterochloris irregularis*, which has not been reported in Antarctica before. Collectively, these results from both field and laboratory could provide a better understanding of specific ecophysiological responses of shade-adapted lichens in the Antarctic region.

keywords: fruticose lichens; *Cladonia borealis*; Antarctic; phytochemistry; poikilohydric; non-photochemical quenching; desiccated state; shade-adapted lichen

4-71 *Chemistry, Multidisciplinary; Engineering, Multidisciplinary; Materials Science, Multidisciplinary; Physics, Applied*

Taking Advantage of Promiscuity of Cold-Active Enzymes

Nandanwar, Sondavid K., Borkar, Shweta Bharat., **Lee, Jun Hyuck.** and Kim, Hak Jun.

Applied Sciences-Basel. 2020. 10(22).

doi: 10.3390/app10228128.

Cold-active enzymes increase their catalytic efficiency at low-temperature, introducing structural flexibility at or near the active sites. Inevitably, this feat seems to be accompanied by lower thermal stability. These characteristics have made cold-active enzymes into attractive targets for the industrial applications, since they could reduce the energy cost in the reaction, attenuate side-reactions, and simply be inactivated. In addition, the increased structural flexibility could result in broad substrate specificity for various non-native substrates, which is called substrate promiscuity. In this perspective, we deal with a less addressed aspect of cold-active enzymes, substrate promiscuity, which has enormous potential for semi-synthesis or

enzymatic modification of fine chemicals and drugs. Further structural and directed-evolutional studies on substrate promiscuity of cold-active enzymes will provide a new workhorse in white biotechnology.

keywords: cold-active enzyme; catalytic efficiency; broad substrate specificity; substrate promiscuity; psychrophile

4-72 *Plant Sciences; Marine & Freshwater Biology*

Taxonomic study of three new Antarctic *Asterochloris* (Trebouxiophyceae) based on morphological and molecular data

Kim, Jong Im., Kim, Yong Jun., Nam, Seung Won., **So, Jae Eun.**, **Hong, Soon Gyu.**, **Choi, Han-Gu.** and Shin, Woongghi.

Algae. 2020. 35(1): 17-32.

doi: 10.4490/algae.2020.35.2.23.

Asterochloris is one of the most common genera of lichen phycobionts in Trebouxiophyceae. *Asterochloris* phycobionts associated with the lichenized fungi *Cladonia* and *Stereocaulon* in King George Island (Antarctica) and Morro Chico (Chile), were isolated and then used to establish clonal cultures. To understand the phylogenetic relationships and species diversity of Antarctic *Asterochloris* species, molecular and morphological data were analyzed by using three microscopy techniques (light, confocal laser and transmission electron) and a multi-locus phylogeny with data from the nuclear-encoded internal transcribed spacer (ITS) rDNA and the actin and plastid-encoded ribulose bisphosphate carboxylase large chain (*rbc*L) coding genes. Morphological data of three Antarctic strains showed significant speciesspecific features in chloroplast while molecular data segregated the taxa into distinct three clades as well. Each species had unique molecular signatures that could be found in secondary structures of the ITS1 and ITS2. The species diversity of Antarctic *Asterochloris* was represented by six taxa, namely, *A. glotnerata*, *A. italiana*, *A. sejongensis*, and three new species (*A. antarctica*, *A. pseudoirregularis*, *A. stereocaulonicola*).

keywords: Antarctica; *Asterochloris*; lichen; photobiont; phylogeny; taxonomy; Trebouxiophyceae

4-73 *Multidisciplinary Sciences*

Temperature Dependency of Proton Pumping Activity for Marine Microbial Rhodopsin from Antartic Ocean

Kim, Se-Hwan., Jung, ByungHoon., **Hong, Soon Gyu.** and Jung, Kwang-Hwan.

Scientific Reports. 2020. 10(1).

doi: 10.1038/s41598-020-58023-5.

Proteorhodopsin (PR) is discovered from marine bacteria and it has proton pumping activity from inside to outside of the cell using light energy. In general, PR classified into two groups by the maximum absorption spectra. In this study, we isolated the two of a full sequence of opsin homologues by PCR from the seawater sample near King George Island, Antarctica. One was the same sequence as the first reported GPR (Green-light absorbing PR) from Monterey Bay. Another named HSG119 was a newly discovered sequence which shows high sequence similarity with BPR (Blue-light absorbing PR). HSG119 has an absorption maximum at 493 nm with broader spectrum at pH7.0 and it can pump protons out of the cell membrane. Interestingly, it showed a similar temperature dependence to GPR(Y200N) that isolated near the North pole.

keywords: Polar environment; blue-light absorbing rhodopsin; membrane protein expression; proton pumping

4-74 *Biochemistry & Molecular Biology; Endocrinology & Metabolism; Toxicology; Zoology*

Temperature elevation stage-specifically increases metal toxicity through bioconcentration and impairment of antioxidant defense systems in juvenile and adult marine mysids

Haque, Md Niamul., Nam, Sang-Eun., **Kim, Bo-Mi.**, **Kim, Kitae.** and Rhee, Jae-Sung.

Comparative Biochemistry and Physiology C-Toxicology & Pharmacology. 2020. 237.

doi: 10.1016/j.cbpc.2020.108831.

Metals are of serious concern due to their toxicity, persistency, and accumulation potential in aquatic animals. However, limited information is available

on the combined effects of metal with temperature elevation, which is one of the future climate changes suggested for the oceans. In this study, the effect of temperature elevation was investigated by analyzing toxicity, bioconcentration, and antioxidant response in juvenile and adult marine mysids upon exposure to 20 °C and 25 °C for 48 h and 96 h. Based on LC_{50} values, toxicity of metals was highly reliant on temperature, exposure period, and age. Elevation in temperature significantly increased the whole metal toxicity in juveniles. Bioconcentration was elevated by increasing exposure period and metal concentration. Significant elevation of malondialdehyde (MDA) and depletion of glutathione (GSH) was measured in juveniles, while significant elevation of both MDA and GSH was detected in adults. Subsequently, enzymatic activities of antioxidant enzymes in catalase (CAT) and superoxide dismutase (SOD) increased significantly in adults at 48 h and 96 h, whereas most activities were significantly lowered in juveniles at 96 h. These results suggest that the early life stage of marine mysids is more sensitive to the combined effect of metal and temperature than adult stage due to an impairment in the induction of the antioxidant defense system.

keywords: Metal; Temperature; Mysid; Toxicity; Oxidative stress; Bioconcentration

4-75 *Pharmacology & Pharmacy*

Terrein suppressed lipopolysaccharide-induced neuroinflammation through inhibition of NF-κB pathway by activating Nrf2/HO-1 signaling in BV2 and primary microglial cells

Kim, Kwan-Woo., Kim, Hye Jin., Sohn, Jae Hak., **Yim, Joung Han.** and 2 others.

Journal of Pharmacological Sciences. 2020. 143(3): 209-218.

doi: 10.1016/j.jphs.2020.01.011.

In the course of our continuous investigation on the bioactive marine-derived fungal metabolites, terrein was isolated from marine-derived fungal strain *Penicillium* sp. SF-7181. Terrein inhibited the overproduction of pro-inflammatory mediators, such as nitric oxide (NO) and prostaglandin E2 (PGE_2), as well as inducible nitric oxide synthase (iNOS) and cyclooxygenase-2 (COX-2) in lipopolysaccharide (LPS) stimulated BV2 and primary microglial cells. This compound also repressed the LPS-induced production of pro-inflammatory cytokines, interleukin (IL)- 1β and IL-6. These inhibitory effects of terrein were associated with the inactivation of the nuclear factor kappa B (NF-κB) pathway through suppression of the translocation of p65/p50 heterodimer into the nucleus, the phosphorylation and degradation of inhibitor kappa B (IκB)-α and the DNA binding activity of the p65 subunit. In addition, terrein induced the protein expression of heme oxygenase (HO)-1 through the activation of nuclear transcription factor erythroid-2 related factor 2 (Nrf2) in BV2 and primary microglial cells. The anti-inflammatory effect of terrein was blocked by pre-treatment with a selective HO-1 inhibitor, suggesting that its antineuroinflammatory effect is mediated by HO-1 induction.

keywords: Terrein; Anti-neuroinflammatory effects; NF-κB; HO-1; Nrf2

4-76 *Chemistry, Medicinal; Chemistry, Organic*

Two New Phenolic Compounds from the Antarctic Lichen *Pertusaria dactylina*

Koo, Man Hyung., Kim, Ji Hee., Park, Hyun., Lee, Jun Hyuck. and **Youn, Ui Joung.**

Chemistry of Natural Compounds. 2020. 56(1).

doi: 10.1007/s10600-020-02936-0.

Two new phenolic compounds, methyl 2-hydroxy-4-methoxy-6-(2-oxopentyl)-benzoate (1) and 4-methoxy-6-pentyl-1,2-dihydroxybenzene (2), together with two known phenolic derivatives, were isolated from the Antarctic lichen *Pertusaria dactylina* (*Pertusariaceae*). The structures of the new compounds were determined by 1D and 2D NMR and HR-MS experiments, as well as by comparison of their data with the published values.

keywords: *Pertusaria dactylina*; Antarctic lichen; *Pertusariaceae*; phenolic compounds

4-77

Weddell seal observations on female and pup behavior and breeding status for four overwintering periods (2015 to 2018) at Barton Peninsula, King George Island, Antarctica

Kim, Yejin., **Ahn, In-Young.**, **Park, Ji Kang.** and **Lee, Won Young.**

CZECH POLAR REPORTS. 2020. 10(1): 1-6.

doi: 10.5817/CPR2020-1-1.

In animal ecology studies, it is a fundamental monitoring work to observe annual breeding cycle. In this study, we report the detailed observations on seven mother and pup pairs of Weddell seal (*Leptonychotes weddellii*) at Barton peninsula, King George Island, Antarctica. Two or three pairs had been observed along the coast on the fast ice in 2015, 2017, and 2018 and no breeding was recorded in 2016. Although it varied among individuals, pups were recorded to be born on 19–25 Sept., began swimming at day 18–19 after birth, and molted at day 21–25. Our observations may provide fundamental breeding information of Weddell seals in our study site and contribute to the future longterm monitoring research of seals.

keywords: annual breeding cycle; *Leptonychotes weddellii*; Barton Peninsula; Antarctica

PART 5

Policy

5-1

Research on Japan's Arctic Policy: Focusing on Assessment of the Importance of the Social Science

Seo, Hyun Kyo.

Journal of Asia-Pacific Studies. 2020. 27(4): 95-125.

doi: 10.18107/japs.2020.27.4.004.

Japan commenced the Arctic activities by joining IASC which was the first Arctic activity of Asian Countries, and has expanded the interest areas by conducing international project for NSR in 1990s and 2000s. And, 'Headquarter for Ocean Policy at the Prime Minister's Office' for managing the Japan's Ocean and Polar Policy was founded in 2007 and Japan got the ad-hoc observer state in 2009 and finally joined the observer group of Arctic Council in 2013. as an after-action of joining, the headquarter formally released the Japan's Arctic Policy in 2015 that was the first Arctic policy of the Japanese government. Japan's Government consisted of 3-axis of policy, that is △Research and Development (R&D), △International Collaboration. △Sustainable Development. Regarding the R&D of Arctic Policy, MEXT organized the Arctic Climate Change Research Project (2011-2016) under GRENE programme. and as a second stage, MEXT initiated the interdisciplinary programme named "Arctic Challenge for Sustainability (ArCS I 2015-2019 leading by NIPR, JAMSTEC, Hokkaido Univ.)' in 2015 which was finished successively in 2019. MEXT had hosted the breakout session at Arctic Circle Assembly for sharing the accomplishments of the ArCS I. with international communities from 2016 to 2019. In 2020 MEXT, on the third stage, launched ArCS II programme which takes more multidisciplinary approach than ArCS I and more domestic research institutions (i.e. Univ., Institute) apart from 3 main institutions joined as the managing institutes of each sub-project. This study conducted the comparative study on GRENE (Arctic Climate Change Research Project), ArCS I, and ArCS II in terms of research themes and the contents of sub projects, portion of Arctic Social science and its role and

relations on A rctic natural science, etc. And the study reviewed the implications based on the outcomes of analysis and research and suggested the directions for the development of Korea's Arctic interdisciplinary programme collaborating Arctic Social Science, Natural Science and Engineering for addressing Arctic Issue and contributing to Policy-Decision.

keywords: Japan's Arctic Policy; GRENE; ArCS Ⅰ; ArCS Ⅱ; Headquarter for Ocean Policy(Japan)

5-2 *Area Studies*

Research on the Development of Korean Polar Policy Masterplan

Seo, Hyun Kyo.

Korean journal of Siberian studies. 2020. 24(1): 65-104.
doi: 10.22892/ksc.2020.24.1.03.

The ministry of Oceans and Fisheries stated '2050 Polar Vision' as an long-term blueprint for the Korean polar policy last December and the National Assembly is preparing to enact the law for promotion of the activities in polar region. These governmental actions includes integration of 'Korea's Arctic policy Masterplan'(Arctic Masterplan) and 'A Masterplan for promotion of research activities in Antarctica'(Antarctic Masterplan) based on 'Act on Activities in the Antarctic Area and the protection of Antarctic Environment' enacted in 2004, which established every 5 years. So, this study reviewed the process of formation of Antarctic regimes including the Antarctic Treaties, and analyzed the Korea's domestic legislation & Antarctic policies which were linked with international Antarctic regimes. Especially Korean government has setup from the 1st Antarctic Masterplan (2007~2011) to the 3rd masterplan (2017~2021) that included detailed actionplans.The study applied the 'Korea's Arctic policy model', which was developed by Dr. SEO Hyunkyo (2019), to categorizing the detailed actionplans of the 3rd Antarctic masterplans (2017-2021: the newest) for the sake of integrating 'Arctic masterplan' and 'Antarctic masterplan'. And as the next step, the study combined it with items of the relevant actionplans of 2nd Arctic Masterplan (2018-2022: the newest). In the same way, the study classified 'actionplans of the 2nd Arctic Masterplan' and 'the actionplans of the 3rd Antarctic Masterplan' by 7 policy strategies of the '2050 polar vision', and combined classified each actionplan of Arctic masterplan and of Antarctic Masterplan.Lastly based on the result of three kinds of integrative way (① 'Korean Arctic Policy Model', ② '2050 polar vision', ③ 'Polar 20 agenda') between Arctic Masterplan and Antarctic Masterplan, the study drew implications and suggested the ideas and ways for the combination of Arctic Masterplan and Antarctic Masterplan to the Korean government.

keywords: Korea's Arctic policy Masterplan; A Masterplan for Promotion of Research Activities in Antarctica; Korea's Arctic Policy Model; 2050 Polar Vision Statement; Polar 20 Agenda

Keyword Index

B

C

D

H

I

M

N

S

T

U

V

W

X

Y

Z

Author Index

K

L

W

X

Y

Compiled by Library of Korea Polar Research Institute

KOPRI ABSTRACTS contains journal articles written by KOPRI researchers and other researchers funded by KOPRI. The following KOPRI authors can be seen as highlighted in bold text.
The ***KOPRI ABSTRACTS*** are published once a year and distributed world wide by KOPRI since launching in 2014.

Korea Polar Research Institute
igloo Library

**26 Songdomirae-ro, Yeonsu-gu,
Incheon, 21990, Korea
www.kopri.re.kr**

ISSN 2289-0734